Synthesis of molecular probes for the hyperpolarization with parahydrogen

DISSERTATION

FOR THE AWARD OF THE DEGREE
"DOCTOR RERUM NATURALIUM"
OF THE GEORG-AUGUST-UNIVERSITÄT GÖTTINGEN

WITHIN THE DOCTORAL PROGRAM
PHYSICS OF BIOLOGICAL AND COMPLEX SYSTEMS (IMPRS-PBCS)
OF THE GEORG-AUGUST UNIVERSITY SCHOOL OF SCIENCE (GAUSS)

SUBMITTED BY

DENIS MOLL

FROM WÜRSELEN, GERMANY

GÖTTINGEN (2022)

Thesis advisory committee (TAC)

Dr. Stefan Glöggler
Max-Planck-Institut für multidisziplinäre Naturwissenschaften (MPINAT), Forschungsgruppe zur NMR-Signalverstärkung, Göttingen, Deutschland.

Jun.-Prof. Dr. Johannes Walker
Georg-August-Universität, organische Synthese in der Fakultät für Chemie, Göttingen, Deutschland.

Prof. Dr. Christian Griesinger
Max-Planck-Institut für multidisziplinäre Naturwissenschaften (MPINAT), NMR-basierte Strukturbiologie, Göttingen, Deutschland.

Members of the examination board

Erster Gutachter: Dr. Stefan Glöggler, MPINAT, Göttingen, Deutschland

Zweiter Gutachter: Jun.-Prof. Dr. Johannes Walker, MPINAT, Göttingen, Deutschland

Further members of the examination board

Prof. Dr. Manuel Alcarazo
Georg-August-Universität, asymmetrische homogene Katalyse in der Fakultät für Chemie, Göttingen, Deutschland.

Dr. Michael John
Georg-August-Universität, NMR-Analytik im Institut für Organische und biomolekulare Chemie, Göttingen, Deutschland.

Prof. Dr. Martin Suhm
Georg-August-Universität, Institut für Physikalische Chemie, Göttingen, Deutschland.

Date of thesis submission: 2.11.2022
Date of thesis defense: 1.12.2022

Promovierendenerklärung

Name Moll, Denis
(Name, Vorname)

Anschrift Zur Hohen Warte 19, 37077 Göttingen
(Straße, PLZ Wohnort)

Ich beabsichtige, eine Dissertation zum Thema 'Synthesis of molecular probes for the hyperpolarization with parahydrogen' an der Georg-August-Universität Göttingen anzufertigen. Dabei werde ich von Herrn Dr. Stefan Glöggler betreut.

Ich gebe folgende Erklärung ab:

1. Die Gelegenheit zum vorliegenden Promotionsvorhaben ist mir nicht kommerziell vermittelt worden. Insbesondere habe ich keine Organisation eingeschaltet, die gegen Entgelt Betreuerinnen und Betreuer für die Anfertigung von Dissertationen sucht oder die mir obliegenden Pflichten hinsichtlich der Prüfungsleistungen für mich ganz oder teilweise erledigt.
2. Hilfe Dritter wurde bis jetzt und wird auch künftig nur in wissenschaftlich vertretbarem und prüfungsrechtlich zulässigem Ausmaß in Anspruch genommen. Insbesondere werden alle Teile der Dissertation selbst angefertigt; unzulässige fremde Hilfe habe ich dazu weder unentgeltlich noch entgeltlich entgegengenommen und werde dies auch zukünftig so halten.
3. Die Ordnung zur Sicherung der guten wissenschaftlichen Praxis an der Universität Göttingen wird von mir beachtet.
4. Eine entsprechende Promotion wurde an keiner anderen Hochschule im In- oder Ausland beantragt; die eingereichte Dissertation oder Teile von ihr wurden/werden nicht für ein anderes Promotionsvorhaben verwendet.

Mir ist bekannt, dass unrichtige Angaben die Zulassung zur Promotion ausschließen bzw. später zum Verfahrensabbruch oder zur Rücknahme des erlangten Grades führen können.

Göttingen, den 2. November 2022

....

(Unterschrift)

II

Acknowledgments

Mit einem Abschluss eines Kapitels, wie diese Dissertation es darstellt, möchte ich den außergewöhnlichen Menschen danken, die mir auf dem Weg hierhin geholfen haben, das zu erreichen. Vielen Dank euch, die mich durch mein Studium und meine Promotion gefördert, gefordert und unterstützt haben. Gerade die letzten drei Jahre, die so stark von der Pandemie geprägt waren, haben gezeigt, dass selbst diese Steine sich miteinander aus dem Weg räumen lassen. Ich danke euch dafür! Darüber hinaus möchte ich an einige Menschen ein paar persönliche Worte richten:

Zuallererst gilt mein Dank dir, Stefan. Danke dir für die überragende Betreuung meiner Arbeit, deine fachliche Unterstützung, dein offenes Ohr bei Problemen jeder Art und deine Hilfe bei der Umsetzung meiner wissenschaftlichen Ideen. Ich kann mich sehr glücklich schätzen so einen guten Supervisor für meine Promotion gehabt zu haben. Danke!

Ich danke Prof. Dr. Ulf Diederichsen für seine Unterstützung in den ersten beiden TAC-Meetings. Ihm gebührt großer Dank für seine Hilfestellungen hinsichtlich der chemischen Arbeit mit lichtsensitiven Molekülen.

Ein großes Dankeschön an Jun.-Prof. Dr. Johannes Walker. Danke dafür, dass du dich sofort bereiterklärt hast, die Aufgaben von Herrn Diederichsen zu übernehmen und die letzten Monate meiner Arbeit zu begleiten, sowie deine neue Sicht auf meine wissenschaftlichen Ergebnisse.

Ich danke zudem Herrn Prof. Dr. Christian Griesinger für die Unterstützung und hilfreiche Diskussion meiner Arbeit während der TAC-Meetings. Ich bedanke mich auch für die Nutzung Ihrer Labore innerhalb des NMR II Departments. Ihre Perspektive auf meine Arbeit hat mir sehr geholfen, vielen Dank!

I want to thank Dr. Stefan Glöggler, Jun.-Prof. Dr. Johannes Walker, Prof. Dr. Christian Griesinger, Prof. Dr. Manuel Alcarazo, Dr. Michael John and Prof. Dr. Martin Suhm for their interest in my PhD work and their commitment as members of my examination committee.

Ein großes Dankeschön gilt meinen früheren und aktuellen Kollegen der Arbeitsgruppe Glöggler. Thank you, Anil Jagtap, Gabriele Stevanato, Henning Schroeder, Lisa Fries, Lukas Kaltschnee, Oscar Sucre, Philip Saul, Salvatore Mamone, Sergey Korchak, Shengjun Yang, Sonja Sternkopf,

Zusammenfassung

Kernresonanzspektroskopie (NMR) und die verwandte Kernresonanztomographie (MRT) ermöglichen es uns Informationen über Moleküle auf atomarer Ebene zu gewinnen und somit Bilder von humanen Geweben und Organen zu erstellen, ohne dabei die Moleküle oder das Gewebe zu zerstören oder mit starker (Röntgen oder radioaktiver) Strahlung zu belasten. Kerne mit magnetischen Momenten ordnen sich in äußeren Magnetfeldern entlang der Magnetfeldlinien an und können durch Radiofrequenzpulse so angeregt werden, dass sie ein Spektrum (NMR) oder ein Bild (MRT) erzeugen. Jedoch nutzen beide Technologien nicht ihr volles Potential aus. Selbst in modernsten Hochfeldmagneten tragen nur ein Bruchteil der beobachtbaren Moleküle zum detektierten Signal bei. Diese geringe sogenannte thermische Polarisation limitiert die Möglichkeiten der Technologie sich Veränderungen auf molekularer Ebene unter physiologischen Bedingungen zu anzuschauen. Der wissenschaftliche Fortschritt ermöglicht es jedoch, dass durch geschickte Manipulation der magnetischen Momente mehr Atome zum detektierten Signal beitragen und somit die Intensitätssteigerungen von bis zu 100.000-fach möglich sind. Mittels der sogenannten Hyperpolarisation lassen sich selbst geringst konzentrierte Moleküle verfolgen. So könnte sich mit bildgebenden Verfahren der Einfluss von Krankheiten auf den menschlichen Körper untersuchen, ohne dabei auf zeitintensive Untersuchungen oder andere, invasive Methoden angewiesen zu sein.

Eine weitverbreitete Methode Moleküle in diesen hyperpolarisierten Zustand zu versetzen, wird gemeinhin „Parawasserstoffinduzierte Hyperpolarisation" (PHIP) genannt. Dabei verwendet man ein Kernspinisomer des Wasserstoffmoleküls, dass sogenannte Parawasserstoff (pH_2), das durch die chemische Reaktion mit einem ungesättigten, isotopisch angereicherten Kontrastmolekül das Molekül selbst hyperpolarisiert. Falls es nicht möglich ist, das gewünschte Produkt durch die Hydrierung direkt herzustellen, kann auf einen ungesättigten Seitenarm zurückgegriffen werden, der nachfolgend durch den Einsatz weiterer Chemikalien abgespalten werden kann.

Durch die Entwicklung hyperpolarisierter Metabolite, das heißt körpereigner Stoffe, könnten zukünftig Kontrastmittel zur Verfügung stehen, die Medizinern nicht nur Auskunft über die Lokalisation, sondern auch über den Status der Krankheit liefern. Metabolite sind Stoffe, die im Körper zum Beispiel zur Energiegewinnung verwendet werden und somit Teil von überlebenswichtigen Prozessen sind. Krebs oder kardiovaskuläre Erkrankungen zählen zu den häufigsten Todesursachen westlicher Länder und haben in ihrer Wirkungsweise erheblichen Einfluss auf den menschlichen Stoffwechsel und die Durchblutung.

Zielsetzung dieser Arbeit war es, biologisch relevante Substanzen, die nicht direkt hydrierbar sind, für die Hyperpolarisation mittels PHIP zugänglich zu machen. Dies umfasste:

1) Der Protonen-Deuterium Austausch an Kontrastmolekülen zur Verlängerung der Verfolgbarkeit.
2) Die Entwicklung von Synthesestrategien zur Herstellung neuartiger Seitenarme mit spezifischen Eigenschaften und deren Kopplung an Metabolite.
3) Die Entwicklung eines Markierungsmoleküls zur Angiographie.
4) Die Hyperpolarisation und die Freisetzung der zu beobachtenden Metabolite in biokompatiblen Lösungen zur Analyse in magnetresonanzbasierten Verfahren.

Dazu wurden zunächst Modifikationen am wichtigen metabolischen Zwischenprodukt Pyruvat durchgeführt. Dieses Molekül entsteht bei der Verdauung von Glukose und stellt einen zentralen Verzweigungspunkt des menschlichen Metabolismus dar. Das Zusammenspiel der neuen Stoffwechselwege ausgehend vom Pyruvat werden je nach Bedarf gesteuert und lokal durch Krankheiten sehr stark beeinflusst. Das langfristige Ziel ist es, hyperpolarisiertes Pyruvat in bildgebenden Verfahren zur Darstellung dieser Veränderung zu nutzen. Darüber hinaus soll auf Grund der veränderten Gewichtung der ausgehenden Stoffwechselwege die Möglichkeit gegeben werden, diese Veränderungen zu quantifizieren und somit differenzierte Diagnosen stellen zu können. Um das Pyruvat im menschlichen Körper länger verfolgbar zu machen, wurden neue, milde Protonen-Deuterium Austauschreaktionen untersucht. Diese Reaktionen ermöglichen in weiteren synthetischen Transformationen einen effektiveren Einsatz der isotopisch markierten Ausgangsstoffe, um effiziente Wege hin zum Kontrastmolekül zu ermöglichen. Deuteriertes Pyruvat wurde im Anschluss an einen neuartigen Seitenarm gekoppelt, der es erstmals ermöglicht, das Metabolit, ohne die Verwendung weiterer Chemikalien, nach der Hyperpolarisation freizusetzen. Diese neue Klasse an Seitenarmen verkürzt so die Aufarbeitungszeit drastisch, sodass ein einfacherer Zugang zu hyperpolarisierten Stoffen geschaffen wurde. Mit diesem auf einer 2-Nitrobenzylstruktur basierenden Seitenarm wurden hochgradig polarisierte Moleküle (über 60% Protonenpolarisation für 1-^{13}C-Acetat, bis zu 30% Protonenpolarisation für 1-^{13}C-Pyruvat) hergestellt, die selbst in wässrigen Lösungen biologische Messungen ermöglichen könnten (^{13}C Polarisationen bis zu 8% in Wasser).

Neben der Untersuchung von metabolischen Prozessen und deren Bildgebung sind gerade für das MRT die Entwicklung neuer Kontrastmittel für zur zum Beispiel die Angiographie von großem Interesse. Die bisher häufig zum Einsatz kommenden Gadolinium Verbindungen lagern sich im

Gehirn ab, wirken sich potentiell auf Kalziumkanäle aus und werden mit allergischen Reaktionen in Verbindung gebracht, weshalb deren Einsatz stark eingeschränkt wurde. Besonders wiederholte Injektionen am selben Tag sind nicht möglich. Insbesondere zur Angiographie bieten sich daher metabolische Endprodukte an, die an keinen weiteren Stoffwechselprozessen beteiligt sind, sondern bis zur Absonderung nur noch im Blutkreislauf zirkulieren. Einer dieser Stoffe ist eine acetyliere Aminosäure aus der Proteindegeneration, das Acetyl-Alanin. Dieser körpereigene Stoff wurde mit einer Vinylgruppe als hyperpolarisierbaren Seitenarm versehen. Die nachfolgende Hyperpolarisation erreichte die höchst gemessenen Polarisationen in injizierbaren Lösungen für stickstoffhaltige Moleküle durch PHIP. Mit Polarisationswerten von über 6% sollten Anwendungen in Lebewesen möglich sein. So böte das N-Acetyl-Vinyl-Alanin ein mögliches Kontrastmittel für die Angiographie mittels MRT ohne die Nachteile eines Metallion-basierten Kontrastmittels wie Gadolinium.

Summary

Nuclear magnetic resonance spectroscopy (NMR) and related nuclear magnetic resonance imaging (MRI) allow us to acquire information about molecules at an atomic level and thereby create images of human tissues and organs without destroying the molecules or the tissue itself nor exposing them to strong (X-ray or radioactive) radiation. Nuclei with magnetic moments arrange themselves along magnetic field lines when placed in an external magnetic field and can be excited by radio frequency pulses to produce a spectrum (NMR) or an image (MRI). However, neither of these technologies exploits their full potential. Even in state-of-the-art high-field magnets, only a fraction of the observable molecules contributes to the detected signal. This low so-called thermal polarization limits the technology's ability to look directly at changes at the molecular level under physiological conditions. However, scientific progress made it possible to increase the number of atoms contributing to the detected signal by clever manipulation of the magnetic moments, thus enabling an increase of intensity by up to 100,000-fold. The so-called hyperpolarization can be used to track even the smallest concentration of molecules. Therefore, imaging techniques could be used to investigate the influence of diseases on the human body without having to rely on long measurements or other methods.

A widely used technique to bring molecules into this hyperpolarized state is called "parahydrogen-induced hyperpolarization" (PHIP). This involves the use of the nuclear spin isomer of a hydrogen molecule, known as parahydrogen (pH_2), which hyperpolarizes an unsaturated, isotopically enriched molecule through chemical reaction. In case it is not possible to produce the desired product directly by hydrogenation, it is necessary to use an unsaturated side arm, which subsequently has to be cleaved by the use of further chemicals.

The development of hyperpolarized metabolites, i. e. substances that are specific to the body, could make contrast agents available in the future that provide medical experts with information not only on the localization but also on the status of the disease. Metabolites are substances that are used in the body, for example to generate energy, and are thus part of processes that are essential for survival. Cancer or cardiovascular diseases are among the most frequent causes of death in western countries, and their mode of action has a considerable influence on human metabolism and blood circulation.

The purpose of this work was to make biologically relevant substances that are not accessible for hyperpolarization using PHIP by direct. This included:

1) The proton-deuterium exchange on tracer molecules to extend their traceability.

2) The development of synthetic strategies to produce novel sidearms with specific properties and their coupling to metabolites.
3) The development of a labeling molecule for angiography.
4) The hyperpolarization and release of the metabolites to be observed in biocompatible solutions for analysis in magnetic resonance-based techniques.

For this purpose, modifications were first performed on the important metabolic intermediate pyruvate. This molecule is formed during the digestion of glucose and represents a branch point of human metabolism. The interplay of new metabolic pathways starting from pyruvate are controlled as needed and are strongly influenced locally by diseases. The long-term goal is to use hyperpolarized pyruvate in imaging techniques to visualize the change in favoring certain pathways. Based on the quantification of these changes, access to differential diagnosis should be possible. To make pyruvate traceable in the human body for longer periods of time, new mild proton-deuterium exchange reactions were investigated to allow effective use of the substances isotopically labelled in the following. Deuterated pyruvate was subsequently coupled to a novel sidearm that, for the first time, allows the metabolite to be released without the use of additional chemicals after hyperpolarization. This new class of sidearm thus dramatically shortens the work-up time, thereby providing easier access to hyperpolarized materials. This sidearm, based on a 2-nitrobenzyl structure, was used to produce highly polarized molecules (over 60% proton polarization for 1-^{13}C acetate, up to 30% proton polarization for 1-^{13}C pyruvate) that could allow biological measurements even in aqueous solutions (^{13}C polarizations up to 8% in water).

In addition to the study of metabolic processes and their imaging, the development of new contrast agents for angiography, for example, are of great interest, especially in MRI. Gadolinium compounds, which have been commonly used up to now, are deposited in the brain, which is why their use has been severely restricted. Metabolic end products, which do not participate in any further metabolic processes but only circulate in the bloodstream until they are secreted, are particularly suitable for the purpose of angiography. One of these substances is an acetylated amino acid from protein degeneration, the acetyl-alanine. This endogenous substance was equipped with a vinyl group as a hyperpolarizable side arm. The subsequent hyperpolarization achieved the highest polarizations measured in injectable solutions for nitrogen-containing molecules using PHIP. With polarization values above 6%, applications in living organisms should be possible. Thus, N-acetyl-vinyl-alanine would offer a possible contrast agent for angiography by MRI.

Publications and Patents

Decoupling of Spin Decoherence Paths near Zero Magnetic Field

Sven Bodenstedt, <u>Denis Moll</u>, Stefan Glöggler, Morgan W. Mitchell, and Michael C. D. Tayler

Rapidly Signal-enhanced Metabolites for Atomic Scale Monitoring of Living Cells with Magnetic Resonance

Y. Ding, S. Korchak, S. Mamone, A. P. Jagtap, G. Stevanato, S. Sternkopf, <u>D. Moll</u>, H. Schroeder, S. Becker, A. Fischer, E. Gerhardt, T. F. Outeiro, F. Opazo, C. Griesinger, S. Glöggler

Patentnummer EP21180465.3
Anmeldedatum 18.6.2021
Eigentümer Max-Planck-Gesellschaft
Erfinder Dr. Stefan Glöggler, Dr. Sergey Korchak, Dr. Anil Jagtap, Dr. Philip Saul, <u>Denis Moll</u>

Titel: Synthesis of vinylated hydroxy esters with applicability in signal enhanced magnetic resonance imaging

Patentnummer EP21180463.8
Anmeldedatum 18.6.2021
Eigentümer Max-Planck-Gesellschaft
Erfinder Dr. Stefan Glöggler, Dr. Sergey Korchak, Dr. Anil Jagtap, Dr. Philip Saul, <u>Denis Moll</u>

Titel: Vinylated keto esters with applicability in signal enhanced magnetic resonance imaging and synthesis

List of Contents

List of Figures

List of Chemical Reactions

List of Tables

Abbreviations

ABBREVIATION	PHRASE
AC	Acetyl
ALT	Alanine transaminase
ALTADENA	adibatic longitudinal transport after dissociation engenders net polarization
ATP	Adenosine triphosphate
COA	Coenzyme A
CT	Computed tomography
DDNP	Dissolution dynamic nuclear polarization
DNP	Dynamic nuclear polarization
E. G.	exempli gratia
ESOTHERIC	Efficient spin order transfer to heteronuclei via relayed INEPT chains
FADH2	Flavin adenine dinucleotide
FDG	18F-fluorodesoxyglucose
HMBC	Heteronuclear multiple bond correlation
I. E.	id est
INEPT	Insensitive nuclei enhanced by polarization transfer
LDH	Lactate dehydrogenase
MOI	Molecule of interest
MPC	Mitochondrial pyruvate carrier
MRI	Magnetic resonance imaging
MW	Microwave
NADPH	Nicotinamide adenine dinculeotide phosphate hydrate
NAVA	N-acetyl vinyle alanine
NMR	Nuclear magnetic resonance
NOE	Nuclear Overhauser effect
OH2	Orthohydrogen
PARA-H2	Parahydrogen
PASADENA	Parahydrogen and synthesis allow dramatically enhanced nuclear alignment
PC	Pyruvate carboxylase

PET	Positron emission tomography
PTFE	Polytetrafluoroethylene
PH2	Parahydrogen
PHIP	Parahydrogen induced polarization
PK	Pyruvate kinase
PYR	Pyruvate
RG	Reciever gain
RT	Room temperature
RTH2	Room temperature hydrogen
SABRE	Signal amplification by reversible exchange
SAH	Side arm hydrogenation
TCA	Tricarboxylic acid cycle
TEMPO	2,2,6,6-tetramethylpiperidinyloxyl
TLC	Thin layer chromatography
UV	Ultra violet light
ZGIG	Inverse gated NMR experiment
ZGPG	Power gated NMR experiment

1   Introduction

Medical breakthroughs over the last century have dramatically increased the average life expectancy and healthy lifespan of human.[1] Developments of small molecules that allow to effectively treat bacterial infections, for example, have contributed their part to the steady increase in general health.[2, 3] However, the aging of society, especially in western countries, has led to an elevated occurrence of diseases such as cancer, neuronal degeneration or circulatory disorders.[4, 5] These pathologies and their consequences accounted for a large proportion of the pre-pandemic deaths and are therefore the focus of worldwide research.[6, 7] It is of fundamental interest to investigate the mode of action of these diseases in depth, especially at the cellular level.[8] This may lead to better therapeutic approaches in the future or to an understanding of a holistic relationship.

In order to observe changes at the cellular level, many imaging techniques have been developed that are particularly well suited for visualizing larger structures such as proteins or entire cell organelles.[9] An excellent example for that is fluorescence microscopy, which makes it possible to visualize proteins and their interactions with the help of so-called fluorescence tags. However, this kind of projection is only possible if the molecule to be observed is sufficiently larger than the available tag. Especially the small molecules, like metabolites, can only be imaged indirectly, if at all. Techniques such as mass spectrometry are capable of detecting even the smallest concentrations of metabolites, but at the expense of the cells' integrity. The technology that allows direct observation of the atoms of a molecule without destroying the cell is nuclear magnetic resonance (NMR) and its sister technique magnetic resonance imaging (MRI). The biggest challenge to the development of contrast agents for MRI is its intrinsically low sensitivity. Only a handful out of a million observable atoms contribute to the detected signal resulting in long measurement times. That said, techniques have been developed to overcome this obstacle in NMR. By enhancements up to 100,000-fold even low concentrated compounds (below 2 mM) provide signals that in the normal regime could only be generated by concentrations of several moles. These methods are based on the phenomenon called hyperpolarization.[10] Hyperpolarization offers the possibility of achieving such a strong signal amplification, that metabolic processes, fast movements or small impacts can be probed and imaged not only in studies at the cellular level but also in whole living organisms or such as humans.[11-13]

Most of diseases mentioned manifest changes in the metabolism of humans, often in a localized manner. In general, what is usually meant when talking about metabolism are the in-cell processes to generate energy, the production of building blocks and the elimination of waste. But many

diseases massively influence the cellular metabolism, especially energy production.[14-17] Either the disease itself can cause massive shifts in the way metabolic processes are performed (such as cancer), or the healthy tissue might react to e. g. infections with a strong immune response which needs more energy compared to healthy tissue. Regarding the energy metabolism, one of the main sources to generate adenosine triphosphate (ATP), nicotinamide adenine dinucleotide phosphate hydrate (NADPH) or flavin adenine dinucleotide (FADH$_2$) as energy carriers, is the glycolysis and related downstream pathways. Glycolysis is the degradation of one molecule of glucose into two molecules of pyruvate while generating two ATP and two NADPH. Pyruvate itself is a major branching point in the human metabolism as it can be (1) consumed in the tricarboxylic acid (TCA) cycle to reach the full potential of energy production, (2) used as a nitrogen carrier in form of alanine participating in the glucose alanine cycle or (3) converted into lactic acid as for example under heavy muscular load (Figure 1). Usually, the most effective energy production is the preferred pathway for healthy cells, but many diseases are known to alter the balance of these in pyruvate connecting pathways. The most prominent example is cancer with the Warburg effect which describes the phenomenon that many tumors favor the conversion of pyruvate into lactate over suppling the α-keto acid to the TCA cycle.[18, 19] The reason why highly proliferating tumors change the metabolism in this direction is not fully understood.[20] Many tumors have mutations in the regulation of the oxidative phosphorylation or the mitochondrial uptake of pyruvate and thus need to fuel the glycolysis by eliminating pyruvate to keep up with the high amounts of energy needed to keep the unlimited proliferation going.[21, 22] Other theories state that the reason might be the low amount of oxygen available to the inner areas of tumors (especially bigger ones), leading to a similar effect observed in muscles under heavy load over a longer period of time.[23]

Currently, the investigation of cancer undergoes several steps from the initial suspicion until the final diagnosis. Usually, a lot of examinations have to be performed, starting from laboratory test of liquid biopsies, tissue biopsies as well as imaging with computed tomography (CT), MRI, positron emission tomography (PET) or ultrasound, in order to validate the diagnosis. The gold standard for cancer imaging is PET. This method uses a radioactively labelled glucose analogue called ^{18}F-fluorodesoxyglucose (FDG) which accumulates in cells with high energy need and then can be visualized via ionizing radiation.[24] The higher the energy demand, the more FDG is taken up, which can be used to identify and map potential tumor areas and metastases or sites of inflammation.[25]

Creating a radiation-free method for clinical applications to not only image where the tumor can be found but also to investigate conversion rates to further understand how the individual cancer behaves can potentially enable a better and more effective treatment.[26-28]
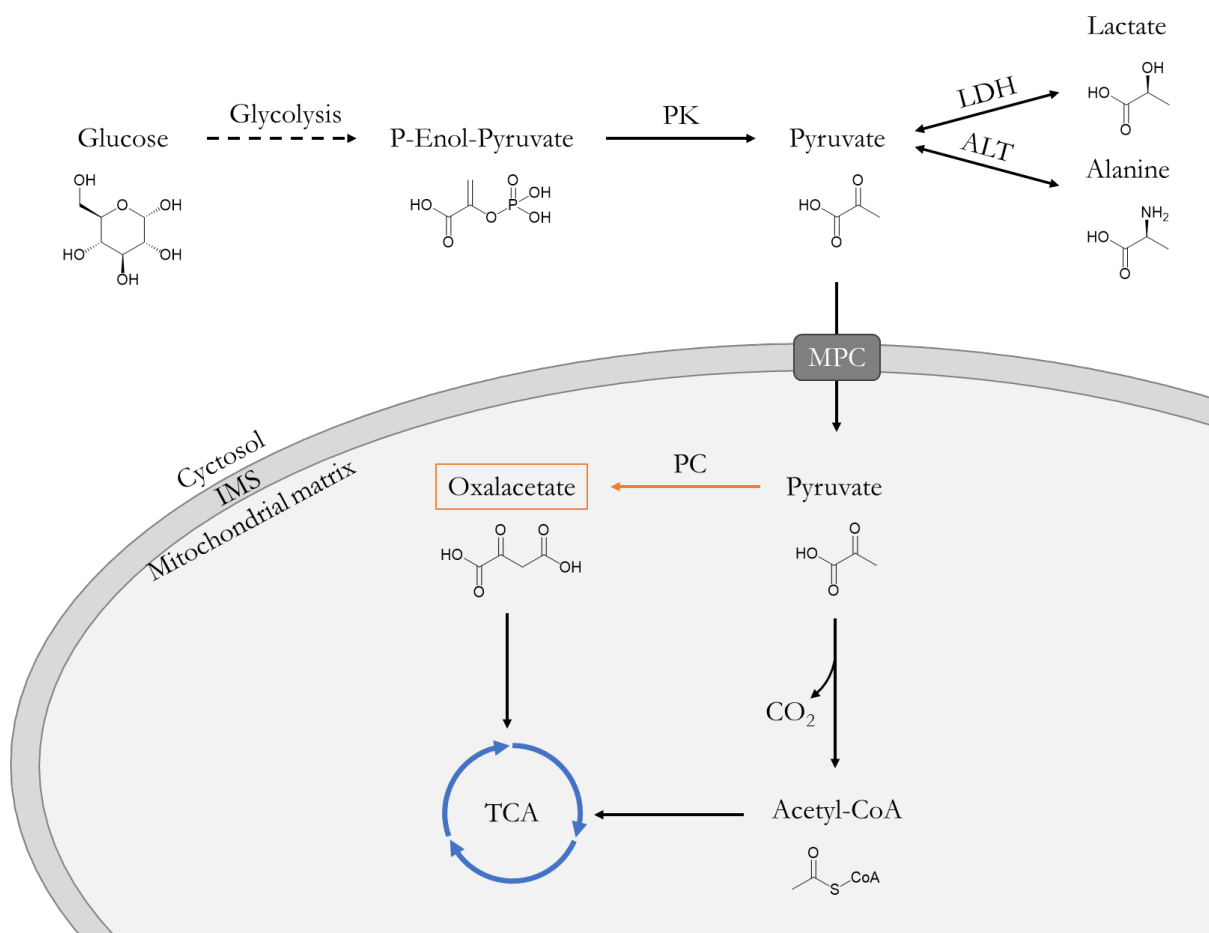
Figure 1 Metabolic pathway of glucose towards pyruvate and the involvement of the mitochondria. Pyruvate is produced from glucose through the glycolysis via phospho-enol-pyruvate (P-Enol-Pyruvate) by the pyruvate kinase (PK). In a bidirectional equilibrium pyruvate can then be converted into lactate by the lactate dehydrogenase (LDH) or into Alanine by the alanine transaminase (ALT). The transport into the mitochondria is performed by the mitochondrial pyruvate carrier (MPC) where pyruvate can access the tricarboxylic acid (TCA) cycle either through decarboxylation by pyruvate dehydrogenase (PDH) providing Acetyl-Coenzyme A (Acetyl-CoA) or by oxalacetate produced prior in the liver or kidney through the pyruvate carboxylase (PC).

For cardiovascular diseases however, not only metabolic information can help to understand how the disease impact the patient. To successfully fight these diseases, medical personnel is highly dependent on good imaging techniques to visualize issues and impacts on the whole system.[14, 27, 29, 30] Thus, the ability to perform both, perfusion studies and fast image acquisition are highly in need. Especially, regarding the imaging of the heart.[31] The continuous movement of the muscle itself severely diminishes imaging quality, which is why the development of contrast agents enabling quick acquisition instead of long measurements would significantly improve the diagnostic information. A major improvement over the currently used contrast agents would be the access to endogenous molecules in form of metabolic end-products to image circulatory disorders. Such metabolic contrast agents could solve safety concerns regarding currently used gadolinium contrast agents. In 2017 many Gd-based contrast agents were banned due to their accumulation in the brain

and their general toxicity as they were found to interfere with calcium-dependent signal transduction pathways.[32-34] Not only do hyperpolarized contrast agents offer a non-toxic alternative to currently used substances. The ability to acquire metabolic data in the form of conversion kinetics offers the possibility to make differentiated statements about the nature and distribution of the diseases.[35-37]

The following chapters will discuss methods and techniques used to enhance signals of molecules in magnetic resonance. This involves the discussion of the physical and chemical requirements for good contrast agents. To understand these, a fundamental knowledge of NMR is required but the concepts needed to understand the experiments performed are explained.

Introduction

1.1 Magnetic resonance

NMR describes the interaction between a magnetically active nucleus and an externally applied magnetic field. A basic requirement is that the total angular momentum of the nucleus (also called nuclear spin) I is not equal to 0. The number of energy states that can be assumed in a magnetic field depends on the magnetic spin quantum number m_I. A nucleus with a spin of $I = \frac{1}{2}$ results in two energy levels ($m_I = 2 \cdot I + 1$) which are degenerate without an external magnetic field B_0 i. e. energetically equivalent. Only by applying a magnetic field the splitting occurs. Upon an interaction of a nucleus with $I = \frac{1}{2}$ like ^{1}H or ^{13}C and an external B_0, the nucleus can align itself with or against the magnetic field. These two states correspond to the energy levels N_0 and N_1 (Figure 2).
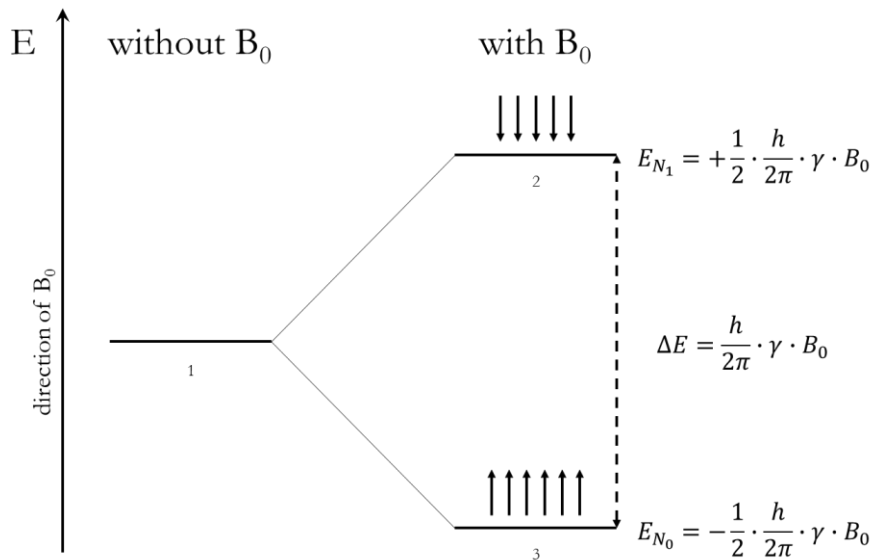
Figure 2 Illustration of the nuclear Zeeman effect. 1) No external B_0 is applied, the energy levels are energetically equal. 2) Exited energy level N_1 in an external magnetic field. 3) Ground state energy level N_0 in an external magnetic field.

This splitting phenomenon is described by the nuclear Zeeman effect. The population difference of the respective energy levels can be calculated by means of the Boltzmann distribution (equation 1), as for $I = \frac{1}{2}$ nuclei at 7 T it holds:

$$\frac{n_1}{n_0} = e^{\frac{-\gamma h B_0}{2\pi k_B T}} = e^{\frac{-267.552 \cdot 10^6 \frac{1}{T \cdot s} 6.63 \cdot 10^{-34} \frac{J}{Hz} * 7\,T}{2\pi \cdot 1.38 \cdot 10^{-23} \frac{J}{K} * 293\,K}} = 0{,}99995 \qquad\qquad 1$$

where n_0 is the number of nuclei in the ground state N_0, n_1 is the number of nuclei in the excited state N_1, γ is the gyromagnetic ratio, h is the Planck constant, B_0 is the magnetic field strength, k_B is the Boltzmann constant and T is the absolute temperature in Kelvin. The here calculated population difference corresponds to the for this work used 7 T magnets. This field strength is quite common for NMR standard and equals the current limits in clinical full-body MRI systems. The Boltzmann distribution results in a small overpopulation of the ground state which can be explained by the small energy difference (ΔE) between the two states (equation 2):

$$\Delta E = \frac{h}{2\pi} \cdot \gamma \cdot B_0 \qquad\qquad 2$$

Where for E_{N_0} holds the negative equation, E_{N_1} holds the positive equation, h is the Planck constant, γ is the gyromagnetic ratio and B_0 is the magnetic field strength. Therefore, the net polarization is considered to be fairly limited due to the small difference in population. Considering the distribution formula (equation 1), the only value to be variable (since temperature, especially in biological applications, is strictly limited) is the magnetic field strength. In the field of magnets, nowadays NMR devices with a field strength of up to 28 T are used, for MRI field strengths of 7 T are common. However, at room temperature, in a magnetic field of 7 T only 25 at 28 T only 100 spins per million contribute to the detected signal. The relative increase is huge, but still not enough to trace a dynamic system such as metabolism in real time. Therefore, techniques to shift the polarization out of the thermal equilibrium are needed.

1.2 Thermal polarization

Polarization by itself is the normalized ratio of the population differences of the energy levels of a given system. For $I = \frac{1}{2}$ nuclei reads:

$$P = \frac{n_0 - n_1}{n_0 + n_1} \qquad\qquad 3$$

where n_0 and n_1 describes the respective populations of spin states N_0 and N_1. Here, for P = 100%, all spins of a system contribute to the measured signal and no signal can be detected for a polarization equal to 0%. In the thermal equilibrium the polarization ($P_{thermal}$) can be calculated by the population differences of the two spin states. For a 7 T magnet and ^1H as observed nucleus it states:

$$P_{thermal} = \frac{e^{\frac{-E_{N_0}}{k_B T}} - e^{\frac{-E_{N_1}}{k_B T}}}{e^{\frac{-E_{N_0}}{k_B T}} + e^{\frac{-E_{N_1}}{k_B T}}}$$

4

$$P_{thermal} = 2.44 \cdot 10^{-5}$$

$$P_{thermal}\% = 0.00244\%$$

where E_N describes the energy of the respective spin states N_0 and N_1, k_B as the Boltzmann constant and T is the absolute temperature. With such low natural polarization values, it is obviously difficult to observe metabolites and other substances at physiological concentrations in living organisms. To illustrate, a thermal polarization of $2.4 \cdot 10^{-3}$ % corresponds to only the volume of a sugar cube being detectable when observing a bathtub full of water. Since cooling down is not realistic in a biological context, other methods of manipulating spin populations must be considered. These so-called hyperpolarization techniques obtain their overpopulation of an energy level from other sources which allows significant overpopulation of one spin state to generate strongly enhanced signals without the usage of a higher substance concentration. By comparing the signals from thermally polarized spectra and those from hyperpolarization experiments it is possible to calculate how many spins contributed to the hyperpolarized signals.

1.3 Hyperpolarization

The spectrum of techniques with the task of producing high spin states that are not in equilibrium are grouped under the term hyperpolarization (Figure 3). Hyperpolarization is defined as a state where more nuclei participate in the generation of the signal compared to thermally polarized counterpart. This means that with a theoretical 100% polarization of the observed nuclei, a signal amplification of up to approx. 50,000-fold at ^{1}H and approx. 160,000-fold at ^{13}C at room temperature are possible. Thus, even with fractions of the possible polarization it is possible, to generate information, which otherwise would have required enormous amounts of measurement time. Some important techniques will be outlined in the following chapters 1.3.1 and 1.3.3.
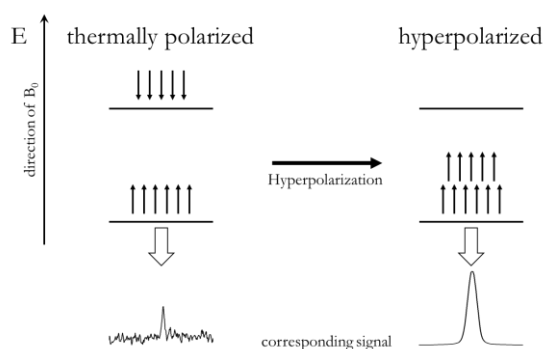
Figure 3 Illustration of a comparison of the spin states of thermally and hyperpolarized samples with arrows representing the alignment direction of the spins. The signals below were acquired within 7 h (64 scans) for the left and 1 second for the right signal. The right signal is 150 times more intense than the left.

1.3.1 Dynamic Nuclear Polarization

One of the most widely used hyperpolarization techniques is dynamic nuclear polarization (DNP), which takes advantage of the much higher polarization of electrons (compared to nuclear spin polarization) to transfer their spin order onto nuclei. DNP comes in a wide variety of styles, with dissolution DNP (dDNP) being the most successful for studying metabolically active molecules such as 1-^{13}C pyruvate.[38, 39]
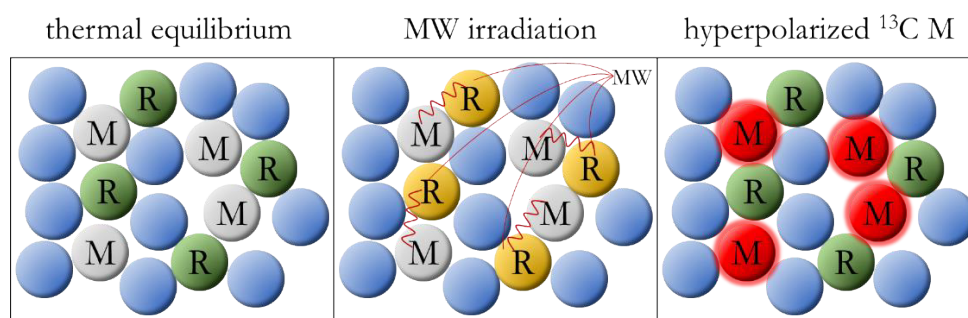
Figure 4 Hyperpolarization by dDNP. Irradiation of a glass matrix containing a free radical R and a ^{13}C-labelled metabolite M with microwaves (MW). The transfer of polarization from the electrons of the radical to the heteronucleus yields a polarized metabolite (M, red) in the glass matrix (blue).[40]

For successful hyperpolarization one needs a so-called hyperpolarization juice consists of a stable free radical compound such as 2,2,6,6-tetramethylpiperidinyloxyl (TEMPO) and the material to be hyperpolarized in solution. It is important that the solvent forms a glass matrix at the targeted temperatures below 2 K, so that the transfer of electron polarization to the heteronucleus can be stimulated by the irradiation of strong microwaves (Figure 4). This process is performed in strong magnetic fields (> 3 T) and leads to the slow build-up of the polarization. Initially, only very long

build-up times were possible (up to 1.5 h)[38], but these could be reduced down to 15 min[41] by not hyperpolarizing the heteronucleus directly but by temporally polarizing the nearby protons and subsequently transferring the acquired polarization to the heteronucleus. After this procedure, the sample must be thawed as quickly as possible to use the solution in NMR studies or to inject it into living organisms (or even in humans). Thus, polarization values of up to 70% have been achieved in the raw juice, however, polarization values for the injectable solution of the hyperpolarized compound are much lower.[42]

Nevertheless, human clinical studies investigating prostate cancer using 1-^{13}C-pyruvate are in progress. With an average polarization of 17% (although polarization attempts under 15% and out of the pH range of 6.7 to 8 were dismissed) 31 patients were investigated to observe the kinetics of 1-^{13}C-lactate formation consistent with the numbers achieved by preclinical trials. It was possible to generate hyperpolarized images of a prior biopsy proven tumor, which was not detectable during the staging examination.[11] That said, bringing more of the many preclinical models for lymphoma, prostate, liver, breast and bone cancers using hyperpolarized metabolites to human studies may help to implement hyperpolarized ^{13}C MRI as a valid and secure method to investigate potential cancerous tissue.[27, 43]

In general, hyperpolarization of pyruvate can be seen as an alternative to PET imaging for cancer with overwhelming advantages. Beside the much larger availability of MRI compared to PET instruments, bypassing radioactive radiation allows for new patient populations because clinicians would no longer need to perform a risk-benefit assessment regarding the harmfulness of radioactivity. Despite the excellent polarization values, there are concerns about the safety of free radical injections into humans leading to studies adding free radical scavengers such as vitamin C to the solution.[44, 45] However, pyruvate is not the only molecule studied using dDNP. In addition to studies with ^{13}C metabolites such as glucose[46], choline[47, 48], a variety of amino acids[49, 50] or bicarbonate[51], even hyperpolarized H_2O[52] was used for angiography studies. These studies, in contrast to 1-^{13}C-pyruvate, where performed in animals, not in humans.

Regardless of the very exciting research and the advancing applications of DNP in biological applications, the technique suffers from several drawbacks. The hyperpolarization process itself is associated with high costs for purchase of a DNP machine as well as maintenance due to the required infrastructure. In addition to the high magnetic field strengths (> 3T), strong microwave emitters and large amounts of liquid helium are required for operation. Not only has the price of the liquid noble gas increased dramatically, but also the availability has decreased significantly due to the COVID-19 pandemic. These aspects, especially in potential clinical applications, considerably limit the access to this powerful technology.

A further concern is that in order to achieve good polarization of the heteronucleus in a short period of time, protons must be hyperpolarized before the polarization can be transferred to heteronuclei. This leads to significantly shorter longitudinal relaxation times T_1 of the ^{13}Cs or ^{15}Ns which should be pursued as long as possible. Direct polarization of deuterated metabolites such as pyruvate would need considerably more time and thus, again is harder to implement in clinical applications. Other hyperpolarization methods, such as PHIP, allow the use of deuteration strategies to significantly extend the T_1 of the heteronuclei.

1.3.2   Parahydrogen

Another intensively studied method is hyperpolarization using parahydrogen (para-H$_2$ or pH$_2$ for short) which is one of four spin isomers of the hydrogen molecule. In addition to the parahydrogen induced polarization (PHIP) where the hydrogen molecule is chemically added to an unsaturated bond, pH$_2$ is also used in a second approach in the form of the signal amplification by reversible exchange (SABRE). SABRE utilizes a reversable binding of the pH$_2$ to a catalyst to transfer the polarization onto the desired substrate.

A simplified way of looking at the origin of different spin isomers is based on the previously presented consideration of the behavior of spins with $I = \frac{1}{2}$. Thus, it was defined that this spin can be in two orientations in the applied magnetic field, with and against the direction of the field. In a molecule like hydrogen however there are two spins which are connected by a covalent bond. As a result, the orientation of the spins with respect to each other is fixed when entering a magnetic field. Simply spoken, this results in two states, a parallel (ortho) and an antiparallel arrangement (para).[53] A more detailed explanation of why there are four spin isomers in total, however, requires the consideration of the quantum mechanics of the molecule.

With the help of the wave function, it is possible to completely define the entirety of the states of this system. This means that if all parts of the wave function of a particle are known, all properties of that particle can be determined. The total wave function consists thus of several partial functions as for example the spin wave function. But quantum mechanics distinguishes between two types of particles in the case of nuclei with a spin. A discrimination is made between particles with an integer spin quantum number, the bosons, and the fermions as particles with a half-integer spin. Fermions, like hydrogen is as an atom with the spin $\frac{1}{2}$, behave according to the Fermi-Dirac statistics. Thereby also the Pauli Principle of indistinguishability of identical particles has to be applied.[54]

Introduction

What does this mean for the H_2 molecule?

The two protons are considered as indistinguishable particles from each other and must therefore be considered as a whole. The consequence is that the total wave equation of the atoms H_a and H_b (when H_a-H_b is the H_2 molecule) is antisymmetric (due to the Pauli Principle). This means the total wave equation of the atoms H_a and H_b are equal in value but with a different sign. The wave function of the H_2 molecule is a result of the product of the different wave functions, which are among others for example the spin wave function and the rotational wave function. Thus, the total wave function is antisymmetric if one (partial) function is symmetric while the other is antisymmetric (equation 5).

$$\Psi_{tot}(H_a, H_b) = -\Psi_{tot}(H_b, H_a) \qquad\qquad 5$$

For the hydrogen molecule, this means that four spin states are possible. If the spin is symmetric, that is I = 1 (when both spins point in the same direction), then three further states fall on the magnetic spin quantum numbers -1, 0 and 1. These spin isomers are called orthohydrogen (oH_2) in their entirety (equation 6).

$$
\begin{aligned}
\text{Triplet, ortho} \quad &
\begin{cases}
|\mathbf{1,1}\rangle = |\alpha, \alpha\rangle \\[4pt]
|\mathbf{1,0}\rangle = \dfrac{1}{\sqrt{2}}|\alpha, \beta\rangle + |\beta, \alpha\rangle \\[4pt]
|\mathbf{1,-1}\rangle = |\beta, \beta\rangle
\end{cases} \\[10pt]
\text{Singlet, para} \quad &
\begin{cases}
|\mathbf{0,0}\rangle = \dfrac{1}{2}|\alpha, \beta\rangle - |\beta, \alpha\rangle
\end{cases}
\end{aligned}
\qquad 6
$$

For the singlet state of parahydrogen, the symmetry of the rotational wave function is the rotational quantum number J. This is satisfied when J adopts an even numerical value. Consequently, the spin must be antisymmetric, that means I = 0. An important physical discrimination between oH_2 and pH_2 is based exactly on the difference between the rotational quantum numbers. This resulted in the experimental proof of the existence of H_2 spin isomers. The para-isomer is at a lower energy level than is possible for oH_2 due to the proportional dependence of the rotational energy on the rotational quantum number J. As described earlier, this J is 0 for pH_2, but is at least 1 for oH_2 (due to anti-parallelism). Phenomenologically, in 1929, Karl-Friedrich Bonhoeffer and Paul Harteck thus succeeded in demonstrating experimentally the thermal conductivity differences of the isomers(which is proportional to the heat capacity).[55]

Introduction

The transition from oH_2 to $pH_2 + h\nu$ is a so-called 'forbidden transition', which has the advantage that without ferromagnetic materials pH_2 has a potential half-life of several years. However, this also means that without appropriate conditions the enrichment would be not possible.[56] At room temperature, H_2 is equally populated over all four spin states (further referred as rtH_2). Yet, by cooling hydrogen down to 20 K in the presence of an appropriate catalyst (e. g. iron oxide), pH_2 can be enriched to almost 100% (Figure 5). When removing the catalyst, the gas can be warmed to room temperature while remaining in the singlet state. Due to the pure spin order in the parahydrogen, the molecule in contrast to the orthohydrogen is NMR silent. This logically is due to the total spin of I = 0. The consequence is that 1) by comparing the signal of oH_2 and pH_2 the actual enrichment level can be determined (equation 7) and 2) in order to make use of the spin order, the hydrogen molecule must interact with the substrate to be hyperpolarized, either by symmetry breaking through chemical reactions or by interaction across a catalyst. The fraction of pH_2 enrichment $\left(f_{pH_2}\right)$ is determined by the following equation 7:[57, 58]

$$f_{pH_2} = 1 - \left(\frac{3\, S_{pH_2}}{4\, S_{rtH_2}}\right) \qquad\qquad 7$$

where S_{pH_2} and S_{rtH_2} represent the integrals of the respective signals of pH_2 and room temperature H_2.
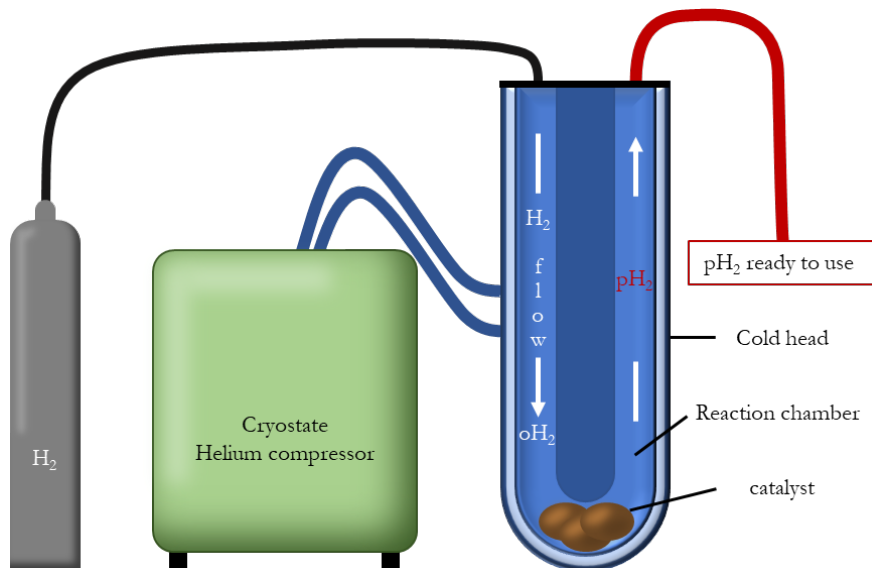

Figure 5 Schematic drawing of a parahydrogen generator consisting of a hydrogen cylinder, a helium cooling compressor and the reaction chamber. A H_2 bottle is connected to the to 20 K cooled reaction chamber. The cooling is ensured by a helium compressor driven cryostat. The cooled H_2 gas is blown over the paramagnetic catalyst yielding after warming to rt in 99.9% enriched parahydrogen.

1.3.3 Hyperpolarization by means of parahydrogen

After the preparation of highly enriched pH_2, there are two methods commonly used to achieve hyperpolarization, one non-hydrogenative (SABRE)[59] and one hydrogenative (PHIP)[60] technique (Figure 6a). In the late 2000s, the spontaneous polarization transfer from pH_2 to a substrate with the help of a Crabtree-like Ir catalyst was first demonstrated. To allow the transfer, it is essential that both hydrogen atoms and the substrate coordinate simultaneously to the metal center.[61, 62] This process is commonly carried out at low magnetic field strengths matching to the couplings of the system but also a pulsed high-field transfer is possible.[63, 64] For both cases, the polarization transfer is only possible if there is a scalar coupling between the protons and the nucleus of the substrate to be hyperpolarized. In addition to the direct hyperpolarization of substrates via the catalyst, so-called carrier molecules are being used to transfer the polarization to the final molecule of interest but with comparably low polarization levels.[65]

However, the centerpiece of the SABRE method is the catalyst and its modifications, which, depending on the substrate, were able to massively increase the efficiency of the transfer. Due to the wide variety of coupling partners, SABRE is able to polarize not only ^1H and ^{13}C[66] atoms but also ^{15}N[67], ^{19}F[68], ^{31}P[69] or ^{29}Si[70], thus providing a very broad spectrum of potential molecules. While the general polarization values tend to be found in the single-digit percentage range, it was possible to successfully polarize free 1-^{13}C pyruvate to over 10% ^{13}C polarization in DMSO, which takes the method one step closer to potential biological applications.[71]
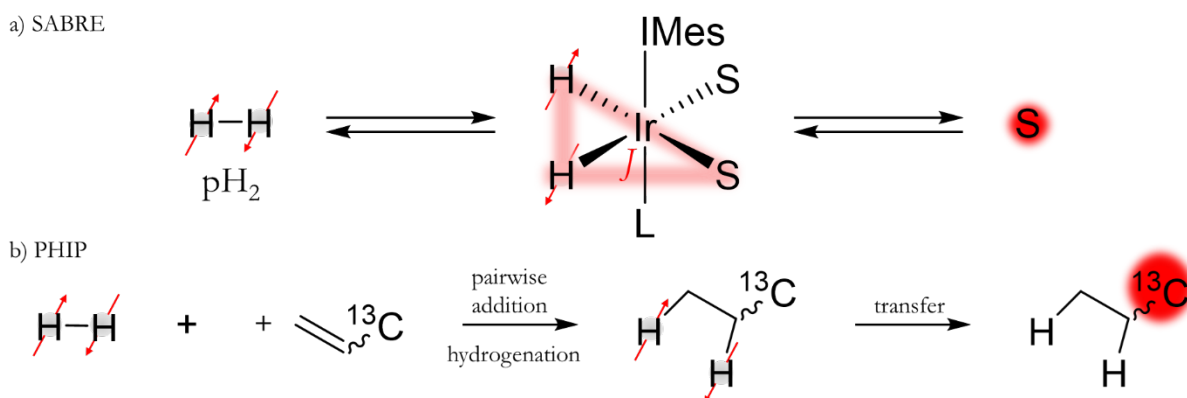

Figure 6 a) Schematic of the SABRE mechanism with the arrows indicating a reversable exchange at the catalytic center of the Iridium complex. b) Hydrogenative addition of parahydrogen on an unsaturated carbon-carbon bond with subsequent polarization transfer.

Introduction

1.3.3.1 Parahydrogen induced Polarization (PHIP)

The most widely used method to access the spin order of parahydrogen is the catalytic hydrogenation of unsaturated bonds. For this purpose, an appropriate syn-adding catalyst (more on this in Chapter 1.3.3.2) has to be used, whereby a pH_2 molecule is hydrogenated as a whole to the unsaturated bond.[10] This catalyst must have extremely high conversion rates to perform the reaction faster than the T_1 of the protons newly added to the molecule can decompose the polarization. There are two methods to perform the hydrogenation. In the PASADENA method (parahydrogen and synthesis allow dramatically enhanced nuclear alignment), both hydrogenation and detection are performed in high field magnets while under ALTADENA conditions (adiabatic longitudinal transport after dissociation engenders net alignment) the unsaturated bond is hydrogenated in weak magnetic fields (around 50 µT equal to the earth magnetic field) and subsequently measured in high field magnets.[72, 73] The type of magnetic field applied during the hydrogenation directly affects the nature of the J-coupling regime of the two protons. While under PASADENA conditions there is a weak coupling regime, under ALTADENA conditions there is a strong coupling between the two protons. The difference between strong and weak coupling is that the coupling constant for weak couplings is much smaller than the difference in chemical shift. For strong coupling regimes exactly the other way around. However, both procedures lead to a significantly different NMR spectrum compared to rtH_2.
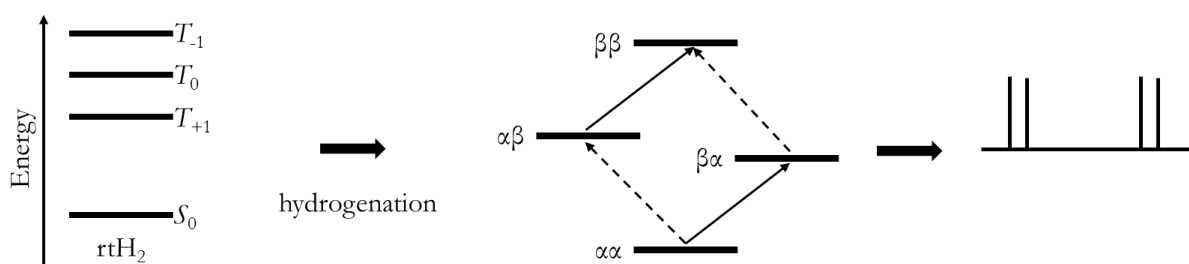

Figure 7 Schematic overview of a hydrogenation with rtH_2 with the respective NMR spectrum. The eigenstates of the AX system are equally populated and represented by horizontal lines.

To understand what changes using pH_2 for hydrogenation reactions, one need to understand how the NMR spectrum arises by hydrogenation with rtH_2. Through the addition the spin system of the dihydrogen changes from an A_2 to an AX system, which can be described by the eigenfunctions of the Zeeman base. The symmetry break leads to a combination of the individual spins. Four different states are formed, where the states $\alpha\beta$ and $\beta\alpha$ have a total spin of 0 and the $\alpha\alpha$ and $\beta\beta$

have one of 1 and -1, respectively.[74] Now, transitions between the energy levels can be excited by the irradiation of rf pulses, inverting one of the two spins. An inversion of both spins is quantum mechanically forbidden (allowed: $\alpha\beta \rightarrow \beta\beta$ forbidden: $\alpha\alpha \rightarrow \beta\beta$). Thus, four possible transitions result in four lines in the spectrum (Figure 7). The intensity of the lines corresponds to the initial polarization (calculated in chapter 1.2).
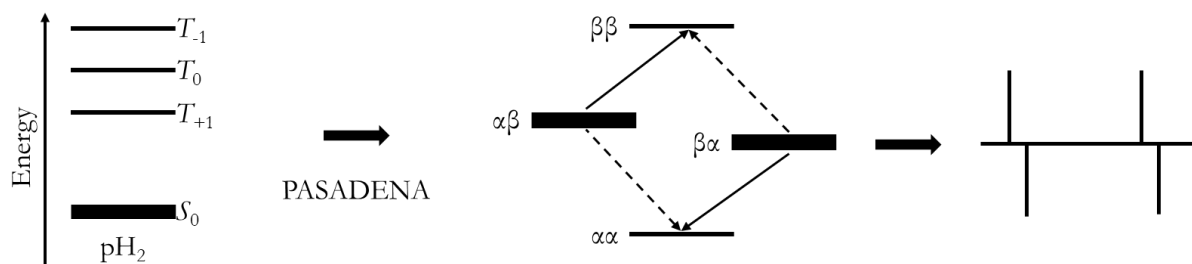

Figure 8 Schematic overview of a hydrogenation with pH_2 under PASADENA conditions for an AX spin system with the respective NMR spectrum. Thick horizontal lines represent overpopulation of the respective energy level, whereas thin lines represent a less populated state. The hydrogenation of the target molecule with the singlet isomer of H_2 leads to an equal population of the eigenstates $\alpha\beta$ and $\beta\alpha$. After the reaction, the typical anti-phase doublets can be acquired.

In the case of hydrogenation with pH_2 under PASADENA conditions, only the S_0 state is populated in the A_2 system (corresponding to the degree of pH_2 enrichment). The hydrogenation divides the population equally between $\alpha\beta$ and $\beta\alpha$. Thus, according to the excitation, a positive and a negative line are formed for $\alpha\beta$ and $\beta\alpha$, respectively (Figure 8). Without considering possible relaxation processes, the intensity of the lines corresponds to $\frac{2}{3}P + -\varepsilon$. As in the spectrum of the reaction with rtH_2, the distance between the lines is equal to the coupling constant J.
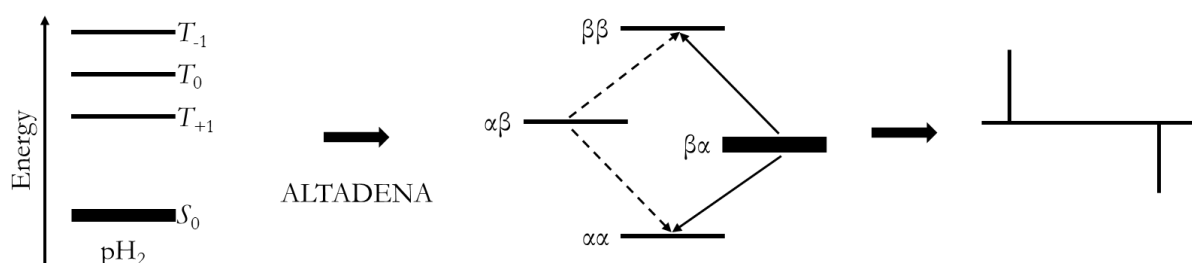

Figure 9 Schematic overview of a hydrogenation with pH_2 under ALTADENA conditions for an AX spin system with the respective NMR spectrum. Thick horizontal lines represent overpopulation of the respective energy level, whereas thin lines represent a less populated state. The hydrogenation of the target molecule at low magnetic fields leads to the overpopulation of the $\beta\alpha$ eigenstate. After the reaction, the typical two peaks with opposing phases can be acquired.

Introduction

Under ALTADENA conditions however, the singlet state follows the eigenstates of the magnetic field, whereby the magnetization bound in S_0 ends up in the $\beta\alpha$ eigenstate of the AX system. As a result, the NMR spectrum differs massively. Due to the overloading of the $\beta\alpha$ state, only two transitions are possible, resulting in two lines with twice the intensity compared to PASADENA lines (in the idealized case, i.e. no relaxation, no time loss due to hydrogenation outside the measuring magnet; Figure 9).

To understand how spins can be manipulated in a way that the introduced polarization is transferred to the heteronuclei a quantum mechanical description of the system has to be given. In order to describe the situation of the pH_2 protons under PASADENA and ALTADENA conditions, the density operator formalism has to be applied to PHIP. The density operator itself is able to describe the effects of pulses or delays on the spin. For an isolated spin $I = \frac{1}{2}$ the density operator ρ can be described as (equation 8):

$$\rho = \frac{1}{2}i + I_x + I_y + I_z$$

8

with i as identity operator, and I_x to I_z as magnetization of the single spin in the rotating frame in association to the cartesian system for x, y and z. For the two-spin system as pH_2 the operator reads:

$$S_0 = |S_0\rangle\langle S_0| = \frac{1i}{4} - \left(I_1^x I_2^x + I_1^y I_2^y + I_1^z I_2^z\right) = \frac{1i}{4} - I_1 \cdot I_2 \qquad 9$$

with I_1 and I_2 representing the entirety of the magnetization for each proton. PASADENA conditions cause the evolution of the terms $I_1^x I_2^x + I_1^y I_2^y$, however the hydrogenation reactions occur over time leading to the scramble of the transversal states. Thus, these terms are negated leaving the following state:

$$\rho_{PASADENA} = I_z^1 \cdot I_z^2 \qquad 10$$

If a RF pulse is applied on the molecule in a high magnetic field with a certain phase (γ) and flip angle (α) the density operator transforms into:

$$\rho_{PASADENA}(\alpha) = \cos^2(\alpha)\ I_z^1 I_z^2 + \cos(\alpha)\sin(\alpha)\ (I_z^1 I_x^2 + I_x^1 I_z^2) + \sin^2(\alpha)\ I_x^1 I_x^2$$

<div align="right">11</div>

That said, only the second term $(I_z^1 I_x^2 + I_x^1 I_z^2)$ is able to create a current in the receiver after the application of a pulse. This is the typical anti-phase signal with a maximal peak intensity at $\alpha = \frac{\pi}{4}$. A typical PASADENA NMR experiment thus consists of the reaction time Δ_1 (also called the bubbling time), a settling time Δ_2, and the 45° pulse to measure the maximum detectable signal (Figure 10).
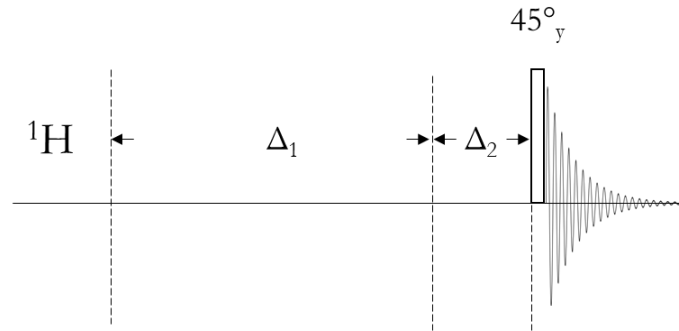
Figure 10 NMR pulse sequence used to perform hyperpolarization experiments at high field with subsequent ¹H acquisition. The rectangle represents a 45° pulse with the subscript indicating the phase. Δ_1 represents the bubbling time needed to fully hydrogenate the substrate and Δ_2 the time for the liquid to settle before performing a 45° pulse. The latter following sequences continue after Δ_2 instead of the 45° pulse.

For ALTADENA conditions however the magnetization evolves under the selective population at the low B-field. Since the spins can occupy either $|\alpha\beta\rangle\langle\alpha\beta|$ or $|\beta\alpha\rangle\langle\beta\alpha|$, the following density operator can be described:

$$\rho_{ALTADENA} = I_x^1 I_x^2 \pm \frac{1}{2}(I_z^1 - I_z^2)$$

<div align="right">12</div>

which evolves to

$$\rho_{ALTADENA}(\alpha) = \cos(\alpha)\sin(\alpha)\ (I_z^1 I_x^2)\ \pm \frac{1}{2}\sin(\alpha)\ (I_x^1 - I_x^2)$$

<div align="right">13</div>

when applying a pulse with a phase (γ) and flip angle (α). The term is composed of the already known part $\cos(\alpha)\sin(\alpha)\ (I_z^1 I_x^2)$ from the PASADENA experiment leading to the generation of an anti-phase signal while the other part $\pm\frac{1}{2}\sin(\alpha)\ (I_x^1 - I_x^2)$ yields a doublet formation. When

applying a pulse with a flip angle of $\alpha = 90°$ pure in-phase signals for each proton are generated, however the phase is altered by 180°.

1.3.3.2 Catalytic hydrogenation and precursor design

To incorporate the protons from pH_2 into the molecule a catalytic reaction is needed. The initial PHIP experiments were performed using the Wilkinson's Catalyst, rodium thriphenylphosphine chloride ($Rh(PPh_3)_3Cl$).[72, 75] The intrinsically stable PPh_3 is able to dissociate from the pre-catalyst allowing the hydrogen molecule to bind by oxidative addition yielding in a Rh^{III} catalytic center. Thus, it is possible for the unsaturated bond to bind to the metal (side-on), whereby the insertion can take place by hydrogenation. The reductive elimination of the now end-on bound alkyl residue can be carried out under recovery of the active catalyst (Scheme 1).
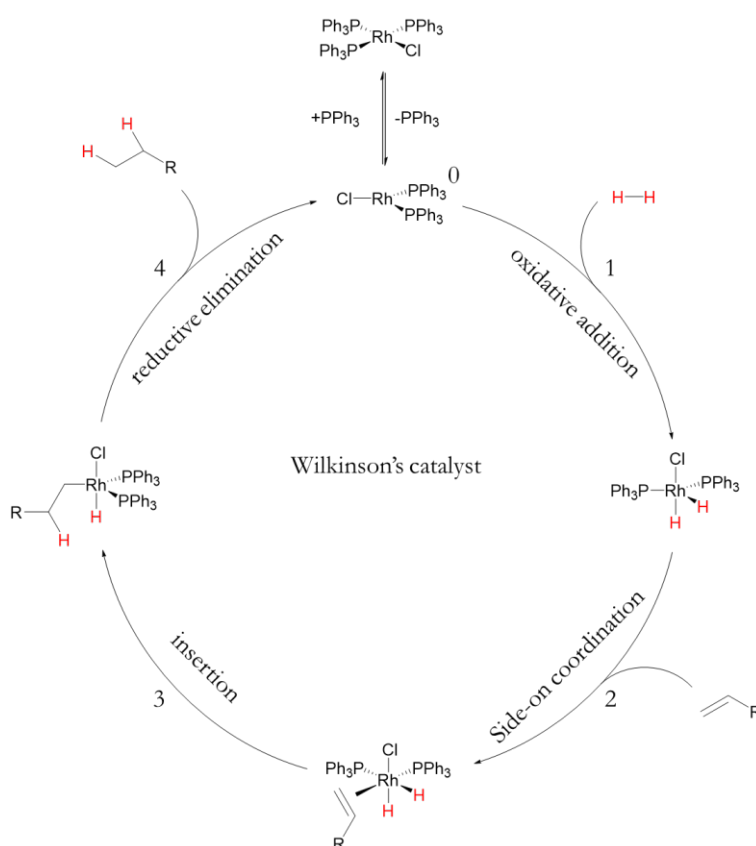
Scheme 1 Syn-hydrogenation of hydrogen to an unsaturated carbon-carbon bond by the Wilkinson's Catalyst. After the catalyst activation (0), the hydrogen molecule is attached to the catalyst by oxidative addition (1). The unsaturated substrate coordinates side-on onto the metal center forming the fully coordinated catalyst (2). Through the insertion the substrate is reduced (3) before the catalyst can undergo reductive elimination (4).

For this work another rhodium-based catalyst [1,4-Bis(diphenylphosphino)butane](1,5-cyclooctadiene)rhodium(I) tetrafluoroborate was mainly used due to the higher turn-over rate, which allows higher polarization values for the systems investigated. The catalytic cycle, however, is running comparably to the Wilkinson's Catalyst. The binding of the hydrogen molecule binding leads to the active catalyst form dissociated from the cyclooctadiene. These catalysts allow to generate polarization levels comparable to those achieved by DNP, leading to promising molecules to investigate biological questions.

An intensively investigated molecule with PHIP, as it is already in use for hyperpolarized in vivo studies of small animals is fumarate. The carboxylic acid made it possible to investigate the detection of necrotic processes and was one of the first PHIP hyperpolarized molecules in animal studies.[76] The precursor with the intrinsic triple bond generates access to the metabolic active molecule without any previous modifications. With a polarization of 12% directly after the transfer (no data on the polarization values of the injected solution available), Stewart et al. were able to show conversion of from 1-13C-fumerate to 1-13C-malate and 4-13C-malate in vivo using an acetaminophen-induced hepatitis mouse model (Figure 11).

in vivo conversion
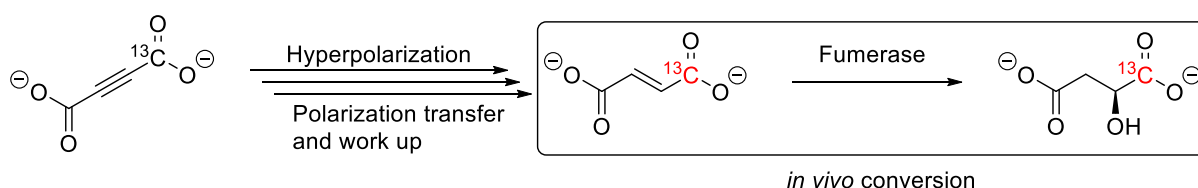
Figure 11 Hyperpolarization process generating 1-13C-fumerate from 1-13C-acetylenedicarboxylate. Subsequently the in vivo conversion from fumarate to malate was observed.

For other biologically relevant metabolites such as pyruvic acid or small amino acids like L-alanine, it is not possible to generate the molecule of interest by simple hydrogenation of an unsaturated carbon-carbon bond. An alternative way to access these molecules is the so-called PHIP side arm hydrogenation (SAH) approach.[77-92] The method describes the introduction of an unsaturated bond via the addition of a side arm acting as the hyperpolarization site. The simplest possible side arm, in terms of atom count and resulting AAX spin system is the vinyl ester, in particular the vinyl-d_3. To make use of SAH, the unsaturated bond has to be placed in proximity to the biologically active moiety of the molecule coupling to the added protons enabling the observation of changes in the chemical shifts of the hyperpolarized atoms. The coupling of the pH$_2$ protons to a heteronucleus like ^{13}C or ^{15}N even across functional groups allows the use of hyperpolarization transfer techniques to generate a high spin order in the molecule of interest (MOI).[77, 78, 93, 94] After

the successful completion of the hydrogenation and polarization transfer is completed successfully the side arm has to be removed to enable the molecules' biological activity.[81, 82, 95] Beside high polarization values long trackabilities of the MOIs are very important to follow biological processes.[96] The relaxation of the observed nucleus needs to be long enough to perform a) the hyperpolarization experiment, b) the purification, c) the release of the metabolite plus the transfer of it into an isotonic aqueous solution, d) the subsequent injection and e) the observation of the biochemical conversions. Since no automated polarizer is commercially available yet, the procedure needs to be well-choreographed to succeed in using these molecules as possible contrast agents.

A very critical part of the PHIP SAH approach is the cleavage of the side arm, which has to be performed fast and to full conversion. Usually, a basic cleavage solution is used to remove the unwanted side arm within a few tens of seconds with a subsequent pH adjustment. To generate a biologically compatible injection solution, the remaining hyperpolarization catalyst has to be removed for example by filtration.[82, 87, 88, 97] All these work up steps require a long half-life of the polarization. A very important way to increase the T_1 and thus reduce escape routes for the polarization is to chemically exchange coupling protons with deuterium atoms.[98, 99] In comparison to protons, deuterium as a quadrupolar nucleus owns a more than 6 times smaller gyromagnetic ratio reducing its interaction with ^{13}C or ^{15}N. Thus, longer T_1 values are commonly seen for many small metabolites like 1-^{13}C-lactate, 1-^{13}C-alanine or 1-^{13}C-glycine. All molecules increased their T_1 values by more than 10%.[99] Notably, deuteration of the hyperpolarization site also leads to 10 times longer T_1 (for vinylated metabolites) resulting in much higher polarization values (vinyl-pyruvate: 6%[90] vinyl-1-^{13}C-pyruvate-d_6: 59%[81]). In general, the synthesis of a good precursor for PHIP SAH must therefore consider the following points:

- Biological relevance of the metabolite
- High polarization values on the target molecule
- Removability of the side arm
- Removability of all toxic components
- Long traceability which may require deuteration

Since the development of PHIP SAH a lot of different molecules have been synthesized to allow for highly polarized pyruvate which is likely to be a suitable contrast agent for a large variety of MRI studies due to its central role in the metabolism.[26, 28, 100] Since many cancer types display an altered pyruvate metabolism, hyperpolarized pyruvate could serve as an endogenous molecule to

image tumors with high accuracy. However, working with pyruvate, itself creates certain challenges. The oxygen, moisture and most probably light-sensitive molecule can undergo many intra- and intermolecular modifications such as dimerization, hydration or cyclization.[101-104] In the biological context it is very useful for the organism to have such a flexible and fast reacting molecule as a branching point of many metabolic pathways, whereas a chemist has to find mild reaction conditions to generate PHIP SAH ready pyruvate esters.
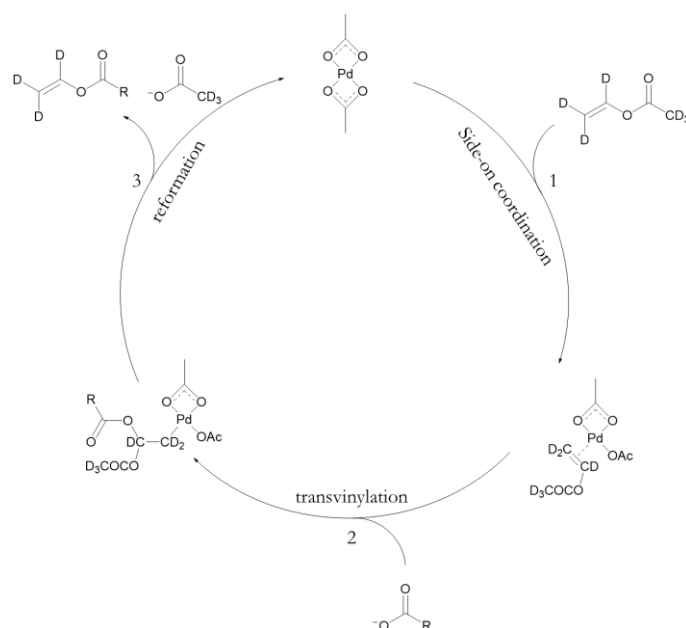
Scheme 2 Proposed mechanism of the transvinylation using palladium acetate. By side-on coordination of vinyl acetate-d_6 a π-complex is formed (1). Through a rearrangement a σ-complex is formed resulting in the nucleophilic attack of a free carboxylate (2). The decomposition of the σ-complex (3) results in the catalyst regeneration and release of the final products.[105]

Most vinylation methods with other substrates are based on the catalytic transvinylation of an access of vinyl acetate, a catalyst (usually palladium-based catalysts are preferred) and a hydroxide together with the to-be-vinylated carboxylic acid.[106, 107] For pyruvate however, the yields of the reaction are very low and for deuterated compounds very expensive due to the needed vinyl-acetate-d_6 (Scheme 2 Figure 12).

Recently, two successful syntheses of vinyl-1-^{13}C-pyruvate-d_6 were published, both have found alternative ways to generate the ester, however with relatively low yields[81] or with not fully characterized side products[83], compared to other ways to excess well polarized 1-^{13}C-pyruvate-d_3, (alternative precursors shown in Figure 12). Nevertheless, hyperpolarization of the vinyl ester led to the highest ^{13}C polarization measured in aqueous solutions of 1-^{13}C-pyruvate-d_3. The difficulty of synthesizing vinyl pyruvate today shows that further options for the preparation of hyperpolarized pyruvate still need to be identified in form of new side arms. One factor in the

work-up of the hyperpolarized material that costs time and thus polarization is the basic cleavage of the side arm. At present, there are no side arms that can be removed without the use of additional chemicals.

The first in vivo studies of 1-^{13}C-pyruvate were performed by Cavallari et. al. in 2018 using a propargyl pyruvate ester with a ready-to-inject ^{13}C polarization of up to 4%.[97] However, the image quality lacked in resolution resulting the localization of 1-^{13}C-lactate and 1-^{13}C-pyruvate to surpass the physical borders of the mouse itself. In 2022 Hune et al. were able to obtain metabolic tumor images of mice diseased with a human melanoma. In their study, 1-^{13}C-pyruvate-d_3 generated through the hyperpolarization of vinyl-1-^{13}C-pyruvate-d_6 with an injection polarization of 12% was used to image metabolic conversions and localize the tumor of the mice.[12] Due to their high polarization, conversions to 1-^{13}C-lactate-d_3 and 1-^{13}C-alanine-d_3 and their kinetics were described. Comparing these results with the initial data derived from dDNP (see Chapter 1.3.1) a PHIP-based approach was able to yield comparable data, which could enable clinical studies in the future.
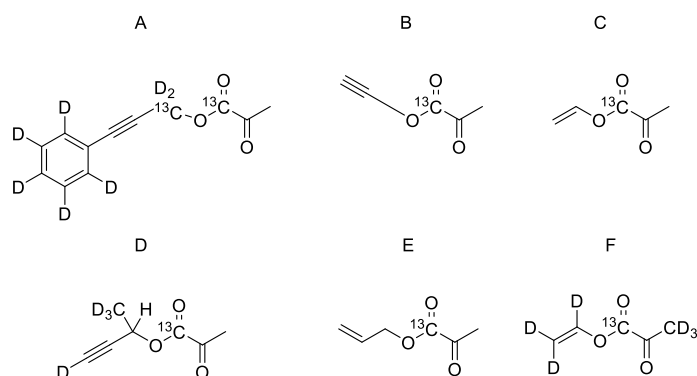
Figure 12 Commonly used 1-^{13}C-Pyruvate PHIP SAH precursor molecules. A) 3-(phenyl-d5)prop-2-yn-1-yl-1-^{13}C-1,1-d_2-2-oxopropanoate-1-^{13}C[82], B) prop-2-yn-1-yl 2-oxopropanoate-1-^{13}C[78], C) vinyl 2-oxopropanoate-1-^{13}C[108], D) but-3-yn-2-yl-1,1,1,4-d_4-2-oxopropanoate-1-^{13}C, E) allyl 2-oxopropanoate-1-^{13}C[90] F) vinyl-d3 2-oxopropanoate-1-^{13}C-d_3[81, 83]

Not only metabolic processes are investigated by PHIP. In the early 2000s, extensive investigations of ^{13}C-labeled, hyperpolarized hydroxyethyl propionate as contrast agents for angiography were performed.[109] High polarization values of 25% directly on ^{13}C immediately after the hyperpolarization (injection values not known) even allowed the in vivo investigation of higher mammals. The in-plane resolution of 0.6 mm^2 gave the opportunity to investigate in detail the perfusion and the cardiovascular system. However, the molecule used was not approved for human studies due to its high toxicity.[109] Further experiments were performed with hyperpolarized water (by DNP, but not PHIP), but due to the short T_1 of the H_2O protons the polarization decays

relatively fast (within seconds).[52, 110, 111] Molecules that have little to no metabolic activity and thus are considered metabolic end products are particularly suitable for observing perfusion. A simple metabolic end product is acetylated amino acids from protein degradation, which are transported from the cells into the bloodstream and then excreted via the kidneys.[112, 113] N-acetyl-alanine in particular is a good starting point from the perspective of precursor synthesis. Alanine and its derivatives have already been successfully hyperpolarized, so this is a promising molecule for angiography.[84, 114]

1.3.3.3 NMR pulse sequences for heteronuclear polarization transfer

The experiments presented in this work were performed under PASADENA conditions. The following chapter therefore assumes that the symmetry breaking of pH_2 is performed in high magnetic fields with fully enriched pH_2.

For the transfer from the protons to a heteronucleus, a spin system must be formed between the two hydrogen atoms and another NMR-active nucleus. Thus, polarization can be transferred even across functional groups as long as the coupling between nuclei is measurable. In the (bio-) chemical analysis of structures, be it small molecules or proteins, polarization transfer pulse sequences have been used as standard analysis methods.[115-117] Heteronuclear multiple bond correlation (HMBC)[118] and insensitive nuclei enhanced by polarization transfer (INEPT)[119] NMR pulse sequences are used to study chemical structures and to transfer the higher natural polarization of protons to nuclei with a lower gyromagnetic ratio such as ^{13}C or ^{15}N. Both methods exploit the J coupling between the nuclei, while other polarization transfer methods based on the Nuclear Overhauser Effect (NOE, not further discussed in this work) rely on cross-relaxation through space.[120]

In order to understand how the spins are manipulated in the used pulse sequence allowing to hyperpolarize the heteronuclei of interest, it is helpful to first review the underlying INEPT sequence. An INEPT experiment derives its signal amplification from two factors:

1) The larger gyromagnetic ratio of the protons compared to ^{13}C and ^{15}N.

2) The faster relaxation of the nuclei with larger gyromagnetic ratios, as this allows the experiment to be repeated more often.

In terms of the INEPT both factors aim to drastically shorten the measurement time of heteronuclear experiments. The pulse sequence itself is based on a combination of a spin echo, the refocusing of spin magnetization and a selective population inversion (SPI). In a spin echo part, a 90° pulse is used on the proton channel to align the magnetization perpendicular to the direction of the magnetic field (± y axis) causing the spins to rotate (i. e. de-phase) at different speeds. After a time t these are fanned out by the irradiation of a 180° pulse (i.e. the inversion of the spins), after a further time t the spins have converged again (i. e. re-phase). The SPI part is performed by simultaneous irradiation of a 180° pulse on S while the 180° of the echo is applied on I. After a further time t another 90° pulse is applied on both channels I and S, which leads to the polarization transfer. During this pulse, the polarization is rotated on the z-axis resulting in the evolution of an antiphase alignment of the magnetization along the same axis. Subsequently, acquisition can be performed on the channel of the more insensitive nucleus, which is directly attached to the proton (Figure 13).
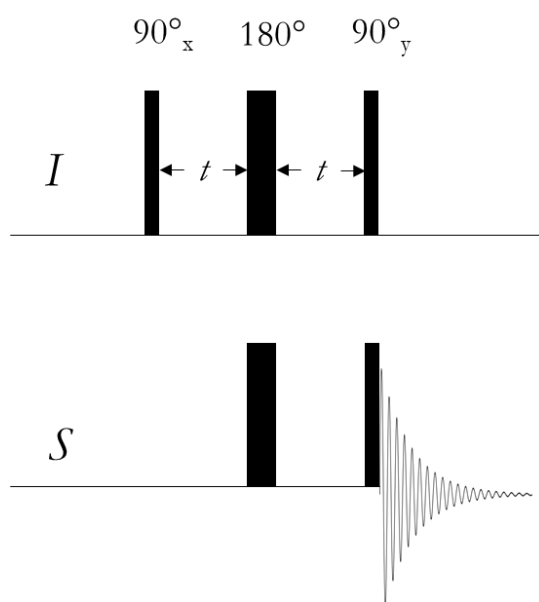
Figure 13 Graphical representation of the INEPT NMR experiment with the dimension I as the sensitive and S as the insensitive nuclei. The thin and large rectangles represent 90° pulses whereas the bolt rectangles represent 180° pulses with their subscripts indicating the phase.

To apply the principle of polarization transfer from the INEPT sequence onto a hyperpolarized ester, Korchak et al. developed the so-called ESOTHERIC (efficient spin order transfer to heteronuclei via relayed INEPT chains) pulsed NMR sequence.[79] For the sequence a three-spin system AAX is at least necessary. Beyond, a variant to transfer the polarization from X to X´, a second heteronucleus coupling to the system, is described. As the hydration was performed under PASADENA conditions, the initial spin order $I_z^1 I_z^2$ was manipulated into the antiphase

magnetization $I_z^1 + S_z^3$ with S as heteronuclear ^{13}C spin. In case of the detection of the polarization on X an INEPT block converts the antiphase magnetization to the ^{13}C$_3$ (Figure 14). The J coupling of the respective nuclei for the formation of coherence is decisive for the delays between the pulses, denoted by Δ in the INEPT sequence, and must be adjusted for optimal transfer to the target atom (with respect to the J coupling) depending on the molecule used. As it is chemically challenging to introduce a vinyl group onto every MOI, the variant to transfer polarization from X to X´ uses another INEPT chain (from ^{13}C$_3$ to ^{13}C$_4$). The first heteronucleus (^{13}C$_3$) here sits on the side arm (see Figure 12 molecule a).

The figure shows the following density operators:

0: $\rho = I_{1z}I_{2z}$
1: $\rho = I_{1x}I_{2x}$
2: $\rho = 2I_{1y}I_{2x}I_{3z}$
3: $\rho = I_{1y}I_{2z}I_{3z}$
4: $\rho = -I_{1x}I_{3z}$
5: $\rho = I_{1z}I_{3x}$
6: $\rho = I_{3y}/2$

Pulse sequence labels: $90°_y$, $180°$, $90°_{-y}$, 180, $90°_y$, $180°$ on ^{1}H and ^{13}C channels.

Delays: $\Delta_A = 1/(2J_{13})$, $\Delta_B = 1/(2J_{13})$, $\Delta_{c_1} = 1/(2J_{13})$
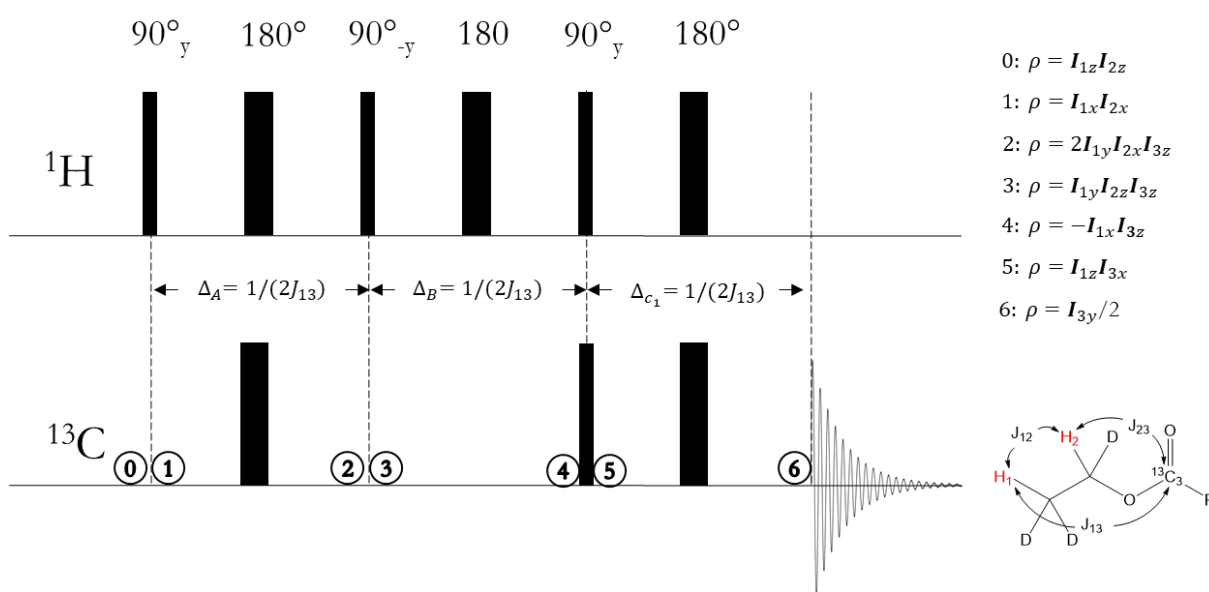
Figure 14 NMR pulse sequence for the transfer of spin order from protons onto heteronuclei in a three-spin system (ESOTHERIC). The thin and large rectangles represent 90° pulses whereas the bolt rectangles represent 180° pulses with their subscripts indicating the phase. The vertical dashed lines indicate the separation of logical blocks within the sequence. The circled numbers and their description on the right describe the density operators of the spins at the certain position.

Based on this pulse sequence (Figure 14), two modifications are important for this work. For the hyperpolarization of amino acids Kaltschnee et al. used an adapted variant with selective C-3 methyl group decoupling (see chapter 3.3.2, Figure 22).[84] For this purpose, a refocusing block with a selective pulse was used for effective decoupling. In 2021, Dagys et al. used a proton relayed approach for non-vinyl side arms to replace the previously used ^{13}C on the side arm as a four-spin system (Figure 15).[86] With this variant, an increased accessibility of new side arm variants was given. The sequence is composed of three consecutive INEPT blocks transferring the polarization to the relay proton H^3 adapting the delays between the pulses to the respective couplings of the protons. To transfer the polarization onto the ^{13}C an adapted INEPT block was used, as proton-

carbon coupling is often in the same regime as $J_{H^1H^3}$. Thus, a delay was calculated by numerical simulation of the spin system to take the scalar coupling into account, while still hyperpolarizing the heteronucleus. Since the transfer to the ^{13}C of the MOI is highly dependent on the efficient transfer to the relay proton, a partial sequence can be used to generate a pure in-phase spectrum of the hyperpolarized H^3.
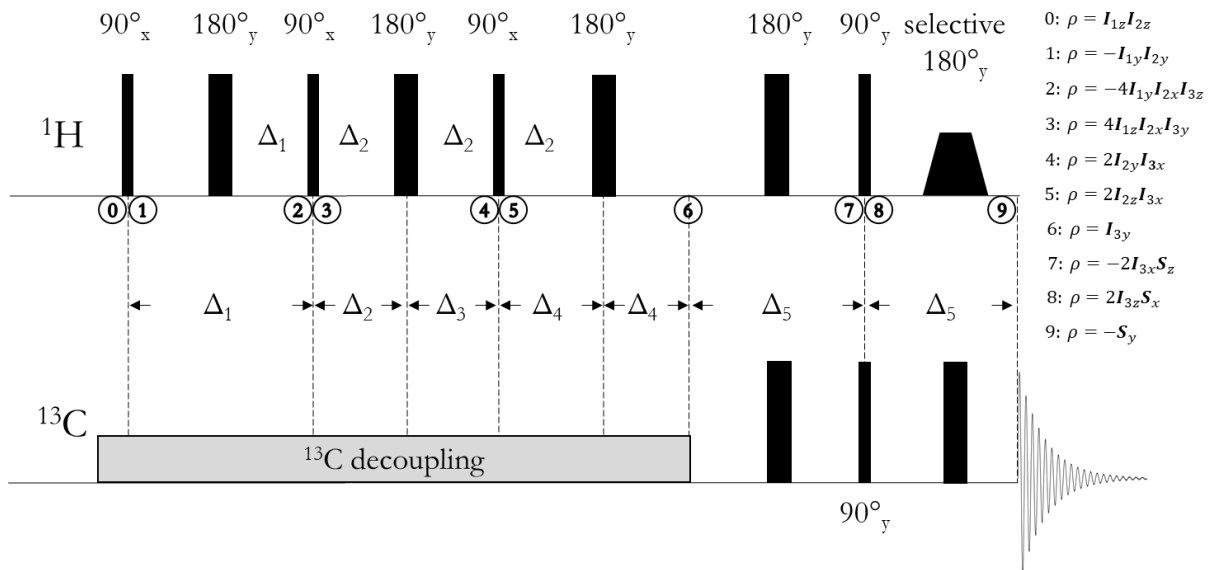

Figure 15 NMR pulse sequence for the transfer of the spin order from protons onto heteronuclei in a four-spin system (Relay-ESOTHERIC). The thin and large rectangles represent 90° pulses whereas the bolt rectangles represent 180° pulses with their subscripts indicating the phase. The vertical dashed lines indicate the separation of logical blocks within the sequence. The circled numbers and their description on the right describe the density operators of the spins at the certain position.

1.4 Aim of the work

The goal of this work was to synthesize precursors to release hyperpolarized endogenous molecules that provide polarization levels enabling the investigation of cellular models and implementation preclinical imaging studies with high polarization and long traceability. This includes, on the one hand, the necessary design of novel side arms for hyperpolarization by means of parahydrogen for molecules that cannot be produced through the hydrogenation of an internal double bond. On the other hand, it also includes the development of effective proton deuterium exchange reactions on isotopically enriched substances as well as the linkage of the contrast agents to the corresponding side arm.

Deuteration at the side arm as well as at the target molecule itself is necessary to eliminate relaxation pathways for polarization, allowing longer observation times by extending the relaxation time T_1. Especially for the isotopically enriched contrast molecules it is particularly important to elaborate clean and efficient deuteration procedures. These often very small molecules are usually very difficult to purify and are used directly after the deuteration for further reactions. Here, focus was the avoidance of by-products, as these lead to lower conversions when linked to the side arm.

For the synthesis of the side arms special attention was paid on providing a novel way to release the metabolites. To this end, cleavage agents such as bases have to be dispensed and novel release mechanisms were employed to shorten the purification process. The longer the time between the hydrogenation reaction and the addition of the hyperpolarized material to the biological organism (cells or animals), the more polarization is lost. By reducing the steps needed to extract the polarized compound, more polarization can be maintained. This could also eliminate possible sources for errors (e. g. incorrect dosing of the base, wrong pH value, etc.) and thus ensure a more stable process to the hyperpolarized compound. To achieve these objectives, modifications were made to the light-sensitive 2-nitrobenzyl moiety, which is known to be used as a light-sensitive protecting group for alcohols and carboxylic acids. By introducing a C-C triple bond as well as its terminal deuteration, high degrees of polarization were reached. The introduced polarization can be transferred to the desired heteronucleus of the target molecule using appropriate pulse sequences such as the proton relayed ESOTHERIC version.

In order to broaden the spectrum of possible MRI applications, an amino acid based biocompatible contrast agent was aimed to be established. Using a deuterated vinyl group as a side arm and specific deuteration of certain sites in the target molecule ensured long traceability and high polarization values. These findings may contribute to place parahydrogen-based hyperpolarization methods in

clinical applications that offer new diagnostic pathways and information to improve imaging dependent medical care.

2 Material and Methods

2.1 General material and methods

In the following section the used chemicals, solvents and consumables are listed. All chemicals and solvents were used without any further purification directly from the bottle (expect otherwise mentioned). Chemicals and solvents stored under inert conditions were transferred under Schlenk conditions using nitrogen as inert atmosphere. The used glassware was cleaned in an acid (2-6 M HCl in H_2O solution) and base (saturated KOH pallets in 2-isopropanol) bath, rinsed with deionized water and dried in an oven. All reactions were carried out under inert conditions with nitrogen as atmospheric gas in flame-dried round bottom flasks equipped with polytetrafluoroethylene (PTFE) coated magnetic stirring bars. If required, due to light sensitivity, all reactions were carried out in brown round bottom glass ware. If not otherwise stated all reactions were performed at 25 °C referred as room temperature. Thin layer chromatography (TLC) was performed under standardized conditions. The (crude) product was applied as a small spot on Macherey-Nagel TLC SIL G UV254 silica-on-glass TLC plates 1 cm above the lower edge. The prepared plates were developed for 6 min in closed chambers containing 5-6 mL solvent mixture. Visualization of the isolated products was performed under UV light ($\lambda = 254$ nm), by I_2 in silica, by phosphomolybdic acid (10 g of the acid in 100 mL EtOH), or by potassium permanganate (1.5 g $KMnO_4$, 10 g K_2CO_3, 100 mg NaOH dissolved in 200 mL H_2O) staining solutions.

If not otherwise stated synthesized compounds were purified with an INTERCHIM puriFlash® XS520Plus system with a UV-Vis detector and the corresponding software InterSoft X with Genius mode which automatically calculate a solvent gradient according to the generated TLC data of the impure compound mixture. The crude mixture was loaded on Celite 503 (2 g of celite for 1 g of crude compound) stuffed into pruiFlash® Dry load Flash column (PF-DLE-F0012). Purification itself was performed using prepacked puriFlash® Silica HP Flash column (PF-30SIHP) in different sizes (F0012, F0020, F0040, F0120) depending on the weight of the crude material.

Concentration in vacuo was performed using an IKA® RV 8 rotary evaporator connected to a VACUUBRAND® MZ 2C membrane pump equipped with a pressure regulator.

The used chemicals and solvents are listed in alphabetical order (Table 1):

Material and Methods

Table 1 Chemicals, their abbreviation or formula and their supplier which were used for this work.

Chemical	Abbreviation /chemical formula	Supplier
[1,4-Bis(diphenylphoshino)butane](1,5-cyclooctadiene)rhodium(I) tetrafluoroborate		Sigma Aldrich
1,1-^{13}C-acetic anhydride-d$_6$	Ac2O-1,1-^{13}C-d$_6$	Sigma Aldrich
1-^{13}C-L-alanine	1-^{13}C-ala	Sigma Aldrich
1-^{13}C-pyurvic acid		Sigma Aldrich
1-^{13}C-sodium pyruvate		Sigma Aldrich
1-Ethyl-3-(3-dimethylaminopropyl)carbodiimide-hydrochloride	EDC HCl	PEPTIPURE
2-Nitrobenzaldehyde	2-NBn	Sigma Aldrich
4,5-Dimethoxy-2-Nitrobenzaldehyde	2-NV	Sigma Aldrich
4-Dimehtylaminopyridine	DMAP	Carl Roth®
Acetic anhydride	Ac$_2$O	Sigma Aldrich
Acetic anhydride-d$_6$	Ac$_2$O-d$_6$	Sigma Aldrich
Acetone		Honeywell Riedel-de Haen
Acetone-d$_6$		VWR Chemicals
Ammonia in H$_2$O 25%	NH$_4$OH in H$_2$O	Sigma Aldrich
Ammonium chloride	NH$_4$Cl	Thermo Scientific
Celite 503		Macherey-Nagel
Chloroform-d	CDCl$_3$	Sigma Aldrich
Deuterium chloride 38% in D2O	DCl in D$_2$O	Carl Roth®
Deuterium oxide	D$_2$O	Sigma Aldrich
Dichloromethane	DCM	Honeywell Riedel-de Haen
Diethyl ether	Et$_2$O	Honeywell Riedel-de Haen
Dowex X-8		Sigma Aldrich
Ethyl acetate	EtOAc	Honeywell Riedel-de Haen
Ethynyl magnesium bromide solution 0.5 M in THF		Sigma Aldrich
L-alanine	L-ala	Sigma Aldrich
Methane sulfonyl chloride	MsCl	Sigma Aldrich
Methanol	MeOH	Thermo Scientific
Palladium acetate	Pd(OAc)$_2$	Sigma Aldrich
Petroleum ether	PE	Honeywell Riedel-de Haen
Potassium hydroxide	KOH	Merck
Pyridine		Sigma Aldrich
Pyruvic acid	Pyr	Sigma Aldrich
Ruthenium on carbon	Ru/C	Sigma Aldrich
Sodium bicarbonate	NaHCO$_3$	Merck

Sodium carbonate	Na_2CO_3	Merck
Sodium chloride	NaCl	Carl Roth®
Sodium hydroxide	NaOH	Sigma Aldrich
Sodium sulphate	Na_2SO_4	Thermo Scientific
Sulfuric acid-d_2 98% in D2O	D_2SO_4	Sigma Aldrich
Tetrahydrofuran	THF	Honeywell Riedel-de Haen
Triethylamine	Et_3N	Sigma Aldrich
Vinyl acetate		Sigma Aldrich
Vinyl acetate-d_6		CDN ISOTOPES
Vinyl magnesium bromide solution 1 M in THF		Sigma Aldrich

2.2 NMR experiments

All analytical NMR spectra were recorded on a BRUKER® AVANCE III HD operating a BRUKER® ULTRASHIELD™ 300 7 T magnet or on a BRUKER® AVANCE NEO operating a BRUKER® ASCEND™ 300 WB 300 7 T magnet. Typically, for all compounds synthesized ^1H spectra (300 MHz) were recorded. For relevant compounds ^2H (300 MHz) and ^{13}C spectra (75 MHz) were measured. If not otherwise stated, ^{13}C spectra where recorded while decoupling protons during the acquisition (inverse gated decoupling (zgig), quantitative analysis) or during the whole experiment (power gated decoupling, (zgpg), maximal signal intensity). For deuterated compounds a double decoupled (proton and deuterium) ^{13}C spectra were recorded to massively decrease measurement time. The analytes were dissolved in deuterated solvents (Acetone-d_6, $CDCl_3$ or D_2O) and transferred to WILMAD® 5 mm high throughput NMR tubes. The ^1H NMR shifts (δ) were calculated relative to tetramethyl silane (TMS; δ = 0.0 ppm) and the respective solvent (Acetone-d_6: δ = 2.20 ppm, Chloroform-d: 7.26 ppm, D_2O: δ = 4.81 ppm for ^1H; Acetone-d_6: δ = 206.26 ppm, Chloroform-d: 79.19 ppm) and expressed in ppm. Spin multiplicities of the protons were reported as s (singlet), d (doublet), t (triplet), q (quartet), qu (quintet) m (multiplet) and br (broad singlet) and the coupling constants were reported in Hz.

2.3 Analysis of deuteration reactions

^1H, ^2H and ^{13}C (zgig experiments for more precise integration) NMR spectra were measured to analyze deuteration reactions. The integrals of the to be replaced protons were related to each other before and after the reaction (see equation 14).

$$100 - \left(100 * \frac{I_{After}}{I_{Before}}\right) = Deuteration \ [\%] \qquad\qquad 14$$

In this case, the NMR experiments must be performed under the same conditions (number of scans, receiver gain, temperature, concentration, sample volume). For the deuteration of mixtures (e. g. pyruvic acid and pyruvate hydrate), the sum of the integrals of the to be replaced protons was set in relation to each other before and after the reaction. Since it cannot be assumed that the concentration of the substances of a mixture is the same before and after the reaction and the reaction velocity of the respective possible deuteration is the same, the ratio of similar carbon atoms (e. g. carboxylic acids in similar chemical environment) was included. Deuterium NMR spectra were used purely as a positive control since the line width leads to strong overlaps of the signals of chemically similar substances.

2.4 Analysis of hyperpolarization experiments

The thermal polarization of nuclei with a spin of $\frac{1}{2}$ can be described using their gyromagnetic ratio γ, the applied magnetic field B_0, the temperature T, along with the constants h and k_B in equation 15:

$$P_{th} = \tanh\left(\frac{h - \gamma B_0}{2 k_B T}\right) \qquad\qquad 15$$

The hyperpolarized signal was integrated in the appropriate region (for example, 1-^{13}C acetate at about 162 ppm) and expressed as H_{hyp}. The thermal signal was measured from experiments before (for ^{1}H polarizations) or after (^{13}C polarizations) the hyperpolarization experiment. The hyperpolarization is calculated from the ratio between the integrals of the hyperpolarized and the thermal signal as well as the receiver gain rg, the number of scans ns and the flip angle θ of the respective experiments(see equation 16).

$$P_{hyp} = \frac{I_{hyp}}{I_{th}} \cdot \frac{ns_{th}}{ns_{hyp}} \cdot \frac{\sin(\theta_{th})}{\sin(\theta_{hyp})} \cdot P_{th} \qquad\qquad 16$$

The hyperpolarization experiments which were performed to release the metabolites were carried out in 200 μL of the appropriate solvent. After the transfer of polarization to the heteronucleus, the NMR tube was taken out of the magnet, the polarization setup was unscrewed and the aqueous solution was added. Depending on the molecule, cleavage of the esters was accomplished using isotonic aqueous solutions containing 150 mM NaCl concentration.

2.5 Design and execution of the hyperpolarization experiments

Parahydrogen was produced in a pH$_2$ generator at 20 K using a Sumitomo Heavy Industries HC-4A He compressor connected to a ColdEdge Technologies reaction chamber controlled by a Lake Shore Cryotronics, Inc. temperature regulator.

Parahydrogenation experiments were performed using a home-built valve and tubing system controlled by the NMR console (Figure 16). The samples containing the analyte in a desired concentration together with the catalyst ((1,5-cyclooctadiene)rhodium(I) tetrafluoroborate) in acetone-d$_6$ were degassed by bubbling N$_2$ gas for one minute through the solution. The hydrogenation was performed by bubbling parahydrogen at 8 bar for a sample optimized time through the solution inside the probe head of the 7 T magnets. The ^{1}H spin order added to the molecule of interest and transferred to the desired atom as described in chapter 1.3.3.3.
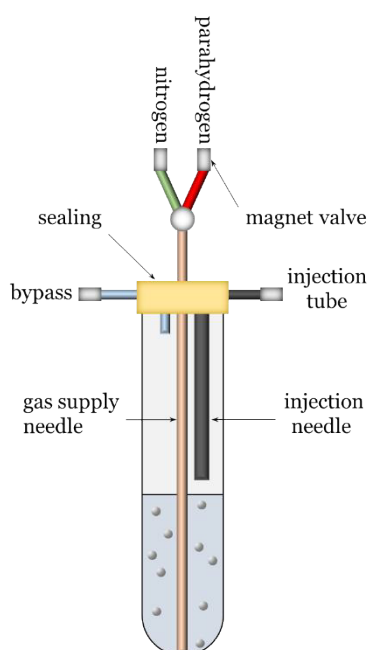
Figure 16 Home-built valve and tubing system. From left to right: light blue bypass; green nitrogen; red parahydrogen; black injection tube. A needle combining the gas supply reaching to the bottom of the 5 mm NMR tube as well as a bypass for pressure release and an injection line are passed the sealing.

2.6 Optical rotation measurements

Optical rotation was determined on a Jasco P-2000 polarimeter. The polarimeter was operated with a Na lamp of wavelength λ = 589 nm. To determine the rotation, five cycles were measured with cycle intervals of 10 s between each measurement. The average was determined from the measurements and compared to reference values and literature. The samples were prepared freshly and in concentrations according to the literature.

2.7 Experimental section

In the following chapter the procedures to synthesize the in this work used chemicals are described including the corresponding analytical data. The respective spectra can be found in the Appendix.

2.7.1   2-oxopropanoicd₃ acid

1
$C_3HD_3O_3$
91.07 g/mol
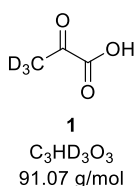
Sodium pyruvate (100 mg, 0.909 mmol, 1 eq.) was dissolved in a 1:1 mixture of THF and D_2O (total volume 1 mL) at 0 °C. Triethyl amine (92 mg, 127 µL, 0.909 mmol, 1 eq.) was added in a dropwise fashion. After 16 h, the reaction was terminated by the addition of solid NaCl (150 mg). The aqueous phase was extracted 20 times with Et_2O (each 2 mL). The combined organic fractions were dried over Na_2SO_4 and concentrated under reduced pressure. The pure acid 1 was found as a clear liquid (D%: 99%, 41 % yield).

^{2}H NMR (46 MHz, D_2O) δ = 2.5 (s, 3 D) ppm.

^{13}C NMR (75 MHz, D_2O) δ = 203.4 (CD_3-CO-COOH) 170.2 (CD_3-CO-COOH), 25.6 (CD_3-CO-COOH) ppm.

2.7.2 2-oxopropanoic-1-^{13}C-d$_3$ acid
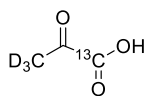
2

C$_2$^{13}CHD$_3$O$_3$

92.07 g/mol

Procedure a:

Sodium pyruvate-1-^{13}C (1 g, 9 mmol, 1eq.) was solved in 9 mL D$_2$O in three neck round bottom flask equipped with a condenser. After cooling the solution to 0 °C D$_2$SO$_4$ (98% in D$_2$O; 0.406 g, 4.053 mmol, 0.218 mL, 0.45 eq.) was added dropwise to the stirring solution. After full addition the reaction was warmed for 5 h to reflux. The deuteration was monitored by NMR. If by that time the pyruvic acid was not fully deuterated another 0.108 mL D$_2$SO$_4$ (98% in D$_2$O; 0.203 g, 2.026 mmol, 0.23 eq.) were added and the reaction was warmed to reflux for another 2 h. After cooling the solution to room temperature 0.75 g solid NaCl was added (fully dissolved by shaking) and the aqueous phase was extracted with Et$_2$O (20 times 3 mL). The combined organic layers were dried over Na$_2$SO$_4$, filtered and concentrated in vacuo (rotary evaporator with a cooling bath temperature of 30 °C). The deuterated acid was found as a pale-yellow oil (yield: 60%, impurity: Et$_2$O).

Procedure b:

1-^{13}C-pyruvic acid (1 g, 11.23 mmol, 1 eq.) was solved in 9 mL D$_2$O. After cooling the solution to 0 °C, NaHCO$_3$ was added in small portions over 45 min (to avoid strong bubbling). The reaction was allowed to warm to room temperature and stirred for 16 h. After this time the pH was adjusted to pH=2 to deuterate the carboxylic acid with 38% DCl in D$_2$O. 0.85 g solid NaCl was added to the solution (fully dissolved by shaking) and the aqueous phase was extracted with Et$_2$O (20 times 3 mL). The combined organic layers were dried over Na$_2$SO$_4$, filtered and concentrated in vacuo (rotary evaporator with a cooling bath temperature of 30 °C).

Procedure c:

Sodium 1-^{13}C-pyruvate (100 mg, 0.901 mmol, 1 eq.) was dissolved in a 1:1 mixture of THF and D$_2$O (total volume 1 mL) at 0 °C. Triethyl amine (91 mg, 126 µL, 0.901 mmol, 1 eq.) was added in a dropwise fashion. After 16 h, the reaction was terminated by the addition of solid NaCl (150 mg). The aqueous phase was extracted 20 times with Et$_2$O (each 2 mL). The combined organic fractions

were dried over Na_2SO_4 and concentrated under reduced pressure. The pure acid 1 was found as a clear liquid (D%: 99%, 40 % yield).

^{2}H NMR (46 MHz, D_2O) δ = 2.5 (s, 3 D) ppm.

^{13}C NMR (75 MHz, D_2O) δ = 203.4 (CD_3-CO-COOH) 170.2 (CD_3-CO-COOH), 25.6 (CD_3-CO-COOH) ppm.

2.7.3   3-benzoyloxy-4-methoxybenzaldehyde
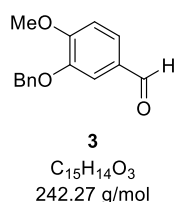
3
$C_{15}H_{14}O_3$
242.27 g/mol

Vanillin (1 g, 6.572 mmol, 1 eq.), benzyl bromide (1.124 g, 6.572 mmol, 1 eq.), potassium carbonate (0.908 g, 6.572 mmol, 1 eq.) and acetonitrile (25.78 mL) were added together in a round bottom flask. The reaction mixture was warmed to reflux for 24 h. After reaction completion, the solvent was evaporated under reduced pressure before taking the resulting residue up with water (25 mL) and dichloromethane (25 mL). The organic layer was dried over Na_2SO_4 and filtered before concentrating the product under reduced pressure. The pure ether 3 was found as a white powder (yield: 99%).

^{1}H NMR (300 MHz, $CDCl_3$) δ = 9.84 (s, 1 H, -CHO), 7.40 (m, 7 H, Ar), 7.02 (d, J = 8.1 Hz, 1H, Ar), 5.27 (s, 2 H, Ar-CH_2-O-Bn), 3.98 (s, 3 H, -OMe), 1.58 ppm.

^{13}C NMR (75 MHz, $CDCl_3$) δ = 190.91 (-CHO), 153.62 (Ar-CH_2-O-Bn), 150.10 (Me-O-Bn), 136.03 (Ar), 130.32 (Ar), 128.74 (Ar), 128.22(Ar), 127.21 (Ar), 126.59 (Ar), 112.42 (Ar), 109.38 (Ar), 70.89 (Ar-CH_2-OBn), 56.08 (Me) ppm.

2.7.4   3-methoxy-4-benzyloxybenzaldehyde
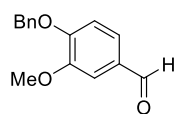
4
$C_{15}H_{14}O_3$
242.27 g/mol

Isovanillin (1 g, 6.572 mmol, 1 eq.), benzyl bromide (1.124 g, 6.572 mmol, 1 eq.), potassium carbonate (0.908 g, 6.572 mmol, 1 eq.) and acetonitrile (24.78 mL) were added together in a round bottom flask. The reaction mixture was warmed to reflux for 24 h. After reaction completion the solvent was evaporated under reduced pressure before taking the resulting residue up with water (25 mL) and dichloromethane (25 mL). The organic layer was dried over Na_2SO_4 and filtered before concentrating the product under reduced pressure. The pure ether 4 was found as a white powder (yield: 99%).

^{1}H NMR (300 MHz, CDCl$_3$) δ = 9.84 (s, 1 H, -CHO), 7.40 (m, 7 H, Ar), 7.04 (d, J = 8.1 Hz, 1H, Ar), 5.20 (s, 2 H, Ar-CH$_2$-O-Bn), 3.99 (s, 3 H, -OMe), 1.58 ppm.

^{13}C NMR (75 MHz, CDCl$_3$) δ = 190.92 (-CHO), 155.19 (Ar-CH$_2$-O-Bn), 148.84 (Me-O-Bn), 136.42 (Ar), 130.13 (Ar), 129.14 (Ar), 128.91 (Ar), 128.76 (Ar), 128.24 (Ar), 126.98 (Ar), 111.55 (Ar), 110.91 (Ar), 70.99 (Ar-CH$_2$-OBn), 56.31 (Me) ppm.

2.7.5   3-benzyloxy-4-methoxy-2-nitrobenzaldehyde
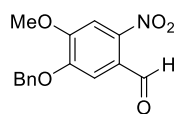
5
$C_{15}H_{13}NO_5$
287.27 g/mol

Fuming nitric acid (1 mL) was cooled to 0 °C in acetic acid (10 mL) before 3-benzoyloxy-4-methoxybenzaldehyde (0.26 g, 1.074 mmol) was added in small protions. After full addition reaction was stirred for 16 h at 0 °C before pouring the solution on ice. The crude is stirred for another 30 min before filtering the precipitate. The precipitate was washed with cold water (3 x 30 mL) and recrystallized form ethyl acetate. The aldehyde 5 was found as a pale-yellow powder (yield: 75%).

^{1}H NMR (300 MHz, CDCl$_3$) δ = 9.83 (s, 1 H, -CHO), 7.45 (m, 6 H, Ar), 7.00 (d, J = 8.15 Hz, 1H, Ar), 5.25 (s, 2 H, Ar-CH$_2$-O-Bn), 3.98 (s, 3 H, -OMe), 1.58 ppm.

^{13}C NMR (75 MHz, CDCl$_3$) δ = 190.95(-CHO), 153.63 (Ar-CH$_2$-O-Bn), 150.10 (Me-O-Bn), 140.73 (Bn-NO$_2$), 136.01 (Ar), 130.31 (Ar), 128.74 (Ar), 128.22 (Ar), 127.22 (Ar), 126.62 (Ar), 112.42 (Ar), 109.39 (Ar), 70.89 (Ar-CH$_2$-OBn), 56.08 (Me) ppm.

2.7.6   3-methoxy-4-benzyloxy-2-nitrobenzaldehyde
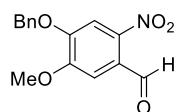
6
C$_{15}$H$_{13}$NO$_5$
287.27 g/mol

Fuming nitric acid (1 mL) was cooled to 0 °C in acetic acid (10 mL) before 3-methoxy-4-benzoyloxybenzaldehyde (0.26 g, 1.074 mmol) was added in small protions. After full addition reaction was stirred for 16 h at 0 °C before pouring the solution on ice. The crude is stirred for another 30 min before filtering the precipitate. The precipitate was washed with cold water (3 x 30 mL) and recrystallized form ethyl acetate. The aldehyde 6 was found as a pale-yellow powder (yield: 55%).

^{1}H NMR (300 MHz, CDCl$_3$) δ = 9.83 (s, 1 H, -CHO), 7.39 (m, 6 H, Ar), 6.99 (d, J = 8.75 Hz, 1H, Ar), 5.21 (s, 2 H, Ar-CH$_2$-O-Bn), 4.01 (s, 3 H, -OMe), 1.58 ppm

^{13}C NMR (75 MHz, CDCl$_3$) δ = 190.82 (-CHO), 153.57 (Ar-CH$_2$-O-Bn), 148.74 (Me-O-Bn), 136.79 (Bn-NO$_2$), 136.31 (Ar), 130.02 (Ar), 128.66 (Ar), 128.13 (Ar), 127.49 (Ar), 126.88 (Ar), 122.47 (Ar), 111.45 (Ar), 110.80 (Ar), 70.89(Ar-CH$_2$-OBn), 56.21 (Me) ppm.

2.7.7   1-(2-nitrophenyl)prop-2-yn-1-ol
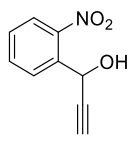
9
$C_9H_7NO_3$
177.16 g/mol

In a 250 mL two-neck flask, equipped with a dropping funnel 2-Nitrobenzaldehyde (5 g, 33.08 mmol, 1 eq.) was dissolved in dry THF (4 mL) and cooled to 0 °C in an ice bath. The ethynyl magnesium bromide 0.5 M in THF (99 mL of the solution containing 49.62 mmol ethynyl magnesium bromide, 1.5 eq.) was transferred to the dropping funnel and added to the stirring solution over 30 min. After full addition the reaction was allowed to warm to room temperature. The full conversion after 2 h was visualized by TLC (1:5 EtOAc PE) and the reaction was quenched with 50 mL of a saturated NH_4Cl in H_2O solution. The aqueous solution was extracted with EtOAc (three times 25 mL). The combined organic fractions were dried over Na_2SO_4, filtered and concentrated in vacuo and purified by column chromatography. After purification the pure alkyne 9 was found as a yellow powder (yield: 99%).

^{1}H NMR (300 MHz, CDCl$_3$) δ = 7.99 (dt, J = 1.15, 7.85 Hz, 2 H, BnH3&4), 7.70 (dt, J = 1.15, 7.85 Hz, 1 H, BnH2), 7.53 (dt, J = 1.15 7.85 Hz 1 H, BnH5), 6.03 (d, J = 2.15 , 1 H, Bn-CHOHR), 3.20 (br, 1 H, OH), 2.66 (d, J = 2.15 Hz, 1 H, Alkyne-H) ppm.

^{13}C NMR (75 MHz, CDCl$_3$) δ =147.80 (Ar), 138.84 (Ar), 133.90 (Ar), 129.54 (Ar), 129.45 (Ar), 125,16 (Ar), 81.7 (-C≡CH), 75.22 (-C≡CH), 60.99 (Bn-CHOHR) ppm.

2.7.8   1-(4,5-dimethoxy-2-nitrophenyl)pro-2-yn-1-ol
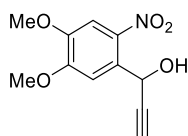
10
$C_{11}H_{11}NO_5$
237.21 g/mol

In a 250 mL two-neck flask, equipped with a dropping funnel 4,5-dimethoxy-2-Nitrobenzaldehyde (5 g, 23,678 mmol, 1 eq.) was dissolved in dry THF (3 mL) and cooled to 0 °C in an ice bath. The ethynyl magnesium bromide 0.5 M in THF (71 mL of the solution containing 35.516 mmol ethynyl magnesium bromide, 1.5 eq.) was transferred to the dropping funnel and added to the stirring

solution over 30 min. After full addition the reaction was allowed to warm to room temperature. The full conversion after 5 h was visualized by TLC (1:5 EtOAc PE) and the reaction was quenched with 50 mL of a saturated NH_4Cl in H_2O solution. The aqueous solution was extracted with EtOAc (three times 25 mL). The combined organic fractions were dried over Na_2SO_4, filtered and concentrated in vacuo and purified by column chromatography. After purification the pure alkyne 10 was found as a brown powder (yield: 99%).

^1H NMR (300 MHz, $CDCl_3$) δ = 7.66 (s, BnH, 1 H), 7.47 (s, BnH, 1 H), 6.12 (d, J = 2.3 Hz, BnCHOHR, 1 H), 4.05 (s, OMe, 3 H), 4.00 (s, OMe, 3 H), 2.66 (d, Alkyne-H, J = 2.3 Hz, 1 H) ppm.

^{13}C NMR (75 MHz, Acetone-d_6) δ = 156.80 (Ar), 137.62 (Ar), 129.75 (Ar), 129.24 (Ar), 128.15 (Ar), 125.05 (Ar), 80.8 (-C≡CH), 74.78 (-C≡CH), 60.49 (Bn-CHOHR), 56.1 (OMe) 56,02 (OMe) ppm.

2.7.9   1-(2-nitrophenyl)prop-2-yn-3-d-1-ol

11
$C_9H_6DNO_3$
178.17 g/mol
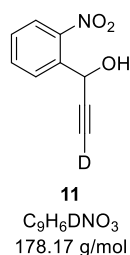
In a 10 mL round bottom flask 9 (0.5 g, 2.82 mmol, 1 eq.) was dissolved in a 1:1 mixture of D_2O and THF (each 2.5 mL) at 0 °C. Et_3N (0.628 g, 6.21 mmol, 0.865 mL, 2.2 eq.) was added dropwise to the vigorously stirring solution. After the addition the cooling bath was removed and the reaction allowed to warm to room temperature. After 16 h the aqueous phase was extracted with EtOAc (three times 10 mL The combined organic fractions were dried over Na_2SO_4, filtered and concentrated in vacuo and purified by column chromatography (1:5 EtOAc PE). The purified deuterated alkyne 11 was found as a pale-yellow powder (yield: 80%, deuteration degree: 95-99%).

^1H NMR (300 MHz, $CDCl_3$) δ = 8.00 (dt, J = 1.15, 7.85 Hz, 2 H, BnH3&4), 7.70 (dt, J = 1.15, 7.85 Hz, 1 H, BnH2), 7.53 (dt, J = 1.15 7.85 Hz 1 H, BnH5), 6.04 (s, 1 H, Bn-CHOHR), 3.20 (br, 1 H, OH) ppm.

^{13}C NMR (75 MHz, $CDCl_3$) δ =147.62 (Ar), 134.93 (Ar), 133.87 (Ar), 129.45 (Ar), 129.34 (Ar), 125.10 (Ar), 81.31 (-C≡CH), 75.05 (-C≡CH), 60.99 (Bn-CHOHR) ppm.

2.7.10 1-(4,5-dimethoxy-2-nitrophenyl)prop-2-yn-3-d-1-ol
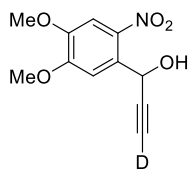
12
$C_{11}H_{10}DNO_5$
238.22 g/mol

In a 10 mL round bottom flask 10 (1.158 g, 6.536 mmol, 1 eq.) was dissolved in a 1:1 mixture of D_2O and THF (each 7 mL) at 0 °C. Et_3N (1.455 g, 14.380 mmol, 1.993 mL, 2.2 eq.) was added dropwise to the vigorously stirring solution. After the addition the cooling bath was removed and the reaction allowed to warm to room temperature. After 16 h the aqueous phase was extracted with EtOAc (three times 10 mL The combined organic fractions were dried over Na_2SO_4, filtered and concentrated in vacuo and purified by column chromatography (1:5 EtOAc PE). The purified deuterated alkyne 12 was found as a pale-yellow powder (yield: 85%, deuteration degree: 95-99%).

^{1}H NMR (300 MHz, $CDCl_3$) δ = 7.74 (s, BnH, 1 H), 7.56 (s, BnH, 1 H), 6.19 (s, BnCHOHR, 1 H), 4.13 (s, OMe, 3 H), 4.07 (s, OMe, 3 H) ppm.

^{13}C NMR (75 MHz, Acetone-d_6) δ = 156.82 (Ar), 137.72 (Ar), 129.72 (Ar), 129.15 (Ar), 128.01 (Ar), 125.15 (Ar), 80.45 (-C≡CH), 74.38 (-C≡CH), 60.78 (Bn-CHOHR), 56.15 (OMe) 56.08 (OMe) ppm.

2.7.11 1-(2-nitrophenyl)prop-2-yn-1-yl-3-d-acetate
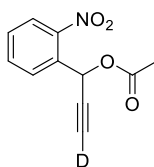

13
$C_{11}H_8DNO_4$
220.20 g/mol

The alkyne 12 (0.097 g, 0.548 mmol, 1 eq.) was dissolved in dry DCM (2.5 mL) at 0 °C. 4-DMAP (0.01 g, 0.048 mmol, 0.15 eq.) and Et_3N (0.11 g, 1.095 mmol, 0.152 mL, 2 eq.) were added. Acetic anhydride (0.084 g, 0.821 mmol, 0.078 mL, 1.5 eq.) was added to the stirring solution. The reaction was warmed to reflux for 3 h. D_2O (1 mL) was added to the reaction mixture. The aqueous phase was extracted with DCM (three times 1 mL). The combined organic fractions were dried over Na_2SO_4, filtered and concentrated in vacuo and purified by column chromatography (1:5

EtOAc PE). The purified ester 3 was found as white solid (yield: 70%; deuteration degree: >95%). From time to time the alkyne was exchanging its' deuterium with a proton. In such cases, the protocol of the synthesis of 12 was repeated with the ester. These reactions led to reduction in yield up to 50%.

^{1}H NMR (300 MHz, CDCl$_3$) δ = 8.00 (dt, J = 1.15, 7.85 Hz, 2 H, BnH3&4), 7.72 (dt, J = 1.15, 7.85 Hz, 1 H, BnH2), 7.56 (dt, J = 1.15 7.85 Hz 1 H, BnH5), 7.06 (s, 1 H, Bn-CHOAcR), 2.13 (s, 3 H, OAc) ppm.

^{13}C NMR (75 MHz, CDCl$_3$) δ = 169.05 (-COOCH$_3$) 147.79 (Ar), 133.56 (Ar), 131.50 (Ar), 129.85 (Ar), 129.32 (Ar), 124.98 (Ar), 61.54 (Bn-CHOHR), 20.58 (COOCH$_3$) ppm.

2.7.12 1-(4,5-dimethoxy-2-nitrophenyl)prop-2-yn-1-yl-3-d-acetate
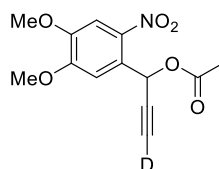
14
C$_{13}$H$_{12}$DNO$_6$
280.25 g/mol

The alkyne 12 (0.3 g, 1.259 mmol, 1 eq.) was dissolved in dry DCM (12.5 mL) at 0 °C. 4-DMAP (0.023 g, 0.189 mmol, 0.15 eq.) and Et$_3$N (0.225 g, 2.519 mmol, 0.308 mL, 2 eq.) were added. Acetic anhydride (0.192 g, 1.738 mmol, 1.776 mL, 1.5 eq.) was added to the stirring solution. The reaction was warmed to reflux for 3 h. D$_2$O (3 mL) was added to the reaction mixture. The aqueous phase was extracted with DCM (three times 2 mL). The combined organic fractions were dried over MgSO$_4$, filtered and concentrated in vacuo and purified by column chromatography (1:5 EtOAc PE). The purified ester 14 was found as white solid (yield: 65%; deuteration degree: >95%). From time to time the alkyne was exchanging its' deuterium with a proton. In such cases, the protocol of the synthesis of 12 was repeated with the ester. These reactions led to reduction in yield up to 50%.

^{1}H NMR (300 MHz, CDCl$_3$) δ = 7.74 (s, BnH, 1 H), 7.56 (s, BnH, 1 H), 6.19 (s, BnCHOHR, 1 H), 4.13 (s, OMe, 3 H), 4.07 (s, OMe, 3 H), 1.65 (s, OAc, 3H) ppm.

^{13}C NMR (75 MHz, Acetone-d$_6$) δ = 169.0 (OCOCH$_3$) 156.82 (Ar), 137.72 (Ar), 129.72 (Ar), 129.15 (Ar), 128.01 (Ar), 125.15 (Ar), 80.45 (-C≡CD), 74.38 (-C≡CD), 60.78 (Bn-CHOHR), 56.15 (OMe) 56.08 (OMe) ppm.

2.7.13 1-(2-nitrophenyl)prop-2-yn-1-yl-3-d-2-oxoproanoate

15
$C_{12}H_8DNO_5$
248.21 g/mol
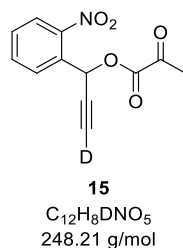
To a to 0 °C cooled solution of 10 (0.107 g, 0.604 mmol, 1 eq.), pyruvic acid (0.1 g, 1.208 mmol, 0.084 mL, 2 eq.) and pyridine (0.239 g, 3.02 mmol, 0.244 mL, 5 eq.) in THF (5 mL) methane sulfonyl chloride (0.138 g, 1.208 mmol, 0.093 mL, 2 eq.) was added dropwise. The reaction was stirred at room temperature for 3 h. D_2O was added to the mixture. The aqueous phase was extracted with Et_2O (three times 1 mL), the organic fractions combined, dried over Na_2SO_4, filtered and concentrated in vacuo. The crude product was purified by column chromatography (10:90 DCM:PE). The pure pyruvate ester 15 was found as a white solid (yield 45%, deuteration degree 95-99%).

^{1}H NMR (300 MHz, $CDCl_3$) δ = 8.10 (dd, J = 1.1, 8.15 Hz, 1 H, BnH), 7.98 (dd, J = 1.1, 8.15 Hz, 1 H, BnH), 7.75 (dt, J = 1.1, 8.10 Hz, 1 H, BnH), 7.60 (dt, J = 1.1 8.10 Hz 1 H, BnH), 6.98 (s, 1 H, Bn-CHOPyrR), 2.5 (s, 3 H, OPyr) ppm.

^{13}C NMR (75 MHz, $CDCl_3$) δ = 190.29 (-COOCOCH$_3$) 159.01 (-COOCOCH$_3$) 147.71 (Ar), 134.14 (Ar), 130.62 (Ar), 130.01 (Ar), 129.69 (Ar), 125.43 (Ar), 77.75 (-C≡CD), 75.35 (-C≡CD), 63.50 (Bn-CHOHR), 26.90 (COOCOCH$_3$) ppm.

2.7.14 1-(4,5-dimethoxy-2-ntirophenyl)prop-2-yn-1yl-3-d-2-oxopropanoate

16
$C_{14}H_{12}DNO_7$
308.26 g/mol
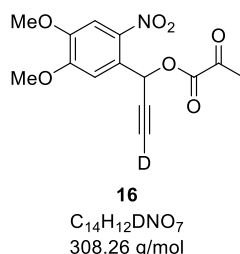
To a to 0 °C cooled solution of 12 (0.500 g, 2.108 mmol, 1 eq.), pyruvic acid (0.186 g, 2.108 mmol, 0.146 mL, 1 eq.) and pyridine (0.417 g, 5.27 mmol, 0.424 mL, 2.5 eq.) in THF (7.5 mL) methane sulfonyl chloride (0.29 g, 2.529 mmol, 0.196 mL, 1.2 eq.) was added dropwise. The reaction was stirred at room temperature for 8 h. D_2O was added to the mixture. The aqueous phase was

extracted with Et_2O (three times 2 mL), the organic fractions combined, dried over Na_2SO_4, filtered and concentrated in vacuo. The crude product was purified by column chromatography (10:90 DCM:PE). The pure pyruvate ester 16 was found as a white solid (yield 25%, deuteration degree 95-99%).

^1H NMR (300 MHz, $CDCl_3$) δ = 7.68 (s, BnH, 1 H), 7.46 (s, BnH, 1 H), 7.23 (s, BnCHOPyrR, 1 H), 4.02 (s, OMe, 3 H), 3.97 (s, OMe, 3 H), 2.50 (s, OPyr, 3 H) ppm.

^{13}C NMR (75 MHz, $CDCl_3$) δ = 190.87 (-$COOCOCH_3$), 159.13 (-$COOCOCH_3$), 153.65 (Ar-OMe), 149.59 (Ar-OMe), 140.28(Ar), 124.76 (Ar), 111.21 (Ar), 108.45 (Ar), 77.20 (-$C\equiv CD$), 75.75 (-$C\equiv CD$), 63.54 (Bn-CHOPyrR), 56.22 (BnOMe), 56.70 (BnOMe) 26.85 (-$COOCOCH_3$) ppm.

2.7.15 1-(2-nitrophenyl)prop-2-yn-1-yl-3-d-acetate-1-^{13}C-d_3
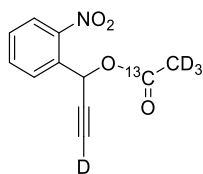
17
$C_{10}{}^{13}CH_5D_4NO_4$
224.21 g/mol

The alkyne 11 (0.200 g, 1.123 mmol, 1 eq.) was dissolved in dry DCM (8.5 mL) at 0 °C. 4-DMAP (0.021 g, 0.168 mmol, 0.15 eq.) and Et_3N (0.200 g, 2.245 mmol, 0.275 mL, 2 eq.) were added. 1,1-^{13}C Acetic anhydride-d_3 (0.185 g, 1.684 mmol, 0.172 mL, 1.5 eq.) was added to the stirring solution. The reaction was warmed to reflux for 3 h. D_2O (5 mL) was added to the reaction mixture. The aqueous phase was extracted with DCM (three times 7 mL). The combined organic fractions were dried over Na_2SO_4, filtered and concentrated in vacuo and purified by column chromatography (1:5 EtOAc PE). The purified ester 17 was found as white solid (yield: 73%; deuteration degree: >95%). From time to time the alkyne was exchanging its' deuterium with a proton. In such cases, the protocol of the synthesis of 11 was repeated with the ester. These reactions led to reduction in yield up to 50%.

^1H NMR (300 MHz, acetone-d_6) δ = 8.10 (dd, J = 1.3, 8.15 Hz, 1 H, BnH), 7.98 (dd, J = 1.3, 8.15 Hz, 1 H, BnH), 7.75 (dt, J = 1.3, 8.10 Hz, 1 H, BnH), 7.60 (dt, J = 1.3 8.10 Hz 1 H, BnH), 7.10 (d, J = 2.85, 1 H, Bn-CHOAcR) ppm.

^{13}C NMR (75 MHz, acetone-d$_6$) δ = 169.05 (-COOCH$_3$) 147.79 (Ar), 133.56 (Ar), 131.50 (Ar), 129.85 (Ar), 129.32 (Ar), 124.98 (Ar), 77.74 (-C≡CD), 75.36 (-C≡CD), 61.54 (Bn-CHOHR), 20.58 (COOCH$_3$) ppm.

2.7.16 1-(2-nitrophenyl)prop-2-yn-1-yl-3-d-2-oxopropanoate-1-^{13}C-3-d$_3$
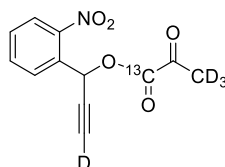
18
C$_{11}$^{13}CH$_5$D$_4$NO$_5$
252.22 g/mol

A solution of EDC·HCl (0.195 g, 1.016 mmol, 0.9 eq.) in DCM (2 mL) was added to a mixture of 1-^{13}C-pyruvate-d$_3$ (0.087 g, 0.96 mmol, 0.069 mL, 0.85 eq.), 11 (0.2 g, 1.129 mmol, 1 eq.) and 4-DMAP (0.117 g, 0.96 mmol, 0.85 eq.) in DCM (5 mL) at -15 °C. The resulting mixture was stirred at -15 °C for 30 min before warming the reaction to room temperature for further 14 h. After this time, D$_2$O (5 mL) was added, the aqueous phase was extracted with DCM (three times 5 mL), the combined organic layers were dried over Na$_2$SO$_4$, filtered and concentrated in vacuo. The crude mixture was purified by column chromatography (10:90 DCM:PE). The deuterated pyruvate ester 18 was found as an off-white solid (yield: 25%, deuteration: 95% (alkyne) and 99% (pyruvate)).

^{1}H NMR (300 MHz, CDCl$_3$) δ = 8.10 (dd, J = 1.1, 8.15 Hz, 1 H, BnH), 7.98 (dd, J = 1.1, 8.15 Hz, 1 H, BnH), 7.75 (dt, J = 1.1, 8.10 Hz, 1 H, BnH), 7.60 (dt, J = 1.1, 8.10 Hz 1 H, BnH), 6.98 (s, 1 H, Bn-CHOPyrR), 2.5 ppm.

^{13}C NMR (75 MHz, CDCl$_3$) δ = 158.85 (-COOCOCH$_3$) 147.85 (Ar), 134.21 (Ar), 130.68 (Ar), 130.05 (Ar), 129.35 (Ar), 125.05 (Ar), 77.93 (-C≡CD), 73.35 (-C≡CD), 62.74 (Bn-CHOHR), 23.90 (COOCOCH$_3$) ppm.

^{2}H NMR (46 MHz, CDCl$_3$) δ = 2.5 (Pyr) ppm.

2.7.17 1-(4,5-dimethoxy-2-nitrophenyl)prop-2-yn-1yl-3-d-acetate-1-^{13}C-d$_3$
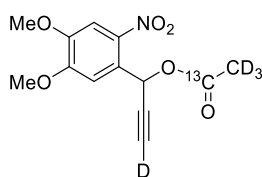
19
C$_{12}$^{13}CH$_9$D$_4$NO$_6$
284.26 g/mol

The alkyne 12 (0.300 g, 1.123 mmol, 1 eq.) was dissolved in dry DCM (12.5 mL) at 0 °C. 4-DMAP (0.023 g, 0.189 mmol, 0.15 eq.) and Et$_3$N (0.225 g, 2.519 mmol, 0.308 mL, 2 eq.) were added. 1,1-^{13}C Acetic anhydride-d$_3$ (0.208 g, 1.889 mmol, 0.193 mL, 1.5 eq.) was added to the stirring solution. The reaction was warmed to reflux for 3 h. D$_2$O (7 mL) was added to the reaction mixture. The aqueous phase was extracted with DCM (three times 7 mL). The combined organic fractions were dried over MgSO$_4$, filtered and concentrated in vacuo and purified by column chromatography (1:5 EtOAc PE). The purified ester 19 was found as white solid (yield: 43%; deuteration degree: >95%). From time to time the alkyne was exchanging its' deuterium with a proton. In such cases, the protocol of the synthesis of 12 was repeated with the ester. These reactions led to reduction in yield up to 50%.

^{1}H NMR (300 MHz, CDCl$_3$) δ = 7.71 (s, BnH, 1 H), 7.42 (s, BnH, 1 H), 7.20 (s, BnCHOAcR, 1 H), 4.09 (s, OMe, 3 H), 4.02 (s, OMe, 3 H) ppm.

^{13}C NMR (75 MHz, Acetone-d$_6$) δ = 168.66 (-COOCD$_3$) 153.28 (Ar), 152.58 (Ar), 149.07 (Ar), 148.49 (Ar), 110.71 (Ar), 108.01 (Ar), 77.22 (-C≡CD), 75.73 (-C≡CD), 61.55 (Bn-CHOHR), 56.15 (OMe) 56.05 (OMe) 23.89 (R-O^{13}COCD$_3$) ppm.

^{2}H NMR (500 MHz, CDCl$_3$) δ = 2.5 (Pyr) ppm.

2.7.18 1-(4,5-dimethoxy-2-nitrophenyl)prop-2-yn-1-yl-3-d-2-oxopropanoate-1-^{13}C-d$_3$
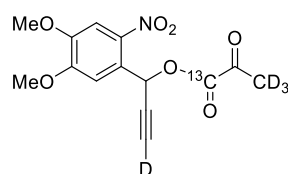
20

C$_{13}$^{13}CH$_9$D$_4$NO$_7$

312.27 g/mol

To a to 0 °C cooled solution of 12 (0.300 g, 1.259 mmol, 1 eq.), pyruvic acid (0.174 g, 1.889 mmol, 0.161 mL, 1.5 eq.) and pyridine (0.498 g, 6.297 mmol, 0.682 mL, 5 eq.) in THF (12.5 mL) methane sulfonyl chloride (0.346 g, 3.023 mmol, 0.234 mL, 2.4 eq.) was added dropwise. The reaction was stirred at room temperature for 8 h. D$_2$O (5 mL) was added to the mixture. The aqueous phase was extracted with Et$_2$O (three times 2 mL), the organic fractions combined, dried over Na$_2$SO$_4$, filtered and concentrated in vacuo. The crude product was purified by column chromatography (10:90 DCM: PE). The pure pyruvate ester 20 was found as a white solid (yield 30%, deuteration degree 95-99%).

¹H NMR (300 MHz, CDCl₃) δ = 7.65 (s, 1 H, Ar), 7.47(s, 1 H, Ar), 6.91 (d, J = 2.75 Hz, 1 H, Ar), 4.05(s, 3 H, OMe), 3.98 (s, 3 H, OMe) ppm.

¹³C NMR (75 MHz, CDCl₃) δ = 191.64 (-COOCOCD₃), 159.14(-COOCOCD₃), 153.67 (Ar), 152.38 (Ar), 142.56 (Ar), 140.38 (Ar), 124.75 (Ar), 111.23 (Ar), 77.02 (-C≡CD), 75.52 (-C≡CD), 63.56 (BNCHOPyrR), 56.73 (OMe), 56.69 (OMe), 26.96 (-COOCOCD₃)

2.7.19 1-(2-nitrophenyl)prop-2-en-1-ol
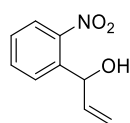
precursor of **21**
$C_9H_9NO_3$
179.18 g/mol

In a 50 mL two-neck flask, equipped with a dropping funnel 2-Nitrobenzaldehyde (0.250 g, 1.654 mmol, 1 eq.) was dissolved in dry THF (20 mL) and cooled to 0 °C in an ice bath. The vinyl magnesium bromide 1 M in THF (1.82 mL, 1.1 eq.) was transferred to the dropping funnel and added to the stirring solution over 30 min. After full addition the reaction was allowed to warm to room temperature. The full conversion after 2 h was visualized by TLC (1:5 EtOAc PE) and the reaction was quenched with 10 mL of a saturated NH_4Cl in H_2O solution. The aqueous solution was extracted with EtOAc (three times 5 mL). The combined organic fractions were dried over Na_2SO_4, filtered and concentrated in vacuo and purified by column chromatography. After purification the pure alkene was found as a yellow powder (yield: 99%).

¹H NMR (300 MHz, CDCl₃) δ = 7.92 (dd, J = 1.15, 8.1 Hz, 1 H, Ar), 7.77 (dd, J = 1.15, 8.1 Hz, 1 H, Ar), 7.64 (dt, J = 1.15, 7.6 Hz, 1H, Ar), 7.45 (dt, J = 1.15, 7.6 Hz, 1H, Ar), 6.07 (ddd, J = 5.2, 10.44, 17.2 Hz, 1 H, -CH=CH₂), 5.80 (dt, J = 1.15, 5.2 Hz, 1 H, BnCHOHR), 5.42 (dt, J = 1.15, 17.18 Hz, 1 H, -CH=CH₂, trans), 5.26 (dt, J = 1.15 ,10.52 Hz, 1 H, -CH=CH₂, cis) ppm.

¹³C NMR (75 MHz, CDCl₃) δ = 148.17 (Ar), 138.09 (-C=CH₂), 137.66 (Ar), 133.70 (Ar), 128.99 (Ar), 128.65 (Ar), 124.69 (Ar), 116.36 (-CH=CH₂), 70.12 (BnCOHR) ppm.

2.7.20 1-(4,5-dimethoxy-2-nitrophenyl)prop-2-en-1-ol
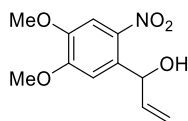
prcursor of **22**
$C_{11}H_{13}NO_5$
239.23 g/mol

In a 50 mL two-neck flask, equipped with a dropping funnel 4,5-dimethoxy-2-nitrobenzaldehyde (0.250 g, 1.654 mmol, 1 eq.) was dissolved in dry THF (20 mL) and cooled to 0 °C in an ice bath. The ethenyl magnesium bromide 1 M in THF (1.82 mL, 1.1 eq.) was transferred to the dropping funnel and added to the stirring solution over 30 min. After full addition the reaction was allowed to warm to room temperature. The full conversion after 2 h was visualized by TLC (1:5 EtOAc PE) and the reaction was quenched with 10 mL of a saturated NH_4Cl in H_2O solution. The aqueous solution was extracted with EtOAc (three times 5 mL). The combined organic fractions were dried over Na_2SO_4, filtered and concentrated in *vacuo* and purified by column chromatography. After purification the pure alkene was found as a yellow powder (yield: 99%).

^{1}H NMR (300 MHz, CDCl$_3$) δ = 7.70 (s, 1 H, ArH), 7.37 (s, 1 H, ArH), 7.07 (d, J = 5.2 Hz, 1 H, BnCHOHR), 6.18 (ddd, J = 5.2, 10.52, 17.08 Hz, 1 H, -CH=CH$_2$), 5.42 (dt, J = 1.2 ,17.08 Hz, 1 H, -CH=CH$_2$, trans), 5.42 (dt, J = 1.2 ,10.52 Hz, 1 H, -CH=CH$_2$, cis) 4.08 (s, 3 H, OMe), 4.05 (s, 3 H, OMe) ppm.

^{13}C NMR (75 MHz, CDCl$_3$) δ =153.8 (Ar), 148.17 (Ar), 138.23(-C=CH$_2$), 133.20 (Ar), 115.93 (Ar), 109.93 (-C=CH$_2$), 108.02 (-C=CH$_2$), 70.12 (Bn-CHOHR) 56.56 (2x OMe) ppm.

2.7.21 1-(2-nitrophenyl)allyl-2-oxopropanoate
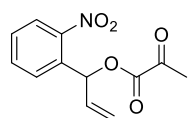
21
$C_{12}H_{11}NO_5$
249.22 g/mol

To a to 0 °C cooled solution of 1-(2-nitrophenyl)prop-2-en-1-ol (0.200 g, 0.1.116 mmol, 1 eq.), pyruvic acid (0.197 g, 2.233 mmol, 0.271 mL, 2 eq.) and pyridine (0.441 g, 5.581 mmol, 0.45 mL, 5 eq.) in THF (8 mL) methane sulfonyl chloride (0.32 g, 2.791 mmol, 0.216 mL, 2.5 eq.) was added dropwise. The reaction was stirred at room temperature for 3 h. D_2O was added to the mixture.

The aqueous phase was extracted with Et_2O (three times 1 mL), the organic fractions combined, dried over Na_2SO_4, filtered and concentrated in vacuo. The crude product was purified by column chromatography (1:4 EtOAc:PE). The pure pyruvate ester 21 was found as a white solid (yield 70%).

^{1}H NMR (300 MHz, $CDCl_3$) δ = 7.92 (dd, J = 1.15, 8.1 Hz, 1 H, Ar), 7.77 (dd, J = 1.15, 8.1 Hz, 1 H, Ar), 7.64 (dt, J = 1.15, 7.6 Hz, 1H, Ar), 7.45 (dt, J = 1.15, 7.6 Hz, 1H, Ar), 6.95 (dt, J = 1.15, 5.8 Hz, 1 H, BnCHOHR), 6.11 (ddd, J = 5.2, 10.44, 17.2 Hz, 1 H, -CH=CH$_2$), 5.45 (dt, J = 1.15, 17.18 Hz, 1 H, -CH=CH$_2$, trans), 5.38 (dt, J = 1.15 ,10.52 Hz, 1 H, -CH=CH$_2$, cis), 2.47 (s, 3 H, Pyr) ppm.

2.7.22 1-(4,5-dimehtoxy-2-nitrophenyl)allyl-oxopropanoate

22
$C_{14}H_{15}NO_7$
309.27 g/mol
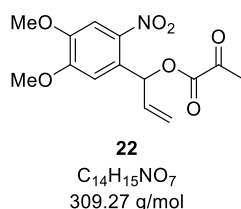
To a to 0 °C cooled solution of 2.7.201-(4,5-dimethoxy-2-nitrophenyl)prop-2-en-1-ol (0.200 g, 0.418 mmol, 1 eq.), pyruvic acid (0.074 g, 0.836 mmol, 0.101 mL, 2 eq.) and pyridine (0.165 g, 2.09 mmol, 0.169 mL, 5 eq.) in THF (3 mL) methane sulfonyl chloride (0.12 g, 1.045 mmol, 0.081 mL, 2.5 eq.) was added dropwise. The reaction was stirred at room temperature for 3 h. D_2O (1 mL) was added to the mixture. The aqueous phase was extracted with Et_2O (three times 1 mL), the organic fractions combined, dried over Mg_sSO_4, filtered and concentrated in vacuo. The crude product was purified by column chromatography (1:4 EtOAc PE). The pure pyruvate ester 22 was found as a white solid (yield 30%).

^{1}H NMR (300 MHz, $CDCl_3$) δ = 7.62 (s, 1 H, ArH), 7.10 (s, 1 H, ArH), 7.08 (dt, J =1.35, 5.4 Hz, 1 H, BnCHOHR), 6.13 (ddd, J = 5.4, 10.52, 17.19 Hz, 1 H, -CH=CH$_2$), 5.42 (ddd, J = 1.2, 1.35, 17.08 Hz, 1 H, -CH=CH$_2$, trans), 5.35 (dt, J = 1.2, 1.35 ,10.52 Hz, 1 H, -CH=CH$_2$, cis) 3.97 (s, 3 H, OMe), 3.95 (s, 3 H, OMe), 2.48 (s, 3 H, Pyr-CH$_3$) ppm.

2.7.23 L-alanine-2-d
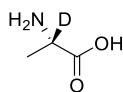
23
$C_3H_6DNO_2$
90.10 g/mol

In a three neck round bottom flask equipped with a condenser L-alanine (3 g, 33.67 mmol, 1 eq.), sodium hydroxide (4.04 g, 101.02 mmol, 3 eq.) and ruthenium on carbon (10% wt, 0.89 g, 8.82 mmol) was dissolved in 68 mL D_2O. The atmosphere was changed from N_2 to H_2 by slowly evacuating the reaction vessel while bubbling H_2 via a needle through the aqueous solution. Then, the reaction was warmed to reflux for 8-36 h (depending on the deuteration ratio checked by NMR). After the reaction was completed, the mixture was cooled to room temperature, filtered through a plug of Celite and the pH was decreased to pH=5 (1 mol DCl in D_2O). Dowex X-8 resin (3 g) was added to the clear solution. The resin was loaded on a filter, the filtrate was removed and the resin was washed with a 25 mL NH_4OH H_2O solution. The solvent was evaporated under reduced pressure while washing the evaporation gas through a 1 M HCl in H_2O washing solution to scavenge the ammonia. The resulting deuterated acid 23 was found as a white powder (yield: 65%, deuteration level: 99.8%)

^1H NMR (300 MHz, D_2O) δ = 1.26 (s, 3 H, $-CH_3$) ppm.

^{13}C NMR (75 MHz, D_2O) δ = 178.89 (COOH), 36.13 ($NHCOOCH_3$), 29.02 (-Me) ppm.

Specific rotation +2,28° (100 mg/mL, H_2O)

2.7.24 (Acetyl)-L-alanine-2-d
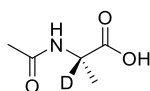
24
$C_5H_5D_4NO_3$
131.13 g/mol

To a solution of the amino acid 23 (2 g, 20.803 mmol, 1 eq.) in dry methanol (35 mL) acetic anhydride (5.097 g, 49.927 mmol, 2.7 eq.) was added. The reaction mixture was heated to reflux for 16 h, then cooled to room temperature before removing all volatiles in vacuo. The resulting colourless oil was crystallized over night at -20 °C. The acetylated amino acid 24 was found as a white crystal (yield 99%).

^{1}H NMR (300 MHz, D$_2$O) δ = 4.7 (q, J = 7.1 Hz, 1 H), 2.14 Hz, (s, 3 H, NHAc), 1.55 (d, J = 7.1 Hz, 3 H, -Me) ppm.

^{13}C NMR (75 MHz, D$_2$O) δ = 176.37 (Ac-COOR), 170.74 (-COOH), 48.28 (CH$_3$-CHNHR-COOH), 22.83 (Ac-CH$_3$), 18.04 (-Me) ppm.

2.7.25 Vinyl (acetyl-d$_3$)-L-alaninate-2-d

25
C$_7$H$_{10}$DNO$_3$
158.19 g/mol
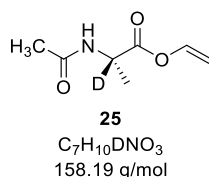
Under gentle warming to 35 °C, the acid 24 (1 g, 7.626 mmol, 1 eq.)was dissolved in vinyl acetate (5.252 g, 61.008 mmol, 5.648 mL, 8 eq.). To the stirring solution KOH (0.043 g, 0.763 mmol, 0.1 eq.) and freshly recrystallized Pd(OAc)$_2$ (0.017 g, 0.076 mmol, 0.01 eq.) was added and the reaction was stirred for 24 h. The crude reaction mixture was filtered through a plug of celite, rinsed with EtOAc (10 mL) and concentrated in vacuo. The crude product was purified by column chromatography (1:9 EtOAc PE). The vinyl ester 25 was found as an off white solid (yield: 60%).

^{1}H NMR (300 MHz, CDCl$_3$) δ = 7.22 (dd, J = 6.21, 13.92 Hz, 1 H, R-O-CH=CH$_2$), 6.17 (s, 1 H, NHAc), 4.96 (dd, J = 1.53, 13.92 Hz, 1 H, R-O-CH=H$_2$, trans), 4.63 (m (overlap of dd and q), dd: J = 1.53, 6.21 Hz q: 7.3 Hz, 1 H dd: R-O-CH=CH$_2$, cis; 1 H q: Me-CHNHR-COOR', 1 H), 2.14 Hz, (s, 3 H, NHAc), 1.55 (d, J = 7.3 Hz, 3 H, -Me) ppm.

2.7.26 L-alanine-1-^{13}C-2-d

26
C$_2$^{13}CH$_6$DNO$_2$
91.09 g/mol
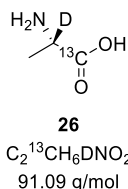
In a three neck round bottom flask equipped with a condenser L-alanine (2 g, 22.2 mmol, 1 eq.), sodium hydroxide (2.664 g, 66.6 mmol, 3 eq.) and ruthenium on carbon (10% wt, 0.100 g) was dissolved in 45 mL D$_2$O. The atmosphere was changed from N$_2$ to H$_2$ by slowly evacuating the reaction vessel while bubbling H$_2$ via a needle through the aqueous solution. Then, the reaction

was warmed to reflux for 8-36 h (depending on the deuteration ratio checked by NMR). After the reaction was completed, the mixture was cooled to room temperature, filtered through a plug of Celite and the pH was decreased to pH=5 (1 mol DCl in D_2O). Dowex X-8 resin (2 g) was added to the clear solution. The resin was loaded on a filter, the filtrate was removed and the resin was washed with a 20 mL NH_3 H_2O solution. The solvent was evaporated under reduced pressure while washing the evaporation gas through a 1 M HCl in H_2O washing solution to scavenge the ammonia. The resulting deuterated acid 26 was found as a white powder (yield: 67%, deuteration level: 99.5%)

^{1}H NMR (300, D_2O) δ = 1.26 (s, 3 H, -CH$_3$) ppm.

^{13}C NMR (75 MHz, D_2O) δ = 179.01 (COOH), 36.43 (NHCOOCH$_3$), 29.19 (-Me) ppm.

2.7.27 (Acetyl-d$_3$)-L-alanine-1-^{13}C-2-d

27
$C_4{}^{13}CH_5D_4NO_3$
136.15 g/mol
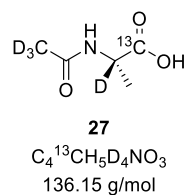
To a solution of the amino acid 26 (0.7 g, 7.857 mmol, 1 eq.) in dry methanol (12 mL) acetic anhydride-d$_6$ (2.166 g, 21.215 mmol, 2.7 eq.) was added. The reaction mixture was heated to reflux for 16 h, then cooled to room temperature before removing all volatiles in vacuo. The resulting colourless oil was crystallized overnight at -20 °C. The acetylated amino acid 27 was found as a white crystal (yield 99%).

^{1}H NMR (300 MHz, D_2O) δ = 1.27 (d, J = 4.22 Hz, -CH$_3$ C-13 coupling) ppm.

^{13}C NMR (75 MHz, CDCl$_3$) δ = 178.87 (-NHCOOCD$_3$), 174.77 (-NHCOOCD$_3$), 169.16 (Me-CDNHR-COOR', 21.10 (Me-CDNHR-COOR'), 19.87 (-NHCOOCD$_3$) ppm.

2.7.28 Vinyl-d$_3$ (acetyl-d$_3$)-L-alaninate-1-^{13}C-2-d
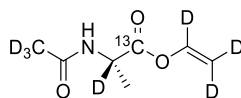
28

C$_6$^{13}CH$_4$D$_7$NO$_3$

165.20 g/mol

Under gentle warming to 35 °C, the acid 27 (0.2 g, 1.469 mmol, 1 eq.)was dissolved in vinyl acetate-d$_6$ (0.759 g, 8.814 mmol, 0.816 mL, 6 eq.). To the stirring solution KOH (0.008 g, 0.147 mmol, 0.1 eq.) and freshly recrystallized Pd(OAc)$_2$ (0.003 g, 0.015 mmol, 0.01 eq.) was added and the reaction was stirred for 24 h. The crude reaction mixture was filtered through a plug of celite, rinsed with EtOAc (5 mL) and concentrated in vacuo. The crude product was purified by column chromatography (1:9 EtOAc PE). The vinyl ester 28 was found as an off white solid (yield: 50%).

^{1}H NMR (300 MHz, acetone-d$_6$) δ = 1.41 (d, J = 4.6 Hz,3 H, CH$_3$ C-13 coupling) ppm.

^{2}H NMR (46 MHz, CDCl$_3$) δ = 7.34 (dd, J = 7.2 Hz, 2 D, -O-CD=CD$_2$), 4.98 (m, 1 D, -O-CD=CD$_2$), 4.62 (m, 2 D, -O-CD=CD$_2$, Me-CDNHR-COOR'), 2.08 (s, 3 D, NHAc-d$_3$) ppm.

^{13}C NMR (75 MHz, acetone-d$_6$) δ = 173.31 (Me-CDNHR-COOR', 170.29 (-NHCOOCD$_3$), 141.18 (-ROCD=CD$_2$), 97.31 (-ROCD=CD$_2$), 28.80 (Me-CDNHR-COOR') 21.10 (Me-CDNHR-COOR'), 16.98 (-NHCOOCD$_3$) ppm.

3 Results

Molecules that are supposed to be hyperpolarized by means of parahydrogen in order to study metabolic processes in living organisms, whether in cell experiments by NMR or in animals or even humans with MRI, require certain properties. Biological activity of the MOI is a prerequisite to investigate metabolomic activities. Without conversion in biochemical processes, it is not possible, to make any statements about the effects of diseases or drugs on the metabolism.

In order to trace these molecules over a long period of time, chemical modifications of their structure are essential to elongate the relaxation times of the observed nuclei. In principle, within the metabolite the atoms, which, for metabolites as a result of the biochemical reaction, cause a significant (i. e. clearly visible) change in their chemical shift, are of particular interest. Especially carbon atoms with their larger spectral width and distribution compared to protons are noteworthy. To reduce the longitudinal relaxation time T_1 of the observed ^{13}C atom, the exchange of surrounding protons to deuterium atoms is necessary. These exchange reactions are realized predominantly by acid-base reactions (in chapter 3.1 for pyruvate) or by catalytic processes (in chapter 3.3 for alanine). Notably, the deuteration of molecules does not only elongate their traceability. Deuteration of the to-be-hydrogenated unsaturated carbon-carbon bonds can further increase the detectable polarization by a factor of ten. New findings regarding the effective and efficient deuteration with little to no side product formation are described to scale synthetic routes up for in vivo studies of animals or even human.

3.1 Deuteration of sodium pyruvate and pyruvic acid

One of the most studied molecules in hyperpolarized magnetic resonance is 1-^{13}C pyruvate, as it is a major branching point in human metabolism. Through the interplay of the various downstream pathways, changes in their ratios can provide information about the condition of the living being. Thereby, imaging methods allow the localization of tumors in living organisms. Hyperpolarization techniques such as PHIP are used to generate signal enhancements of +10,000-fold enabling the performance of metabolic studies under physiological conditions. Besides the required polarization levels, the longest possible traceability (T_1 dependent) is needed to make slower conversions to certain downstream metabolites visible. However, to reduce the couplings between the observed

atoms (e. g. 1-^{13}C of pyruvate) and protons (such as those of the methyl group of pyruvate) that lead to rapid relaxation by the reduction of T_1 of the previously introduced polarization, robust deuteration methods have to be established (molecule 1 & 2, Scheme 3).
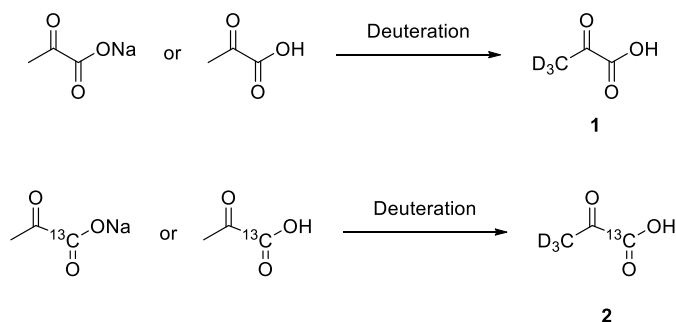
Scheme 3 General reaction scheme for the deuteration of sodium pyruvate or pyruvic acid at the respective methyl group under appropriate conditions for natural abundance pyruvate and ^{13}C pyruvate respectively.

Due to the high reactivity of the molecule, reactions with pyruvate lead to the formation of undesirable by-products such as dimers of the pyruvate itself. These unwanted products massively effect the following modifications, such as esterifications, needed to access hyperpolarization via side arm hydrogenation. Effective deuteration of the terminal methyl group lead to increased polarization values and thus might also help other hyperpolarization methods to achieve higher order of spin polarization as for example SABRE. To reduce the side product formation while achieving the highest possible degree of deuteration, the pyruvate with natural abundance ^{13}C was tested under various reaction conditions before using the commercially available isotopically enriched pyruvate sources (Na-1-^{13}C-pyruvate or 1-^{13}C-pyruvic acid). In addition to the literature-known procedures using deuterated sulfuric acid (with sodium pyruvate) and sodium bicarbonate (for pyruvic acid), deuteration was attempted using sodium carbonate in D_2O and amine-based bases (Et$_3$N and pyridine) in a solvent mixture of D_2O and THF.[86] For all reactions a concentration of 0.1 g/mL and an equimolar ratio of base to pyruvate were used. All reactions were performed under inert atmospheres, the reagents were added over a significant amount of time at 0 °C to ensure that overloading the mixture does not impact the later yield.

The reactions were monitored by NMR spectroscopy after 5 and 16 h each (^{1}H and ^{13}C spectra) and analyzed with respect to their resulting products. For NaHCO$_3$, Na$_2$CO$_3$ and D$_2$SO$_4$, the reaction at room temperature did not yield deuterated pyruvate (i. e. less than 5%). These were warmed to 80 °C for 5 h. For most conditions, side product formation was unavoidable. Besides the through pH adjustment back convertible hydropyruvate-d$_3$, parapyruvate A, hydroparapyruvate B and zymonic acid C (Figure 17) were found in different concentrations.
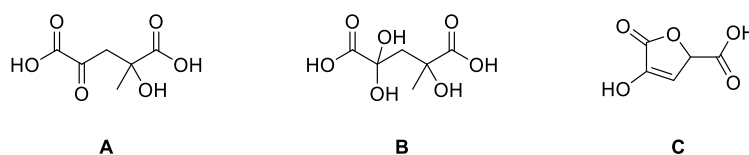
Figure 17 Structure of the molecules parapyruvate 3, hydroparapyruvate 4 and zymonic acid 5 as the main side products of deuteration reactions with sodium pyruvate or pyruvic acid.

As a reference to the starting material of each reaction, a solution with a concentration of 0.1 g/mL of the pyruvate (acid and sodium salt) was measured by NMR. In the sample of sodium pyruvate, traces of parapyruvate were found while the sample mainly contained pyruvate (90%) and pyruvate hydrate (9%, see Table 2 a). In the sample of the free acid 10% impurities were found (1% A, 1% B, and 8%C, see Table 2 b). It is known from the literature, that these impurities can be found in commercially available pyruvic acid. The results of the deuteration experiments are shown in Table 2.

Table 2 Determination of the products as well as their degree of deuteration starting from sodium pyruvate (a) and pyruvic acid (b) by NMR (for a detailed description of the calculation see chapter 2.3; for a detailed list of the measured integrals of each spectrum see the appendix). With "-" indicating that the respective side product was not formed and "*" indicating that not quantifiable traces of the respective side product was found.

a)

from Na-Pyruvate	in D_2O		with $NaHCO_3$		with Na_2CO_3		with Et_3N in THF/D_2O		with D_2SO_4	
products	yield	D degree	yield	D degree	yield	D degree	yield	D degree	yield	D degree
Pyruvate	91,47%	0,00%	42,12%	85,42%	61,50%	99,46%	52,85%	98,71%	39,48%	100,00%
Hydropyruvate	8,53%	0,00%	*	*	*	*	-	-	-	-
Parapyruvate	-	-	40,57%	99,41%	19,20%	98,43%	47,15%	99,25%	60,52%	100,00%
Hydroparapyruvate	-	-	17,31%	99,77%	19,29%	85,34%	-	-	-	-
Zymonic acid	-	-	-	-	-	-	-	-	-	-

b)

from pyruvic acid	in D_2O		with $NaHCO_3$		with Na_2CO_3		with Et_3N in THF/D_2O		with D_2SO_4	
products	yield	D degree	yield	D degree	yield	D degree	yield	D degree	yield	D degree
Pyruvate	34,73%	0,00%	49,69%	26,22%	29,15%	99,89%	40,78%	99,50%	30,04%	59,48%
Hydropyruvate	65,27%	0,00%	10,37%	54,11%	0,00%	0,00%	0,00%	0,00%	36,18%	53,02%
Parapyruvate	*	*	14,18%	94,66%	31,29%	98,20%	*	*	*	*
Hydroparapyruvate	*	*	3,74%	0,00%	12,74%	99,09%	*	*	*	*
Zymonic acid	*	*	*	*	*	*	*	*	*	*

3.2 Synthesis of 2-nitrobenzyl based side arms for the hyperpolarization with parahydrogen

All established side arms for the hyperpolarization of pyruvate need to undergo a chemically induced cleavage reaction (see chapter 1.3.3.2). This cleavage procedure is time consuming and thus results in lower polarization values. By synthesizing a new class of side arms based on a 2-nitrobenzyl framework, a chemical-free cleavage was targeted. To investigate the impact of modifications of the benzyl ring on the hyperpolarization levels, a 4,5 dimethoxy-2-nitrobenzyl derivative was prepared. In addition, a strategy for further modifications of the aromatic ring was developed starting from (iso-)vanillin as a generally available building block. The shown aldehydes in Scheme 4 can be directly converted into the respective polarizable side arms under standardized reaction conditions ready for the esterification with the MOI. After the deuteration of the terminal alkyne a broad scope of esterification procedures for acetate and pyruvate as well as their ^{13}C labelled counterparts were fine-tuned.
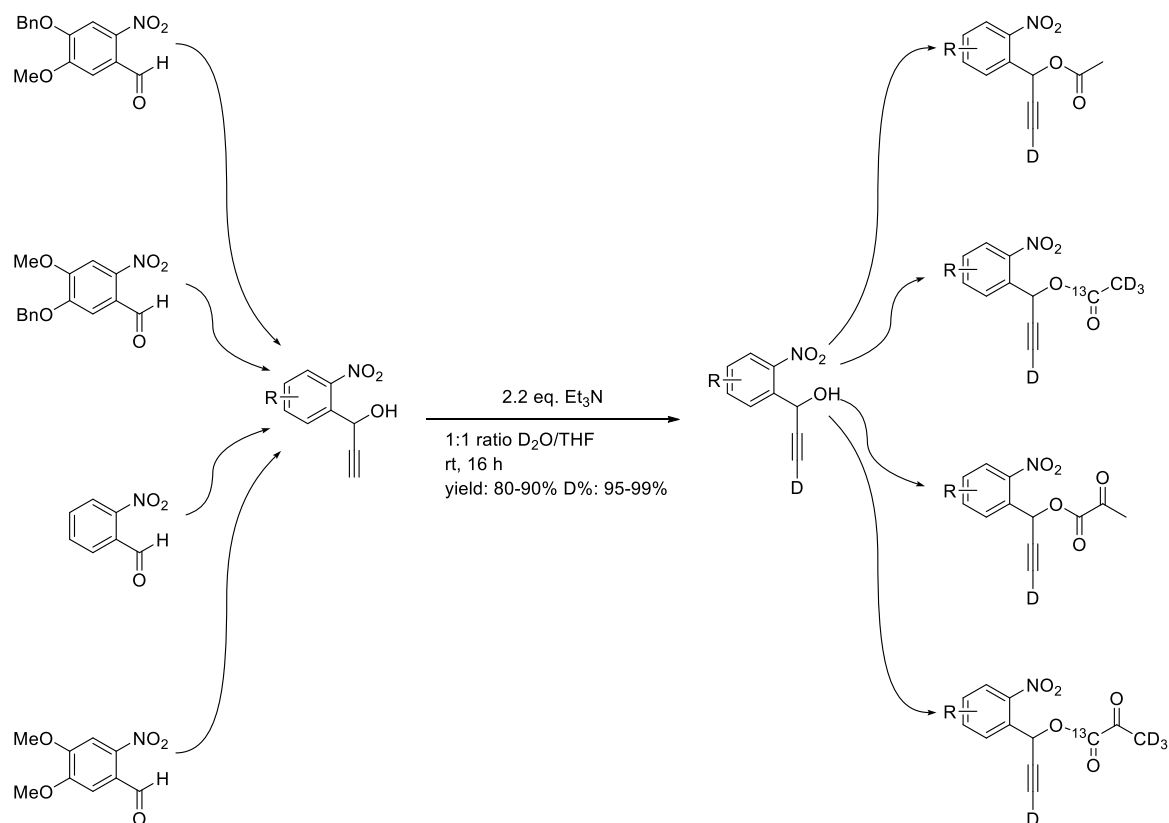
Scheme 4 Different derivatives of 2-nitrobenzaldehyde based on (iso-)vanillin and 4,5-dimethoxy-2-nitrobenzaldehyde and their respective transformation to their secondary alcohol using a Grignard reagent. Deuteration of the triple bond under standardized conditions allowed the formation of the subsequent esters based on acetate and pyruvate and their deuterated and ^{13}C-labelled compounds, respectively.

Upon that, hyperpolarization of the precursors was performed under PASADENA conditions using highly enriched pH_2 yielding highly polarized metabolites through a proton-relayed version of the ESOTHERIC pulse sequence (Figure 15, Scheme 5).
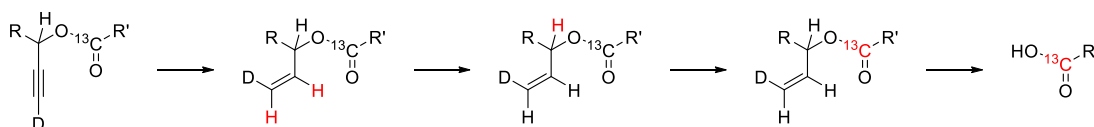
Scheme 5 Typical sequence of the transfer of polarization after hydrogenation of the triple bond. The spin order is transferred to the heteronucleus by linking several INEPT sequences via the relay proton. After the transfer is completed, the MOI is released.

3.2.1 Synthesis of side arms

Starting from vanillin and iso-vanillin, the benzylic alcohols were first protected using potassium carbonate and benzyl bromide in high yields allowing to use the aldehydes in the next reaction without further purification. Nitration was carried out using fuming nitric acid and acetic acid yielding in the nitrobenzyl compounds 4 and 6 (Scheme 6).
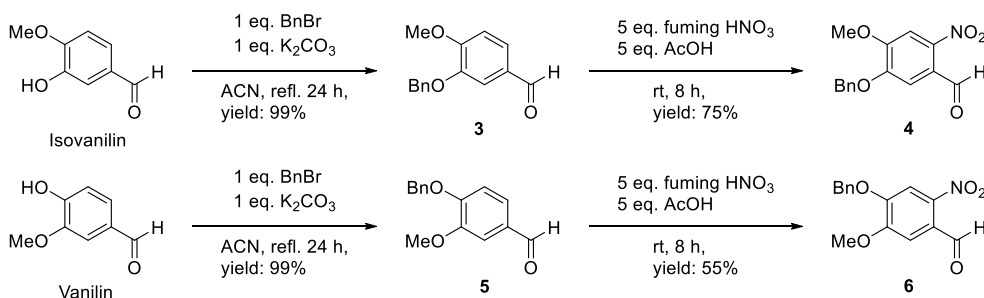
Scheme 6 Synthetic transformations of iso-vanillin via the benzyl-protected alcohols to the nitrated aldehydes 5-(benzyloxy)-4-methoxy-2-nitrobenzaldehyde 4 and 4-(benzyloxy)-5-methoxy-2-nitrobenzaldehyde 6.

To investigate the coupling of the respective side arm with acetate and pyruvate, the 4,5-dimethoxy-2-nitrobenzaldehyde (also known as 6-nitroveratraldehyde, short form 6-NV) and 2-nitrobenzaldehyde (short form 2-NBn) were converted to the respective secondary alcohols using standard Grignard conditions under full conversion. Deuterium-proton exchange of the terminal triple bonds was achieved in a solvent mixture of D_2O and THF using Et_3N for the deprotonation. Purification by column chromatography was performed due to small impurities (Scheme 7).
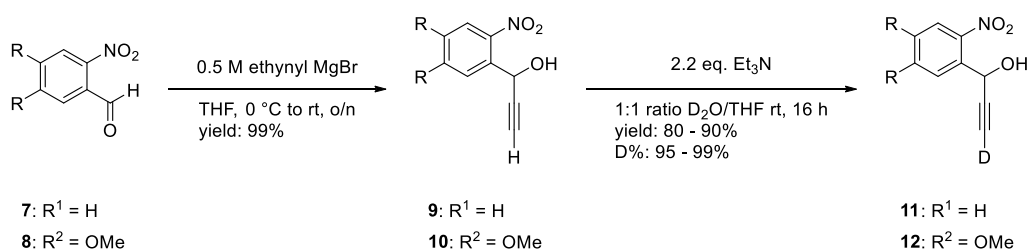
Scheme 7 Grignard reaction of the aldehydes 7 and 8 to the alcohols 9 and 10 using ethynyl magnesium bromide. These alcohols were used for a terminal deuterium-proton exchange reaction under basic conditions yielding the alcohols 11 and 12. Weather the latter alcohol functional groups were also deuterated was not investigated.

Since ^{13}C-enriched and deuterated molecules 1-^{13}C-acetic acid-d_3 and 1-^{13}C-pyruvate-d_3 (planned to be used for the hyperpolarization experiments) are cost intensive, the esterifications were first optimized with respect to their yield with the unlabeled variants. Therefore, the alcohols 11 and 12 were coupled with acetic acid or the anhydride under the conditions mentioned in Table 3. From time to time the reaction conditions of Entry 1 and 2 led to partial re-protonation of the terminal alkyne. Deuteration was achieved comparable to the initial exchange reaction but with 1.1 eq. Et_3N instead of 2.2 eq. resulting in fully deuterated esters within 16 h with a yield of 90%. The major side product of these reactions was the starting material 11 or 12 yet protonated at the alkyne position. To enhance the reactivity the reactions were also performed at 40 °C and 60 °C (for DCM reflux), which did not lead to the desired result of higher yields. To avoid effects of residual water the reactions were also tested in presence of molecular sieves with, however, no beneficial results.

Table 3 Screening of reaction conditions for the esterification of secondary alcohols (R^1: 1-(2-nitrophenyl)prop-2-yn-3-d-1-ol 11; R^2 1-(4,5-dimethoxy-2-nitrophenyl)prop-2-yn-3-d-1-ol 12) and acetic acid forming the esters (R^1: 1-(2-nitrophenyl)prop-2-yn-1-yl-3-d acetate 13), R^2: 1-(4,5-dimethoxy-2-nitrophenyl)prop-2-yn-1-yl-3-d acetate 14). Procedures adapted from [121-123].
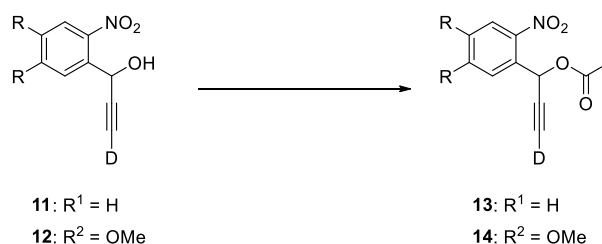
Entry	Conditions at 100 mg scale	isolated yield	
		R^1	R^2
1	0.2 eq. 4-DMAP, 2 eq. Et$_3$N 1.5 eq. acetic anhydride, rt, DCM	75	70
2	0.2 eq. 4-DMAP, 2 eq. Et$_3$N 1.5 eq. acetic acid, rt, DCM	45	34
3	1.25 eq MsCl, 2.5 eq. pyridine, 2 eq. acetic acid, rt, THF	51	45
4	2.5 eq MsCl, 5 eq. pyridine, 2 eq. acetic acid, rt, THF	40	32
5	1 eq. pyridine, acetic acid, reflux, DCM	10	8

In addition to the conditions that led to good yields with acetic acid and concerning the generally higher sensitivity of pyruvate, more esterification conditions of the alcohols 11 and 12 with pyruvic acid were performed. Methods converting the -OH into a halide followed by nucleophilic attacks of the pyruvate on the carbon did not lead to the desired product (Table 4). In general, more attention had to be paid to the slow addition of reagents. Otherwise, the increased occurrence of side reactions was observed. For the acetate, heating and the use of molecular sieves did not improve product formation.

Table 4 Screening of reaction conditions for the esterification of secondary alcohols and pyruvic acid forming their respective ester (R[1]: 1-(2-nitrophenyl)prop-2-yn-1-yl-3-d 2-oxopropanoate 15, R[2]: 1-(4,5-dimethoxy-2-nitrophenyl)prop-2-yn-1-yl-3-d 2-oxopropanoate 16). Procedures adapted from [121-123].

11: R[1] = H
12: R[2] = OMe
15: R[1] = H
16: R[2] = OMe
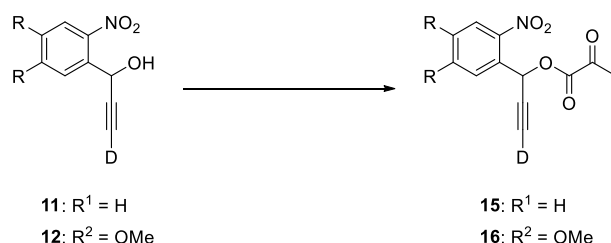
Entry	Conditions at 100 mg scale	Isolated yield [%]	
		R[1]	R[2]
1	1.2 eq. SOCl$_2$, 1.1 eq. sodium pyruvate, rt, DMF	0	0
2	1.2 eq. SOCl$_2$, 1.1 eq. pyruvic acid, rt, DCM	0	0
3	1 eq. DCC, 0.15 eq. 4-DMAP, 1 eq. pyruvic acid, rt, DMF	55	40
4	1.25 eq MsCl, 2.5 eq. pyridine, 2 eq. pyruvic acid, rt, DMF	12	10
5	1.25 eq MsCl, 2.5 eq. pyridine, 2 eq. pyruvic acid, rt, THF	62	50
6	2.5 eq MsCl, 5 eq. pyridine, 2 eq. pyruvic acid, rt, THF	41	43
7	0.9 eq. EDC, 0.85 eq. 4-DMAP, 0.85 eq. pyruvic acid, rt, DCM	22	18
8	a) PBr$_3$, Et$_2$O b) 1 eq. sodium pyruvate, rt, DCM	0	0
9	p-toluene sulfonic acid 1.1 eq., rt, toluene	0	0

Based on Table 3 entry 1, esterifications of 1,1-^{13}C-acetic acid-d$_3$ with alcohols 11 and 12 were executed. The yield was on average 15% lower than with the not enriched acetate. Variation of the equivalents of the used reagents, changing reaction time and temperature did not improve the product formation. For pyruvate the esterifications with the freshly prepared 1-^{13}C-pyruvate-d$_3$ also afforded lower yields. Here, losses of up to 40% were observed in the esterification of alcohol 11 under the conditions of entry 5 Table 4 (Scheme 8). Consequently, the DCC-based protocol (entry

3) was also carried out for esterification in addition to the conditions mentioned in entry 4. In general, aqueous work up conditions lead to the decomposition of the product. By filtration through celite and evaporation of the volatiles most of the reagents were removed. The purification was performed using a celite-based pre-column leading to reagent-free fractions of the product. Since the rf values of the product and the starting material were identical under standard column conditions, dichloromethane was used as polar component of the elution solvent (non-polar component petroleum ether).

11: R^1 = H
12: R^2 = OMe

17: R^1 = H
19: R^2 = OMe

11: R^1 = H
12: R^2 = OMe

18: R^1 = H
20: R^2 = OMe
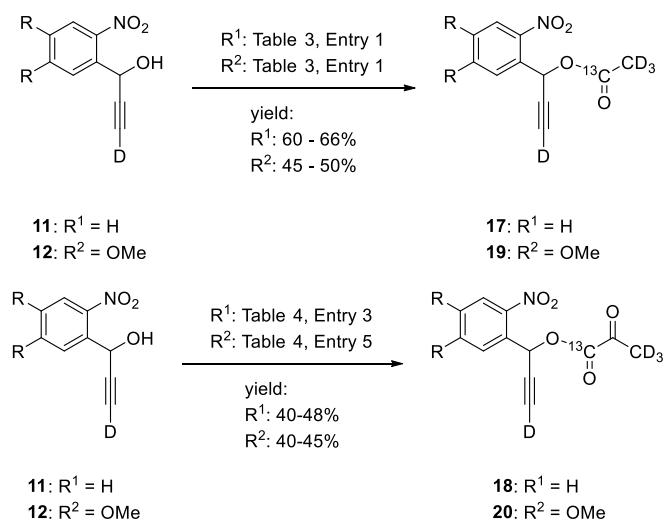
Scheme 8 Synthesis of the 1-^{13}C-acetate-d_3 ester (R^1: 1-(2-nitrophenyl)prop-2-yn-1-yl-3-d-acetate-1-^{13}C-d_3 17), R^2: 1-(4,5-dimethoxy-2-nitrophenyl)prop-2-yn-1yl-3-d-acetate-1-^{13}C-d_3 19) and 1-^{13}C-pyruvate-d_3 (R^1: 1-(2-nitrophenyl)prop-2-yn-1-yl-3-d-2-oxopropanoate-1-^{13}C-3-d_3 19), R^2 1-(4,5-dimethoxy-2-nitrophenyl)prop-2-yn-1-yl-3-d-2-oxopropanoate-1-^{13}C-d_3 20) according to the respective conditions mentioned in Table 3 and Table 4.

The esters 17, 18, 19 and 20 were used for the subsequent hyperpolarization experiments (Figure 18).
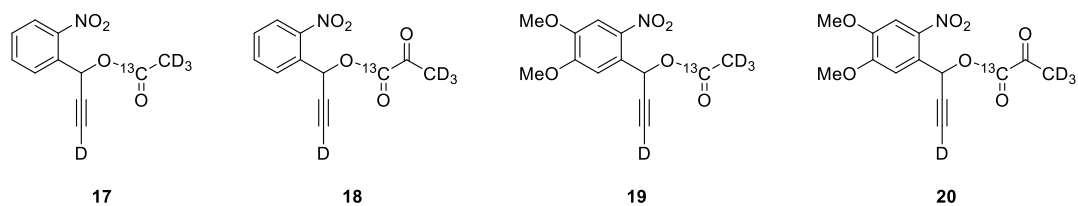
Figure 18 Structures of the precursors for hyperpolarization experiments.

3.2.2 Hyperpolarization of ^{13}C enriched metabolites with parahydrogen

Since the optimal transfer of the spin order introduced by the parahydrogen via the so-called relay proton to the heteronucleus ^{13}C is strongly dependent on the accuracy of the applied pulses, the allyl ester derivatives of the esters 19 and 20 were prepared. Analogously to the reactions with the alkyne group, the allyl magnesium bromide was used to form the respective secondary alcohols. Since deuteration was not needed in this case, the optimal reaction conditions from the formation of the compounds 19 and 20 were used to form the allyl esters 21 and 22. These allowed the measurement of J–couplings which were necessary to calculate the delays between the pulses of the NMR experiments (Table 6).

Table 5 Couplings between the protons of the allyl esters 21 and 22 as they occur after the hydrogenation of 19 or 20 with parahydrogen during hyperpolarization experiments. Couplings of H^{1b} to any other proton are negligible as it is replaced with a deuterium atom in the hyperpolarization experiments (due to deuterated alkynyl bond). The couplings of the H^3 and the ^{13}C of the MOI were determined through the hyperpolarized spectra acquired later on.

21: R^1 = H
22: R^2 = OMe
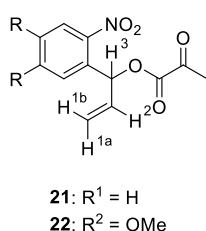
Coupling of Protons	for R^1 in Hz	for R^2 in Hz
1a to 1b	<1	<1
1a to 2	10.53	10.51
1a to 3	1.37	1.25
1b to 2	17.19	17.19
2 to 3	5.65	5.78

In order to achieve the highest polarization possible, the fundamental hydrogenation parameters were determined for 2 mM substrate concentration (esters 17 to 20). These involved the hydrogenation time (bubbling time), the ratio of catalyst to substrate concentration and the reaction temperature. These parameters were used for all subsequent spin manipulations performed using the (fractioned) NMR pulse program shown in chapter 1.3.3.3 Figure 15 (Table 6).

Table 6 Optimized parameters for hyperpolarization experiments used for all hyperpolarization experiments with the esters 17 to 20. The full data set can be found in the Appendix.

	R^1		R^2	
	1-^{13}C-acetate-d$_3$	1-^{13}C-pyruvate-d$_3$	1-^{13}C-acetate-d$_3$	1-^{13}C-pyruvate-d$_3$
	17	18	19	20
bubbling time	10 s	12 s	10 s	12 s
settling time	0.2 s	0.35 s	0.2 s	0.35 s
[ester]	2 mM	2 mM	2 mM	2 mM
[cat]	2 mM	2 mM	2 mM	2 mM
solvent	acetone-d$_6$	acetone-d$_6$	acetone-d$_6$	acetone-d$_6$
T	50 °C	50 °C	50 °C	50 °C

Since the polarization is planned to be transferred from the former pH$_2$ protons onto the relay proton H^3, the used pulse sequence was separated into the corresponding fragment allowing to measure in-phase polarization on the relay proton. For each molecule the polarization values were determined at every position during the hyperpolarization transfer, at protons H^1 and H^2 (originating from parahydrogen), H^3 (the relay proton) as well as on the ^{13}C. To release the metabolite from the side arm water was added manually to the hyperpolarized solution before placing the NMR tube back into the magnet. Consequently, for the cleavage experiments the spins had to be aligned with the magnetic field using a so-called z-flip pulse. Hydrolysis experiments were only performed for the 2-nitrobenzylpropynyl esters 17 and 18. The results of the experiments are shown in Table 7.

Table 7 Polarization values of the hyperpolarized precursors and released metabolites (-: not performed, /: unsuccessful). The hyperpolarization experiments were performed according to the conditions listed in Table 6. In the table P_{hyper} corresponds to the measured hyperpolarization in percent with ± indicating the range of the determined polarization values and σ as the standard deviation. The polarization values were determined by referencing the respective hyperpolarized signal with the integral of the thermal polarized spectrum of the H^3 proton acquired before the hyperpolarization experiment.

	H^1		H^3 Pol		^{13}C Pol		cleaved	
Compound	P_{hyper} [%]	σ	P_{hyper} [%]	σ	P_{hyper} [%]	σ	P_{hyper} [%]	σ
2-NBn-1-^{13}C-acetate-d$_3$ 17	61.58±1.28	1.11	37.63±1.71	2.07	20.58±0.68	0.58	4.21±1.46	2.70
2-NBn-1-^{13}C-pyruvate-d$_3$ 18	27.02±1.28	1.12	15.66±1.04	0.93	11.31±0.83	1.4	5.51±0.23	0.22
6-NV-1-^{13}C-acetate-d$_3$ 19	51.59±3.68	4.61	33.15±1.13	1.78	29.31±1.33	1.15	-	-
6-NV-1-^{13}C-pyruvate-d$_3$ 20	21.90±1.62	1.91	7.71±0.59	0.89	/	/	/	/

The values shown here have been calculated assuming full conversion of the alkyne to alkene and fully enriched pH_2. 33% of the polarization measurable on the H^1 and H^2 protons could still be detected on the ^{13}C after the transfer (33.41% for 17 and 41.85% for 18). For the 19, even 56.81% of the initial spin order could be retained. However, for the pyruvate ester 20, no successful transfer to the ^{13}C could be performed. The coupling constants of the ^{13}C to H^3 together with the chemical shift of the protons led to a poor transfer to the ^{13}C of the pyruvate, so that the data obtained could not be used for a proper analysis.

Hyperpolarization of the esters was performed under the conditions listed in Table 6. In the corresponding ^1H spectrum of 2-NBn-Ac (recorded with a 45° flip angle), 2 antiphase signals can be detected (Figure 19 a). The signal at around 6.2 ppm is associated with the added proton H-2 and has a 20% lower signal intensity than the H-1 at 5.2 ppm due to the couplings. The signal of the H-1 is increased by a factor of 33,000 compared to the thermally polarized one. The same pattern can be seen for all other esters as well, so that this lower intensity of the H-2 can be seen as a property of the side arm.
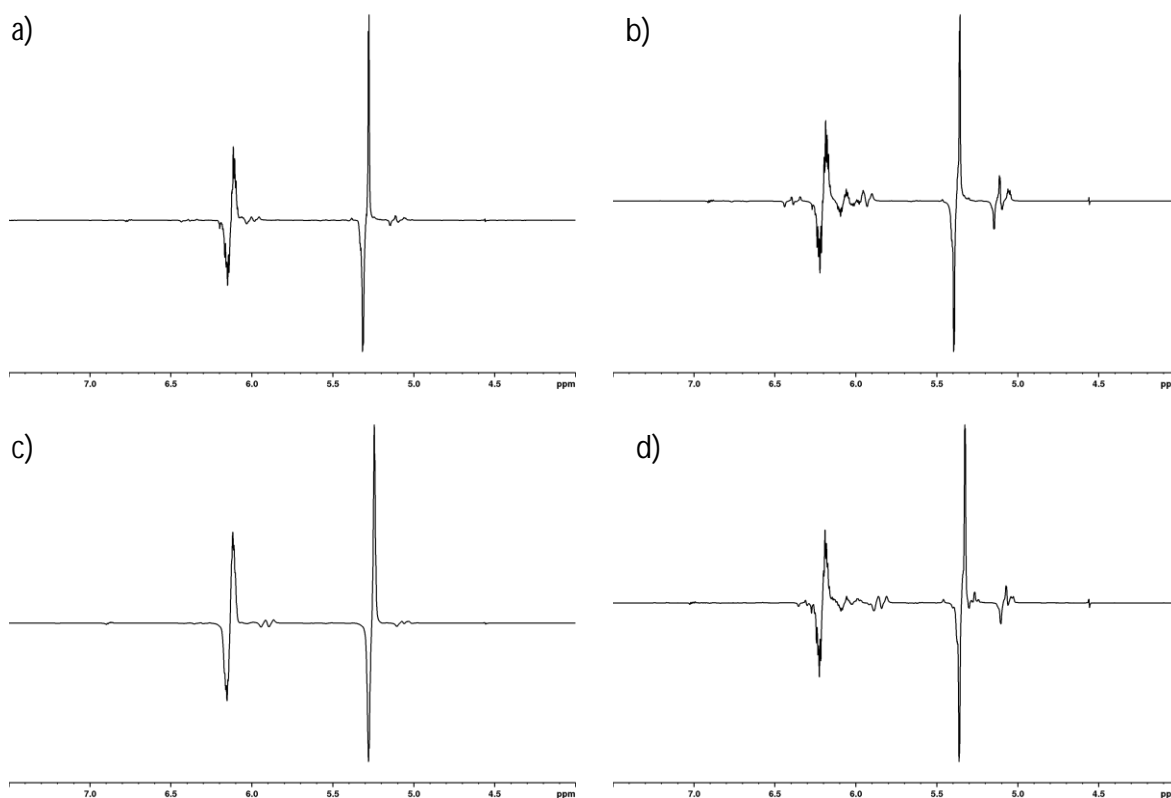
Figure 19 Overview of the 1H NMR 45° flip angle experiments of the hyperpolarized esters 17 (a), 18 (b), 19 (c), and 20 (d). The respective signals correspond to a) 33,000, b) 22,000, c) 12,000, and d) 3,200-fold signal enhancement compared to the thermally polarized signal. The small anti-phase signals shifted towards 5.8 and 5 ppm, respectively, may occur from catalyst bound species.

The release of the respective acetates and pyruvates of 17 and 18 could be achieved by the addition of water within a couple of seconds. After the hyperpolarization of a 2 mM substrate solution in 200 µL acetone-d_6, the NMR tube was transported through the magnetic field, the valve and tubing system was removed and 200 µL of 150 mM NaCl in water solution was added leading to 4.2% and 5.5% polarization on 1-^{13}C acetate and 1-^{13}C pyruvate measured after the return to the magnet. These experiments were performed multiple times until a quick handling was guaranteed and stable polarization values were measured over three consecutive experiments.

For the transfer of the polarization to the H-3 relay proton, block 1 of the pulse relayed ESOTHERIC NMR pulse sequence (Chapter 1.3.3.3) was used. The signal of the proton was amplified up to 18000 times (for 2-NBn-Ac-d_3). However, the most efficient transfer was obtained with 6-NV-Ac. Here, 65% of the initial polarization was obtained. For all molecules it was not possible to carry over the complete spin order from protons H^1 and H^2 to H^3. Losses during the transfer may be attributed to the non-zero J coupling of H^1 and H^3 (Figure 20).
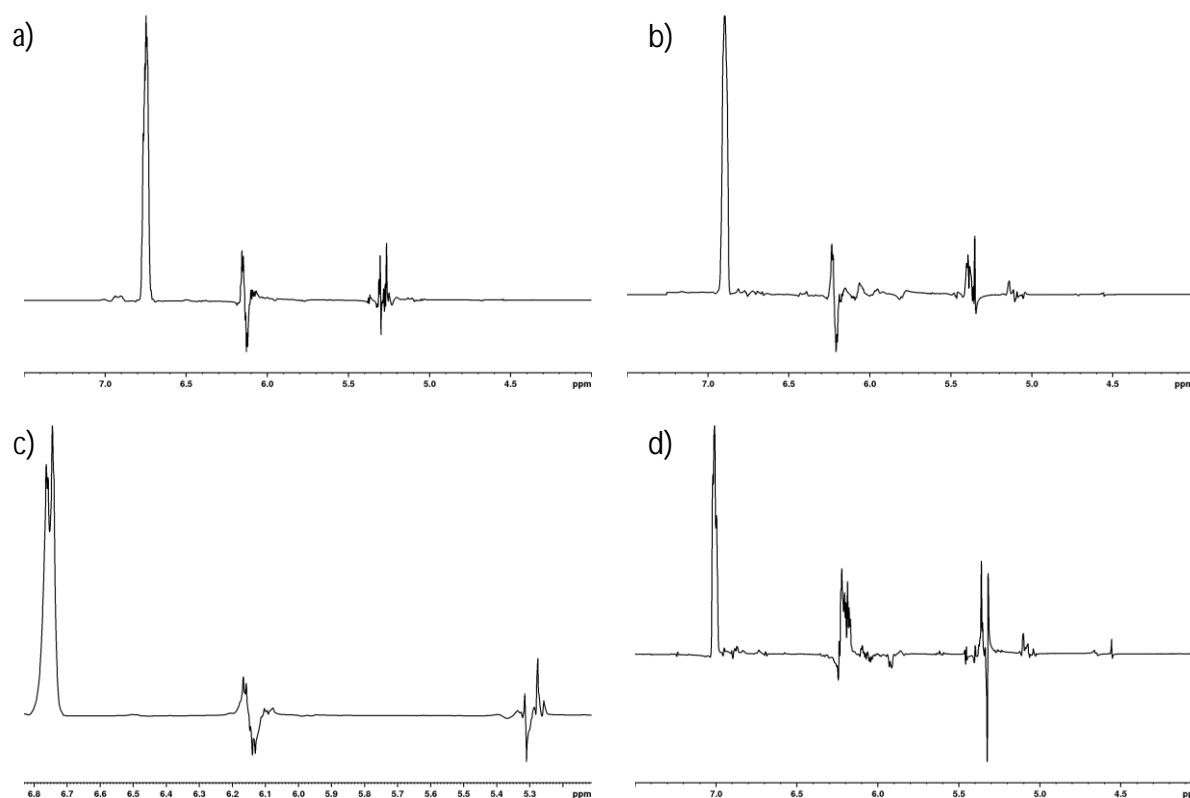
Figure 20 Zoomed spectra of the hyperpolarized ^{1}H spectra of the relay proton H-3. Here, spectra of the ester 17 (a), 18 (b), 19 (c) and 20 (d) with respective enhancements over their thermal signal of 17,000 (a), 15,000 (b), 7,000 (c) and 3,500-times (d). Especially for spectrum d, but also for spectra a-c an incomplete transfer from protons H-1 at around 5.25 ppm and H-2 at around 6.25 ppm is visible.

For the transfer to the heteronucleus, the length of pulse τ_4 was determined by numerical simulation. These simulations (see Appendix) resulted in delays with a certain efficiency for the transfer from H^3 to the ^{13}C. For the acetate esters a delay of 0.49 s for both side arms with an efficiency of 60% and 90% was determined, while the simulations suggested 0.617 s for the ester 18 and 0.444 s for the ester 20 with 75% and 50% efficiencies respectively.

The free metabolites were released with sufficiently high polarizations for cellular applications (^{13}C polarization acetate: 4.21% and pyruvate: 5.51%(Figure 21). As of note, the signals increased by a factor of 10,000-times (for the 1-^{13}C-pyruvate) allow 1 mM of hyperpolarized metabolite to have the same intensity as a 10 M solution of the same thermally polarized substance.

a)   b)
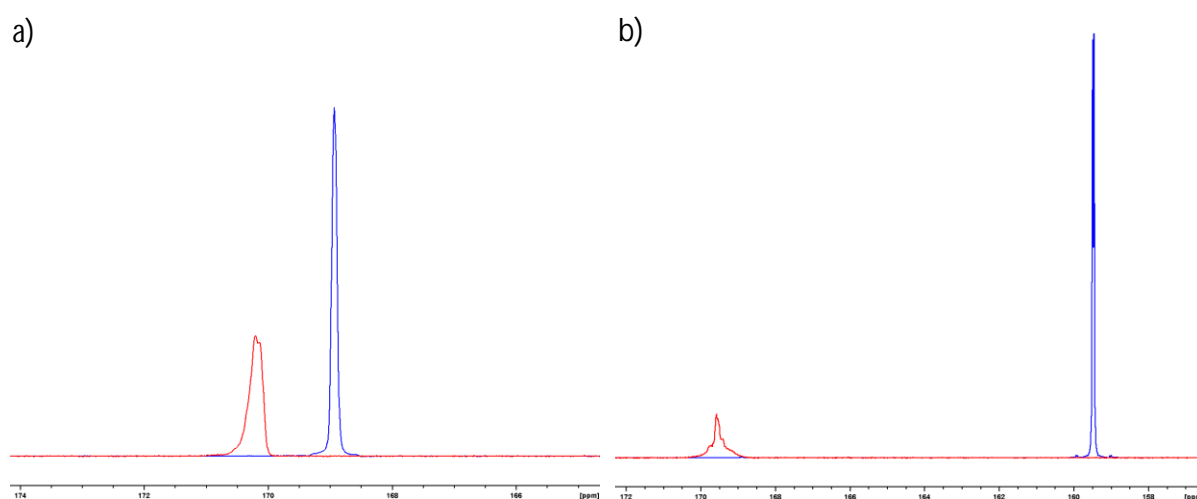
Figure 21 Zoomed ^{13}C NMR spectra of hyperpolarized 1-^{13}C-acetate-d_3 (spectrum a) and 1-^{13}C-pyruvate-d_3 (spectrum b) as an overlay of their hyperpolarized precursor (blue) and free metabolites (red). A clear shift of the signal before and after the cleavage (especially for the 1-^{13}C-pyruvate in b) indicates an excellent cleavage with no ester remaining in both cares. The hyperpolarized signals of the esters correspond to a signal enhancement of 9,000 and 10,000 for 1-^{13}C-acetate-d_3 and 1-^{13}C-pyruvate-d_3, respectively. The line broadening of the released molecule can be accounted to the inhomogeneity of the magnetic field, i. e. the sample was not shimmed as a fast measurement was required to maximize the measurable polarization.

3.3 Synthesis and hyperpolarization of N-acetyl-vinyl-d$_3$-1-^{13}C-alanine-2-d

Since the imaging with MRI is not only limited to metabolically active substances, a molecule for the investigation of blood flow and perfusion by hyperpolarized contrast agents was aimed to be synthesized. This molecule should both, not undergo any enzymatic conversion in the bloodstream and not be taken up into cells (except for clearance). For this purpose, the protein degradation product N-acetyl-alanine was considered suitable. A vinyl group was aimed to be incorporated at the carboxylic acid acting as the hyperpolarization site. For effective transvinylation with vinyl acetate as moiety source, acetylation of the amine must be performed beforehand as these reactions usually do not work out with strongly coordinating amines leading to very low yields regarding the desired ester product. Initially, all synthetic transformations were performed and optimized on the unlabeled variants of the molecules. In the following chapters, the results of the synthesis and the hyperpolarization are presented.

3.3.1 Synthesis of N-Acetyl-vinyl-d$_3$-L-1-^{13}C-alanine-2 (NAVA)

L-alanine was deuterated using the heterogeneous catalyst ruthenium on carbon (Ru/C) the C-2 of alanine reducing the couplings between this proton and the ^{13}C in the desired precursor. A 99% enantiomeric purity, 99.8% deuteration and 65% yield were obtained in the resulting amines 23 and 26. Subsequent acetylation of 23 and 26 was carried out in extra-dry methanol with acetic anhydride by full conversion (molecules 24 and 27). For the isotopically enriched molecule 26, the deuterated version of acetic anhydride was used to avoid any unforeseen interactions with the ^{13}C. Initially, the transvinylation did not produce large quantities of the desired esters 25 and 28. A large amount of the carboxylic acid had not dissolved in the vinyl acetate. By slightly heating the mixture at the beginning of the reaction, the acetylated alanine was dissolved and the desired product could be prepared. Different equivalents of vinyl acetate with regard to the cost intensive deuterated version were tested. Eight equivalents of vinyl acetate with respect to the used acetyl alanine gave the desired ester with 60% yield. The reactions with the isotopically labelled alanine gave similar yields over all three reaction steps Scheme 9.
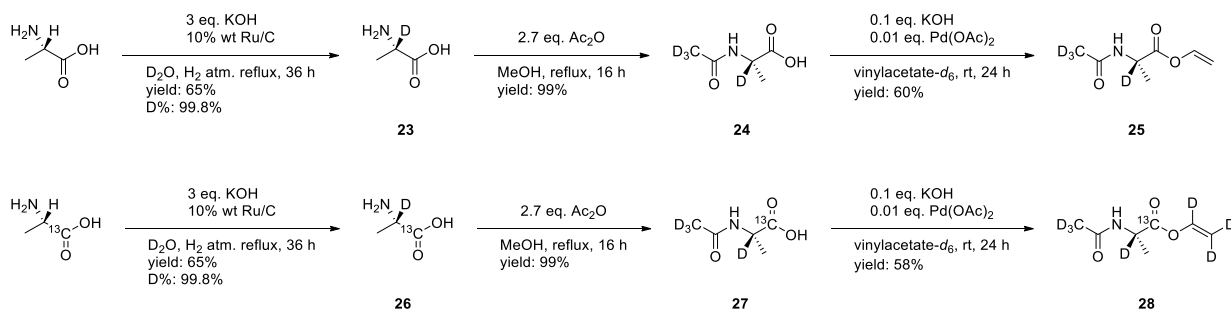
Scheme 9 Three step synthesis of the labeled and unlabeled versions of NAVA.

3.3.2 Hyperpolarization of NAVA

As described in chapter 3.2.2, the hyperpolarization of NAVA (28) was optimized with respect to the ratio of substrate to catalyst, the reaction time as well as the temperature. Only acetone-d_6 was considered as a reaction solvent, since a full dissolution in chloroform was not possible. Other solvents such as deuterated methanol would have needed an extensive exploration of a new purification method after the full hyperpolarization process in order to generate a biocompatible injection solution. To determine the initial polarization generated by the hydrogenation with parahydrogen, a ^{1}H experiment with 45° flip angle was used. On average, the measured spectra revealed an average polarization of 30%. Transferring the spin order from the protons onto the ^{13}C, an adapted version of the ESOTHERIC pulse sequence was used. For the relayed INEPT chains used in the ESOTHERIC sequence the couplings of the molecule had to be determined accurately (Figure 22).
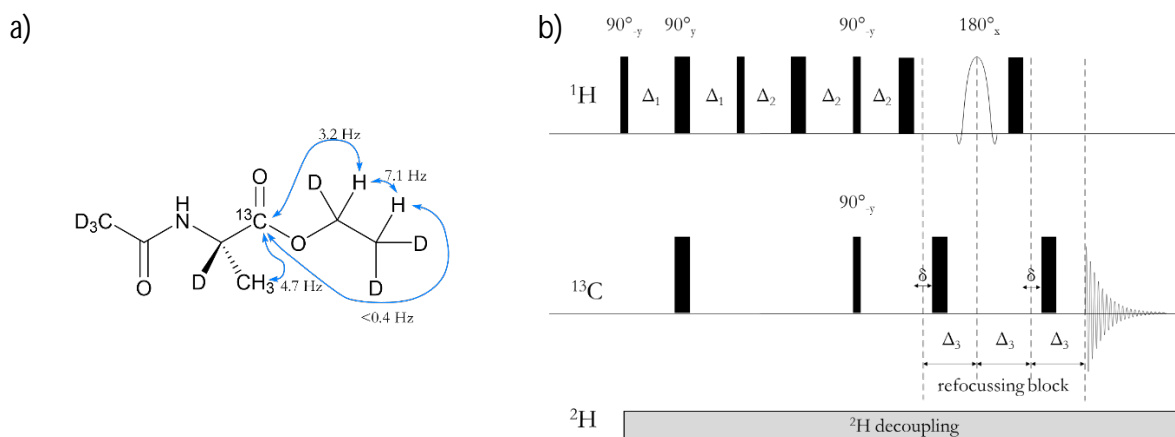
Figure 22 a) Detailed description of the coupling constants of the through parahydrogenation added protons at the ethyl group, the alanine methyl group and the C-1 ^{13}C. b) Modified ESOTHERIC pulse sequence with the durations between pulses of Δ_1 = 79.1 ms, Δ_2 = 79.1 ms, Δ_3 = 35.2 ms and the shift timing δ used for the decoupling of the methyl groups' protons from the 1-^{13}C.

Results

Since the coupling of the methyl group to the $C\alpha$ within the alanine moiety would cause drastic polarization losses during the transfer process, a block for selective ^{1}H decoupling was added to the sequence (Figure 22). By using the modified refocusing block 92% of the proton polarization was transferred to the [13]C. On the heteronucleus, an average of 28% polarization was measured, representing an enhancement of 50.000 times compared to the thermal signal.

The optimal reaction time for hyperpolarization of the vinyl ester was determined to be 10 s by means of ^{1}H polarization. Thus, polarization values of 30% were achieved (Figure 23 a).The transfer from protons to carbon was achieved with transfer rates (92%) and polarization levels of 28%. For the hyperpolarized material to be biocompatible, a workup procedure was performed for solvent exchange and catalyst removal. The time, the system was under vacuum, could be adopted from previous studies. By using the syringe filter, most of the catalyst was removed. This entire process required an average of 30 s (Figure 23 b).

a)   b)
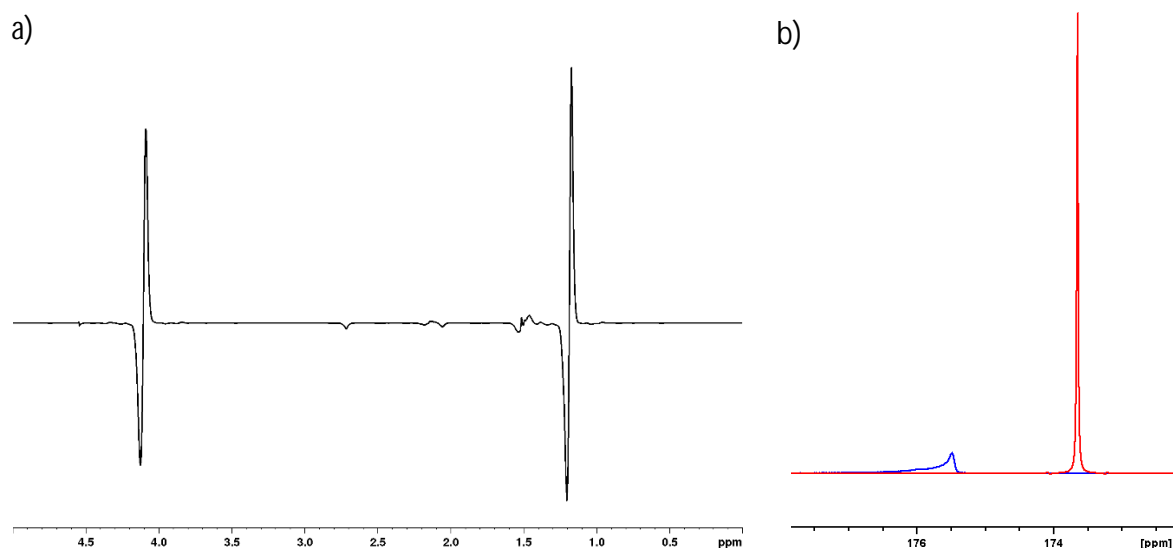
Figure 23 Zoomed ^{1}H and ^{13}C NMR spectra of hyperpolarized NAVA. In spectrum a) the signals of the hyperpolarized protons at 4.11 ppm and 1.19 ppm corresponding to the methylene and methyl protons added through parahydrogenation. The integrals of the signals are 13500 times enhanced compared to the thermal signal intensity (equals 30% polarization. In the ^{13}C spectrum b) the hyperpolarized signals of the 1-^{13}C of the alanine are shown in acetone-d_3 directly after the reaction in red and after the purification procedure in water in blue. The signal at 173.6 ppm in the red spectra is enhanced by 50.000 times while the blue signal at 175.5 ppm is enhanced by 12500 compared to their thermal intensity. The chemical shift difference can be accounted to solvent and temperature effects (hyperpolarization at 50 °C, aqueous solution at rt).

Since the hyperpolarized alanine derivative is intended to be available for injection into living animals, a purification procedure was carried out after the polarization transfer was completed. This requires the solvent acetone to be removed by evaporation and the rhodium complex by filtration. Previous experiments showed that the use of special syringe filters is perfectly sufficient to reduce the remaining rhodium concentration well below the lethargic dose for rodents. The

purification procedure follows a well-timed choreography starting immediately after the transfer. After the release of the overpressure, the isotonic saline solution is added. The NMR tube is placed under vacuum and subsequently the aqueous solution of the hyperpolarized material is drawn up through a filter using a syringe. For the evaluation of the polarization still present, the syringe volume was added to a fresh NMR tube, but the liquid is also ready to be injected into an animal. After the purification steps, an average polarization of 6.63% was measured (Figure 24).

Figure 24 Purification procedure for hyperpolarized compounds in organic solvents. After the transfer (outer left spectrometer, t = 10 s), the NMR tube is taken out of the magnet and the isotonic aqueous solution (A) is added while a strong vacuum is applied (second spectrometer from the left, t = 20 s). Since the aqueous solution contains some rhodium complex (most of it precipitated) the solution is filtered (C) and ready to I) be injected into a fresh NMR tube (B and D) or II) or transported to the animal imaging system.

4 Discussion

The access to novel precursor molecules for hyperpolarization with parahydrogen are of great medical interest.[124] The hyperpolarized substances can be used to obtain metabolic data in real time, providing information about the state of a disease or assisting in making a comprehensive diagnosis.[27] Other molecules could provide valuable information about the cardiovascular system without metabolic activity. In order to perform such medical examinations, it is necessary to synthesize novel molecules that allow high polarization values and long observation times. For this in this work proton deuterium exchange reactions were performed (extended observation time), new side arms for hyperpolarization were prepared and these were linked to significant molecules.

4.1   Deuteration of sodium pyruvate and pyruvic acid

For the investigation of biological systems, the longest possible traceability of the molecules investigated is desired. Thus, a robust deuteration of 1-^{13}C pyruvate, either from sodium 1-^{13}C pyruvate or 1-^{13}C pyruvic acid, must be established. Even though the influence of deuteration of the target molecule is well known only little focus was paid to the exploration of effective deuteration methods in terms of in coupling ranges of the observed nuclei and the hyperpolarization site, especially regarding pyruvate. As pyruvate is known to be a potent contrast agent for MRI cancer studies, which (hyperpolarized by DNP) is already in clinical trials, high quality procedures reducing side products while affording high yields are needed. Pyruvate itself is a sensitive molecule that, for example, reacts with itself to form parapyruvate or zymonic acid if stored for too long. The purification of pyruvate is difficult on a laboratory scale due to its chemical and physical properties. Chromatographic methods often lead to decomposition and distillation is difficult because removal from organic extracts leads to the formation of dimers as well as azeotropic mixtures with the organic solvents.

In the literature, the deuteration of Na-1-^{13}C-pyruvate using D_2SO_4 in D_2O under high temperatures and the reaction of 1-^{13}C pyruvic acid with sodium bicarbonate in D_2O are used. However, even by repeating the described procedures several times, it was not possible to achieve the outstanding yields and degrees of deuteration, especially for sodium bicarbonate. These syntheses led to the production of undesirable by-products such as parapyruvate, hydroparapyruvate or zymonic acid in significant amounts. In order to improve the effectiveness

of the proton-deuterium exchange, different bases were tested for deuteration with both pyruvate sources (Table 2, chapter 3.1). For proof of principle, these reactions were carried out exemplarily with the non-labelled compounds.

The deuteration using D_2SO_4, which is well known for sodium 1-^{13}C pyruvate deuteration reactions, provided the conversion of 60% of the starting material to parapyruvate in addition to excellent degrees of deuteration (over 99% deuteration, overall yield 39%). Significantly better yields in terms of the pyruvate were obtained by using sodium carbonate for deuteration. Here, too, very high deuterium contents (over 99%) and 60% yields were obtained for the pyruvate-d_3.Using the free acid as starting material, very good deuteration (99.5% D incorporation) and acceptable pyruvate yields were produced using Et3N and a 1:1 mixture of heavy water and THF. In this process, hardly any by-product formation could be observed.

One section of the reactions which usually results in high losses of the compound, is the work up procedure. Due to the fact that the desired product is the carboxylic acid and not the sodium salt, pH adjustments to fully protonate the functional group were unavoidable to extract pyruvate from the aqueous phase. On average over 20 extraction steps were necessary to remove the α keto acid entirely. Evaporation of the organic solvents had to be performed very carefully due to co-evaporation and a low boiling point of the deuterated pyruvates themselves. Although the boiling point of pyruvate has a variety of reported temperatures (from 62 °C reported by TCI Chemicals to 165 °C reported by Sigma Aldrich) no literature data was available for deuterated pyruvate or even 1-^{13}C-pyruvate-d_3. During the studies we found that pyruvate-d_4 is even more volatile with a boiling point of roughly 54 °C. These findings explain why for all reactions at least traces of the extraction solvents were found to be present in the NMR spectra (see Appendix).

For a laboratory scale the described deuteration with the amine base was sufficient to accomplish the desired purity. Losses of 40% and more seem under the here tested conditions are unavoidable. For large scale production of precursors for the in vivo investigation using hyperpolarized 1-^{13}C-pyruvate-d_3 by means of parahydrogen, an approach to use deuterated starting materials synthesizing deuterated pyruvate directly, not by proton-deuterium exchange, may be considered.

4.2   Synthesis and hyperpolarization of 2-Nitrobenzyl based side arms

One of the most effective ways to hyperpolarize metabolites with parahydrogen is to use unsaturated sidearms with a subsequent transfer of the polarization from the added protons to the target moiety. Many of the highly metabolized molecules contain a carboxylic acid function, which

allows the assembly of esters. Simple structures such as vinyl esters are particularly popular, since they offer an established and effective transfer of polarization by using a specific pulse sequence (for example, ESOTHERIC). For the use in biological systems, however, it is usually necessary to cleave off the unwanted side arm making the metabolite accessible for biological conversions. Yet, this is not possible without the use of additional chemicals. Hydrolysis of vinyl pyruvate for example, requires a 75 mM solution of Na_2CO_3 followed by pH neutralization. The process takes time and, in the end, costs polarization, which would help to elongate the time to observe downstream metabolism. Therefore, a new class of side arms was developed for this work based on the light sensitive ortho-nitrobenzyl group. The side arm was equipped with a propargyl moiety as hyperpolarization side and coupled with acetates and pyruvates (both with natural abundance isotopes and ^{13}C and ^{2}H enrichment). It was examined how the influence of further modifications on the benzyl ring affects the polarization. For this purpose, derivatives based on (iso-)vanillin and 4,5-dimethoxy-2-nitrobenzaldehyde were prepared. In order to introduce the nitro group into the aromatic system (of isovanillin and vanillin), a benzyl protection of the aromatic alcohol was used favoring the C-2 nitration. Otherwise, the strong -I and -M effect of the aldehyde in position 1 would have led to the preferred nitration of the C-3. However, it was possible to produce good yields of the C-2 nitrated arenes due to the high steric hindrance as well as control of the reaction temperature. The influence of the bulkiness of the protection group on the nitration was reduced when used on the C-5 OH (iso-vanillin) compared to the C-4 OH (vanillin).

The incorporation of the unsaturated bond was achieved by Grignard reaction of the aldehyde. The ethynyl magnesium bromide Grignard was used because the deuteration of terminal triple bonds is well established and, in contrast to a possible allyl alternative, no corresponding deuterated Grignard had to be elaborately prepared. Effective deuteration was achieved using a solvent mixture of D_2O and THF and the base Et_3N. In contrast to alternative proton deuterium exchange reactions using K_2CO_3 in acetonitrile and D_2O, consistently no by-product formation was observed so that the amino base based method could be regarded as more robust.

For the esterification with the corresponding carboxylic acids, various methods for the formation of the secondary esters were tested. Here, optimization was mainly performed with respect to the final yield, but also with respect to the usage of the deuterated and ^{13}C labelled acids. However, the results were not completely transferable to the isotopically enriched metabolites. Various factors such as the kinetic isotope effect may have had an influence here.[125, 126] The latter describes the influence of the heavy isotopes on the reactivity and energy of the transition states. Simplified, the reactivity is reduced by the increase of the atomic radius, while the energy required to form bonds increases resulting less reactive reagents leading to lower yields during transformations involving

the respective nuclei. The 1-^{13}C-pyruvate-d_3 esters proved to be particularly difficult here. In chapter 4.1, the deuteration of pyruvate was discussed in more detail. The majority of esterifications were carried out using D_2SO_4 deuterated pyruvate, which is why a large proportion of the material used was contaminated with parapyruvate. Proton deuterium exchange achieved by Et_3N for pyruvate was used in the later stages of the work resulting in slightly improved yields.

In general, the synthesized sidearms would be polarized very well. Excellent values were obtained with proton polarizations of up to 62%. It should be noted that the acetates achieve more than twice as strong proton polarizations as the pyruvate esters (2-NBn: 2.27 times higher; 6-NV: 2.35 times higher).

The significantly lower polarization of a keto acid may be explained by several phenomena. Due to the additional keto group, there can be a stronger interaction between substrate and catalyst, which then leads to relaxation due to the paramagnetic behavior of the rhodium catalyst. In addition, the longer reaction time also affects the detectable polarization due to relaxation processes. For both systems, acetate and pyruvate ester, there is another common source for the loss of polarization. At the catalyst itself, the binding of the parahydrogen can partially convert the hydrogen back to orthohydrogen, again due to the paramagnetic rhodium center. Previous experiments showed that around 20% of the parahydrogen can be converted back to oH_2.[93]

Considering the calculated transfer efficiency to the ^{13}C, molecules 17, 18, and 19 performed very well under the tested conditions. Only the ester 20 exhibited undesirable mixing of spin states because of H^1-H^3-coupling of 1.25 Hz and H^3-1-^{13}C coupling of 2.75 Hz. As a result, a pure in-phase spin state of the ^{13}C signal could not be detected.

The hydrolysis of the esters 17 to 20 was investigated based on the challenges regarding the polarization transfer using the 4,5-dimethoxy-2-nitrobenzyl side arm using only the esters of 2-NBn. Adding water immediately after the hyperpolarization resulted in the cleavage of the ester without the need of additional irradiation with light. Interestingly, the water sensitivity seemed to be purely the case after the hyperpolarization at the elevated temperatures of the reaction. The alkyne ester itself was stable for several minutes even at pH values of 5 or 9 respectively over a period of 10 minutes (maybe even longer, observation was stopped after this time, spectra see appendix). This allows reagent-free hydrolysis without the light-induced generation of radicals that could have potentially led to relaxation of polarization.

Initially, the cleavage of the precursor resulting in free MOIs was aimed to be performed by UV light, comparable to the commonly known usage of these moieties.[127-129] Under these circumstances a photon induces a radical formation in the NO_2 group leading to an electronical

rearrangement through the benzyl ring and the abstraction of the relay proton (Scheme 10). Thus, a negatively charged oxygen of the nitro group is able to perform an intramolecular ring formation unstable enough to decompose into the metabolite of interest and nitroso containing side arm. During the experiments it was found that the secondary allyl esters were dissociating by the addition of water, which is needed for biological applications.
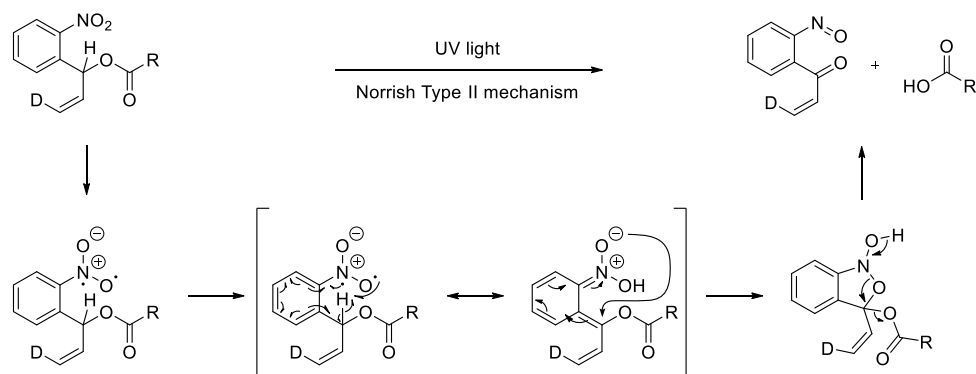
Scheme 10 Intended UV light induced cleavage of the side arm. The light induces radical formation in the nitro group by breaking the N=O π-bond leading to a diradical exited state. The electron rearrangement through the benzyl ring leads to a nucleophilic attack of the nitro oxygen forming a five membered ring. The instability of this construct lead to decomposition of the ring structure releasing the desired carboxylic acid.[130]

Due to the aimed photo liability, it was proposed to let cells take up the whole precursor and then irradiate the sample with UV light leading to a distinct starting point of tracing metabolic action and thus resulting in more precise measurements regarding the conversion kinetics. For the cleavage an optical fiber surrounded NMR tube was prepared yielding in a homogeneous irradiation of the whole sample. Due to the anticipated internalization of the precursor, modifications on the benzyl ring were planned for the delivery of the pyruvate to certain compartments of the cell. However, the unexpected release of the metabolite by the addition of water opens up a new perspective of the potential usability of this molecule.

Yet, the actual cleavage mechanism was not further investigated. Due to the resulting allyl group and the similarities to the alloc protection group a few different ways can be proposed. The simplest explanation is the instability of the secondary ester and the resulting greater sensitivity to nucleophiles such as water. Furthermore, the interaction of the double bond with the catalyst could further weaken the ester bond and thus further facilitate hydrolysis. As a result, the release of the carboxylic acid could be greatly facilitated. A further option is the adaptation of the deprotection mechanism of the allyl protecting group.[131-133] Oxidative addition of the allyl with the rhodium catalyst after the coordination results in the π-allyl Rh intermediate. Decarboxylation takes place before water, as a nucleophile, can perform a reductive attack on the π-complex. The complex then

decomposes releasing the side arm (Scheme 11). Usually, palladium on carbon is used to perform these deprotection reactions but a few examples can be found, where rhodium-based catalysts were used. Generally, these reactions take several hours for completeness, but here a few seconds were needed for full conversion. This might be due to the equimolar concentration of the catalyst and the substrate.
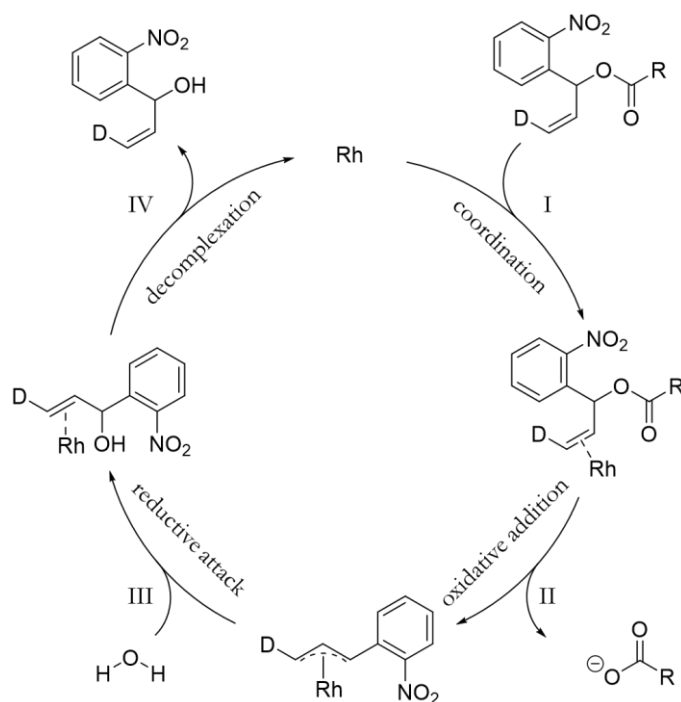
Scheme 11Proposed catalytic ester hydrolysis adapted from the alloc deprotection mechanism with Rh as representation of the hydrogenation catalyst 1,4 Bis-(diphenylphosphino)-butane) rhodium. The catalytic cycle initiates with the coordination of the allyl group (I). This may already have happened during the hydrogenation with pH_2. The oxidative addition can form a π-complex leading to the hydrolysis of the ester and the release of the carboxylic acid (II). Water can act as a nucleophile attacking the π-complex (III) leading to the decomposition of the catalyst substrate interaction (IV).

In comparison to the measured polarization directly after the transfer, the spin order of the free 1-^{13}C-pyruvate-d_3 is quite lower. However, most of the polarization is currently lost in the process of removing the sample from the magnet and performing the cleavage by hand. Since no pH adjustment is required as no base is needed for the release, this molecule perfectly suits the purpose of automatization. For every molecule a tedious tuned cleavage procedure has to be elaborated regarding the used base, their concentration and the respective salt content when the molecule is concerned to be used for injection into living beings. With this presented side arm, it might be possible to avoid these problems especially for (pH) sensitive molecules, since the ester cleavage can be induced by water for the here presented molecules. Of course, if this side arm is aimed to

be used as a general hyperpolarization moiety coupled to a variety of different carboxylic acids water sensitivity has to be proven on each individual construct.

4.3 Synthesis and hyperpolarization of N-acetyl-vinyl-d₃-L-1-¹³C-alanine-2-d

In the early 2000s, parahydrogen hyperpolarized ^{13}C labelled contrast agents were for the first time tested for angiography in animals. The used hydroxyethylproponate achieved high ^{13}C polarizations of over 30% with T_1 times of 45 s. However, this molecule was unsuitable for human studies due to its toxicity. Therefore, a new contrast agent based on endogenous substances was developed for angiography imaging. In particular, degradation products that are tolerated in higher concentrations and not taken up into the cells can be used for this purpose. Thus, N-acetyl-alanine, a common degradation product of proteolysis, proved to be suitable. To hyperpolarize the alanine, an unsaturated carbon-carbon bond was introduced by means of a deuterated vinyl group. An internal unsaturated carbon-carbon bond was not considered to be used due to the close proximity of the amine possibly leading to a more complex hydrogenation reaction. As vinyl esters are well established, it was preferred to use the side arm approach instead of an intrinsically hyperpolarization site.

4.3.1 Synthesis of N-Acetyl-vinyl-d₃-L-1-¹³C-alanine-2-d

Under consideration of the insights gained with earlier work using hyperpolarization techniques with alanine, certain modifications to the chemical structure had to be made. As described by Kaltschnee et al. the coupling of the ^{13}C to the C-2 proton led to fast relaxation of the polarization, in this work, the proton at the chiral center was replaced by a deuterium atom. To avoid any further unknown interactions, the acetyl group protecting the nitrogen was introduced deuterated. In addition, the vinyl group used had to be deuterated, otherwise losses of polarization of an order of magnitude could be expected here as well (Scheme 12). Deuteration of the methyl group was not possible. All tested methods known from the deuteration of pyruvic acid (Chapter 3.1) were tested, without the desired deuteration degrees. Repetition, temperature adjustments and more equivalents of reagents did not improve the exchange over a very small degree. An NMR pulse sequence already established in the laboratory could be used for selective decoupling of the methyl group. This only required small adjustments of the coupling constant-dependent timing for the pulses determined by adjusting simulations implemented by L. Kaltschnee (see Appendix).
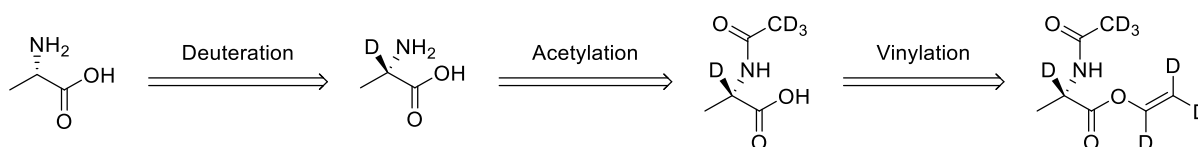
Scheme 12 Synthesis of N-Acetyl-vinyl-d$_3$-L-alanine-2-d.

For the proton deuterium exchange, a procedure known from the literature was carried out. When performing the reaction, special attention was paid on a good mixing of the reaction while the hydrogen was flowing through. The dissolved H$_2$ activates the surface of the catalyst, allowing D$_2$O to bind and perform proton deuterium exchange through the surface interaction (Figure 25). The reaction takes place with preservation of chirality. From the proposed mechanism, it can be assumed that the interaction of C and N with two neighboring Ru atoms form a rigid dimetallic cycle. This allows only the exchange of proton to deuterium under the retention of the chirality.[134]
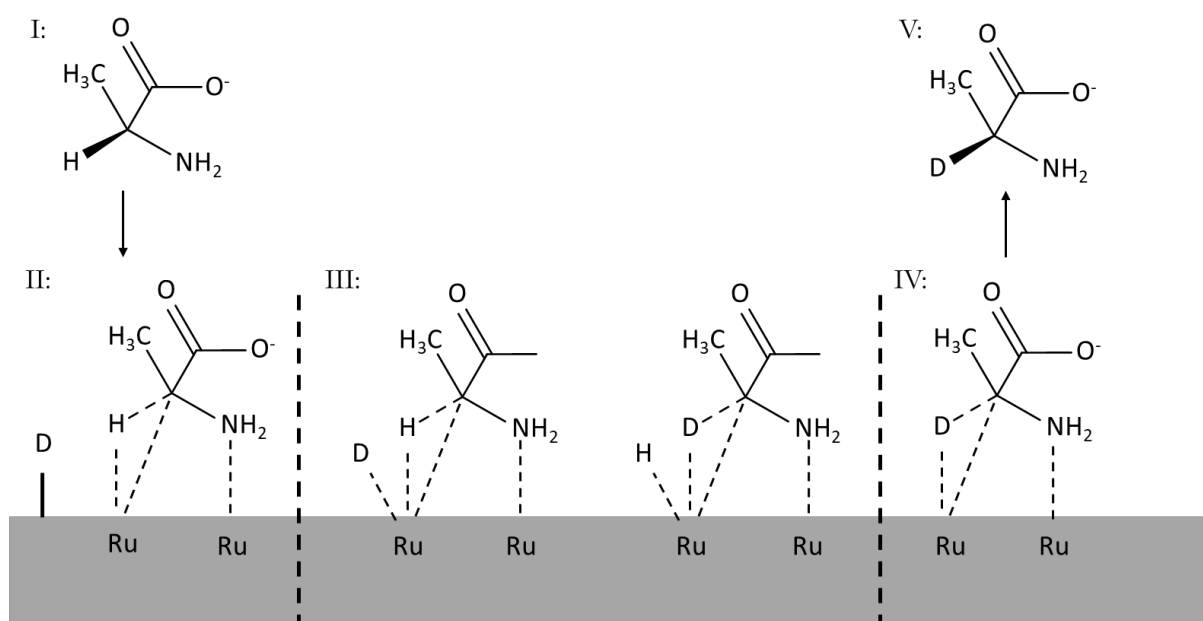
Figure 25 Mechanism for deuteration of alanine with H2 as activator of Ru/C catalyst at 100 °C. I) Association of the amino acid to the catalyst. II) C-H activation by rhodium. III) H/D exchange at the catalytic center. IV) Reductive elimination of the alanine. V) Removal of the amino acid from the catalyst.

The chirality was confirmed by optical rotation measurements. To double check that 1-^{13}C-L-alanine is in the right confirmation it was not only compared to literature/distributor values but also with L-alanine-d$_4$ showing comparable values (optical rotation of: 1-^{13}C-alanine-2-d: 2.27; L-alanine-d$_4$: 2.35; L-alanine, from literature: 2.42). The little lower value of 1-^{13}C-alanine-2-d can be explained by the isotopically enriched 1-^{13}C of the synthesized alanine.

Acetylation of the amine was achieved under standard conditions and full conversion. Regarding the transvinylation, again some losses had to be considered for the isotope-enriched synthesis with

1-^{13}C-alanine. As with the 1-^{13}C labelled substances from Chapter 4.2, isotope effects can similarly be assumed to be involved. Over the entire synthesis, yields of 35.6% for the unlabeled alanine and 34.4% for the 1-^{13}C-alanine can be reported. Since the final product is hygroscopic, a water free storage had to be ensured to avoid contamination leading to lower polarization values.

4.3.2   Hyperpolarization of N-Acetyl-vinyl-d$_3$-L-1-^{13}C-alanine-2-d

Hyperpolarization with parahydrogen focuses primarily on downstream metabolites of the glucose metabolism and thus also the citric acid cycle in the development of imaging contrast agents. However, amino acids also offer exciting applications and facilitate the study of other pathologies. Previous attempts to polarize amino acids or their derivatives and subsequently transfer those into water have yielded quite low polarizations. Polarizations of 4.4% were only achieved on an alanine side arm and only in D_2O. Injection of larger quantities of D_2O leads to problems for the organism which is why H_2O is the preferred solvent for injections. With the hyperpolarization of acetyl-protected vinyl alanine here, polarizations of 6.63% were reached in protonated water.

To ensure the most effective transfer to the ^{13}C, the adapted ESOTHERIC sequence was fine-tuned. The influence of the so-called settling time, i. e. the time in which the pH$_2$ bubbles drift upwards from the liquid, should not be underestimated. This time differs significantly from the time used for the pyruvate and acetate esters (Ala:0.5 s, pyruvate: 0.35 s, acetate 0.25 s). It can be assumed that due to the close proximity of the amine to the unsaturated C-C bond, longer residence times occur at the catalytic center. Especially in the case of free amines, this effect is so pronounced that significant losses of polarization can be observed.

The polarization transferred to the ^{13}C was mainly lost during the z-flip prior the removal of the NMR tube from the magnet. During this process a loss of roughly half of the polarization (depending on how well the sample was shimmed) can be expected. For further studies, a shaped pulse for the transfer of the polarization into the Z direction can be elaborated to reduce the loss of polarization during this process. Since the whole work up procedure took about 30 a reduction of polarization to a ¼ was anticipated as the preservation of polarization in this case is mainly T_1 dependent (T_1= 31 sec).

The results presented in this section show that it is possible to bring amino acid derivatives to inducible polarization values. The measurements shown here exhibit a consistency that ethically justifies the use of NAVA as a potential contrast agent for angiography.

5 Outlook

In this work, new approaches to signal amplification using parahydrogen for magnetic resonance-based techniques are presented. To this end, new solutions regarding the problem of deuteration of pyruvate were found, new synthetic routes to access the first additive-free release of metabolites in the SAH approach were examined, and the first amino acid derivative hyperpolarized with parahydrogen was investigated in living animals.

Reactions involving sensitive substances such as pyruvate are often accompanied by undesirable byproducts. Here, a mild deuteration approach to complete hydrogen deuterium exchange was established. In contrast to previous methods, this does not require strong inorganic acids or bases, operates in a biphasic solvent system, and thus allows a lower by-product access to deuterated pyruvate on a laboratory scale. The extent to which this approach can be transferred to larger scales has not been further explored. However, it was clearly shown that the selection of raw materials (e.g. pyruvic acid) can introduce impurities into further syntheses, which may have a negative impact on subsequent transformations.

Here, for the first time, hyperpolarized metabolite precursor constructs were cleaved by the addition of water to give bioavailable pyruvate and acetate. In the process, a facile synthesis of potent sidearms was established that could display proton polarizations of up to 62% and carbon polarizations of up to 28%. The release of MOIs also occurred within a few seconds. Regarding this sidearm metabolite construct, we expect easier access to hyperpolarized molecules in the future without having to perform time-consuming or elaborate purification procedures.

Access to hyperpolarized amino acids and their derivatives has proven to be extremely difficult with parahydrogen-based techniques. With the high-yield preparation of N-acetyl-vinyl-alanine, it is now possible for the first time to bring amino acid derivatives to ^{13}C polarization levels above 6% ^{13}C polarization. This opens up new possibilities in terms of clinical diagnostics, metabolism studies as well as angiography.

We hope that the successful hyperpolarization of amino acids and the easier access to metabolites such as pyruvate will play an important role in the evolution away from contrast agents, whose long-term effects on the human body are unknown, towards endogenous substances that can give

us a deeper and more accurate insight into diseases in a way that conventional heavy metal contrast agents simply are not able to do.

6 References

[1] D. A. Leon, Trends in European life expectancy: a salutary view. International Journal of Epidemiology 2011, 40, 271-277.

[2] F. R. Lichtenberg, How many life-years have new drugs saved? A three-way fixed-effects analysis of 66 diseases in 27 countries, 2000–2013. International Health 2019, 11, 403-416.

[3] J. D. C. Buxbaum, Michael E; Fendrick, A Mark; Cutler, David M, Contributions Of Public Health, Pharmaceuticals, And Other Medical Care To US Life Expectancy Changes, 1990-2015. Health Affairs 2020, 39, 1546-1556.

[4] W. MacNee, R. A. Rabinovich, G. Choudhury, Ageing and the border between health and disease. European Respiratory Journal 2014, 44, 1332-1352.

[5] T. Niccoli, L. Partridge, Ageing as a Risk Factor for Disease. Current Biology 2012, 22, R741-R752.

[6] J. S. Rana, S. S. Khan, D. M. Lloyd-Jones, S. Sidney, Changes in Mortality in Top 10 Causes of Death from 2011 to 2018. J Gen Intern Med 2021, 36, 2517-2518.

[7] F. B. Ahmad, R. N. Anderson, The Leading Causes of Death in the US for 2020. JAMA 2021, 325, 1829-1830.

[8] M. A. Rubin, Understanding Disease Cell by Cell. Science 2002, 296, 1329-1330.

[9] H. Zhu, J. Fan, J. Du, X. Peng, Fluorescent Probes for Sensing and Imaging within Specific Cellular Organelles. Accounts of Chemical Research 2016, 49, 2115-2126.

[10] C. R. Bowers, D. P. Weitekamp, Transformation of Symmetrization Order to Nuclear-Spin Magnetization by Chemical Reaction and Nuclear Magnetic Resonance. Physical Review Letters 1986, 57, 2645-2648.

[11] S. J. Nelson, J. Kurhanewicz, D. B. Vigneron, P. E. Z. Larson, A. L. Harzstark, M. Ferrone, M. van Criekinge, J. W. Chang, R. Bok, I. Park, G. Reed, L. Carvajal, E. J. Small, P. Munster, V. K. Weinberg, J. H. Ardenkjaer-Larsen, A. P. Chen, R. E. Hurd, L.-I. Odegardstuen, F. J. Robb, J. Tropp, J. A. Murray, Metabolic Imaging of Patients with Prostate Cancer Using Hyperpolarized [1-^{13}C]Pyruvate. Science Translational Medicine 2013, 5, 198ra108-198ra108.

[12] T. Hune, S. Mamone, H. Schroeder, A. P. Jagtap, S. Sternkopf, G. Stevanato, S. Korchak, C. Fokken, C. A. Müller, A. B. Schmidt, D. Becker, S. Glöggler, Metabolic Tumor Imaging with Rapidly Signal-Enhanced 1-^{13}C-Pyruvate-d_3. ChemPhysChem, n/a.

[13] K. Golman, O. Axelsson, H. Jóhannesson, S. Månsson, C. Olofsson, J. S. Petersson, Parahydrogen-induced polarization in imaging: Subsecond ^{13}C angiography. Magnetic Resonance in Medicine 2001, 46, 1-5.

References

[14]   R. Ventura-Clapier, A. Garnier, V. Veksler, Energy metabolism in heart failure. The Journal of Physiology 2004, 555, 1-13.

[15]   M. Ogawa, H. Fukuyama, Y. Ouchi, H. Yamauchi, J. Kimura, Altered energy metabolism in Alzheimer's disease. Journal of the Neurological Sciences 1996, 139, 78-82.

[16]   T. N. Seyfried, L. M. Shelton, Cancer as a metabolic disease. Nutrition & Metabolism 2010, 7, 7.

[17]   F. Yin, H. Sancheti, I. Patil, E. Cadenas, Energy metabolism and inflammation in brain aging and Alzheimer's disease. Free Radical Biology and Medicine 2016, 100, 108-122.

[18]   L. R. Gray, S. C. Tompkins, E. B. Taylor, Regulation of pyruvate metabolism and human disease. Cellular and Molecular Life Sciences 2014, 71, 2577-2604.

[19]   O. Warburg, F. Wind, E. Negelein, The Metabolism of Tumors in the Body. Journal of General Physiology 1927, 8, 519-530.

[20]   I. Martínez-Reyes, N. S. Chandel, Cancer metabolism: looking forward. Nature Reviews Cancer 2021, 21, 669-680.

[21]   J. M. Garcia-Heredia, A. Carnero, Decoding Warburg's hypothesis: tumor-related mutations in the mitochondrial respiratory chain. Oncotarget 2015, 6.

[22]   B. L. Woolbright, G. Rajendran, R. A. Harris, J. A. Taylor, III, Metabolic Flexibility in Cancer: Targeting the Pyruvate Dehydrogenase Kinase:Pyruvate Dehydrogenase Axis. Molecular Cancer Therapeutics 2019, 18, 1673-1681.

[23]   J. M. Brown, A. J. Giaccia, The Unique Physiology of Solid Tumors: Opportunities (and Problems) for Cancer Therapy. Cancer Research 1998, 58, 1408-1416.

[24]   R. Bar-Shalom, A. Y. Valdivia, M. D. Blaufox, PET imaging in oncology. Seminars in Nuclear Medicine 2000, 30, 150-185.

[25]   W. T. Rahman, D. J. Wale, B. L. Viglianti, D. M. Townsend, M. S. Manganaro, M. D. Gross, K. K. Wong, D. Rubello, The impact of infection and inflammation in oncologic ^{18}F-FDG PET/CT imaging. Biomedicine & Pharmacotherapy 2019, 117, 109168.

[26]   K. M. Brindle, S. E. Bohndiek, F. A. Gallagher, M. I. Kettunen, Tumor imaging using hyperpolarized ^{13}C magnetic resonance spectroscopy. Magnetic Resonance in Medicine 2011, 66, 505-519.

[27]   Z. J. Wang, M. A. Ohliger, P. E. Z. Larson, J. W. Gordon, R. A. Bok, J. Slater, J. E. Villanueva-Meyer, C. P. Hess, J. Kurhanewicz, D. B. Vigneron, Hyperpolarized ^{13}C MRI: State of the Art and Future Directions. Radiology 2019, 291, 273-284.

[28]   K. Golman, R. i. t. Zandt, M. Lerche, R. Pehrson, J. H. Ardenkjaer-Larsen, Metabolic Imaging by Hyperpolarized ^{13}C Magnetic Resonance Imaging for in vivo Tumor Diagnosis. Cancer Research 2006, 66, 10855-10860.

References

[29] K. Golman, J. S. Petersson, P. Magnusson, E. Johansson, P. Åkeson, C.-M. Chai, G. Hansson, S. Månsson, Cardiac metabolism measured noninvasively by hyperpolarized ^{13}C MRI. Magnetic Resonance in Medicine 2008, 59, 1005-1013.

[30] A. J. M. Lewis, D. J. Tyler, O. Rider, Clinical Cardiovascular Applications of Hyperpolarized Magnetic Resonance. Cardiovascular Drugs and Therapy 2020, 34, 231-240.

[31] S. Wann, J. Tunio, Current challenges and future directions in cardiac imaging. Journal of the Saudi Heart Association 2010, 22, 121-124.

[32] S. Aime, P. Caravan, Biodistribution of gadolinium-based contrast agents, including gadolinium deposition. Journal of Magnetic Resonance Imaging 2009, 30, 1259-1267.

[33] R. J. McDonald, J. S. McDonald, D. F. Kallmes, M. E. Jentoft, D. L. Murray, K. R. Thielen, E. E. Williamson, L. J. Eckel, Intracranial Gadolinium Deposition after Contrast-enhanced MR Imaging. Radiology 2015, 275, 772-782.

[34] V. Gulani, F. Calamante, F. G. Shellock, E. Kanal, S. B. Reeder, Gadolinium deposition in the brain: summary of evidence and recommendations. The Lancet Neurology 2017, 16, 564-570.

[35] C. C. Tang, K. L. Poston, T. Eckert, A. Feigin, S. Frucht, M. Gudesblatt, V. Dhawan, M. Lesser, J.-P. Vonsattel, S. Fahn, D. Eidelberg, Differential diagnosis of parkinsonism: a metabolic imaging study using pattern analysis. The Lancet Neurology 2010, 9, 149-158.

[36] C. Plathow, W. A. Weber, Tumor Cell Metabolism Imaging. Journal of Nuclear Medicine 2008, 49, 43S-63S.

[37] R. E. Hurd, Y.-F. Yen, A. Chen, J. H. Ardenkjaer-Larsen, Hyperpolarized ^{13}C metabolic imaging using dissolution dynamic nuclear polarization. Journal of Magnetic Resonance Imaging 2012, 36, 1314-1328.

[38] J. H. Ardenkjær-Larsen, B. Fridlund, A. Gram, G. Hansson, L. Hansson, M. H. Lerche, R. Servin, M. Thaning, K. Golman, Increase in signal-to-noise ratio of > 10,000 times in liquid-state NMR. Proceedings of the National Academy of Sciences 2003, 100, 10158-10163.

[39] S. Hu, H. A. I. Yoshihara, R. Bok, J. Zhou, M. Zhu, J. Kurhanewicz, D. B. Vigneron, Use of hyperpolarized [1-^{13}C]pyruvate and [2-^{13}C]pyruvate to probe the effects of the anticancer agent dichloroacetate on mitochondrial metabolism in vivo in the normal rat. Magnetic Resonance Imaging 2012, 30, 1367-1372.

[40] P. Nikolaou, B. M. Goodson, E. Y. Chekmenev, NMR Hyperpolarization Techniques for Biomedicine. Chemistry – A European Journal 2015, 21, 3156-3166.

[41] A. Bornet, R. Melzi, A. J. Perez Linde, P. Hautle, B. van den Brandt, S. Jannin, G. Bodenhausen, Boosting Dissolution Dynamic Nuclear Polarization by Cross Polarization. The Journal of Physical Chemistry Letters 2013, 4, 111-114.

References

[42]   S. Jannin, A. Bornet, R. Melzi, G. Bodenhausen, High field dynamic nuclear polarization at 6.7T: Carbon-13 polarization above 70% within 20min. Chemical Physics Letters 2012, 549, 99-102.

[43]   J. Kurhanewicz, D. B. Vigneron, J. H. Ardenkjaer-Larsen, J. A. Bankson, K. Brindle, C. H. Cunningham, F. A. Gallagher, K. R. Keshari, A. Kjaer, C. Laustsen, D. A. Mankoff, M. E. Merritt, S. J. Nelson, J. M. Pauly, P. Lee, S. Ronen, D. J. Tyler, S. S. Rajan, D. M. Spielman, L. Wald, X. Zhang, C. R. Malloy, R. Rizi, Hyperpolarized ^{13}C MRI: Path to Clinical Translation in Oncology. Neoplasia 2019, 21, 1-16.

[44]   G. Brix, E. A. Nekolla, D. Nosske, J. Griebel, Risks and safety aspects related to PET/MR examinations. European Journal of Nuclear Medicine and Molecular Imaging 2009, 36, 131-138.

[45]   S. Anderson, J. T. Grist, A. Lewis, D. J. Tyler, Hyperpolarized ^{13}C magnetic resonance imaging for noninvasive assessment of tissue inflammation. NMR in Biomedicine 2021, 34, e4460.

[46]   T. Harris, H. Degani, L. Frydman, Hyperpolarized ^{13}C NMR studies of glucose metabolism in living breast cancer cell cultures. NMR in Biomedicine 2013, 26, 1831-1843.

[47]   C. Gabellieri, S. Reynolds, A. Lavie, G. S. Payne, M. O. Leach, T. R. Eykyn, Therapeutic Target Metabolism Observed Using Hyperpolarized ^{15}N Choline. Journal of the American Chemical Society 2008, 130, 4598-4599.

[48]   H. Allouche-Arnon, A. Gamliel, C. M. Barzilay, R. Nalbandian, J. M. Gomori, M. Karlsson, M. H. Lerche, R. Katz-Brull, A hyperpolarized choline molecular probe for monitoring acetylcholine synthesis. Contrast Media & Molecular Imaging 2011, 6, 139-147.

[49]   S. Hu, M. Zhu, H. A. I. Yoshihara, D. M. Wilson, K. R. Keshari, P. Shin, G. Reed, C. von Morze, R. Bok, P. E. Z. Larson, J. Kurhanewicz, D. B. Vigneron, In vivo measurement of normal rat intracellular pyruvate and lactate levels after injection of hyperpolarized [1-^{13}C] alanine. Magnetic Resonance Imaging 2011, 29, 1035-1040.

[50]   G. Batsios, C. Najac, P. Cao, P. Viswanath, E. Subramani, Y. Saito, A. M. Gillespie, H. A. I. Yoshihara, P. Larson, S. Sando, S. M. Ronen, In vivo detection of γ-glutamyl-transferase up-regulation in glioma using hyperpolarized γ-glutamyl-[1-^{13}C] glycine. Scientific Reports 2020, 10, 6244.

[51]   F. A. Gallagher, M. I. Kettunen, S. E. Day, D.-E. Hu, J. H. Ardenkjær-Larsen, R. i. t. Zandt, P. R. Jensen, M. Karlsson, K. Golman, M. H. Lerche, K. M. Brindle, Magnetic resonance imaging of pH in vivo using hyperpolarized ^{13}C-labelled bicarbonate. Nature 2008, 453, 940-943.

[52]   J. H. Ardenkjaer-Larsen, C. Laustsen, S. Bowen, R. Rizi, Hyperpolarized H_2O MR angiography. Magnetic Resonance in Medicine 2014, 71, 50-56.

References

[53] M. Matsumoto, J. H. Espenson, Kinetics of the Interconversion of Parahydrogen and Orthohydrogen Catalyzed by Paramagnetic Complex Ions. *Journal of the American Chemical Society* 2005, 127, 11447-11453.

[54] L. T. Kuhn, *Hyperpolarization Methods in NMR Spectroscopy*, Springer Berlin Heidelberg, 2016.

[55] K. F. Bonhoeffer, P. Harteck, Experimente über Para- und Orthowasserstoff. *Naturwissenschaften* 1929, 17, 182-182.

[56] J.-B. Hövener, A. N. Pravdivtsev, B. Kidd, C. R. Bowers, S. Glöggler, K. V. Kovtunov, M. Plaumann, R. Katz-Brull, K. Buckenmaier, A. Jerschow, F. Reineri, T. Theis, R. V. Shchepin, S. Wagner, P. Bhattacharya, N. M. Zacharias, E. Y. Chekmenev, Parahydrogen-Based Hyperpolarization for Biomedicine. *Angewandte Chemie International Edition* 2018, 57, 11140-11162.

[57] B. Feng, A. M. Coffey, R. D. Colon, E. Y. Chekmenev, K. W. Waddell, A pulsed injection parahydrogen generator and techniques for quantifying enrichment. *Journal of Magnetic Resonance* 2012, 214, 258-262.

[58] S. Wagner, Conversion rate of para-hydrogen to ortho-hydrogen by oxygen: implications for PHIP gas storage and utilization. *Magnetic Resonance Materials in Physics, Biology and Medicine* 2014, 27, 195-199.

[59] A. M. Balu, S. B. Duckett, R. Luque, Para-hydrogen induced polarisation effects in liquid phase hydrogenations catalysed by supported metal nanoparticles. *Dalton Transactions* 2009, 5074-5076.

[60] T. C. Eisenschmid, R. U. Kirss, P. P. Deutsch, S. I. Hommeltoft, R. Eisenberg, J. Bargon, R. G. Lawler, A. L. Balch, Para hydrogen induced polarization in hydrogenation reactions. *Journal of the American Chemical Society* 1987, 109, 8089-8091.

[61] R. W. Adams, J. A. Aguilar, K. D. Atkinson, M. J. Cowley, P. I. P. Elliott, S. B. Duckett, G. G. R. Green, I. G. Khazal, J. López-Serrano, D. C. Williamson, Reversible Interactions with para-Hydrogen Enhance NMR Sensitivity by Polarization Transfer. *Science* 2009, 323, 1708-1711.

[62] K. D. Atkinson, M. J. Cowley, S. B. Duckett, P. I. P. Elliott, G. G. R. Green, J. López-Serrano, I. G. Khazal, A. C. Whitwood, Para-Hydrogen Induced Polarization without Incorporation of Para-Hydrogen into the Analyte. *Inorganic Chemistry* 2009, 48, 663-670.

[63] A. N. Pravdivtsev, K. L. Ivanov, A. V. Yurkovskaya, P. A. Petrov, H.-H. Limbach, R. Kaptein, H.-M. Vieth, Spin polarization transfer mechanisms of SABRE: A magnetic field dependent study. *Journal of Magnetic Resonance* 2015, 261, 73-82.

<center>References</center>

[64]   S. L. Eriksson, J. R. Lindale, X. Li, W. S. Warren, Improving SABRE hyperpolarization with highly nonintuitive pulse sequences: Moving beyond avoided crossings to describe dynamics. *Science Advances* 2022, 8, eabl3708.

[65]   S. S. Roy, K. M. Appleby, E. J. Fear, S. B. Duckett, SABRE-Relay: A Versatile Route to Hyperpolarization. *The Journal of Physical Chemistry Letters* 2018, 9, 1112-1117.

[66]   I. Adelabu, P. TomHon, M. S. H. Kabir, S. Nantogma, M. Abdulmojeed, I. Mandzhieva, J. Ettedgui, R. E. Swenson, M. C. Krishna, T. Theis, B. M. Goodson, E. Y. Chekmenev, Order-Unity 13C Nuclear Polarization of [1-^{13}C] Pyruvate in Seconds and the Interplay of Water and SABRE Enhancement. *ChemPhysChem* 2022, 23, e202100839.

[67]   B. E. Kidd, J. L. Gesiorski, M. E. Gemeinhardt, R. V. Shchepin, K. V. Kovtunov, I. V. Koptyug, E. Y. Chekmenev, B. M. Goodson, Facile Removal of Homogeneous SABRE Catalysts for Purifying Hyperpolarized Metronidazole, a Potential Hypoxia Sensor. *The Journal of Physical Chemistry C* 2018, 122, 16848-16852.

[68]   N. M. Ariyasingha, J. R. Lindale, S. L. Eriksson, G. P. Clark, T. Theis, R. V. Shchepin, N. V. Chukanov, K. V. Kovtunov, I. V. Koptyug, W. S. Warren, E. Y. Chekmenev, Quasi-Resonance Fluorine-19 Signal Amplification by Reversible Exchange. *The Journal of Physical Chemistry Letters* 2019, 10, 4229-4236.

[69]   M. J. Burns, P. J. Rayner, G. G. R. Green, L. A. R. Highton, R. E. Mewis, S. B. Duckett, Improving the Hyperpolarization of ^{31}P Nuclei by Synthetic Design. *The Journal of Physical Chemistry B* 2015, 119, 5020-5027.

[70]   A. M. Olaru, A. Burt, P. J. Rayner, S. J. Hart, A. C. Whitwood, G. G. R. Green, S. B. Duckett, Using signal amplification by reversible exchange (SABRE) to hyperpolarise ^{119}Sn and ^{29}Si NMR nuclei. *Chemical Communications* 2016, 52, 14482-14485.

[71]   P. TomHon, M. Abdulmojeed, I. Adelabu, S. Nantogma, M. S. H. Kabir, S. Lehmkuhl, E. Y. Chekmenev, T. Theis, Temperature Cycling Enables Efficient ^{13}C SABRE-SHEATH Hyperpolarization and Imaging of [1-^{13}C]-Pyruvate. *Journal of the American Chemical Society* 2022, 144, 282-287.

[72]   C. R. Bowers, D. P. Weitekamp, Parahydrogen and synthesis allow dramatically enhanced nuclear alignment. *Journal of the American Chemical Society* 1987, 109, 5541-5542.

[73]   M. G. Pravica, D. P. Weitekamp, Net NMR alignment by adiabatic transport of parahydrogen addition products to high magnetic field. *Chemical Physics Letters* 1988, 145, 255-258.

[74]   L. Buljubasich, M. B. Franzoni, K. Münnemann, in Hyperpolarization Methods in NMR Spectroscopy (Ed.: L. T. Kuhn), Springer Berlin Heidelberg, Berlin, Heidelberg, 2013, pp. 33-74.

[75]   J. A. Osborn, F. H. Jardine, J. F. Young, G. Wilkinson, The preparation and properties of tris(triphenylphosphine)halogenorhodium(I) and some reactions thereof including catalytic homogeneous hydrogenation of olefins and acetylenes and their derivatives. Journal of the Chemical Society A: Inorganic, Physical, Theoretical 1966, 1711-1732.

[76]   N. J. Stewart, H. Nakano, S. Sugai, M. Tomohiro, Y. Kase, Y. Uchio, T. Yamaguchi, Y. Matsuo, T. Naganuma, N. Takeda, I. Nishimura, H. Hirata, T. Hashimoto, S. Matsumoto, Hyperpolarized ^{13}C Magnetic Resonance Imaging of Fumarate Metabolism by Parahydrogen-induced Polarization: A Proof-of-Concept in vivo Study. ChemPhysChem 2021, 22, 915-923.

[77]   E. Cavallari, C. Carrera, T. Boi, S. Aime, F. Reineri, Effects of Magnetic Field Cycle on the Polarization Transfer from Parahydrogen to Heteronuclei through Long-Range J-Couplings. The Journal of Physical Chemistry B 2015, 119, 10035-10041.

[78]   F. Reineri, T. Boi, S. Aime, ParaHydrogen Induced Polarization of ^{13}C carboxylate resonance in acetate and pyruvate. Nature Communications 2015, 6, 5858.

[79]   S. Korchak, S. Yang, S. Mamone, S. Glöggler, Pulsed Magnetic Resonance to Signal-Enhance Metabolites within Seconds by utilizing para-Hydrogen. ChemistryOpen 2018, 7, 344-348.

[80]   E. Cavallari, C. Carrera, S. Aime, F. Reineri, ^{13}C MR Hyperpolarization of Lactate by Using ParaHydrogen and Metabolic Transformation in Vitro. Chemistry – A European Journal 2017, 23, 1200-1204.

[81]   Y. Ding, S. Korchak, S. Mamone, A. P. Jagtap, G. Stevanato, S. Sternkopf, D. Moll, H. Schroeder, S. Becker, A. Fischer, E. Gerhardt, T. F. Outeiro, F. Opazo, C. Griesinger, S. Glöggler, Rapidly Signal-enhanced Metabolites for Atomic Scale Monitoring of Living Cells with Magnetic Resonance. Chemistry–Methods 2022, 2, e202200023.

[82]   S. Mamone, A. P. Jagtap, S. Korchak, Y. Ding, S. Sternkopf, S. Glöggler, A Field-Independent Method for the Rapid Generation of Hyperpolarized [1-^{13}C] Pyruvate in Clean Water Solutions for Biomedical Applications. Angewandte Chemie International Edition 2022, 61, e202206298.

[83]   A. Brahms, A. N. Pravdivtsev, T. Stamp, F. Ellermann, F. D. Sönnichsen, J.-B. Hövener, R. Herges, Synthesis of ^{13}C and ^{2}H Labeled Vinyl Pyruvate and Hyperpolarization of Pyruvate. Chemistry – A European Journal 2022, 28, e202201210.

[84]   L. Kaltschnee, A. P. Jagtap, J. McCormick, S. Wagner, L.-S. Bouchard, M. Utz, C. Griesinger, S. Glöggler, Hyperpolarization of Amino Acids in Water Utilizing Parahydrogen on a Rhodium Nanocatalyst. Chemistry – A European Journal 2019, 25, 11031-11035.

References

[85]   S. Glöggler, S. Wagner, L. S. Bouchard, Hyperpolarization of amino acid derivatives in water for biological applications. *Chemical Science* 2015, 6, 4261-4266.

[86]   L. Dagys, A. P. Jagtap, S. Korchak, S. Mamone, P. Saul, M. H. Levitt, S. Glöggler, Nuclear hyperpolarization of (1-^{13}C)-pyruvate in aqueous solution by proton-relayed side-arm hydrogenation. *Analyst* 2021, 146, 1772-1778.

[87]   S. Korchak, M. Emondts, S. Mamone, B. Blümich, S. Glöggler, Production of highly concentrated and hyperpolarized metabolites within seconds in high and low magnetic fields. *Physical Chemistry Chemical Physics* 2019, 21, 22849-22856.

[88]   E. Cavallari, C. Carrera, S. Aime, F. Reineri, Metabolic Studies of Tumor Cells Using [1-^{13}C] Pyruvate Hyperpolarized by Means of PHIP-Side Arm Hydrogenation. *ChemPhysChem* 2019, 20, 318-325.

[89]   K. V. Kovtunov, D. A. Barskiy, R. V. Shchepin, O. G. Salnikov, I. P. Prosvirin, A. V. Bukhtiyarov, L. M. Kovtunova, V. I. Bukhtiyarov, I. V. Koptyug, E. Y. Chekmenev, Production of Pure Aqueous ^{13}C-Hyperpolarized Acetate by Heterogeneous Parahydrogen-Induced Polarization. *Chemistry – A European Journal* 2016, 22, 16446-16449.

[90]   N. V. Chukanov, O. G. Salnikov, R. V. Shchepin, K. V. Kovtunov, I. V. Koptyug, E. Y. Chekmenev, Synthesis of Unsaturated Precursors for Parahydrogen-Induced Polarization and Molecular Imaging of 1-^{13}C-Acetates and 1-^{13}C-Pyruvates via Side Arm Hydrogenation. *ACS Omega* 2018, 3, 6673-6682.

[91]   P. Saul, S. Mamone, S. Glöggler, Hyperpolarization of ^{15}N in an amino acid derivative. *RSC Advances* 2022, 12, 2282-2286.

[92]   C. Carrera, E. Cavallari, G. Digilio, O. Bondar, S. Aime, F. Reineri, ParaHydrogen Polarized Ethyl-[1-^{13}C] pyruvate in Water, a Key Substrate for Fostering the PHIP-SAH Approach to Metabolic Imaging. *ChemPhysChem* 2021, 22, 1042-1048.

[93]   S. Korchak, S. Mamone, S. Glöggler, Over 50 % ^{1}H and ^{13}C Polarization for Generating Hyperpolarized Metabolites—A para-Hydrogen Approach. *ChemistryOpen* 2018, 7, 672-676.

[94]   R. V. Shchepin, D. A. Barskiy, A. M. Coffey, I. V. Manzanera Esteve, E. Y. Chekmenev Efficient Synthesis of Molecular Precursors for Para-Hydrogen-Induced Polarization of Ethyl Acetate-1-^{13}C and Beyond. *Angewandte Chemie International Edition* 2016, 55, 6071-6074.

[95]   E. Cavallari, C. Carrera, S. Aime, F. Reineri, Studies to enhance the hyperpolarization level in PHIP-SAH-produced C13-pyruvate. *Journal of Magnetic Resonance* 2018, 289, 12-17.

[96]   N. Chattergoon, F. Martínez-Santiesteban, W. B. Handler, J. H. Ardenkjær-Larsen, T. J. Scholl, Field dependence of T_1 for hyperpolarized [1-^{13}C] pyruvate. *Contrast Media & Molecular Imaging* 2013, 8, 57-62.

References

[97]   E. Cavallari, C. Carrera, M. Sorge, G. Bonne, A. Muchir, S. Aime, F. Reineri, The ^{13}C hyperpolarized pyruvate generated by ParaHydrogen detects the response of the heart to altered metabolism in real time. Scientific Reports 2018, 8, 8366.

[98]   O. G. Salnikov, R. V. Shchepin, N. V. Chukanov, L. Jaigirdar, W. Pham, K. V. Kovtunov, I. V. Koptyug, E. Y. Chekmenev, Effects of Deuteration of ^{13}C-Enriched Phospholactate on Efficiency of Parahydrogen-Induced Polarization by Magnetic Field Cycling. The Journal of Physical Chemistry C 2018, 122, 24740-24749.

[99]   C. Taglang, D. E. Korenchan, C. von Morze, J. Yu, C. Najac, S. Wang, J. E. Blecha, S. Subramaniam, R. Bok, H. F. VanBrocklin, D. B. Vigneron, S. M. Ronen, R. Sriram, J. Kurhanewicz, D. M. Wilson, R. R. Flavell, Late-stage deuteration of ^{13}C-enriched substrates for T_1 prolongation in hyperpolarized ^{13}C MRI. Chemical Communications 2018, 54, 5233-5236.

[100]   W. Dastrù, D. Longo, S. Aime, Contrast agents and mechanisms. Drug Discovery Today: Technologies 2011, 8, e109-e115.

[101]   T. Harris, A. Gamliel, J. Sosna, J. M. Gomori, R. Katz-Brull, Impurities of [1-^{13}C] Pyruvic Acid and a Method to Minimize Their Signals for Hyperpolarized Pyruvate Metabolism Studies. Applied Magnetic Resonance 2018, 49, 1085-1098.

[102]   S. A. Margolis, B. Coxon, Identification and quantitation of the impurities in sodium pyruvate. Analytical Chemistry 1986, 58, 2504-2510.

[103]   S.-C. Chang, I. Lee, H. Ting, Y.-J. Chang, N.-C. Yang, Parapyruvate, an Impurity in Pyruvate Supplements, Induces Senescence in Human Fibroblastic Hs68 Cells via Inhibition of the α-Ketoglutarate Dehydrogenase Complex. Journal of Agricultural and Food Chemistry 2018, 66, 7504-7513.

[104]   A. Esposito, A. Lukas, J. E. Meany, Y. Pocker, The reversible enolization and hydration of pyruvate: possible roles of keto, enol, and hydrated pyruvate in lactate dehydrogenase catalysis. Canadian Journal of Chemistry 1999, 77, 1108-1117.

[105]   A. A. Ketterling, A. S. Lisitsyn*, A. V. Nosov, V. A. Likholobov, Carboxylic acid transvinylation as catalysed by complexes of palladium acetate with phenanthroline-like ligands. Applied Catalysis 1990, 66, 123-131.

[106]   J. Ziriakus, T. K. Zimmermann., A. Pöthig, M. Drees, S. Haslinger, D. Jantke, F. E. Kühn, Ruthenium-Catalyzed Transvinylation – New Insights. Advanced Synthesis & Catalysis 2013, 355, 2845-2859.

[107]   H. Nakagawa, Y. Okimoto, S. Sakaguchi, Y. Ishii, Synthesis of enol and vinyl esters catalyzed by an iridium complex. Tetrahedron Letters 2003, 44, 103-106.

References

[108] A. Svyatova, V. P. Kozinenko, N. V. Chukanov, D. B. Burueva, E. Y. Chekmenev, Y.-W. Chen, D. W. Hwang, K. V. Kovtunov, I. V. Koptyug, PHIP hyperpolarized [1-^{13}C]pyruvate and [1-^{13}C]acetate esters via PH-INEPT polarization transfer monitored by ^{13}C NMR and MRI. Scientific Reports 2021, 11, 5646.

[109] L. E. Olsson, C.-M. Chai, O. Axelsson, M. Karlsson, K. Golman, J. S. Petersson, MR coronary angiography in pigs with intraarterial injections of a hyperpolarized ^{13}C substance. Magnetic Resonance in Medicine 2006, 55, 731-737.

[110] K. Wigh Lipsø, E. S. S. Hansen, R. S. Tougaard, C. Laustsen, J. H. Ardenkjær-Larsen, Renal MR angiography and perfusion in the pig using hyperpolarized water. Magnetic Resonance in Medicine 2017, 78, 1131-1135.

[111] K. W. Lipsø, E. S. S. Hansen, R. S. Tougaard, C. Laustsen, J. H. Ardenkjær-Larsen, Dynamic coronary MR angiography in a pig model with hyperpolarized water. Magnetic Resonance in Medicine 2018, 80, 1165-1169.

[112] B. Polevoda, F. Sherman, Nα-terminal Acetylation of Eukaryotic Proteins*. Journal of Biological Chemistry 2000, 275, 36479-36482.

[113] P. Van Damme, K. Hole, A. Pimenta-Marques, K. Helsens, J. Vandekerckhove, R. G. Martinho, K. Gevaert, T. Arnesen, NatF Contributes to an Evolutionary Shift in Protein N-Terminal Acetylation and Is Important for Normal Chromosome Segregation. PLOS Genetics 2011, 7, e1002169.

[114] J. Chen, E. P. Hackett, J. Singh, Z. Kovács, J. M. Park, Simultaneous Assessment of Intracellular and Extracellular pH Using Hyperpolarized [1-^{13}C]Alanine Ethyl Ester. Analytical Chemistry 2020, 92, 11681-11686.

[115] M. Sattler, J. Schleucher, C. Griesinger, Heteronuclear multidimensional NMR experiments for the structure determination of proteins in solution employing pulsed field gradients. Progress in Nuclear Magnetic Resonance Spectroscopy 1999, 34, 93-158.

[116] L. Castañar, T. Parella, in Annual Reports on NMR Spectroscopy, Vol. 84 (Ed.: G. A. Webb), Academic Press, 2015, pp. 163-232.

[117] H. Günther, NMR Spectroscopy, Vol. 3rd Edition, Wiley-VCH Verlag GmbH & Co. KGaA, Weinheim, 2013.

[118] A. Bax, M. F. Summers, Proton and carbon-13 assignments from sensitivity-enhanced detection of heteronuclear multiple-bond connectivity by 2D multiple quantum NMR. Journal of the American Chemical Society 1986, 108, 2093-2094.

[119] G. A. Morris, R. Freeman, Enhancement of nuclear magnetic resonance signals by polarization transfer. Journal of the American Chemical Society 1979, 101, 760-762.

[120] A. W. Overhauser, Polarization of Nuclei in Metals. Physical Review 1953, 92, 411-415.

References

[121] B. Neises, W. Steglich, Simple Method for the Esterification of Carboxylic Acids. *Angewandte Chemie International Edition in English* 1978, 17, 522-524.

[122] P. J. Serafinowski, P. B. Garland, Novel Photoacid Generators for Photodirected Oligonucleotide Synthesis. *Journal of the American Chemical Society* 2003, 125, 962-965.

[123] R. Shen, B. Luo, J. Yang, L. Zhang, L.-B. Han, Convenient synthesis of allenylphosphoryl compounds via Cu-catalysed couplings of P(O)H compounds with propargyl acetates. *Chemical Communications* 2016, 52, 6451-6454.

[124] S. H. Jørgensen, N. Bøgh, E. S. S. Hansen, M. Væggemose, H. Wiggers, C. Laustsen, Hyperpolarized MRI – An Update and Future Perspectives. *Seminars in Nuclear Medicine* 2022, 52, 374-381.

[125] J. Bigeleisen, M. G. Mayer, Calculation of Equilibrium Constants for Isotopic Exchange Reactions. *The Journal of Chemical Physics* 1947, 15, 261-267.

[126] J. E. Baldwin, S. S. Gallagher, P. A. Leber, A. S. Raghavan, R. Shukla, Deuterium Kinetic Isotope Effects and Mechanism of the Thermal Isomerization of Bicyclo[4.2.0]oct-7-ene to 1,3-Cyclooctadiene. *The Journal of Organic Chemistry* 2004, 69, 7212-7219.

[127] Y. V. Il'ichev, J. Wirz, Rearrangements of 2-Nitrobenzyl Compounds. 1. Potential Energy Surface of 2-Nitrotoluene and Its Isomers Explored with ab Initio and Density Functional Theory Methods. *The Journal of Physical Chemistry A* 2000, 104, 7856-7870.

[128] M. Gaplovsky, Y. V. Il'ichev, Y. Kamdzhilov, S. V. Kombarova, M. Mac, M. A. Schwörer, J. Wirz, Photochemical reaction mechanisms of 2-nitrobenzyl compounds: 2-Nitrobenzyl alcohols form 2-nitroso hydrates by dual proton transfer. *Photochemical & Photobiological Sciences* 2005, 4, 33-42.

[129] P. Klán, T. Šolomek, C. G. Bochet, A. Blanc, R. Givens, M. Rubina, V. Popik, A. Kostikov, J. Wirz, Photoremovable Protecting Groups in Chemistry and Biology: Reaction Mechanisms and Efficacy. *Chemical Reviews* 2013, 113, 119-191.

[130] F. Bley, K. Schaper, H. Görner, Photoprocesses of Molecules with 2-Nitrobenzyl Protecting Groups and Caged Organic Acids. *Photochemistry and Photobiology* 2008, 84, 162-171.

[131] D. R. Vutukuri, P. Bharathi, Z. Yu, K. Rajasekaran, M.-H. Tran, S. Thayumanavan, A Mild Deprotection Strategy for Allyl-Protecting Groups and Its Implications in Sequence Specific Dendrimer Synthesis. *The Journal of Organic Chemistry* 2003, 68, 1146-1149.

[132] K. Nakayama, K. Uoto, K. Higashi, T. Soga, T. Kusama, A Useful Method for Deprotection of the Protective Allyl Group at the Anomeric Oxygen of Carbohydrate Moieties Using Tetrakis(triphenylphosphine)palladium. *Chemical & Pharmaceutical Bulletin* 1992, 40, 1718-1720.

References

[133] M. J. Zacuto, F. Xu, One-Step RhCl$_3$-Catalyzed Deprotection of Acyclic N-Allyl Amides. The Journal of Organic Chemistry 2007, 72, 6298-6300.

[134] C. Taglang, L. M. Martínez-Prieto, I. del Rosal, L. Maron, R. Poteau, K. Philippot, B. Chaudret, S. Perato, A. Sam Lone, C. Puente, C. Dugave, B. Rousseau, G. Pieters, Enantiospecific C$_\alpha$H Activation Using Ruthenium Nanocatalysts. Angewandte Chemie International Edition 2015, 54, 10474-10477.

7 Appendix

7.1 Deuteration of pyruvate

The following tables show the analysis of the deuteration experiments of sodium pyruvate (Table 8) and pyruvic acid (Table 9).

Table 8 Analytical data of the deuteration of sodium pyruvate.

Reaction	chemical	Peak	1H Integral	1H ppm	C-1 Integral	C-1 ppm	C-2 Integral	C-2 ppm	C-3 Integral	C-3 ppm	1H rel. ratio: other peaks in the spectrum	1H rel. ratio: sum of SM integral	sum of SM integral	13C C-1	13C C-2	13C C-3
Na Pyruvate	Pyruvate	Me-3H	5412186385953	2,45	2688436800	170,04	4032052800	205,84	13659379368	26,53	0,91	0,91	0,93	0,93	0,88	0,92
	Hydropyruvate	Me-3H	5044648855904	1,58	207452228	178,65	559675592	93,88	1110520848	25,29	0,09	0,09	0,07	0,07	0,12	0,08
	Parapyruvate	CH₂	-		-	-	-	-	-	-						
		Me-3H	-		-	-	-	-	-	-						
	Hydroparapyruvate	CH₂	-		-	-	-	-	-	-						
		Me-3H	-		-	-	-	-	-	-						
	Zymonic acid	1H	-		-	-	-	-	-	-						
		Me-3H	-		-	-	-	-	-	-						
NaHCO3	Pyruvate	Me-3H	3634287013888	2,39	1393830622	169,82	1905663871	205,35	+	+	0,86	0,06	0,48	0,42	0,54	
	Hydropyruvate	Me-3H	420896862208	1,50	*	*	*	*	*	*	0,10	0,01				
	Parapyruvate	CH₂	140477702144	3,20	1342415766	182,35	1099442566	203,52	-	-	0,03	0,00	0,46	0,41	0,31	
		Me-3H	23582359552	1,20	572743030	169,09	542225494	73,57	866132661	26,27	0,01	0,00	0,20	0,17	0,15	1,00
	Hydroparapyruvate	CH₂	-		-	-	-	-	-	-						
		Me-3H	-		-	-	-	-	-	-						
	Zymonic acid	1H	-		-	-	-	-	-	-						
		Me-3H	-		-	-	-	-	-	-						
Na2CO3	Pyruvate	Me-3H	198189355008	2,33	3324844506	168,28	1519623349	203,35	*	*	0,07	0,00	1,15	0,62	0,69	
	Hydropyruvate	Me-3H	381877161984	1,42	*	*	+	+	*	*	0,13	0,01				
	Parapyruvate	CH₂	178699599872	3,26	1038155699	182,30	+	+	256180378	54,54	0,06	0,00	0,36	0,19		1,00
		Me-3H	16733423208	1,35	1043057246	169,02	687582664	73,37	+	+	0,56	0,03	0,36	0,19	0,31	
	Hydroparapyruvate	CH₂	6058078208	2,58	*	*	*	*	*	*	0,00	0,00				
		Me-3H	537925300224	1,27	*	*	*	*	*	*	0,18	0,01				
	Zymonic acid	1H	-		-	-	-	-	-	-						
		Me-3H	-		-	-	-	-	-	-						
D2O THF Et3N	Pyruvate	Me-3H	402173968384	2,32	1236832488	169,14	1812075592	203,72	-	-	0,32	0,01	0,43	0,53	0,74	
	Hydropyruvate	Me-3H	-		-	-	-	-	-	-						
	Parapyruvate	CH₂	207918723072	3,26	1103294230	182,07	*	*	256180378	54,54	0,16	0,00	0,38	0,47		
		Me-3H	66380321776	1,36	*	*	629708396	73,36	*	*	0,52	0,01			0,26	
	Hydroparapyruvate	CH₂	-		-	-	-	-	-	-						
		Me-3H	-		-	-	-	-	-	-						
	Zymonic acid	1H	-		-	-	-	-	-	-						
		Me-3H	-		-	-	-	-	-	-						
D2SO4	Pyruvate	Me-3H	6017842	2,21	1295949242	162,51	2743837154	195,99	4834927420	24,93	0,27	0,00	0,45	0,39	1,00	0,38
	Hydropyruvate	Me-3H	-		-	-	-	-	-	-						
	Parapyruvate	CH₂	2778588	3,11	1986836328	174,70	523319	211,62	7790684812	24,27	0,12	0,00	0,69	0,61	0,00	0,62
		Me-3H	13579288	1,32	*	*	*	*	*	*	0,61	0,00				
	Hydroparapyruvate	CH₂	-		-	-	-	-	-	-						
		Me-3H	-		-	-	-	-	-	-						
	Zymonic acid	1H	-		-	-	-	-	-	-						
		Me-3H	-		-	-	-	-	-	-						

Table 9 Analytical data of the deuteration of pyruvic acid.

Reaction	chemical	Peak	1H Integral	1H ppm	C-1 Integral	C-1 ppm	C-2 Integral	C-2 ppm	C-3 Integral	C-3 ppm	1H: rel. ratio – other peaks in the spectrum	1H: rel. ratio – sum of SM integral	sum of SM integral	13C C-1	13C C-2	13C C-3
Pyruvic acid	Pyruvat	Me-3H	29476392743391	2,36	2026824536	163,12	3010310532	196,53	8194582900	25,54	0,33	0,33	0,35	0,35	0,34	0,42
	Hydropyruvate	Me-3H	56642519961585	1,47	3809061384	174,77	5704031560	92,51	11042239668	24,97	0,63	0,63	0,65	0,65	0,65	0,56
	Parapyruvate	CH2	56512942729	3,29	*	*	*	*	*	*	0,00	0,00				
		Me-3H	218367291415	1,28	*	*	*	*	*	*	0,00	0,00				
	Hydroparapyruvate	CH2	78721951347	2,79	*	*	*	*	*	*	0,00	0,00				
		Me-3H	161484647860	1,09	*	*	*	*	*	*	0,00	0,00				
	Zymonic acid	1H	663489835892	6,35	*	*	52364984	141,97	353003368	120,80	0,01	0,01				
		Me-3H	2701798205718	1,59	2899638192	169,94	4372925092	205,25	13477695640	26,65	0,03	0,03			0,01	0,02
NaHCO3	Pyruvat	Me-3H	54161089339392	2,34	6052252780	178,69	363224128	93,93	603980672	26,08	0,83	0,60	0,50	0,64	0,74	0,89
	Hydropyruvate	Me-3H	4283167465472	1,35	827441888	182,38	625064808	203,44	*	*	0,07	0,05	0,10	0,13	0,06	0,04
	Parapyruvate	CH2	681208934400	3,27	218083208	172,87	547185628	73,59	1077540336	26,37	0,01	0,01	0,14	0,18	0,11	
		Me-3H	5212399710208	1,47	*	*	*	*	*	*	0,08	0,06				
	Hydroparapyruvate	CH2	467030638592	2,57	*	*	*	*	*	*	0,01	0,01				
		Me-3H	127015882752	1,05	*	*	*	*	*	*	0,00	0,00	0,04	0,05	0,09	0,07
	Zymonic acid	1H	23090024448	5,98	*	*	*	*	*	*	0,00	0,00				
		Me-3H	27203470231	1,63	*	*	*	*	*	*	0,00	0,00				
Na2CO3	Pyruvat	Me-3H	28697518080	2,38	1701031522	169,13	1876097062	203,73	1579506868	25,65	0,03	0,00	0,29	0,40	0,36	0,42
	Hydropyruvate	Me-3H	+	1,30	*	*	*	*	*	*						
	Parapyruvate	CH2	505925451776	3,22	1825931846	182,38	694250348	205,42	2204619076	26,38	0,58	0,01	0,31	0,43	0,13	
		Me-3H	1048111161052	1,23	743481846	169,83	2632372526	73,54	*	*	0,12	0,00	0,13	0,17	0,51	0,58
	Hydroparapyruvate	CH2	8504842805	2,31	*	*	*	*	*	*	0,01	0,00				
		Me-3H	93129908817	1,39	*	*	*	*	*	*	0,11	0,00				
	Zymonic acid	1H	9425362082	6,33	*	*	*	*	*	*	0,01	0,00				
		Me-3H	123154315794	1,00	2379632848	169,13	3387789596	203,47	6578526788	26,55	0,14	0,00				
D2O THF Et3N	Pyruvat	Me-3H	183944597504	2,31	-	-	-	-	-	-	0,80	0,00	0,41	1,00		
	Hydropyruvate	Me-3H			-	-	-	-	-	-						
	Parapyruvate	CH2	-		-	-	-	-	-	-						
		Me-3H	-		-	-	-	-	-	-						
	Hydroparapyruvate	CH2	-		-	-	-	-	-	-						
		Me-3H	-		-	-	-	-	-	-						
	Zymonic acid	1H	35811762176	6,39	*	*	*	*	*	*	0,16	0,00				
		Me-3H	10446584601	1,60	*	*	*	*	*	*	0,05	0,00				
D2SO4	Pyruvat	Me-3H	10955081895936	2,29	17531111098	161,69	1862443429	195,14	30328479914	24,89	0,42	0,12	0,30	0,45	0,38	0,42
	Hydropyruvate	Me-3H	15299548145664	1,42	2111637527	174,04	3052659126	92,13	41822212596	24,30	0,58	0,17	0,36	0,55	0,62	0,58
	Parapyruvate	CH2	-		-	-	-	-	-	-						
		Me-3H	-		-	-	-	-	-	-						
	Hydroparapyruvate	CH2	-		-	-	-	-	-	-						
		Me-3H	-		-	-	-	-	-	-						
	Zymonic acid	1H	7539593216	6,29	*	*	*	*	*	*	0,00	0,00				
		Me-3H	92524118016	1,62	*	*	*	*	*	*	0,00	0,00				

7.2   NMR Spectra

Appendix

Appendix

1 pyruvic acid-d₃

Spectrum 1 ¹H NMR spectrum of 1 pyruvic acid-d₃ in D₂O.

Spectrum 2 ²H NMR spectrum of 1 pyruvic acid-d₃ in D₂O.

Spectrum 3 ^{13}C NMR spectrum of 1 pyruvic acid-d$_3$ in D$_2$O.

2 1-^{13}C-pyruvic acid-d$_3$

Spectrum 4 ^{1}H NMR spectrum of 2 1-^{13}C-pyruvic acid-d$_3$ in D$_2$O.
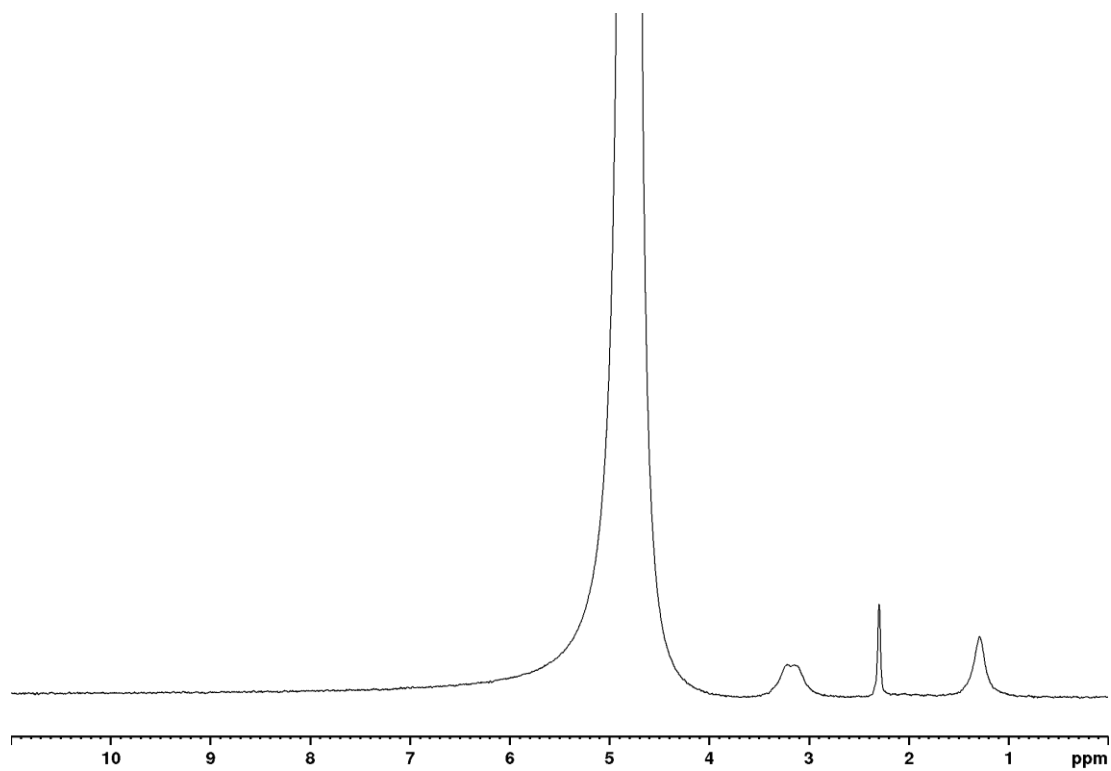
Spectrum 5 ^{2}H NMR spectrum of 2 1-^{13}C-pyruvic acid-d$_3$ in D$_2$O.

Spectrum 6 ^{13}C NMR spectrum of 2 1-^{13}C-pyruvic acid-d$_3$ in D$_2$O.

Appendix

3 3-(benzyloxy)-4-methoxybenzaldehyde

Spectrum 7 ¹H NMR spectrum of 3 3-(benzyloxy)-4-methoxy-benzaldehyde in CDCl₃.

Spectrum 8 ¹³C NMR spectrum of 3 3-(benzyloxy)-4-methoxy-benzaldehyde in CDCl₃.

4 5-(benzyloxy)-4-methoxy-2-nitrobenzahldehyde
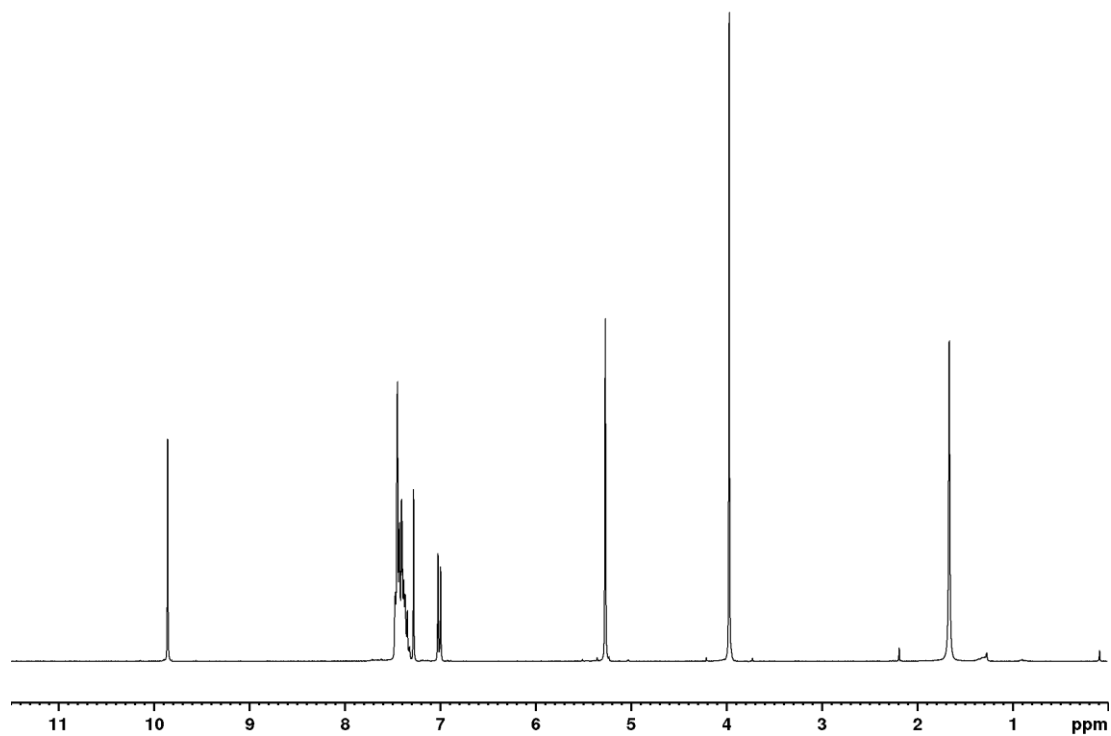
Spectrum 9 ^{1}H NMR spectrum of 4 5-(benzyloxy)-4-methoxy-2-nitrobenzahldehyde in CDCl$_3$.
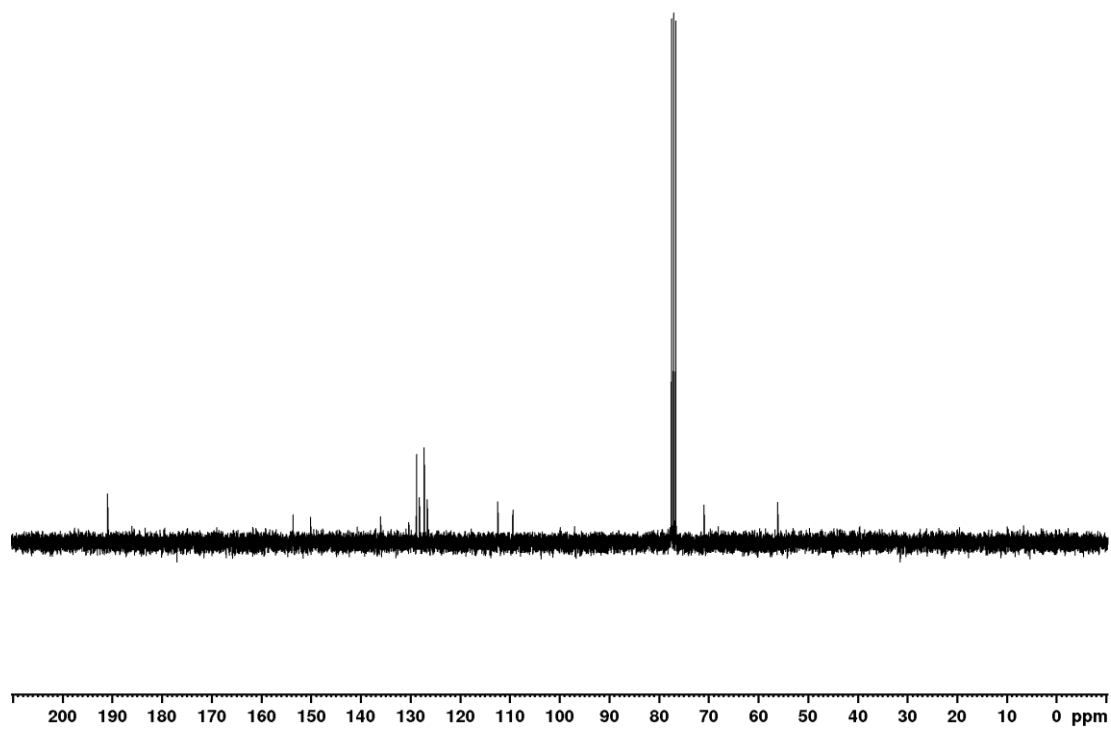
Spectrum 10 ^{13}C NMR spectrum of 4 5-(benzyloxy)-4-methoxy-2-nitrobenzahldehyde in CDCl$_3$.

Appendix

5 3-benzyloxy-4-methoxy-2-nitrobenzaldehyde
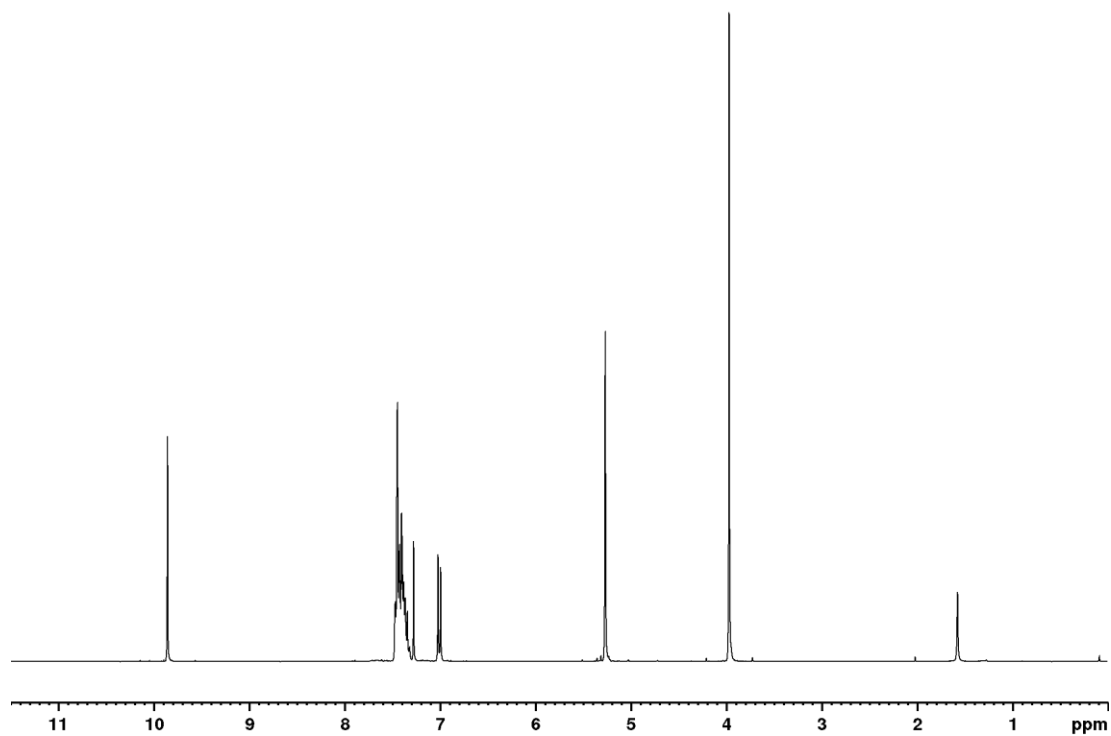
Spectrum 11 ^{1}H NMR spectrum of 5 4-(benzyloxy)-3-methoxybenzaldehyde in CDCl$_3$.
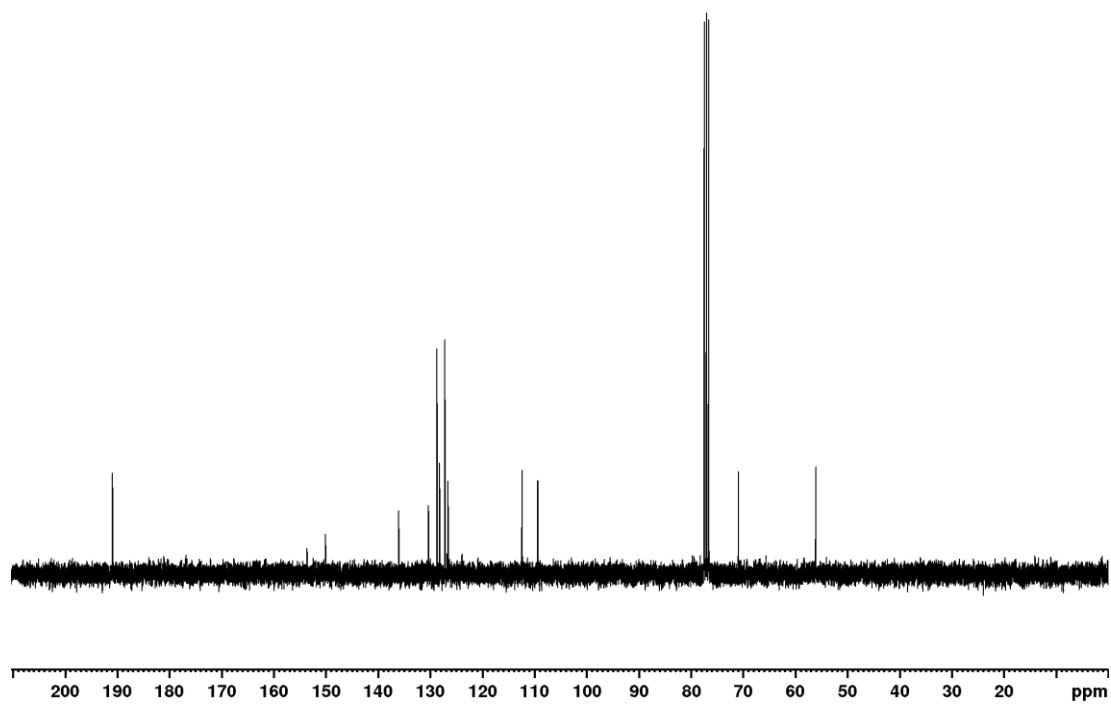
Spectrum 12 ^{13}C NMR spectrum of 5 4-(benzyloxy)-3-methoxybenzaldehyde in CDCl$_3$.

125

6 4-(benzyloxy)-5-methoxy-2-nitrobenzaldehyde
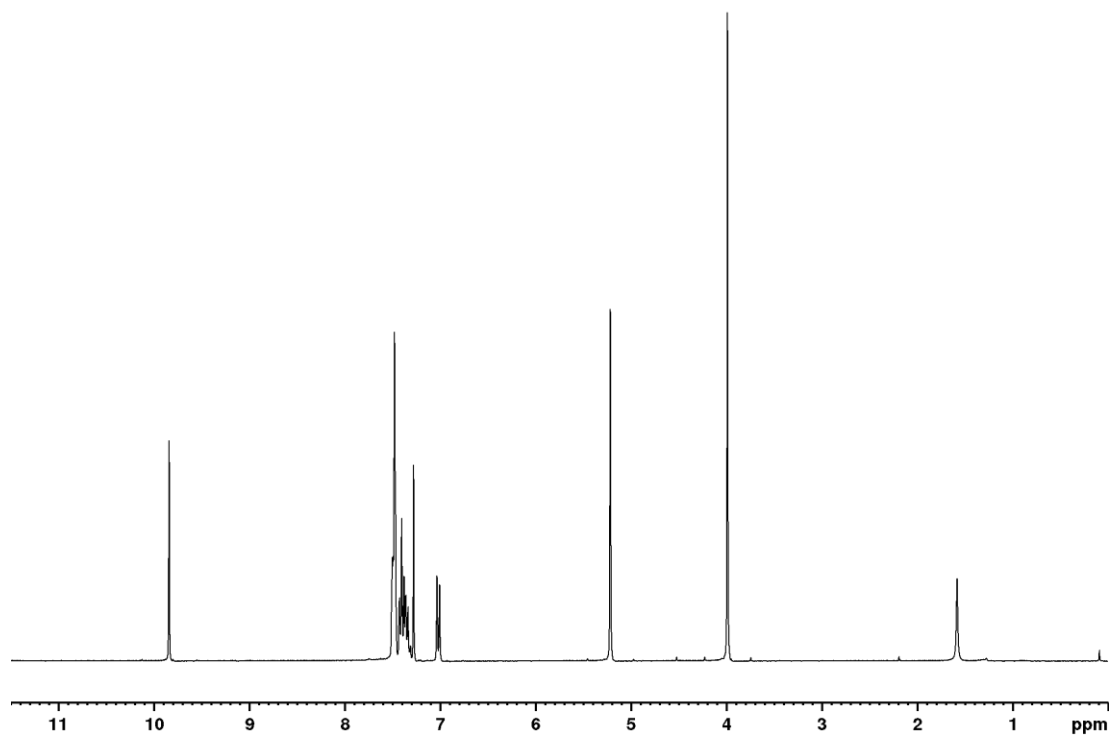
Spectrum 13 ^{1}H NMR spectrum of 6 4-(benzyloxy)-5-methoxy-2-nitrobenzaldehyde in CDCl$_3$.
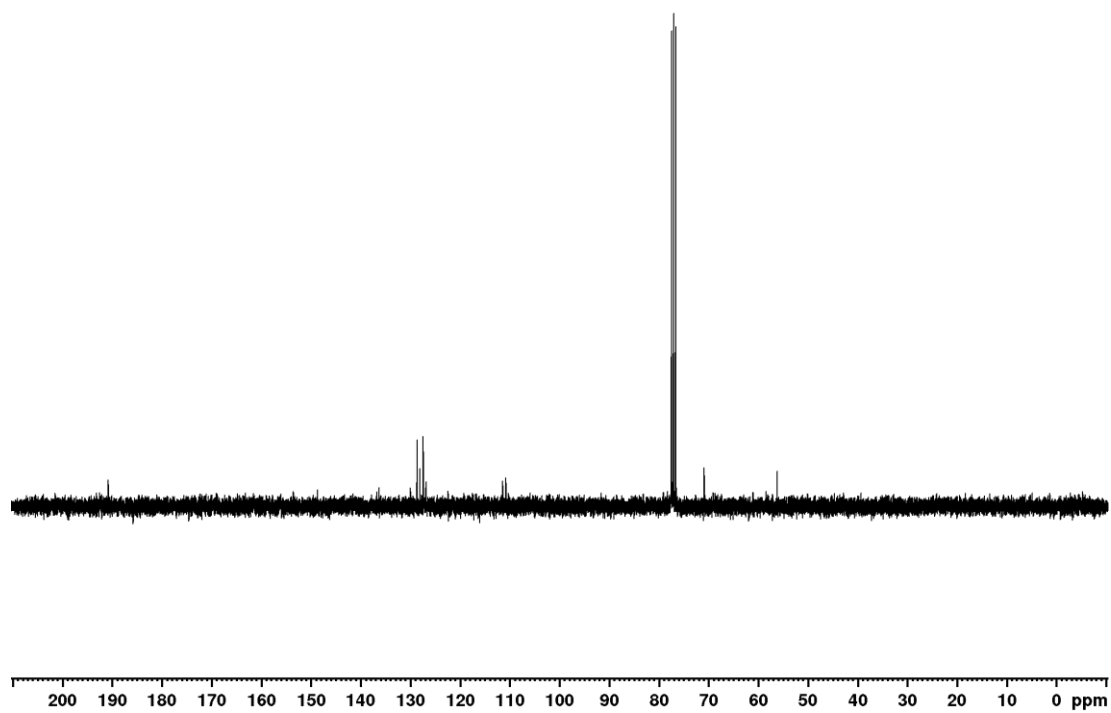
Spectrum 14 ^{13}C NMR spectrum of 6 4-(benzyloxy)-5-methoxy-2-nitrobenzaldehyde in CDCl$_3$.

9 1-(2-nitrophenyl)prop-2-yn-1-ol

Spectrum 15 ^{1}H NMR spectrum of 9 1-(2-nitrophenyl)prop-2-yn-1-ol in CDCl$_3$.
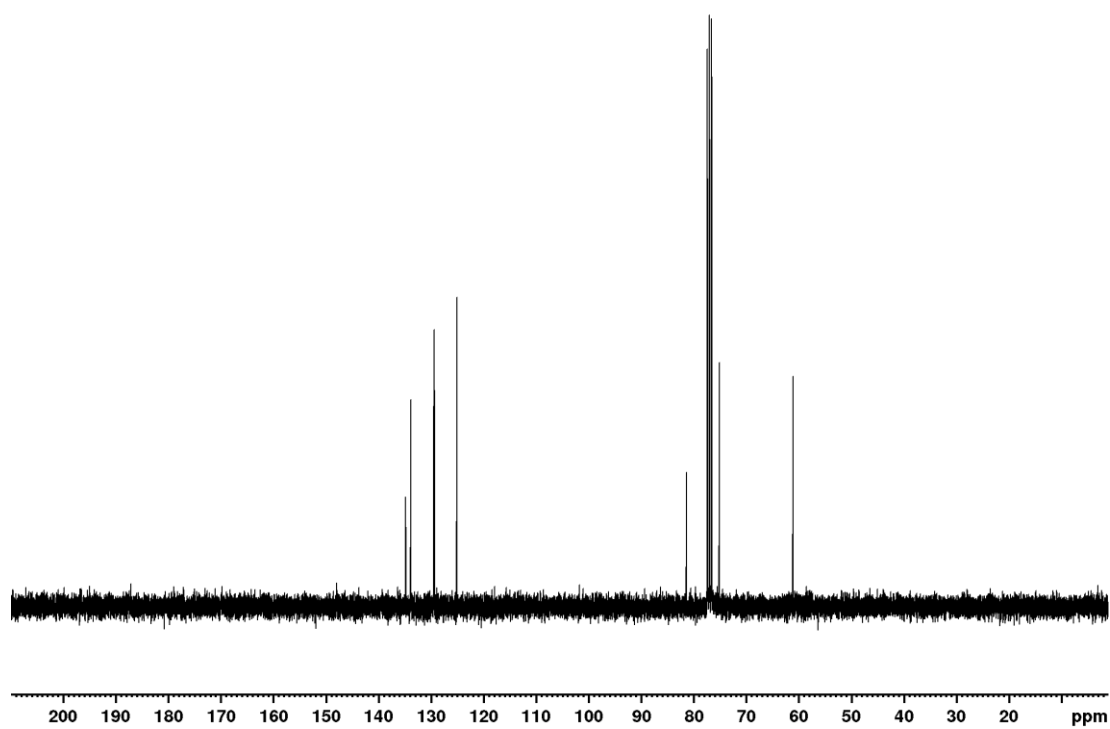
Spectrum 16 ^{13}C NMR spectrum of 9 1-(2-nitrophenyl)prop-2-yn-1-ol in CDCl$_3$.

10 1-(4,5-dimethoxy-2-nitrophenyl)pro-2-yn-1-ol
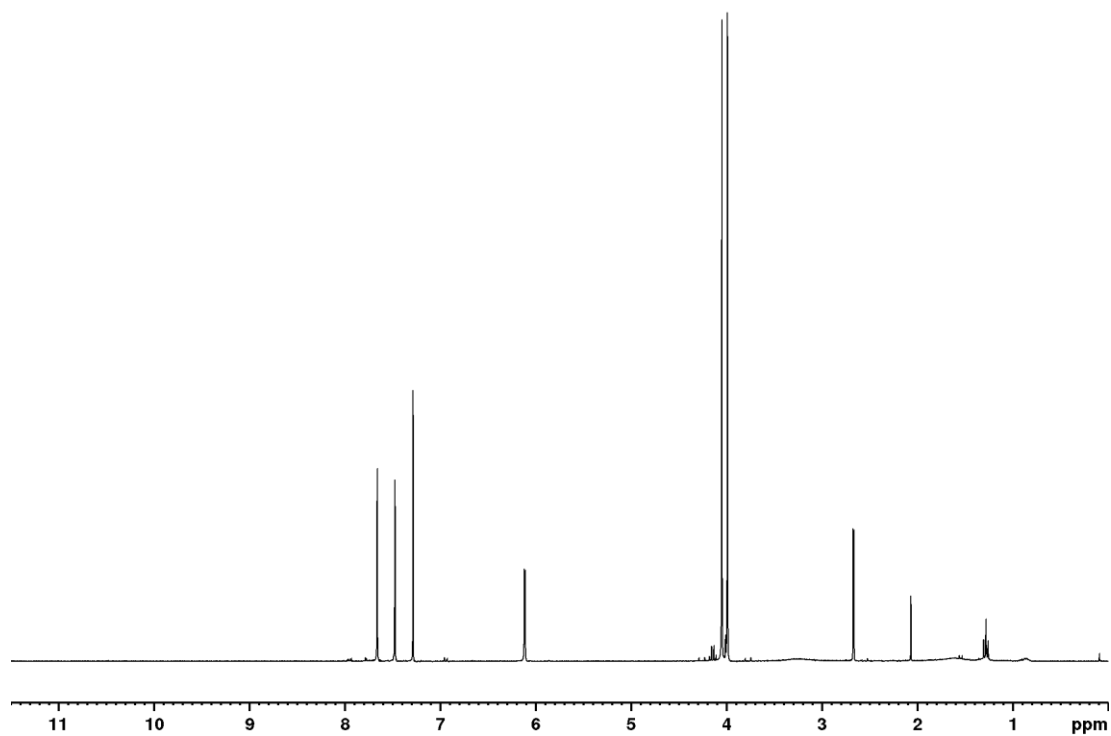
Spectrum 17 ^{1}H NMR spectrum of 10 1-(4,5-dimethoxy-2-nitrophenyl)pro-2-yn-1-ol in CDCl$_3$.
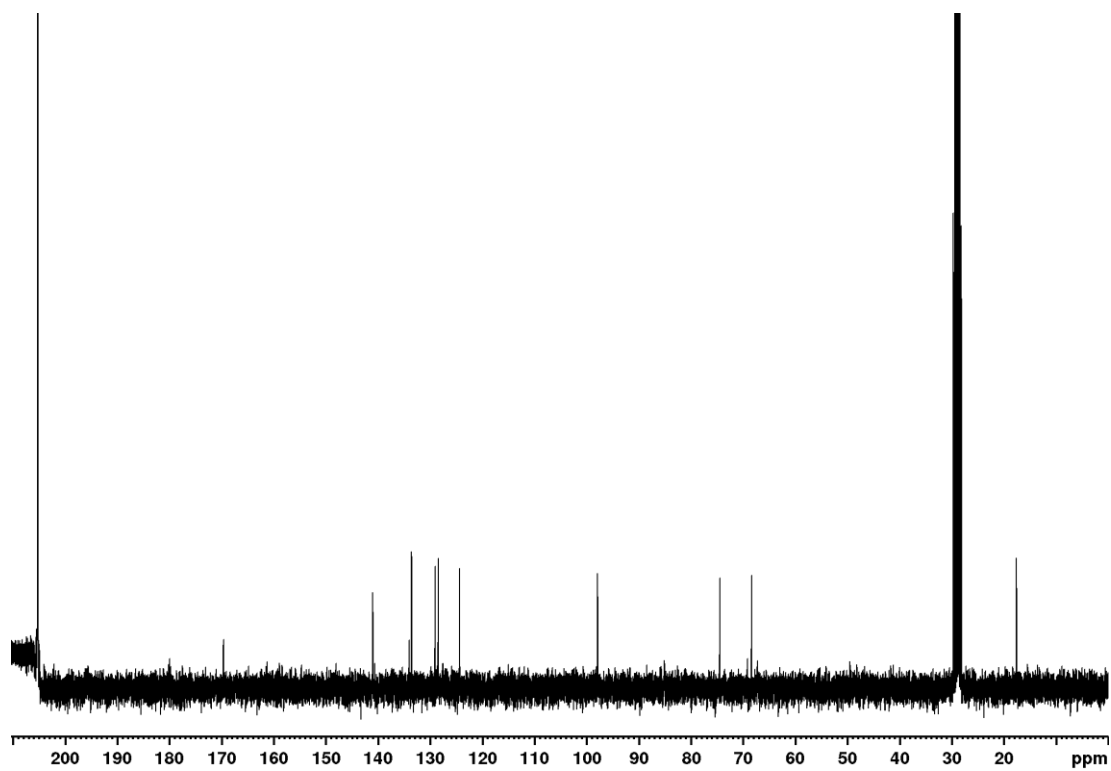
Spectrum 18 ^{13}C NMR spectrum of 10 1-(4,5-dimethoxy-2-nitrophenyl)pro-2-yn-1-ol in CDCl$_3$.

11 1-(-2-nitrophenyl)pro-2-yn-3-d-1-ol
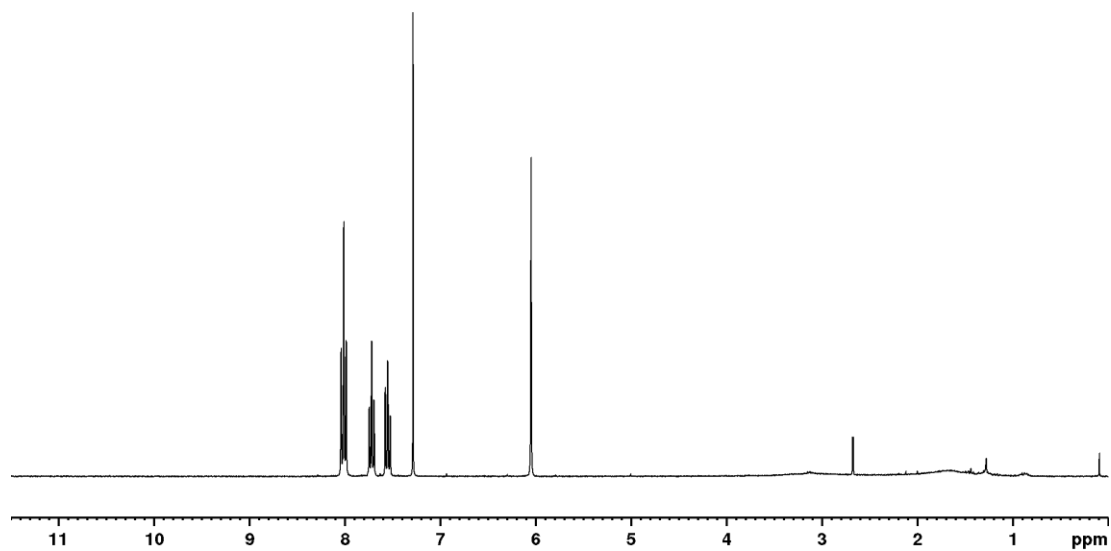
Spectrum 19 ^{1}H NMR spectrum of 11 1-(-2-nitrophenyl)pro-2-yn-3-d-1-ol in CDCl$_3$.
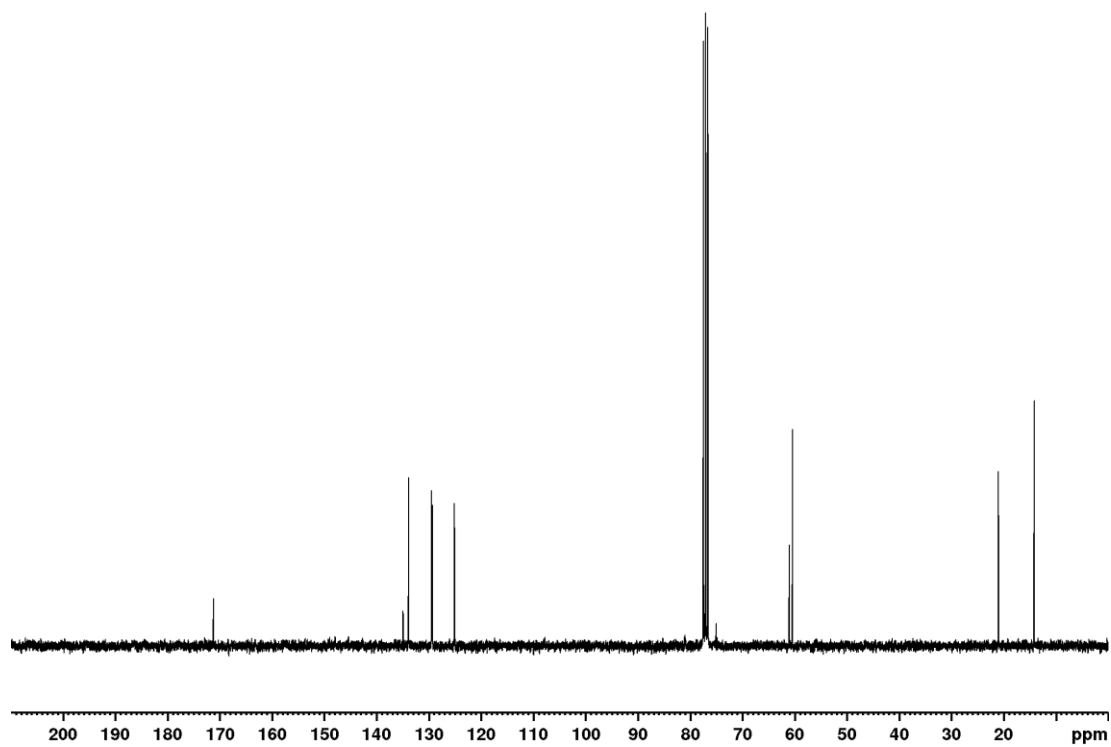
Spectrum 20 ^{13}C NMR spectrum of 11 1-(2-nitrophenyl)pro-2-yn-3-d-1-ol in CDCl$_3$.

12 1-(4,5-dimethoxy-2-nitrophenyl)pro-2-yn-3-d-1-ol
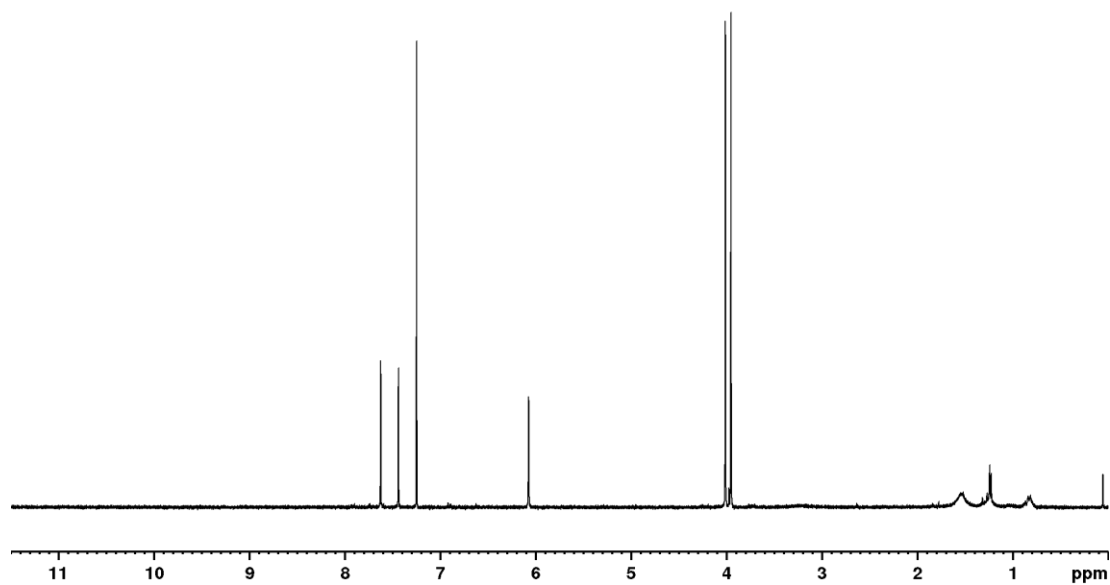
Spectrum 21 ^{1}H NMR spectrum of 12 1-(4,5-dimethoxy-2-nitrophenyl)pro-2-yn-3-d-1-ol in CDCl$_3$.
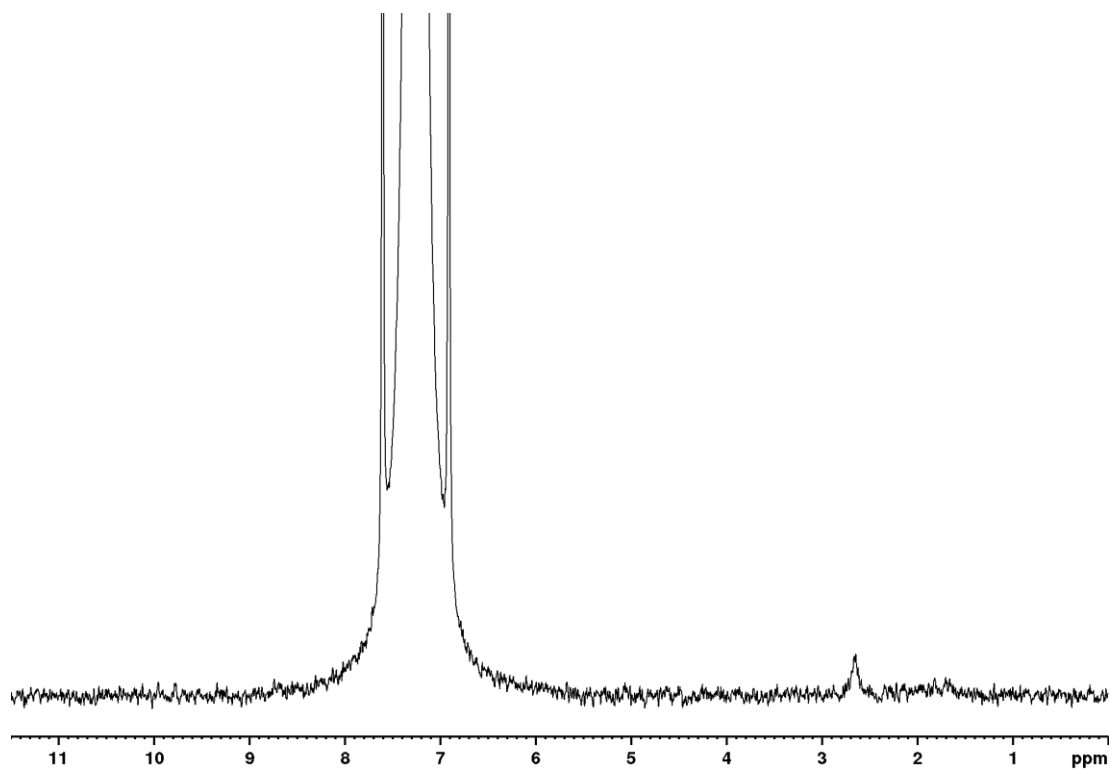
Spectrum 22 ^{2}H NMR spectrum of 12 1-(4,5-dimethoxy-2-nitrophenyl)pro-2-yn-3-d-1-ol in CDCl$_3$.

13 1-(2-nitrophenyl)prop-2-yn-1-yl-3-d-acetate
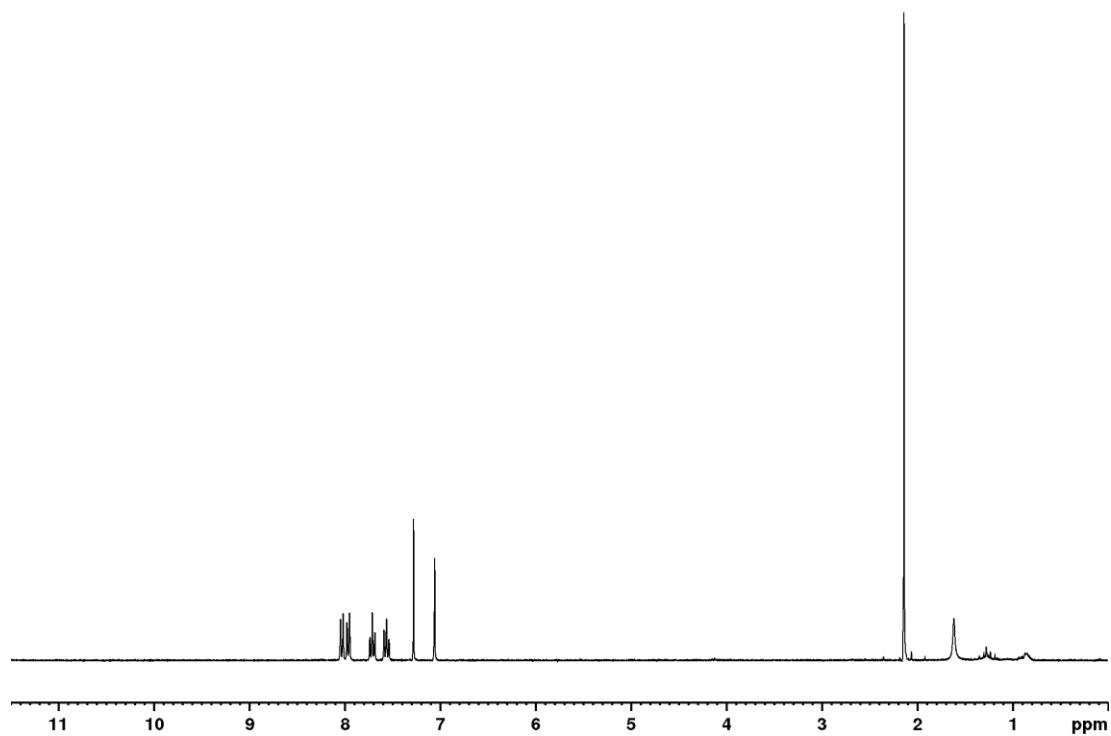
Spectrum 23 ^{1}H NMR spectrum of 13 1-(2-nitrophenyl)prop-2-yn-1-yl-3-d-acetate in CDCl$_3$.
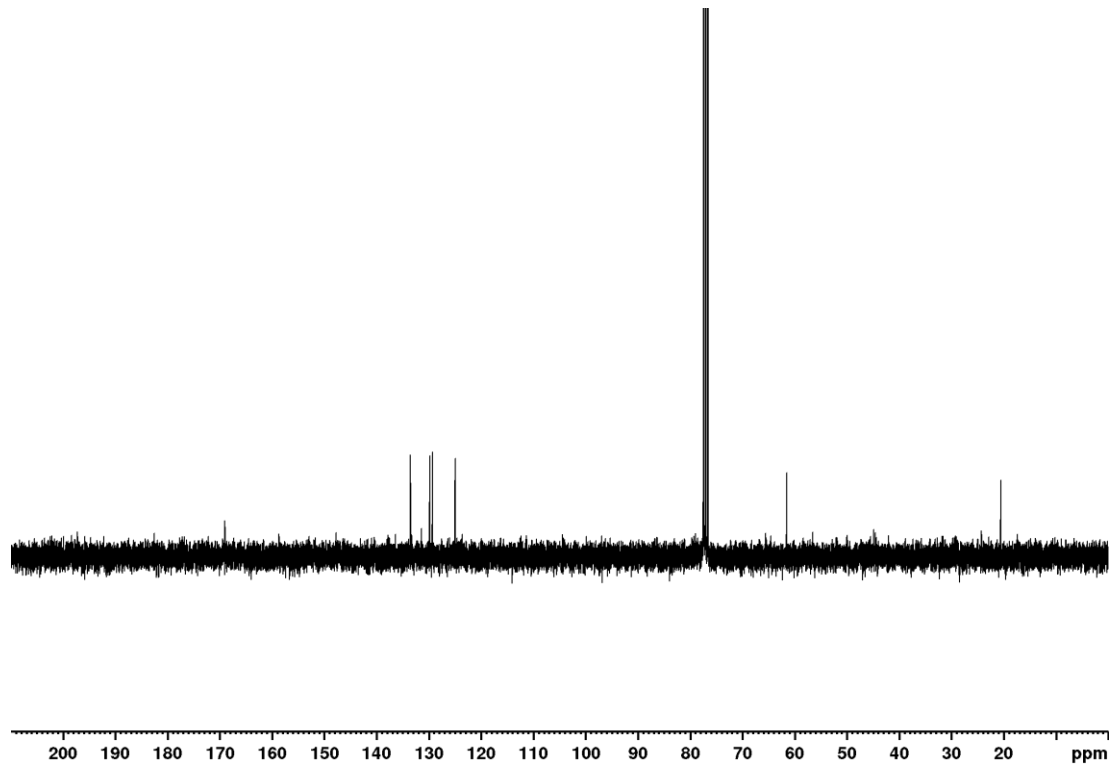
Spectrum 24 ^{13}C NMR spectrum of 13 1-(2-nitrophenyl)prop-2-yn-1-yl-3-d-acetate in CDCl$_3$.

14 1-(4,5-dimethoxy-2-nitrophenyl)prop-2-yn-1-yl-3-d-acetate
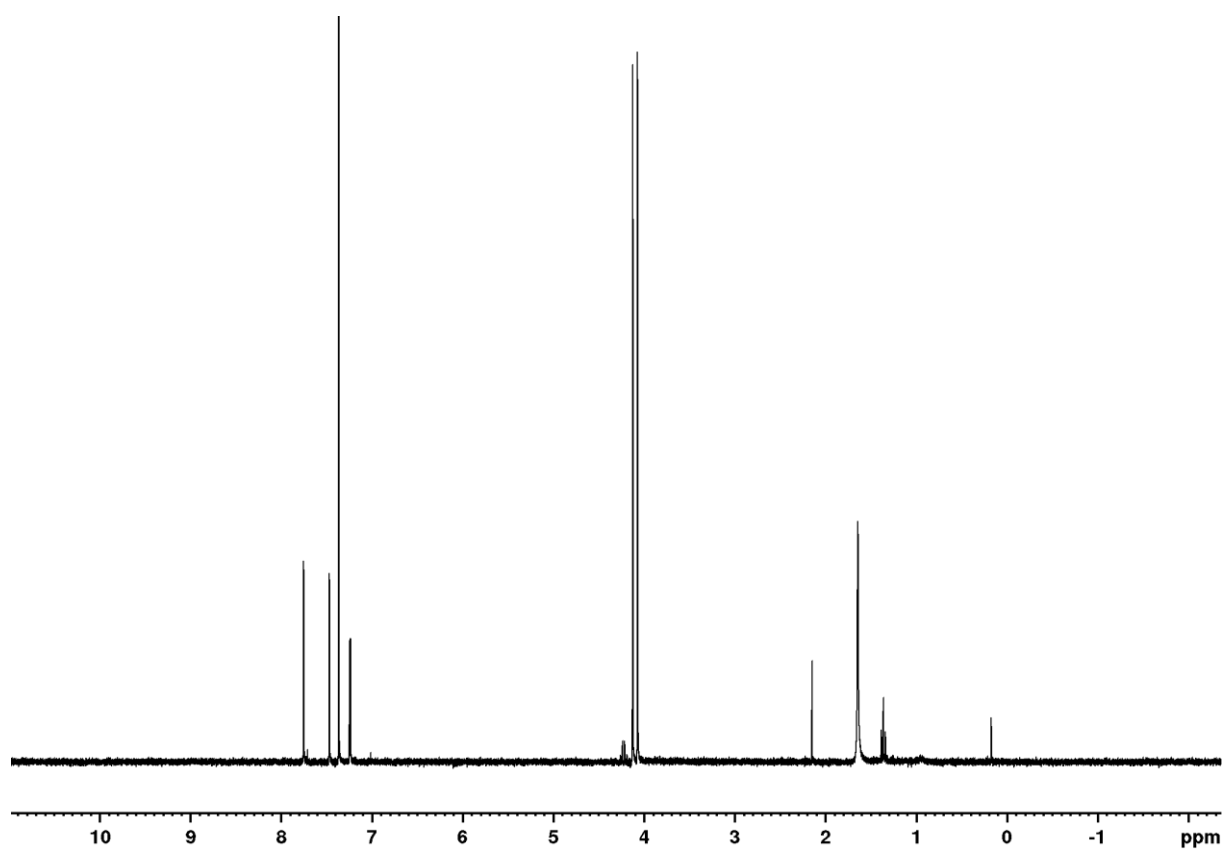
Spectrum 25 ^{1}H NMR spectrum of 14 1-(4,5-dimethoxy-2-nitrophenyl)prop-2-yn-1-3-d-acetate

15 1-(2-nitrophenyl)prop-2-yn-1-yl-3-d-2-oxoproanoate
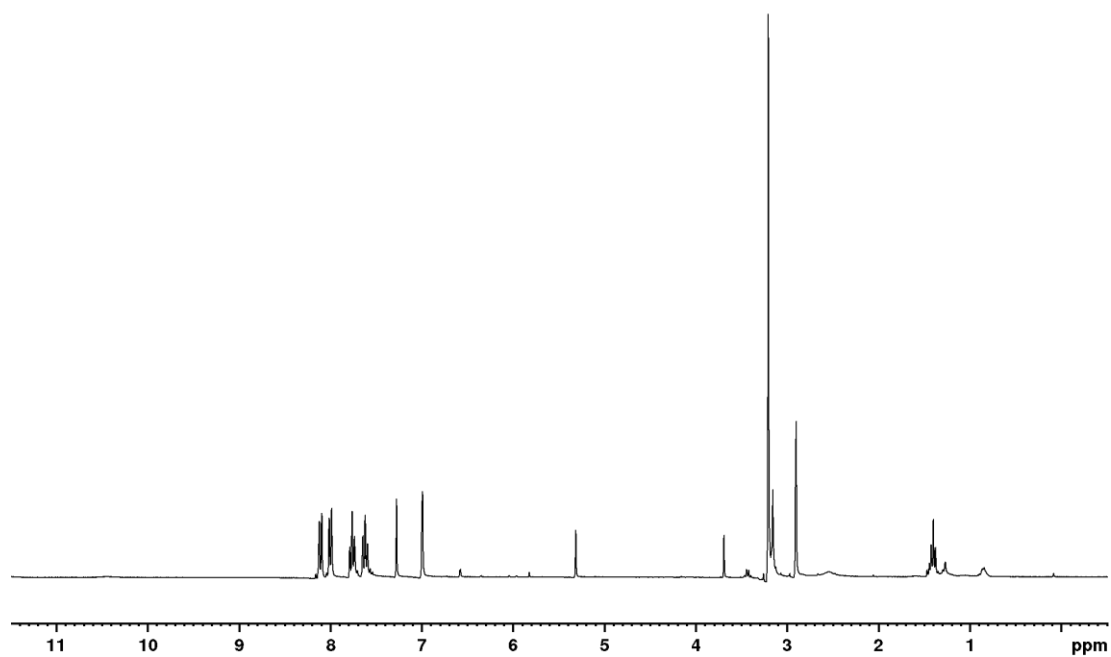
Spectrum 26 ¹H NMR spectrum of 15 1-(-2-ntirophenyl)prop-2-yn-1yl-3-d-2-oxopropanoate in CDCl₃.
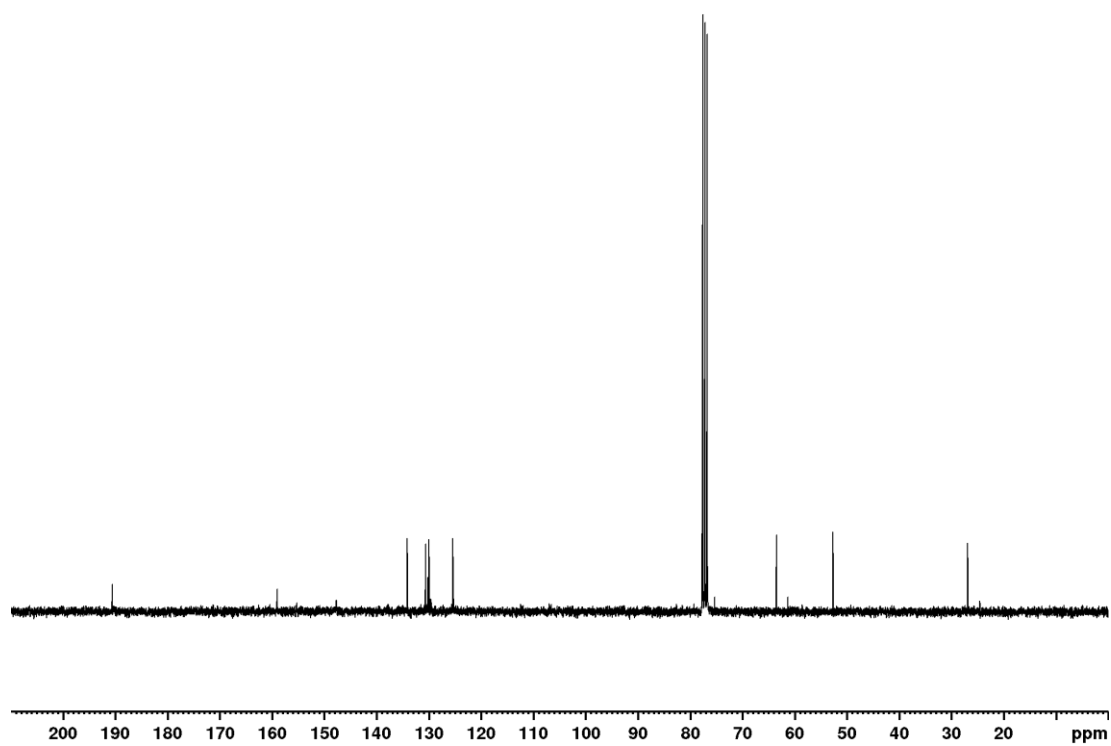
Spectrum 27 ¹³C NMR spectrum of 15 1-(2-ntirophenyl)prop-2-yn-1yl-3-d-2-oxopropanoate in CDCl₃.

Appendix

16 1-(4,5-dimethoxy-2-ntirophenyl)prop-2-yn-1yl-3-d-2-oxopropanoate
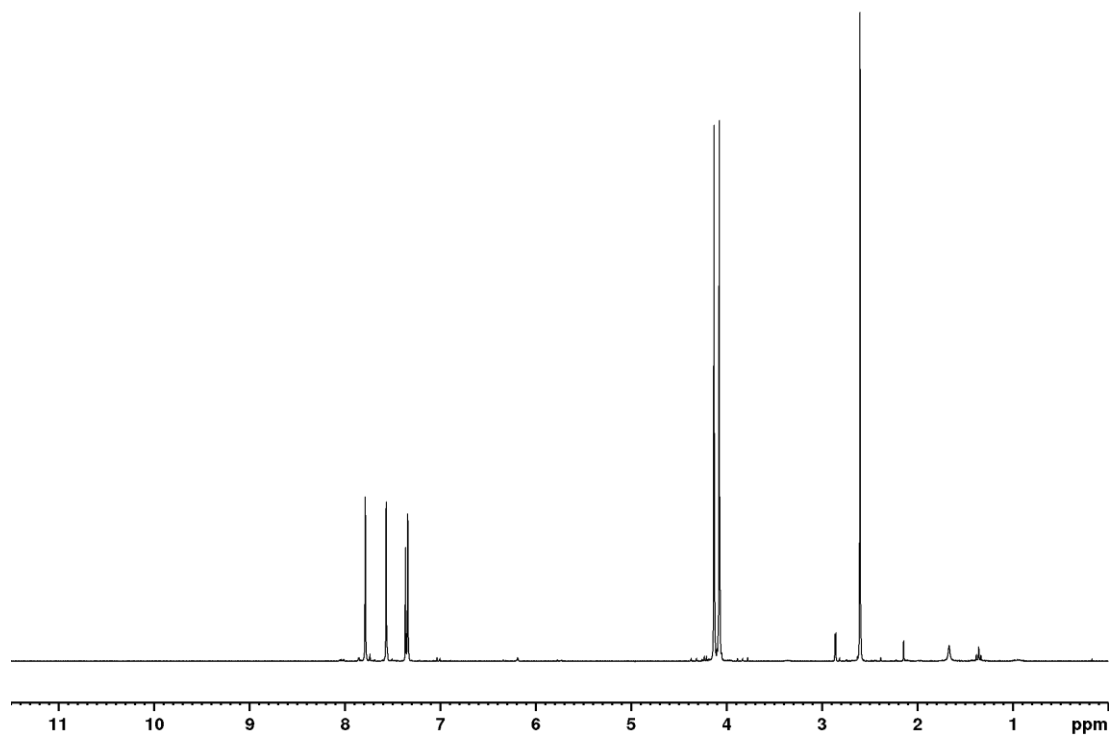
Spectrum 28 1H NMR spectrum of 16 1-(4,5-dimethoxy-2-ntirophenyl)prop-2-yn-1yl-3-d-2-oxopropanoate in acetone-d_6.
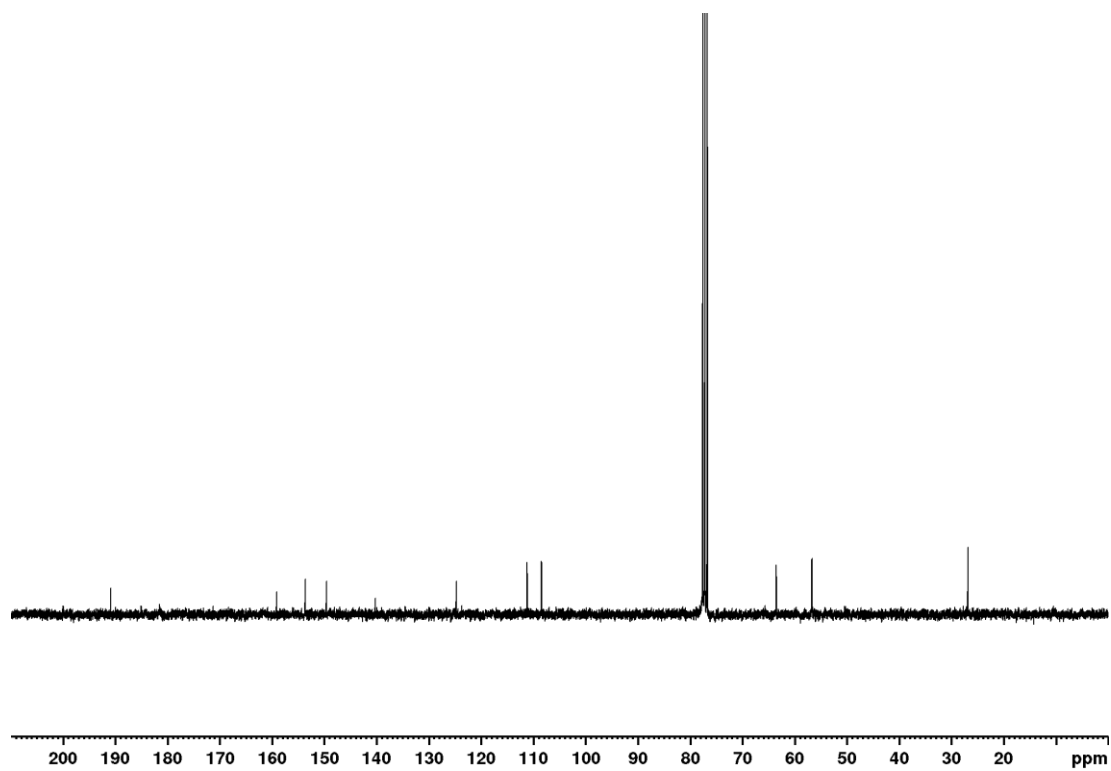
Spectrum 29 13C NMR spectrum of 16 1-(4,5-dimethoxy-2-ntirophenyl)prop-2-yn-1yl-3-d-2-oxopropanoate in CDCl$_3$.

17 1-(2-nitrophenyl)prop-2-yn-1-yl-3-d-acetate-1-^{13}C-d$_3$
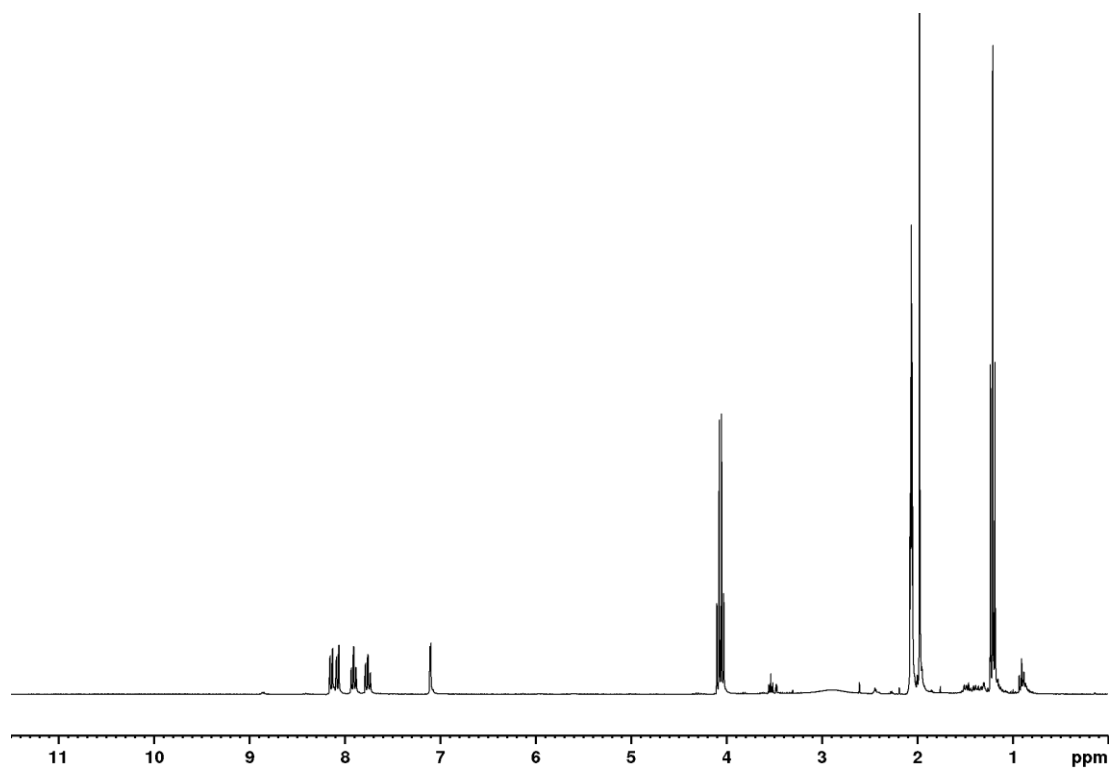
Spectrum 30 ^{1}H NMR spectrum of 17 1-(2-nitrophenyl)prop-2-yn-1-yl-3-d-acetate-1-^{13}C-d$_3$ in acetone-d$_3$
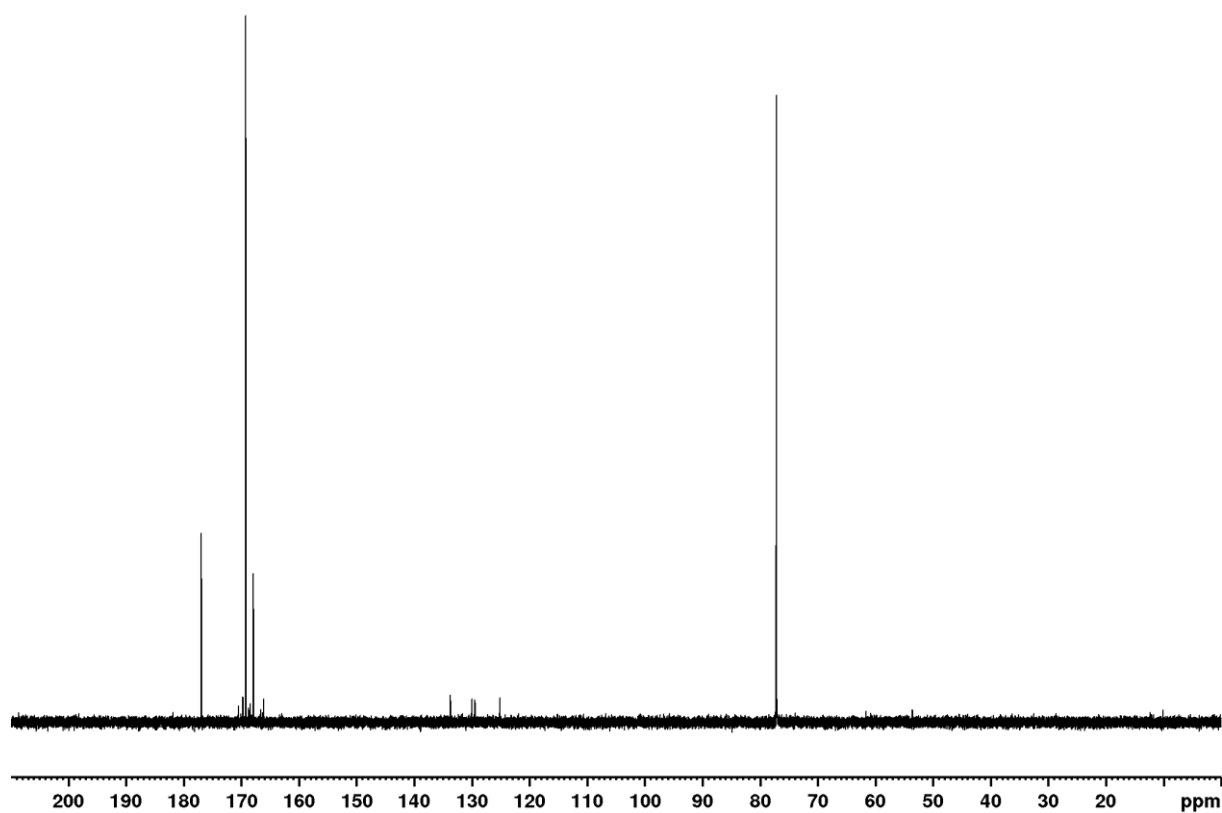
Appendix

18 1-(4,5-dimethoxy-2-nitrophenyl)prop-2-yn-1yl-3-d-acetate-1-^{13}C-d$_3$
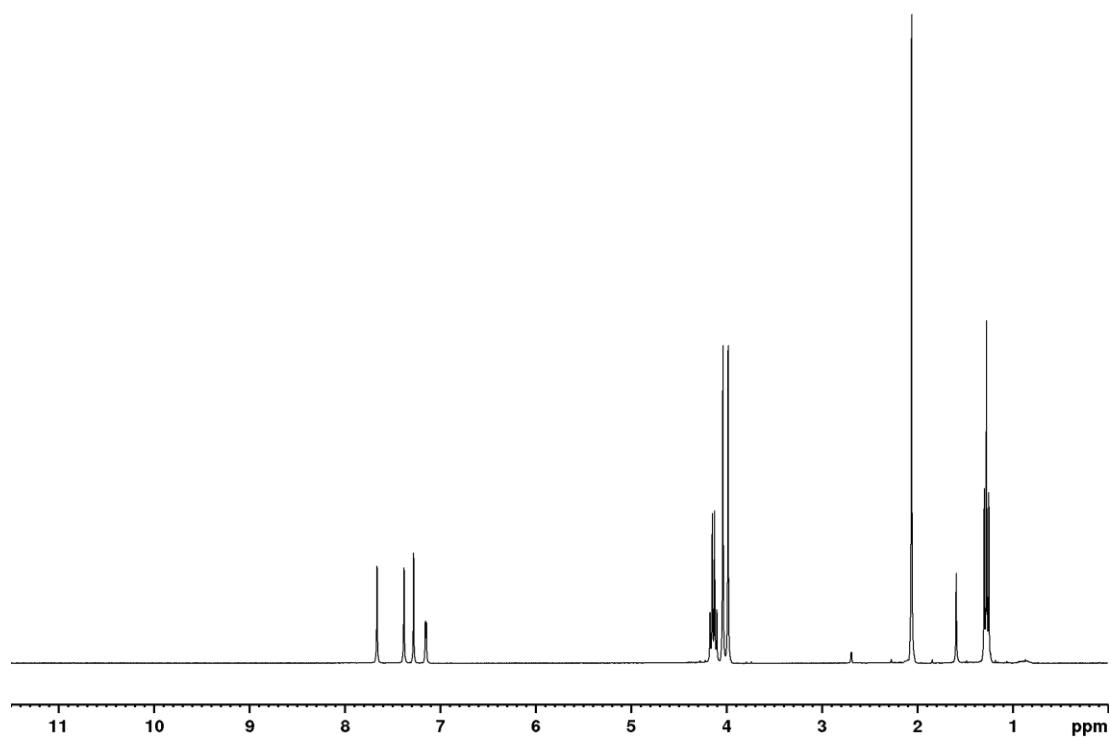
Spectrum 31 ^{1}H NMR spectrum of 18 1-(4,5-dimethoxy-2-nitrophenyl)prop-2-yn-1yl-3-d-acetate-1-^{13}C-d$_3$ in D$_2$O.
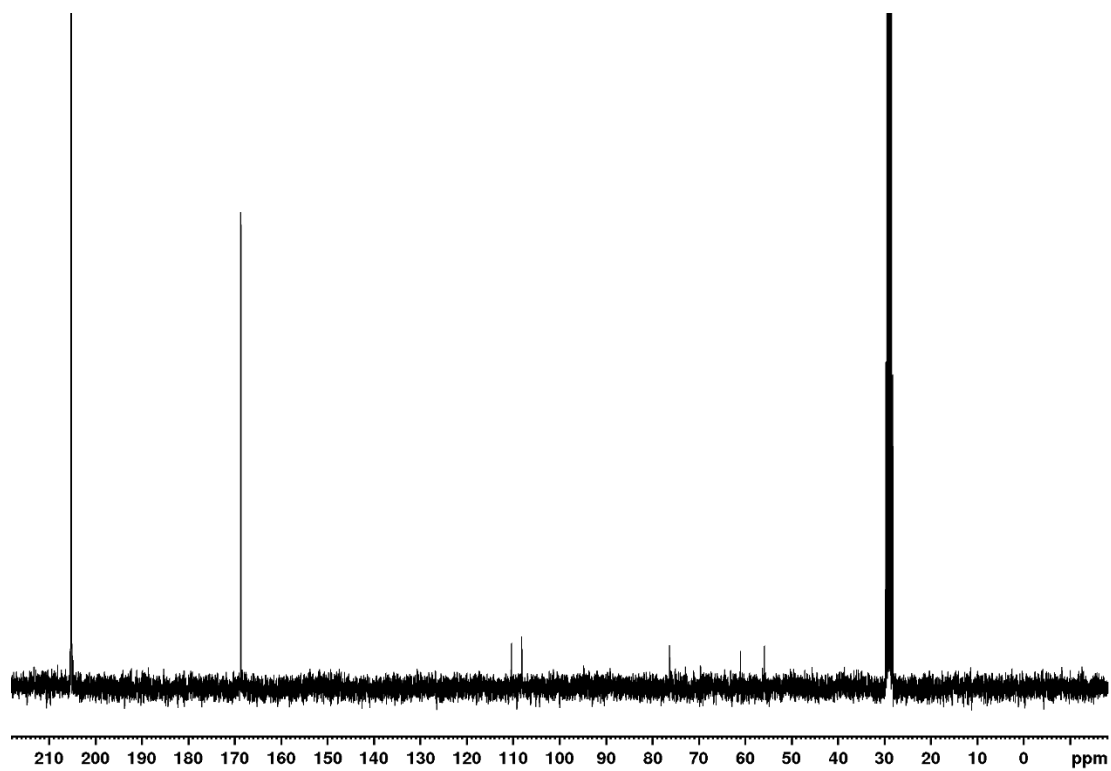
Spectrum 32 ^{13}C NMR spectrum of 18 1-(4,5-dimethoxy-2-nitrophenyl)prop-2-yn-1yl-3-d-acetate-1-^{13}C-d$_3$ in D$_2$O

Appendix

19 1-(2-nitrophenyl)prop-2-yn-1-yl-3-d-2-oxopropanoate-1-^{13}C-3-d$_3$
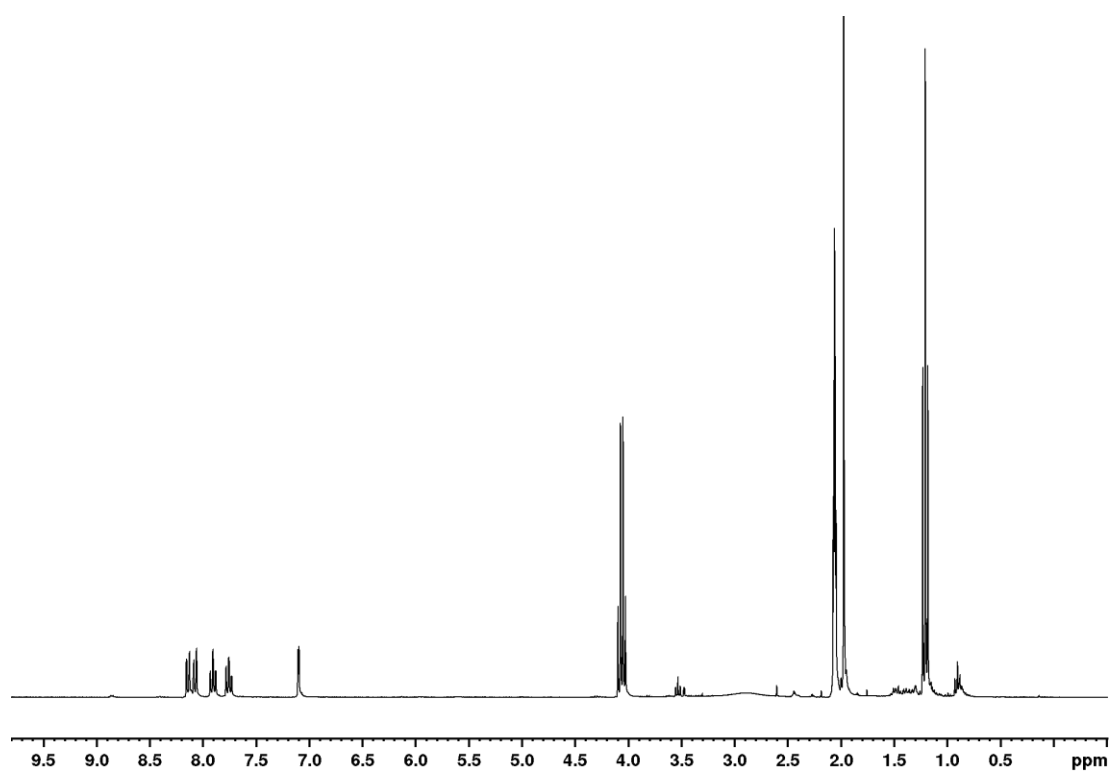
Spectrum 33 ^{1}H NMR spectrum of 19 1-(2-nitrophenyl)prop-2-yn-1-yl-3-d-2-oxopropanoate-1-^{13}C-3-d$_3$ in CDCl$_3$
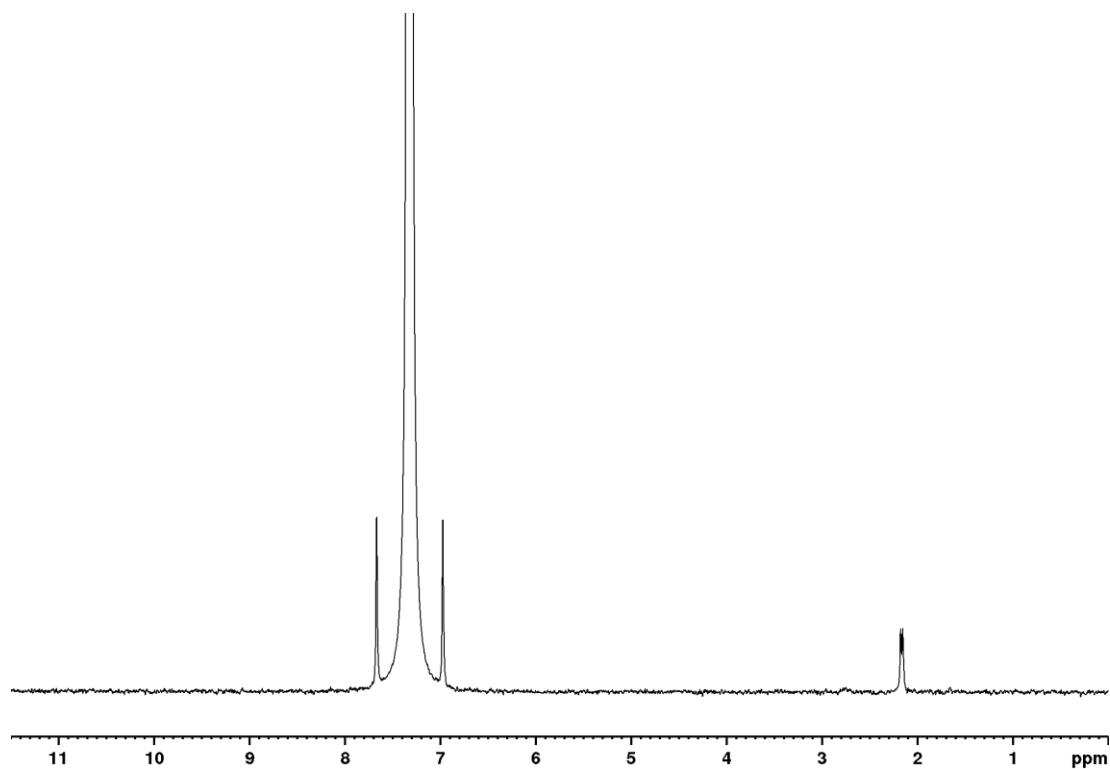
Spectrum 34 ^{2}H NMR spectrum of 19 1-(2-nitrophenyl)prop-2-yn-1-yl-3-d-2-oxopropanoate-1-^{13}C-3-d$_3$ in CDCl$_3$
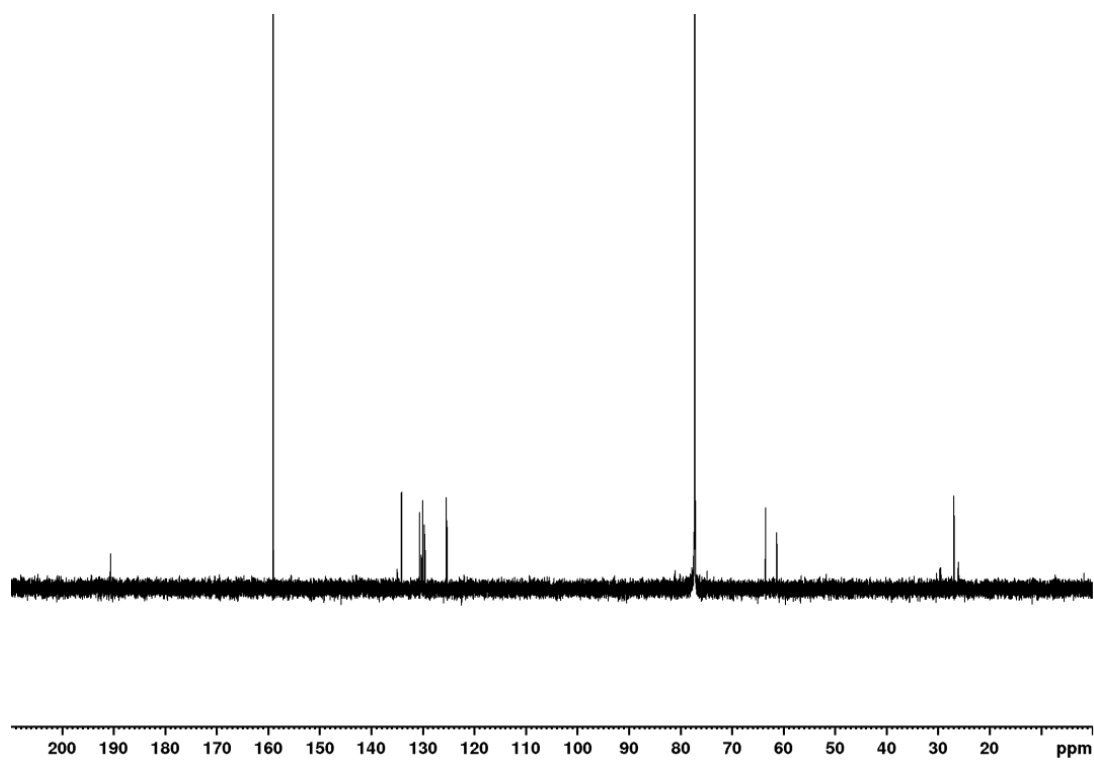
Spectrum 35 ^{13}C NMR spectrum of 19 1-(2-nitrophenyl)prop-2-yn-1-yl-3-d-2-oxopropanoate-1-^{13}C-3-d$_3$ in CDCl$_3$

20 1-(4,5-dimethoxy-2-nitrophenyl)prop-2-yn-1-yl-3-d-2-oxopropanoate-1-^{13}C-d$_3$
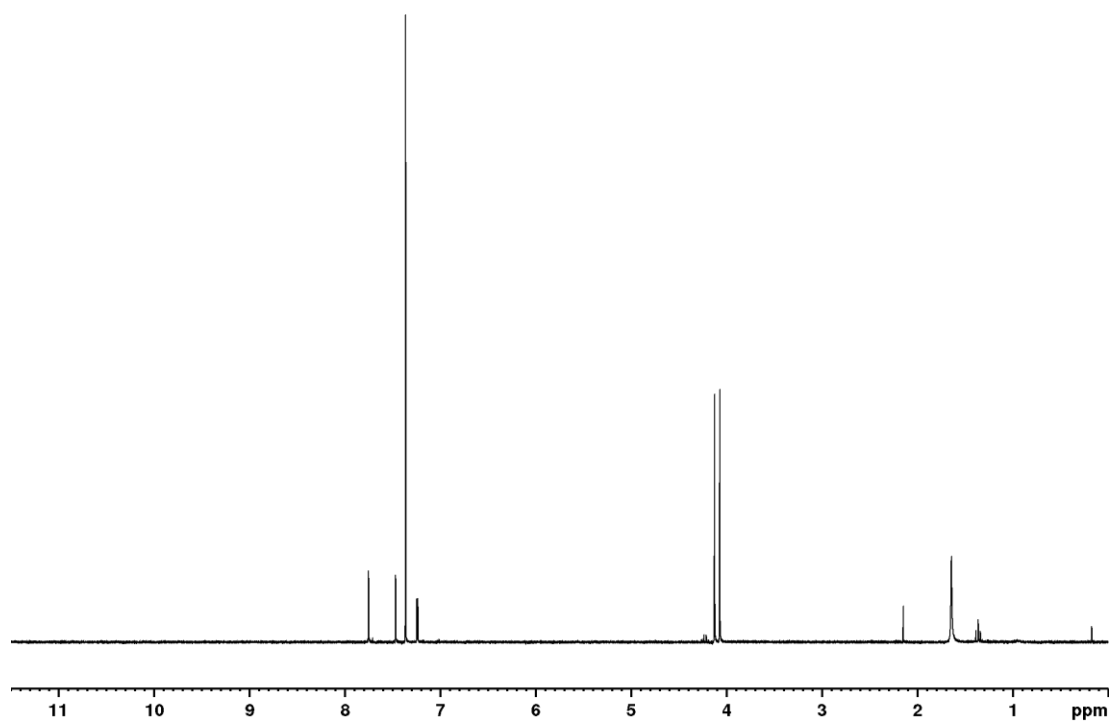
Spectrum 36 ^{1}H NMR spectrum of 20 1-(4,5-dimethoxy-2-nitrophenyl)prop-2-yn-1-yl-3-d-2-oxopropanoate-1-^{13}C-d$_3$ in CDCl$_3$.
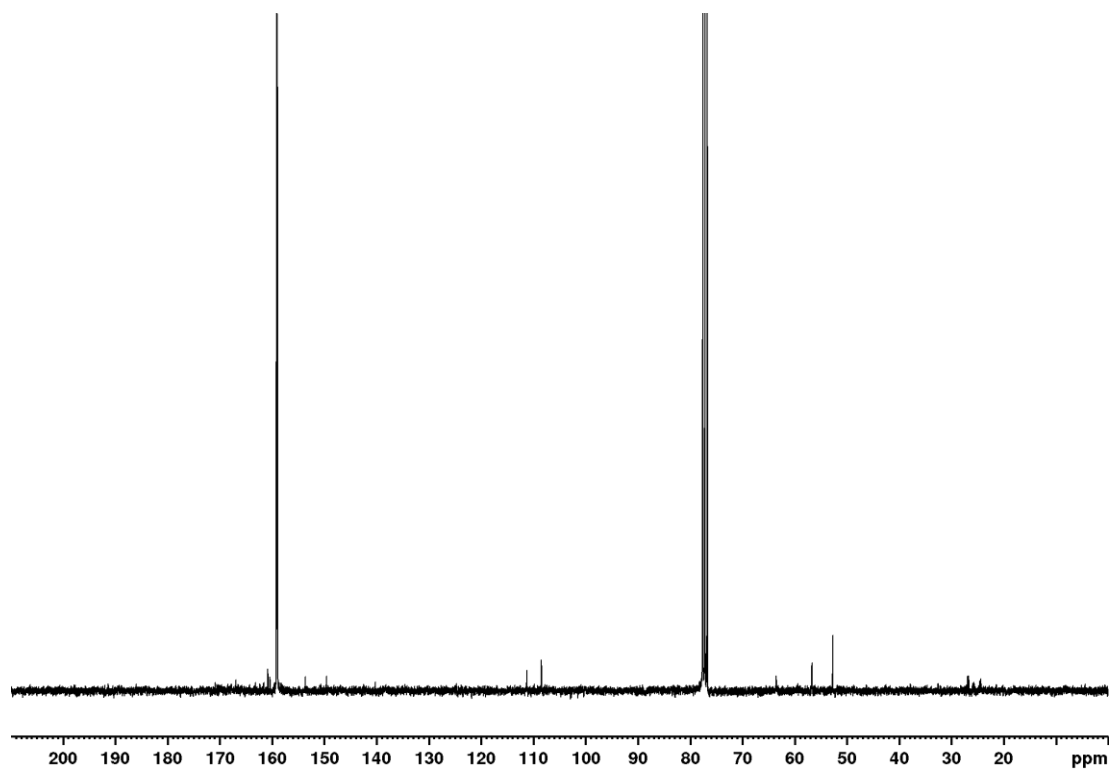
Spectrum 37 ^{13}C NMR spectrum of 20 1-(4,5-dimethoxy-2-nitrophenyl)prop-2-yn-1-yl-3-d-2-oxopropanoate-1-^{13}C-d$_3$ in CDCl$_3$.

Appendix

21 1-(2-nitrophenyl)allyl-2-oxopropanoate
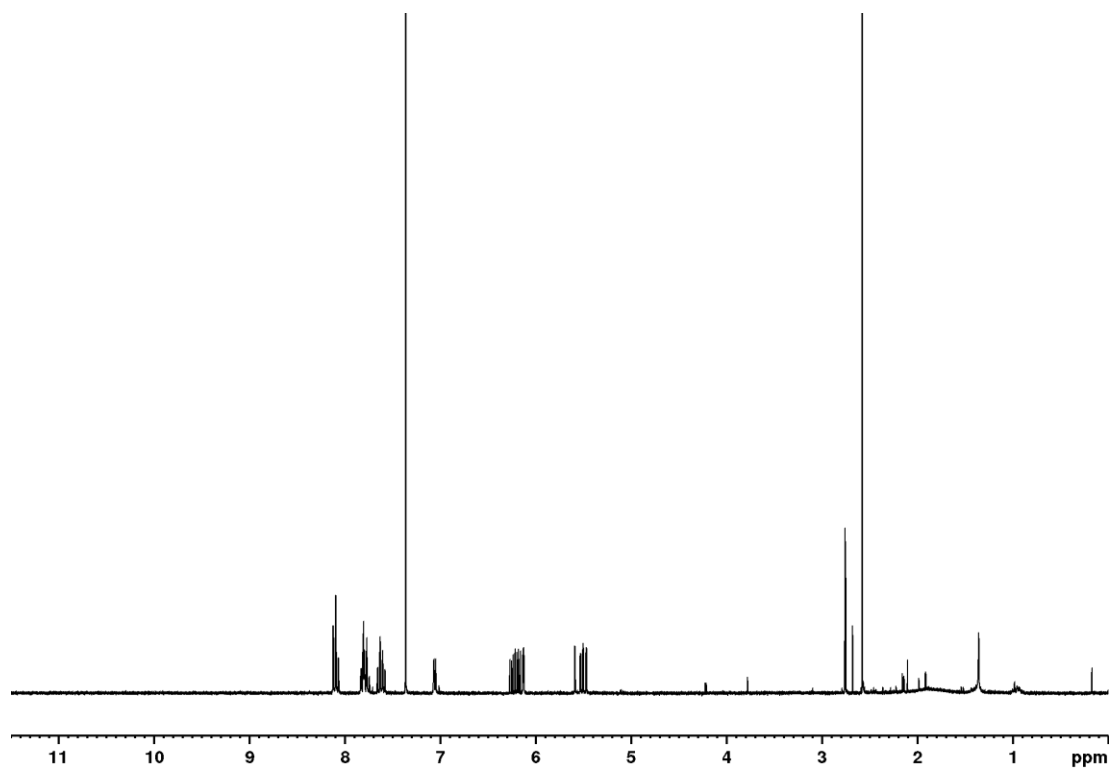
Spectrum 38 ^{1}H NMR spectrum of 21 1-(2-nitrophenyl)allyl-2-oxopropanoate in CDCl$_3$.
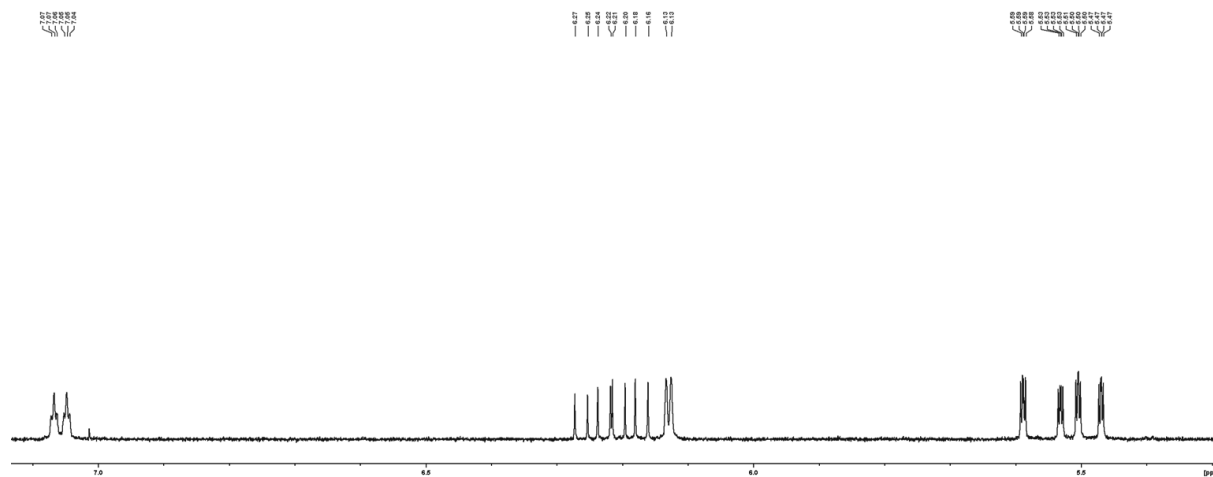
Spectrum 39 Zoomed ^{1}H NMR spectrum of 21 1-(2-nitrophenyl)allyl-2-oxopropanoate in CDCl$_3$.

Appendix

22 1-(4,5-dimehtoxy-2-nitrophenyl)allyl-oxopropanoate
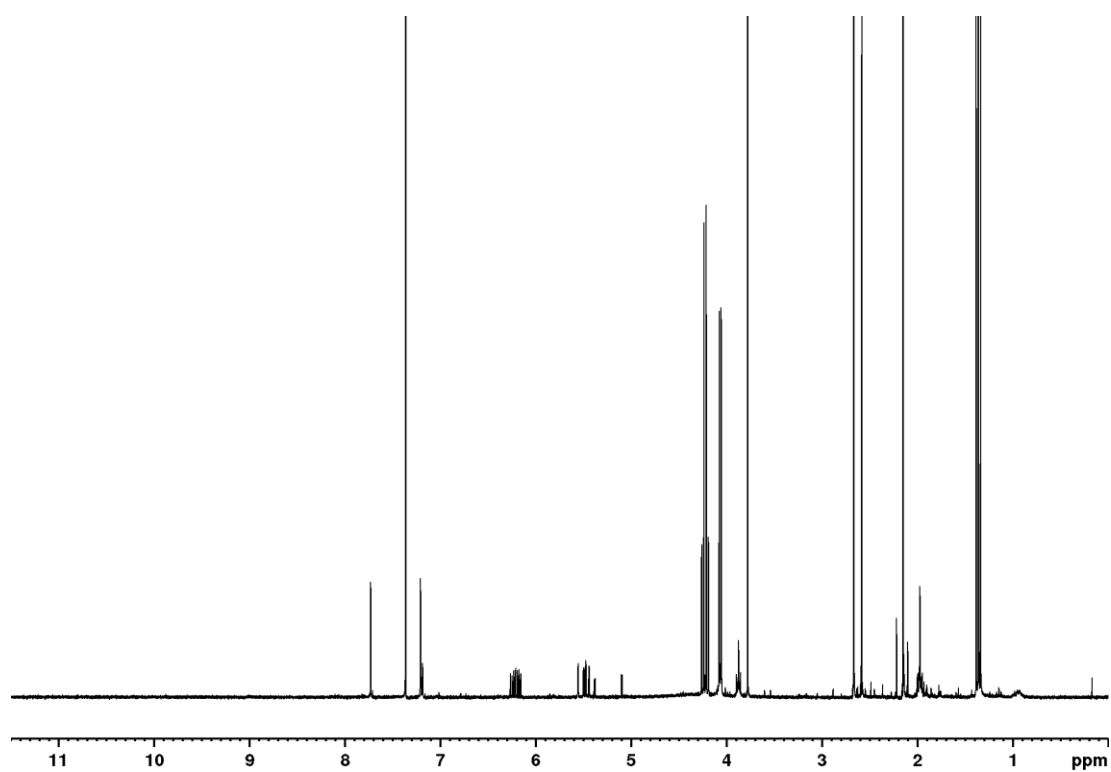
Spectrum 40 ¹H NMR spectrum of 22 1-(4,5-dimehtoxy-2-nitrophenyl)allyl-oxopropanoate in CDCl₃.
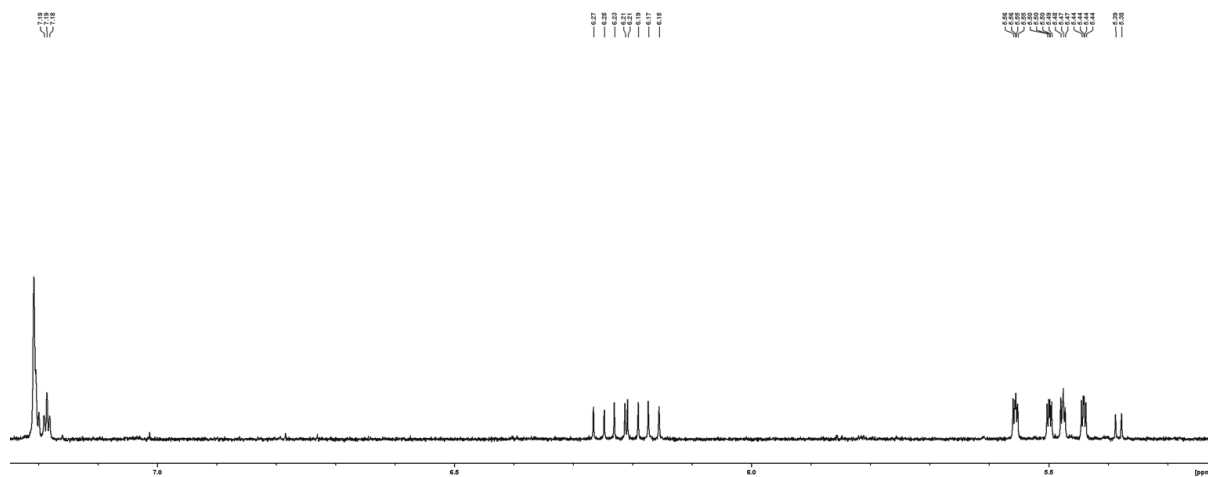
Spectrum 41 Zoomed ¹H NMR spectrum of 22 1-(4,5-dimehtoxy-2-nitrophenyl)allyl-oxopropanoate in CDCl₃.
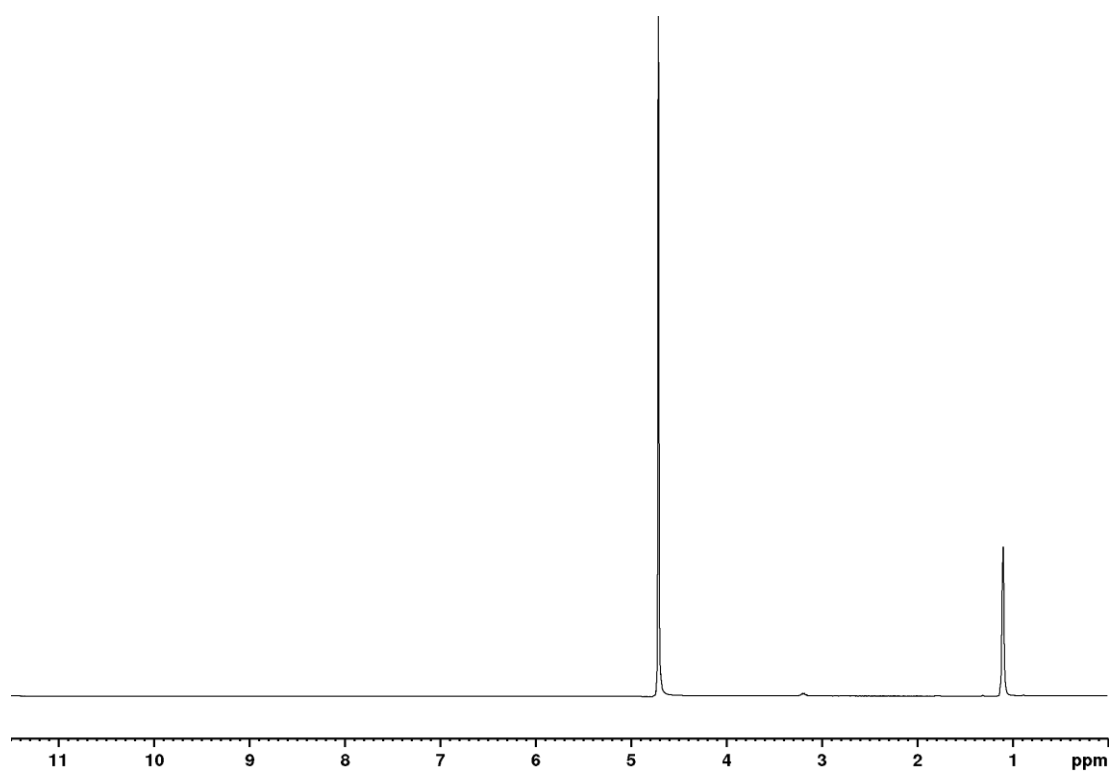
23 L-alanine-2-d

Spectrum 42 ^{1}H NMR spectrum of 23 L-alanine-2-d in D$_2$O.

24 (Acetyl-d₃)-L-alanine-2-d
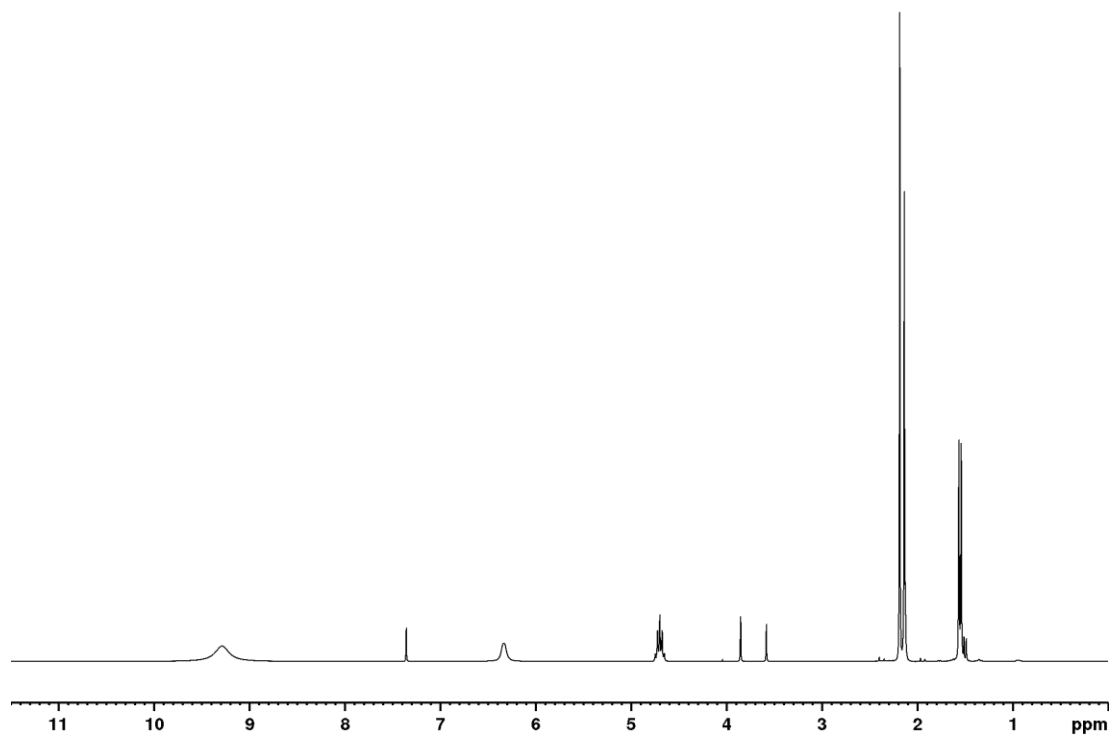
Spectrum 43 ^{1}H NMR spectrum of 24 (acetyl-d$_3$)-L-alanine-2-d in CDCl$_3$.
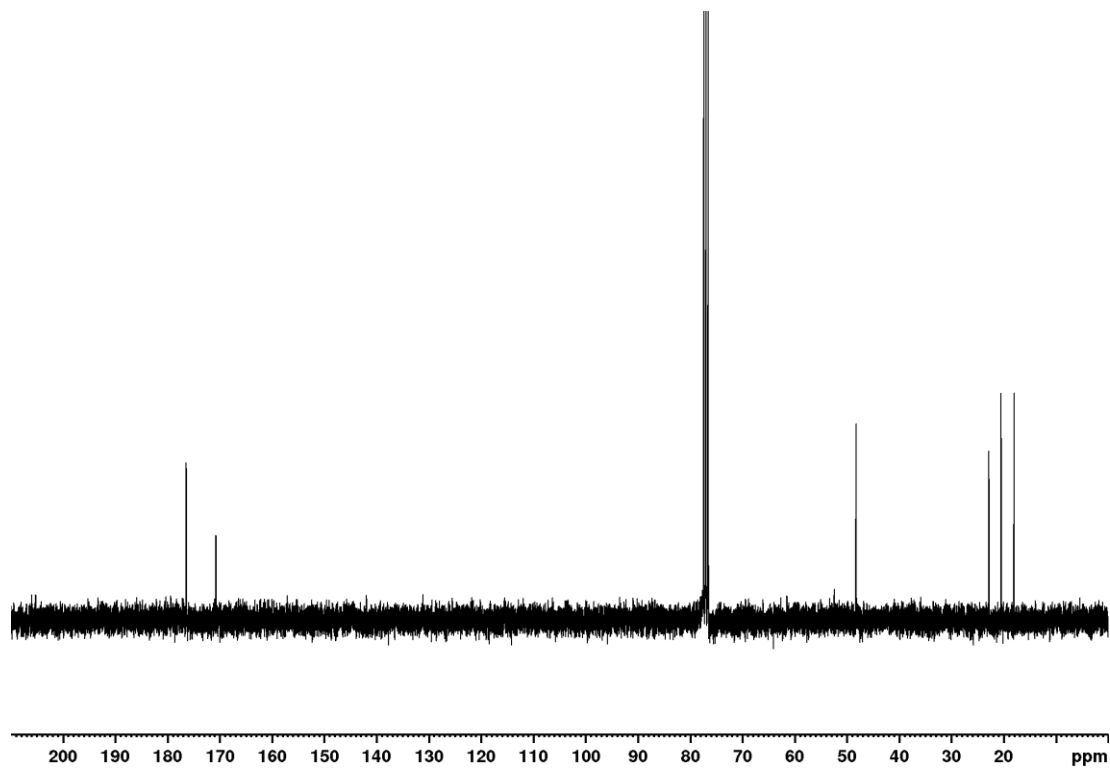
Spectrum 44 ^{13}C NMR spectrum of 24 (acetyl-d$_3$)-L-alanine-2-d in CDCl$_3$.

25 Vinyl (acetyl-d$_3$)-L-alaninate-2-d
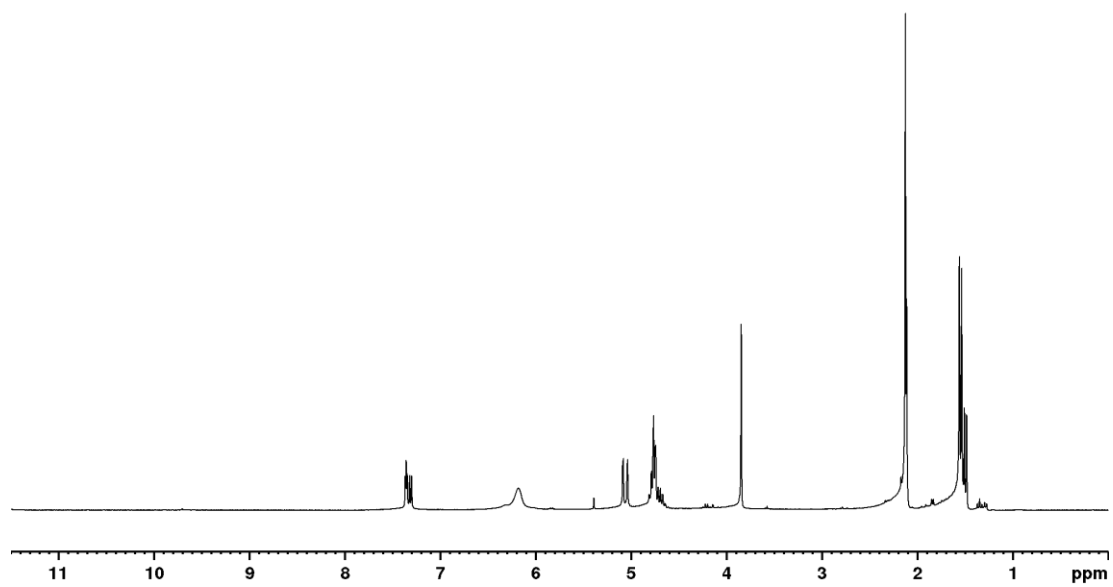
Spectrum 45 ^{1}H NMR spectrum of 25 vinyl (acetyl-d$_3$)-L-alanine-2-d in CDCl$_3$.
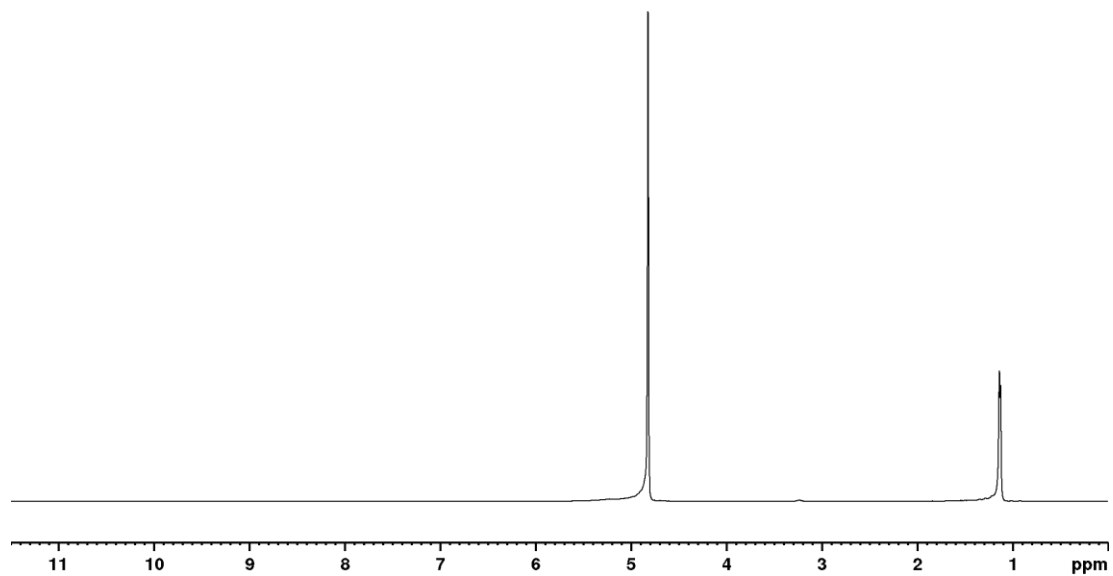
26 L-alanine-1-^{13}C-2-d

Spectrum 46 ^{1}H NMR spectrum of 26 L-alanine-1-^{13}C-2-d in D$_2$O.
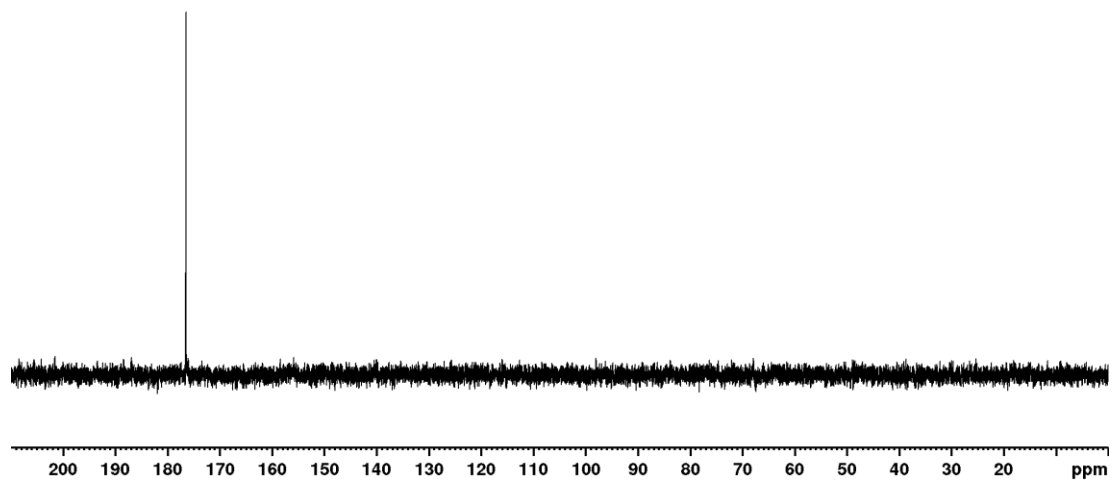
Spectrum 47 ^{13}C NMR spectrum of 26 L-alanine-1-^{13}C-2-d in D$_2$O.

27 (Acetyl-d$_3$)-L-alanine-1-^{13}C-2-d
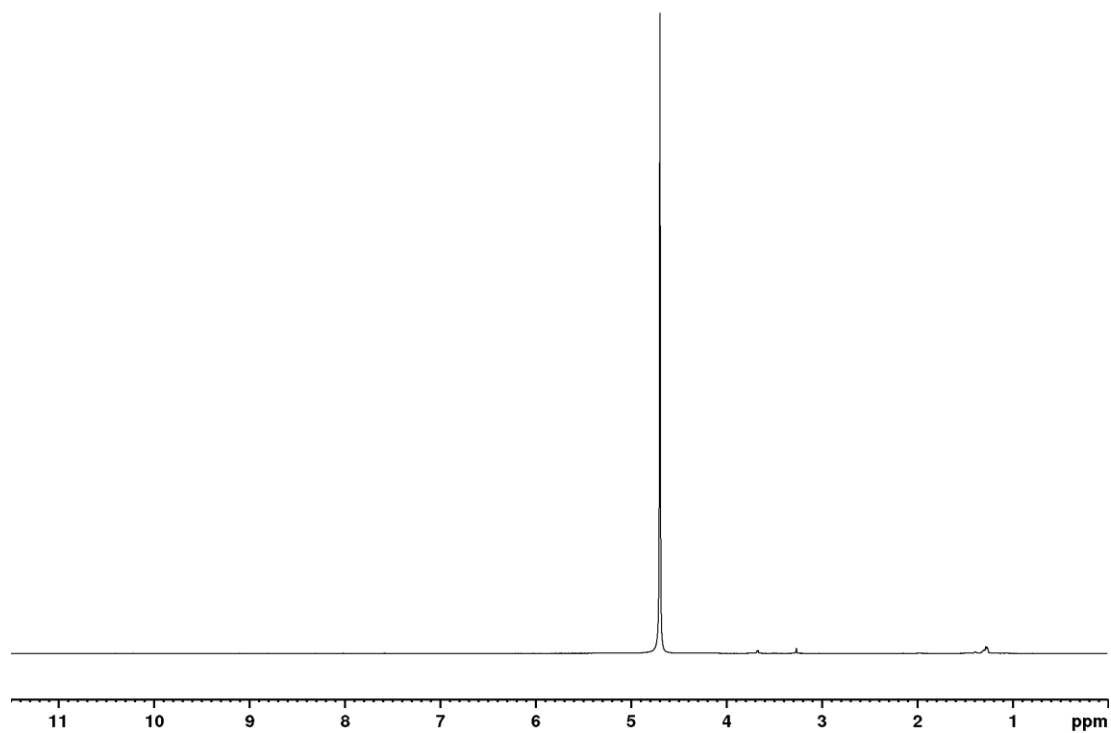
Spectrum 48 ^{1}H NMR spectrum of 27 (acetyl-d$_3$)-L-alanine-1-^{13}C-2-d in D$_2$O.
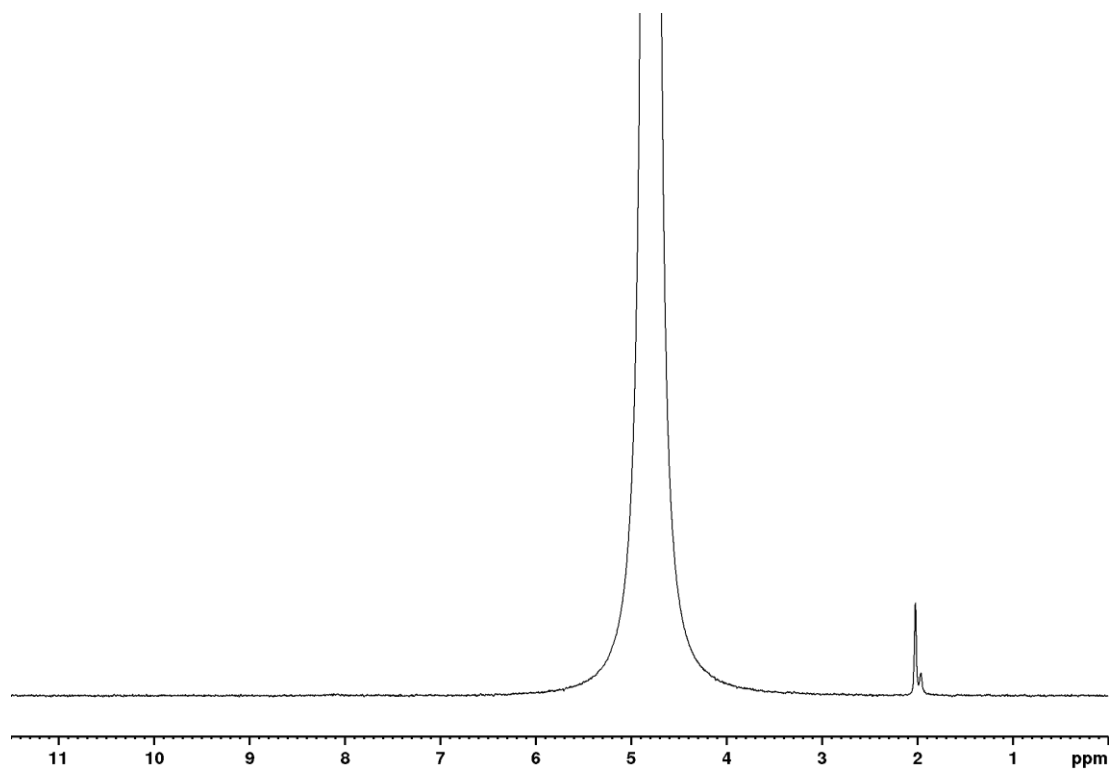
Spectrum 49 ^{2}H NMR spectrum of 27 (acetyl-d$_3$)-L-alanine-1-^{13}C-2-d in D$_2$O.

28 Vinyl-d₃ (acetyl-d₃)-L-alaninate-1-¹³C-2-d
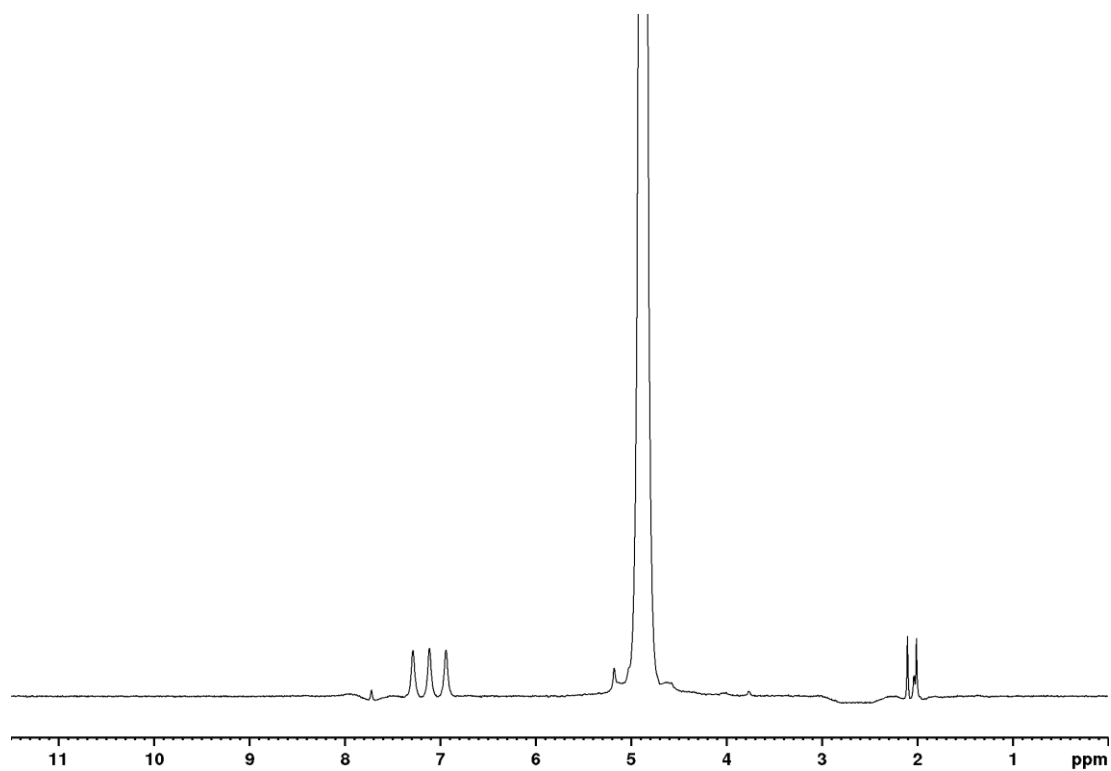
Spectrum 50 ¹H NMR spectrum of 28 vinyl-d₃ (acetyl-d₃)-L-alanine-1-¹³C-2-d in D₂O.
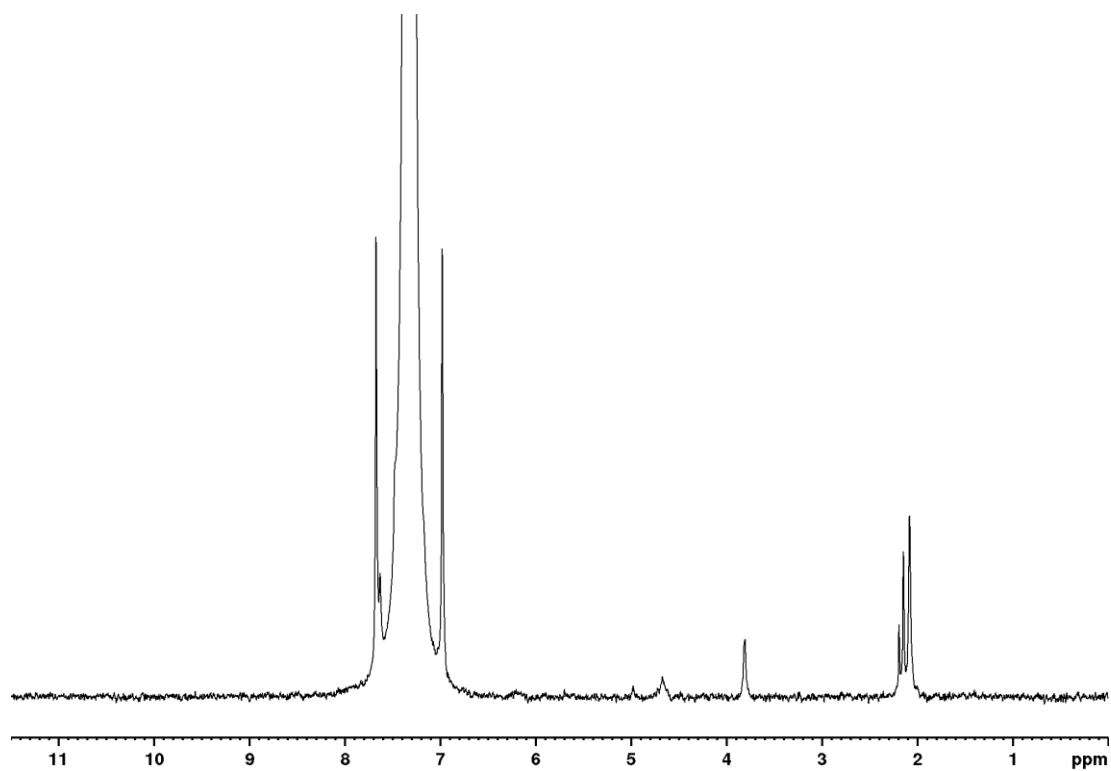
Spectrum 51 ²H NMR spectrum of 25 vinyl-d₃ (acetyl-d₃)-L-alanine-¹³C -2-d in CDCl₃
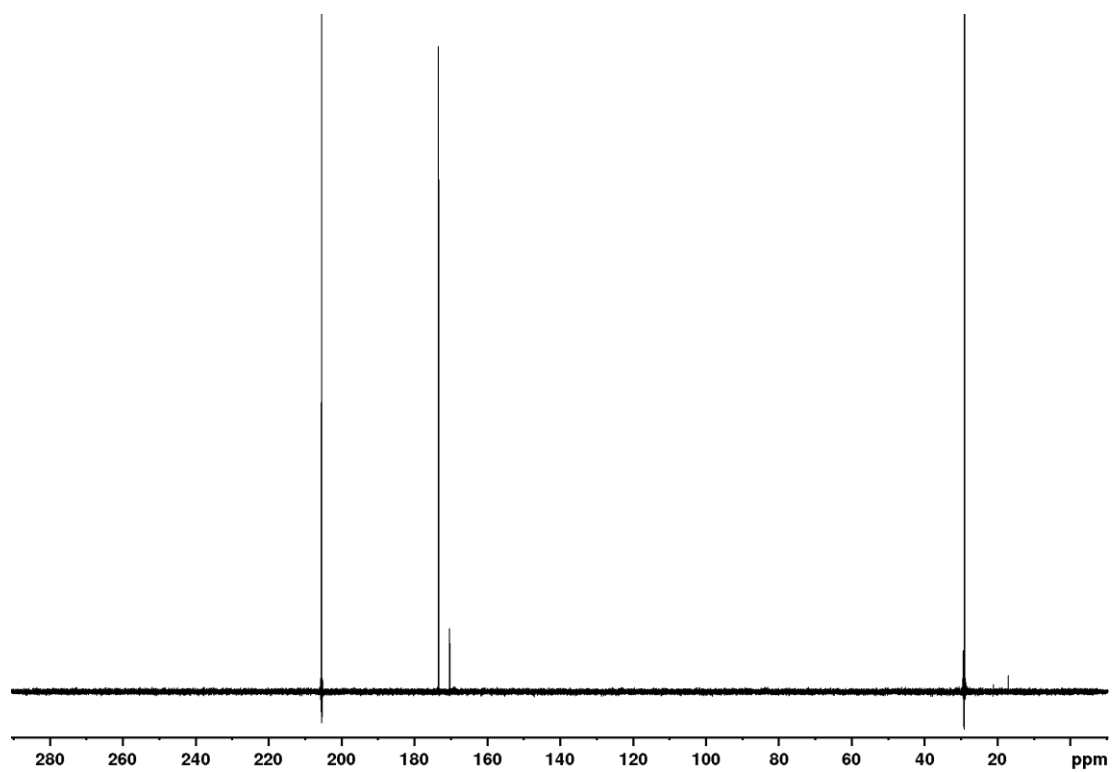
Spectrum 52 ^{13}C NMR spectrum of 28 vinyl-d$_3$ (acetyl-d$_3$)-L-alanine-1-^{13}C-2-d in acetone-d$_6$.

7.3 Hyperpolarized spectra

In the following section, for repeated experiments, three representative hyperpolarized spectra of the respective molecules are shown.

7.3.1 1-(2-nitrophenyl)prop-2-yn-1-yl-3-d-acetate-1-^{13}C-d$_3$
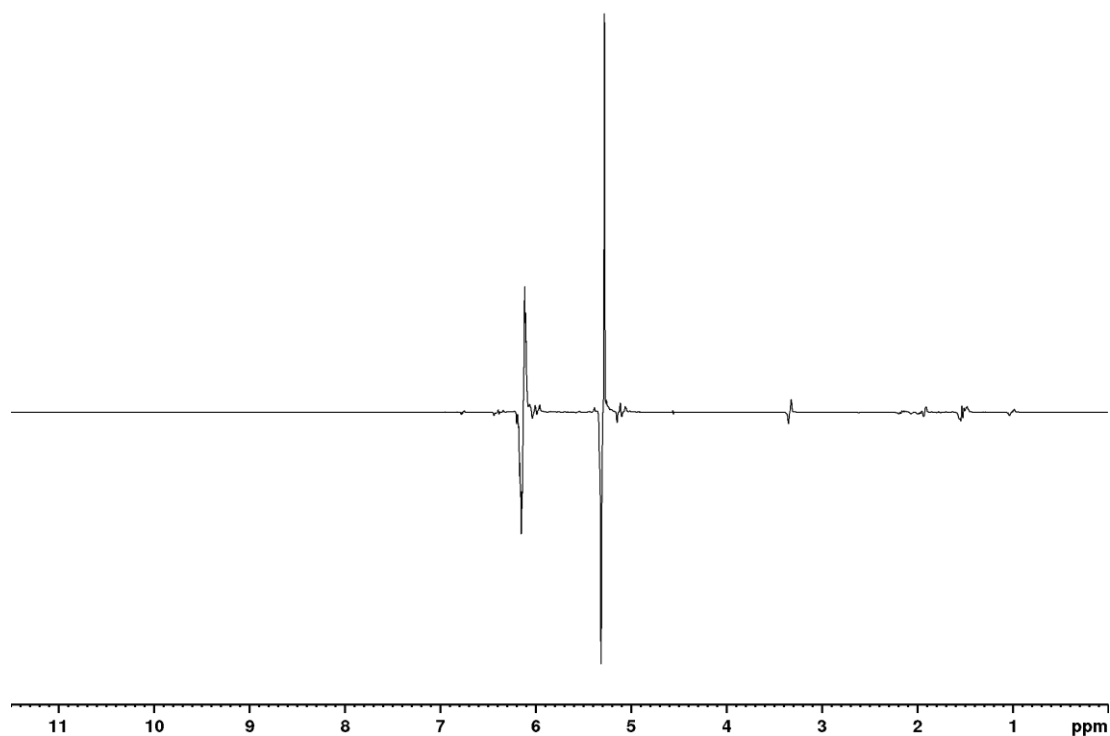
Spectrum 53 ^{1}H spectrum of hyperpolarized 17 in acetone-d$_6$ after a 45° pulse.
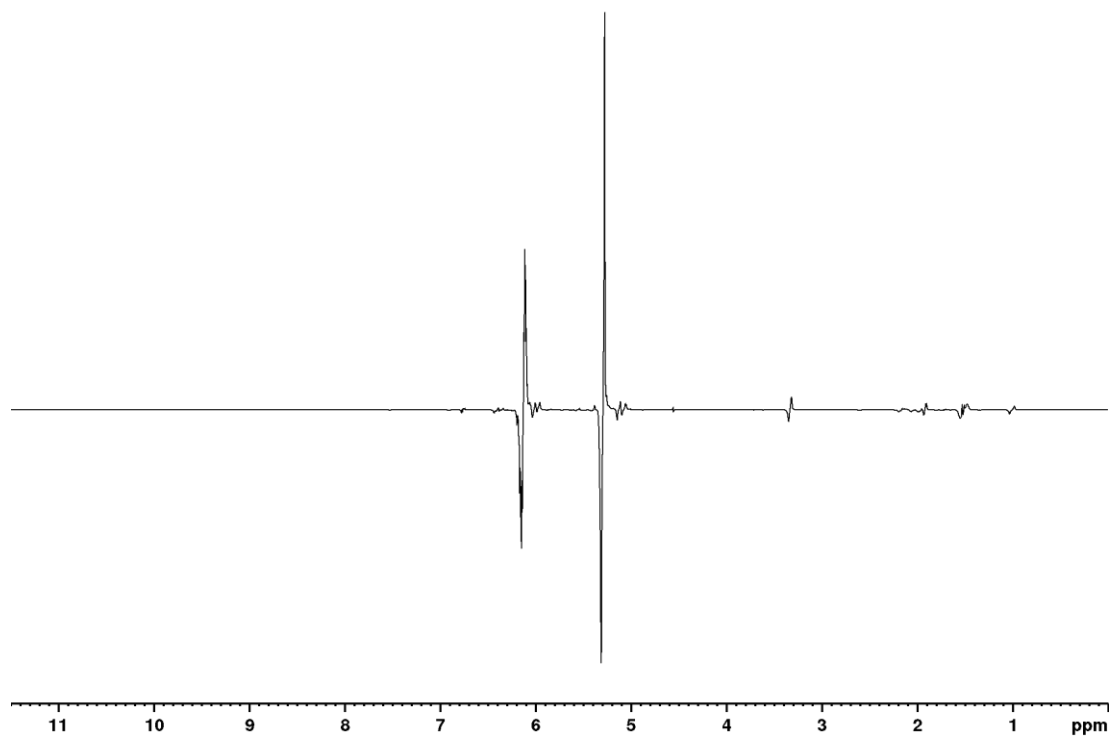
Spectrum 54 ^{1}H spectrum of hyperpolarized 17 in acetone-d$_6$ after a 45° pulse.
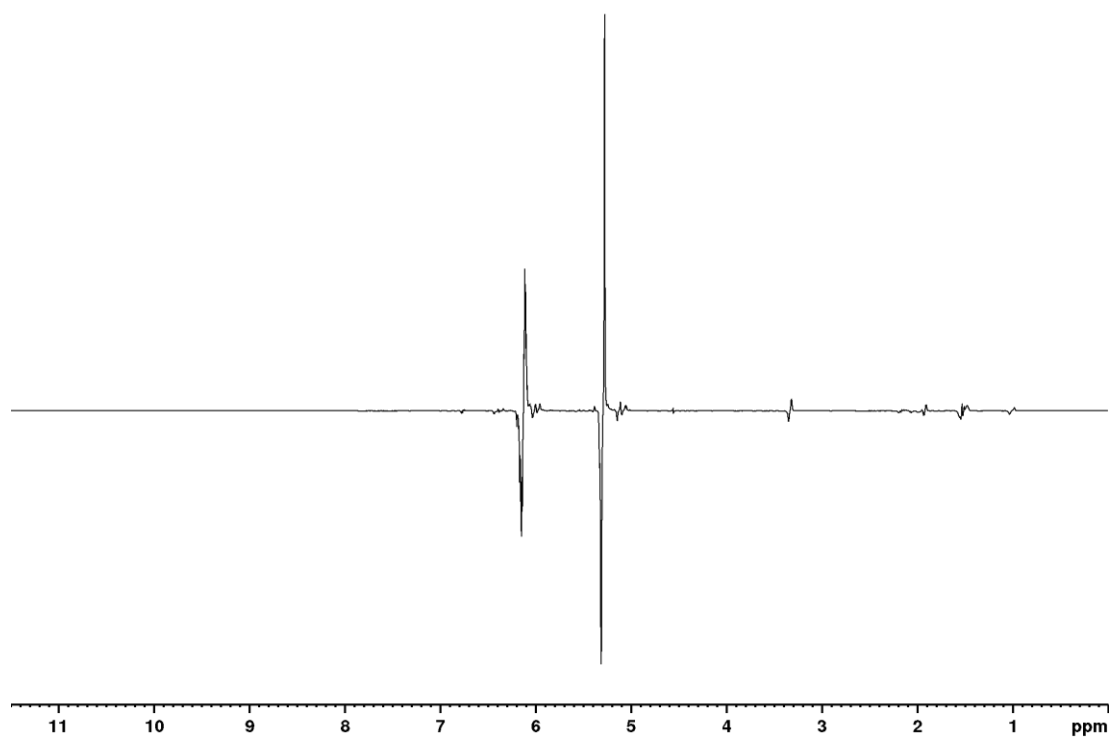
Spectrum 55 ^{1}H spectrum of hyperpolarized 17 in acetone-d$_6$ after a 45° pulse.
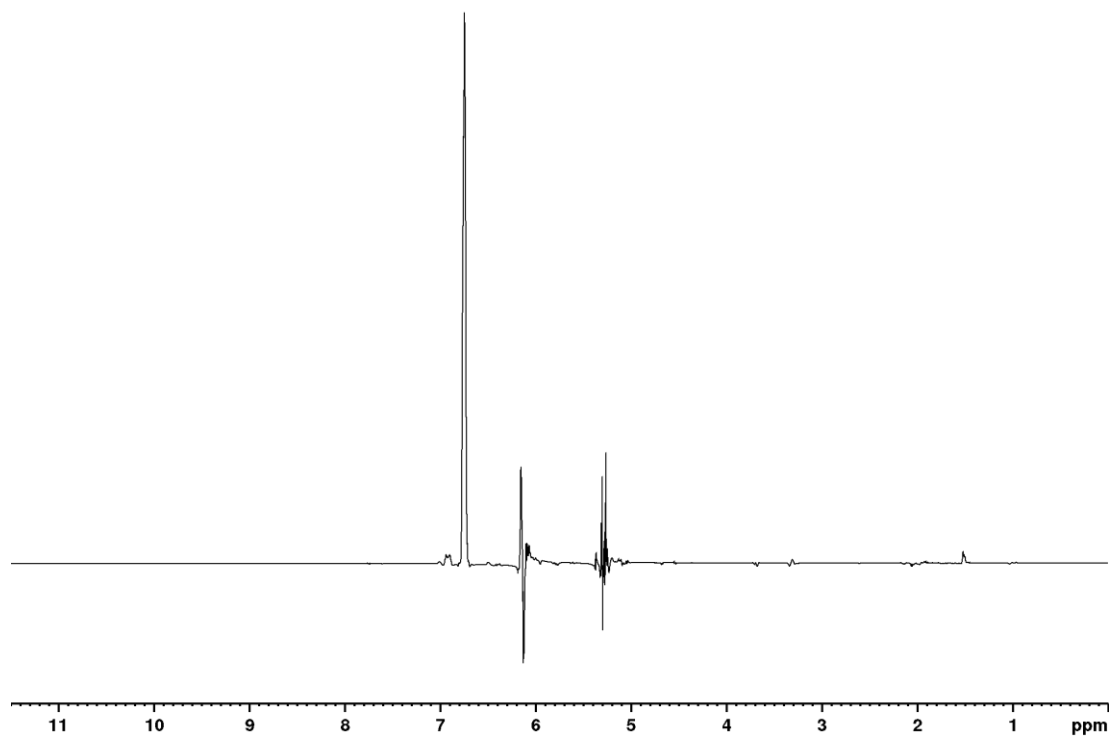
Spectrum 56 ^{1}H spectrum of hyperpolarized 17 in acetone-d$_6$ after the polarization transfer to H^3.
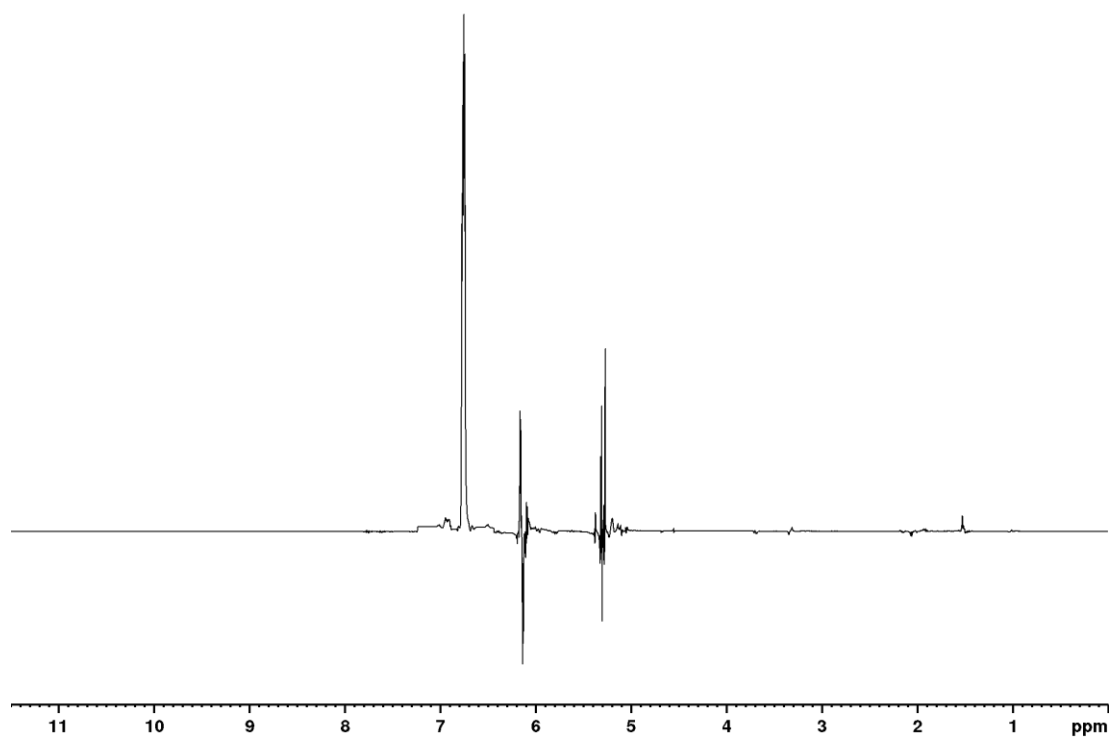
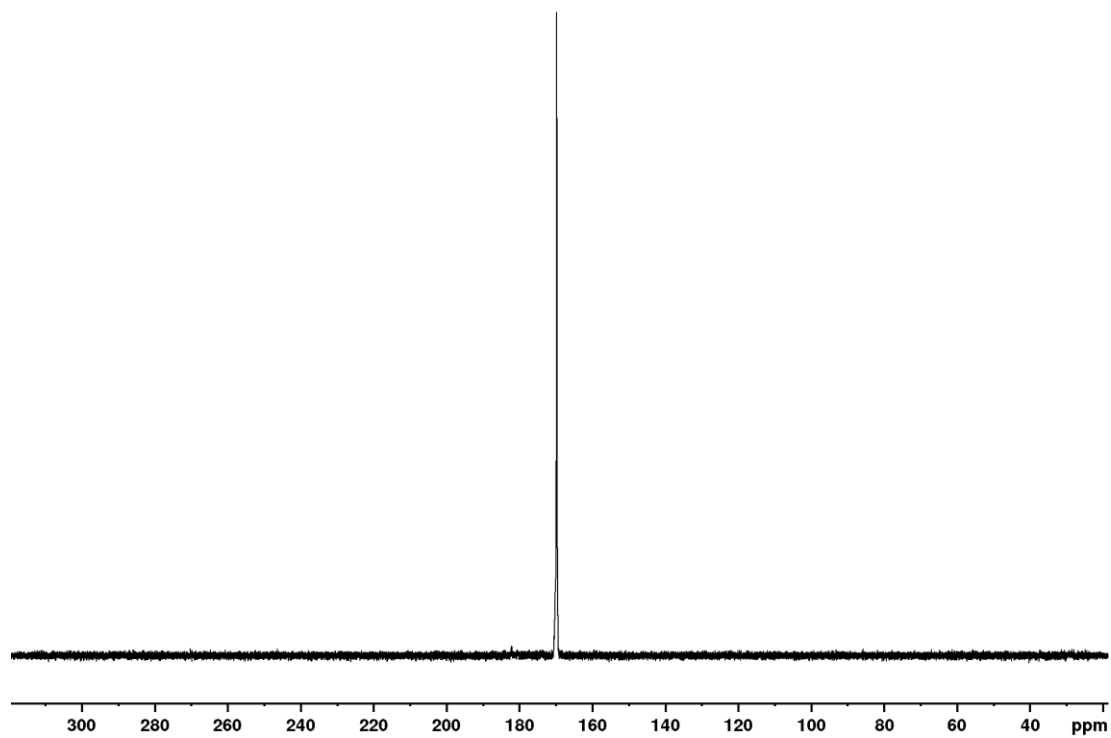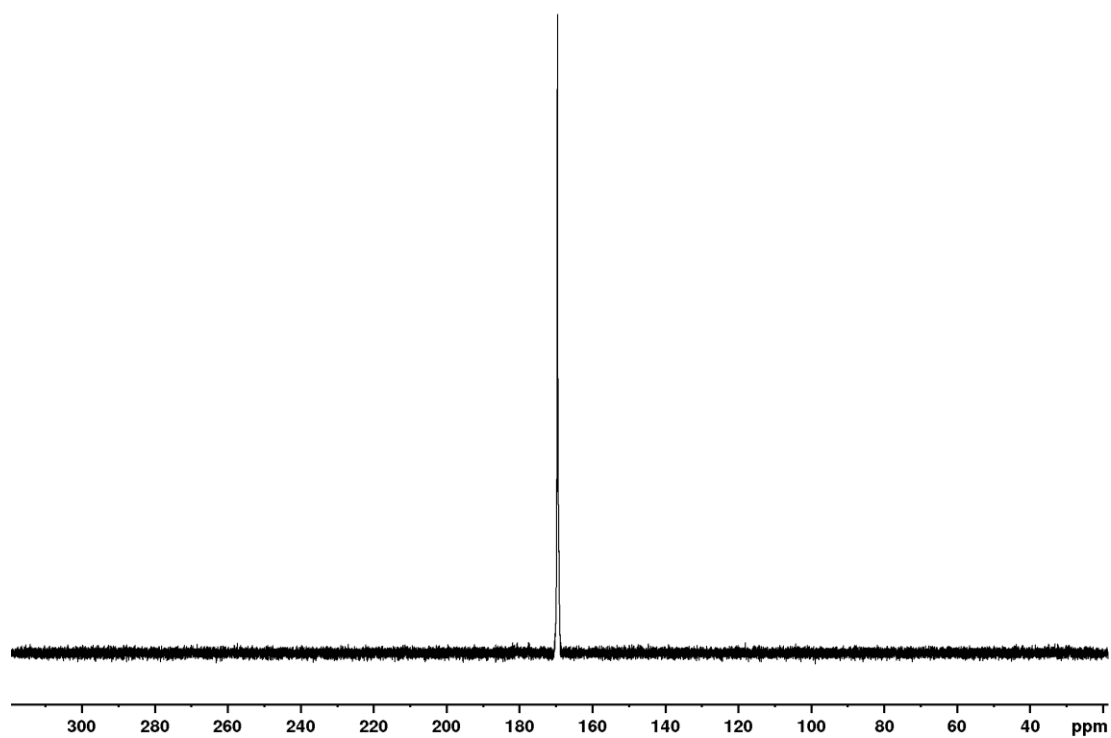Spectrum 57 ^{1}H spectrum of hyperpolarized 17 in acetone-d$_6$ after the polarization transfer to H^3.
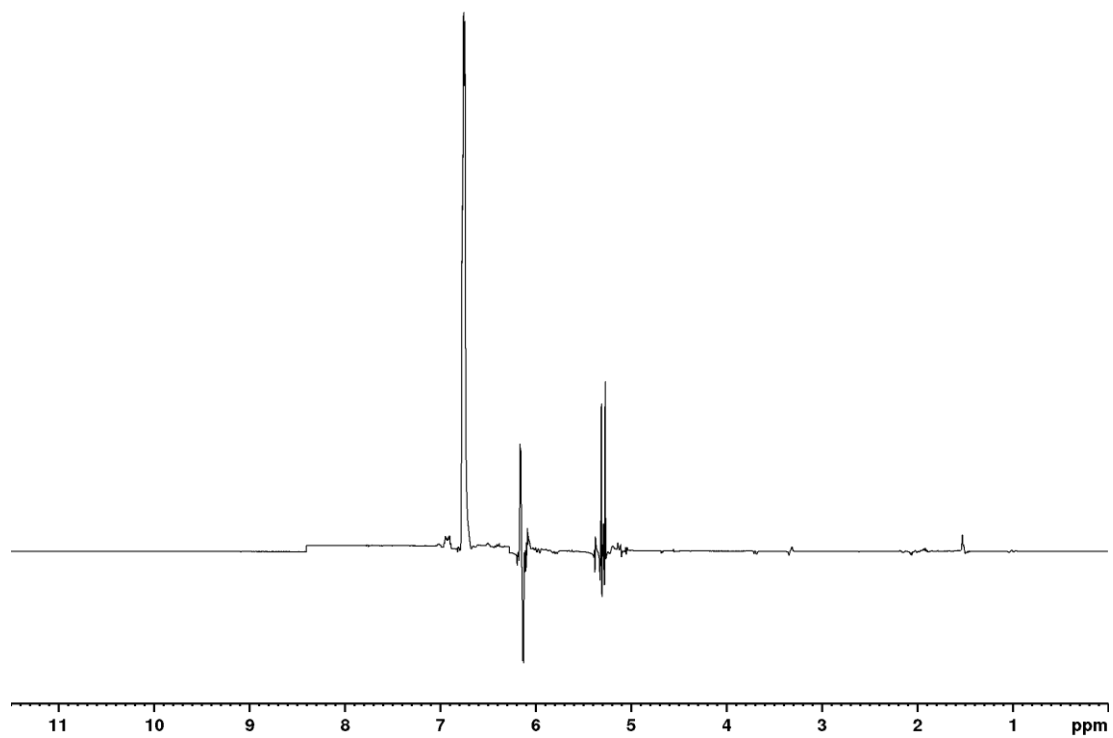
Spectrum 58 ^{1}H spectrum of hyperpolarized 17 in acetone-d_6 after the polarization transfer to H^3.
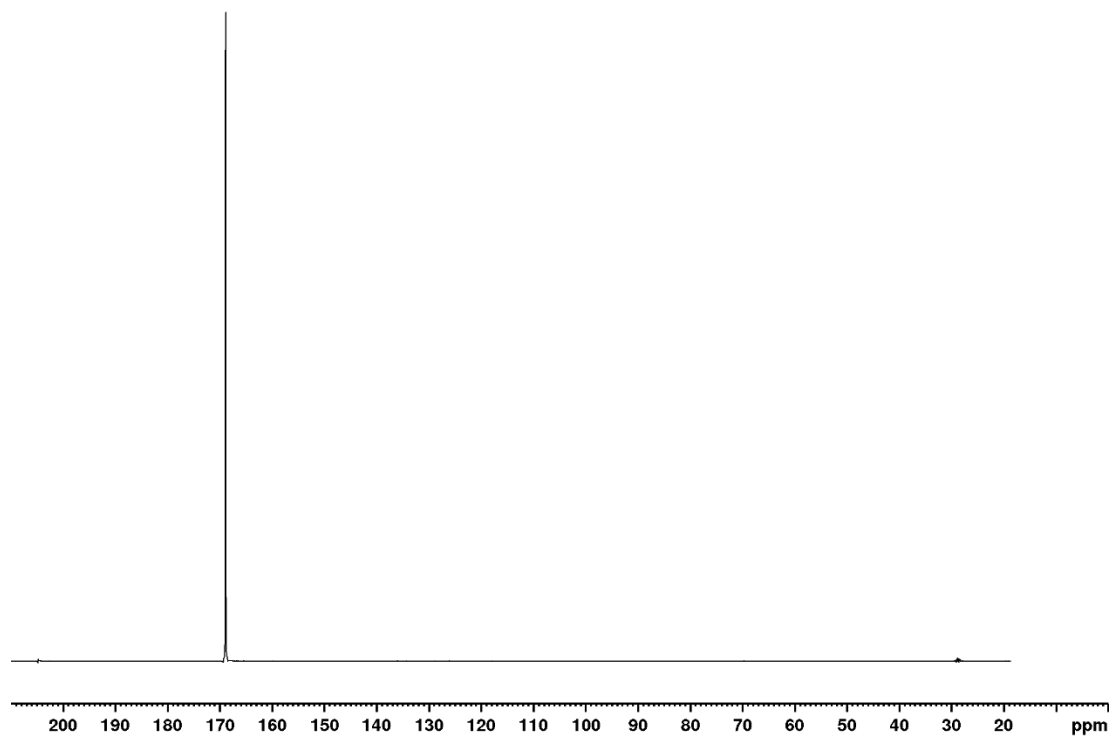
Spectrum 59 ^{13}C spectrum of hyperpolarized 17 in acetone-d$_6$ after the polarization transfer.
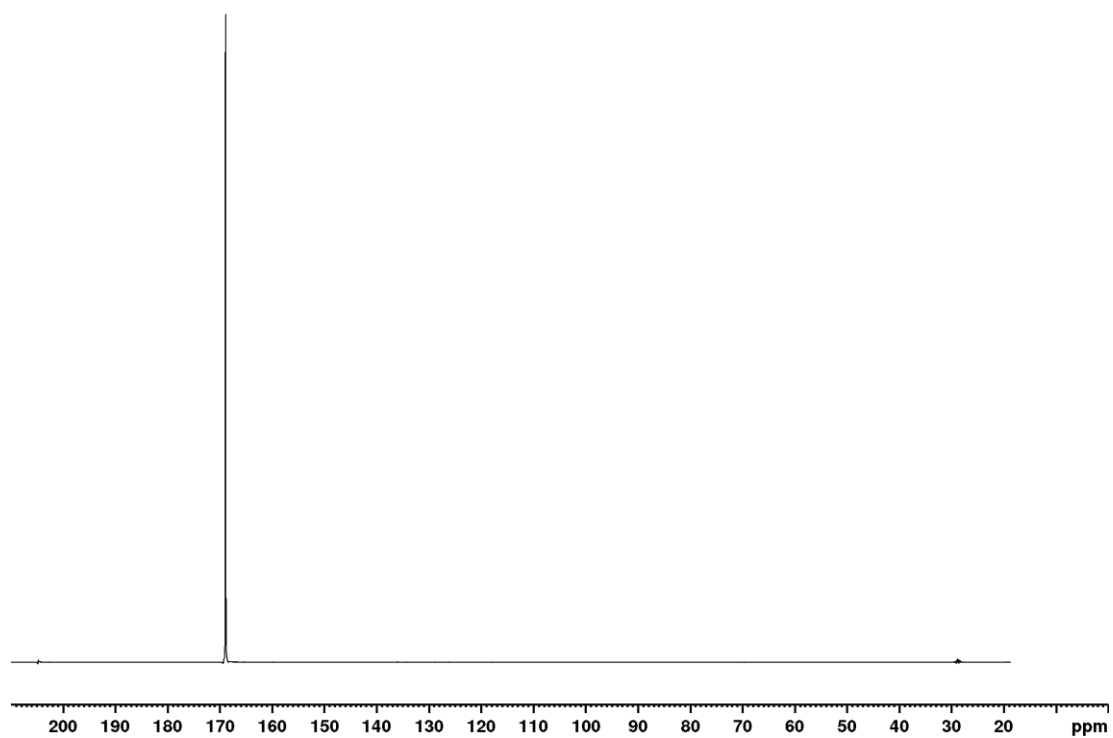
Spectrum 60 ^{13}C spectrum of hyperpolarized 17 in acetone-d$_6$ after the polarization transfer.
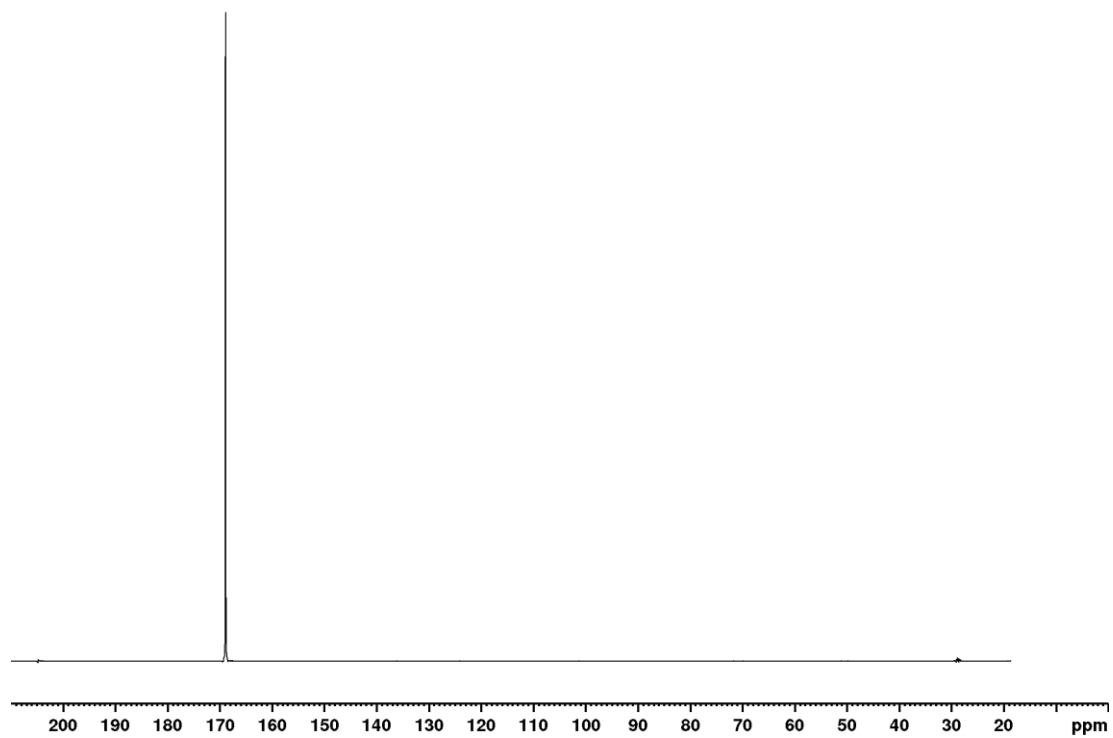
Spectrum 61 ^{13}C spectrum of hyperpolarized 17 in acetone-d$_6$ after the polarization transfer.
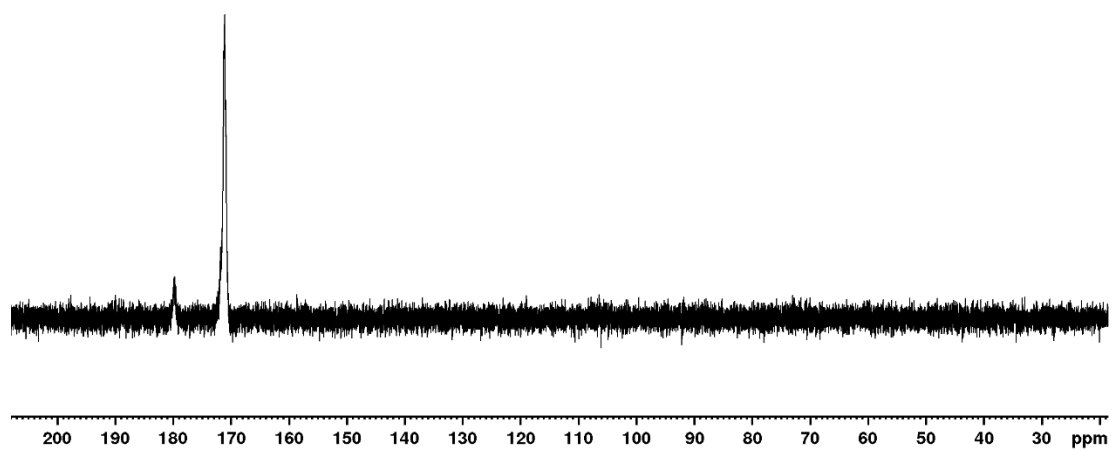
Spectrum 62 ^{13}C spectrum of hyperpolarized 17 in acetone-d$_6$ after the aqueous cleavage.
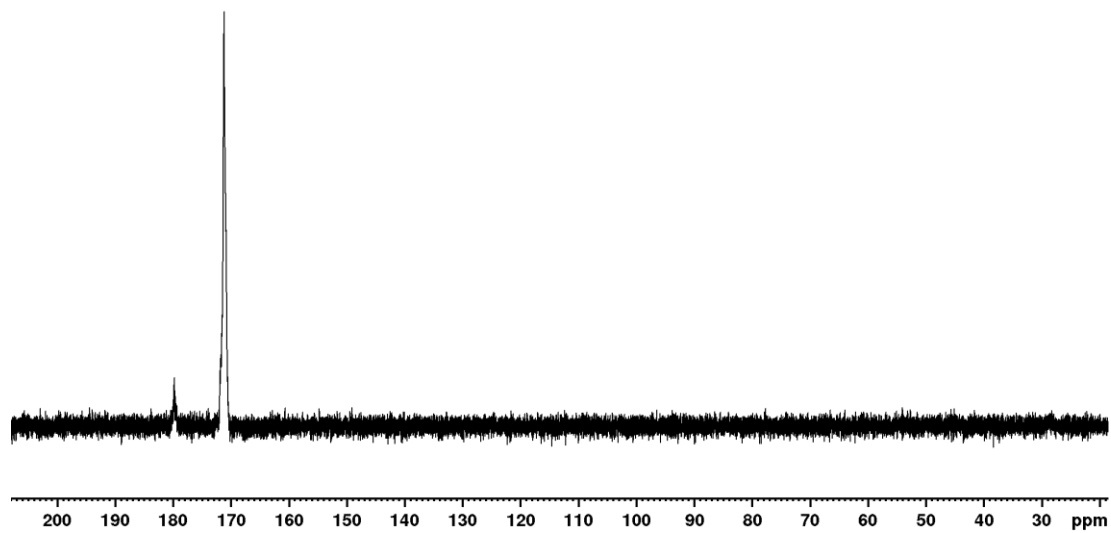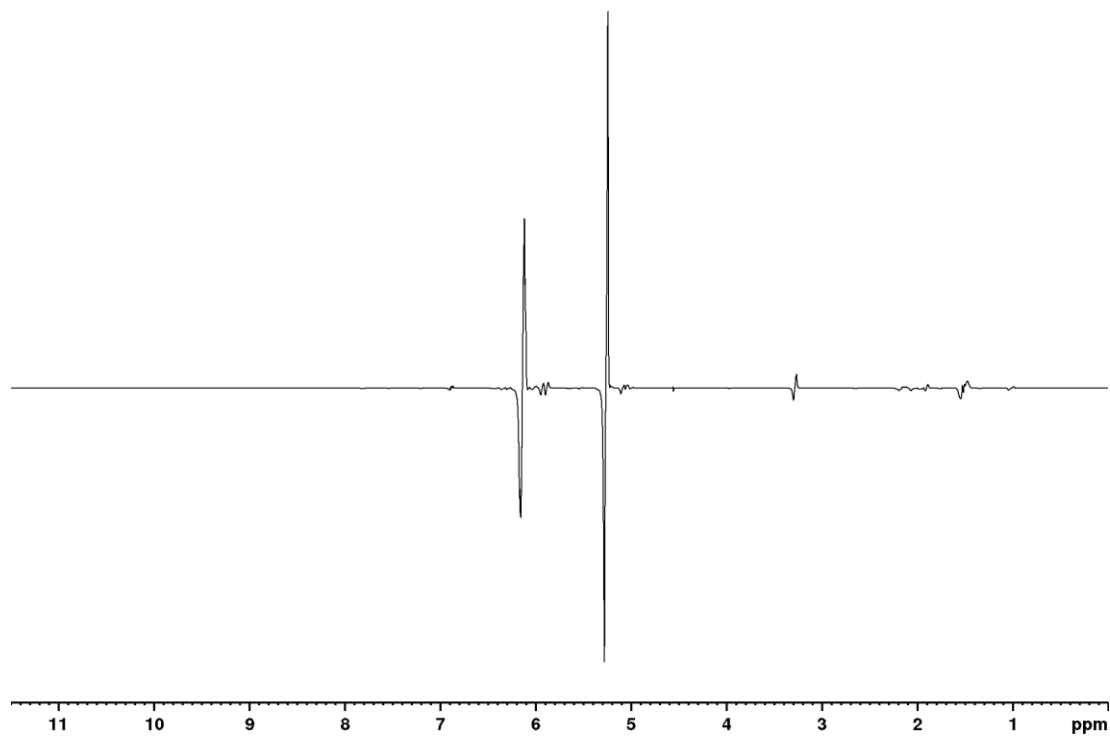
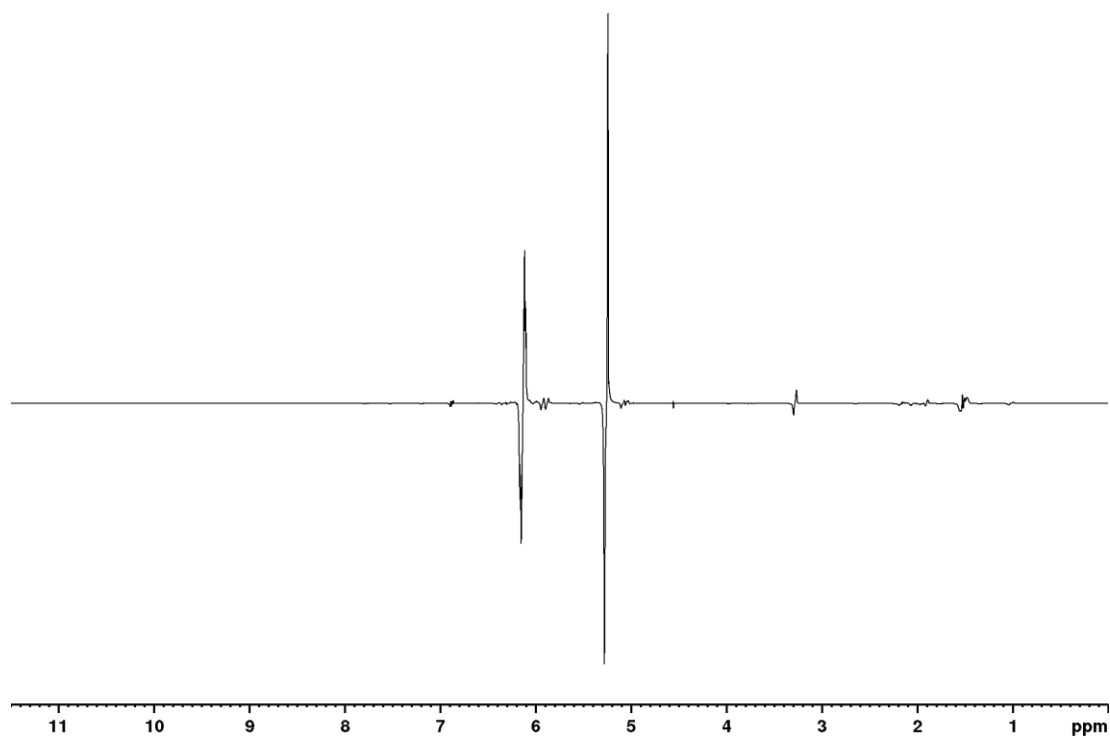Spectrum 63 ^{13}C spectrum of hyperpolarized 17 in acetone-d$_6$ after the aqueous cleavage.
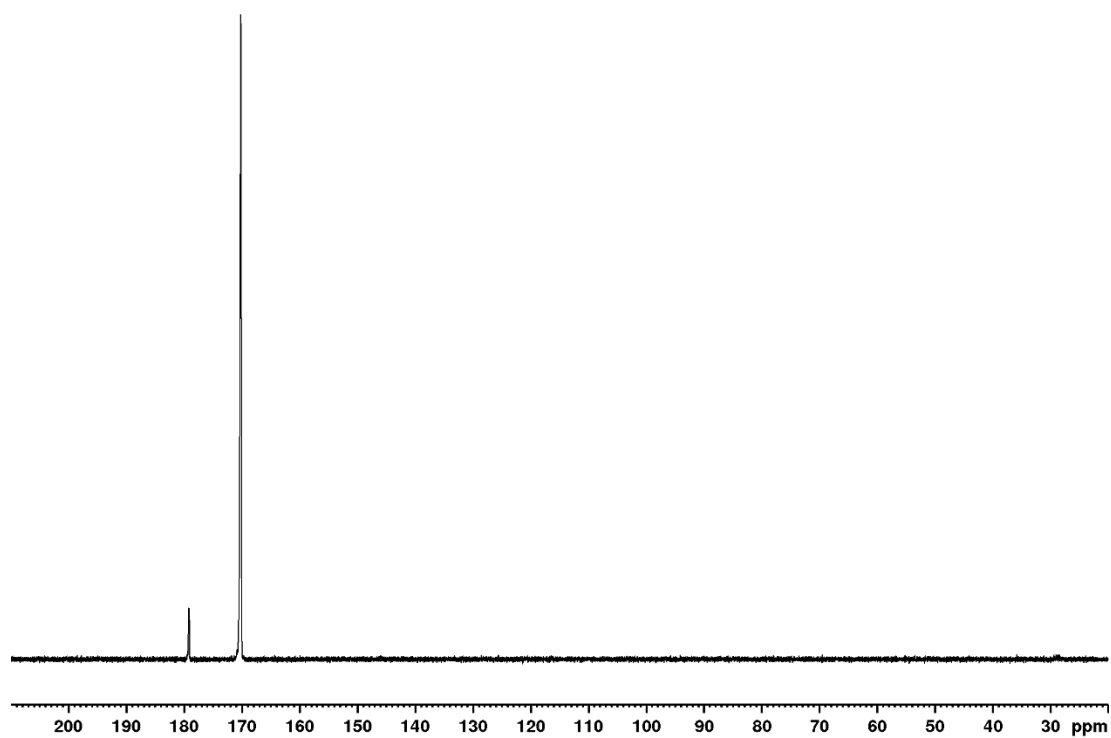
Spectrum 64 ^{13}C spectrum of hyperpolarized 17 in acetone-d$_6$ after the aqueous cleavage.

7.3.2   1-(2-nitrophenyl)prop-2-yn-1-yl-3-d-2-oxopropanoate-1-^{13}C-3-d$_3$
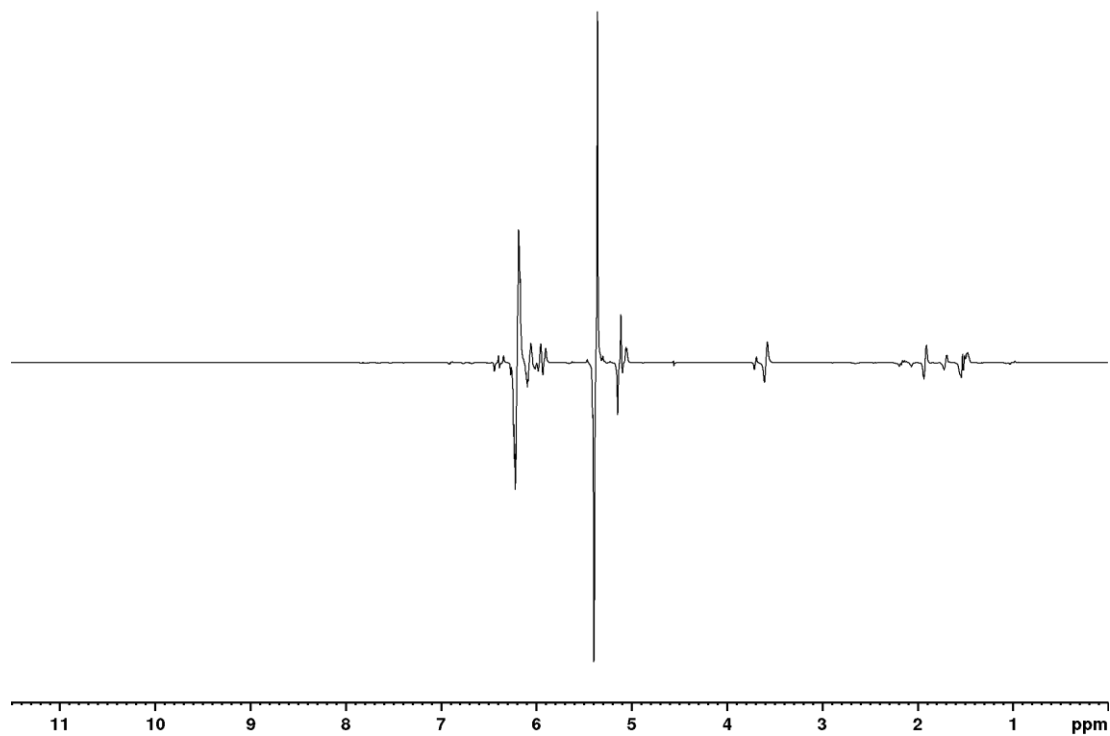
Spectrum 65 ^{1}H spectrum of hyperpolarized 18 in acetone-d$_6$ after a 45° pulse.
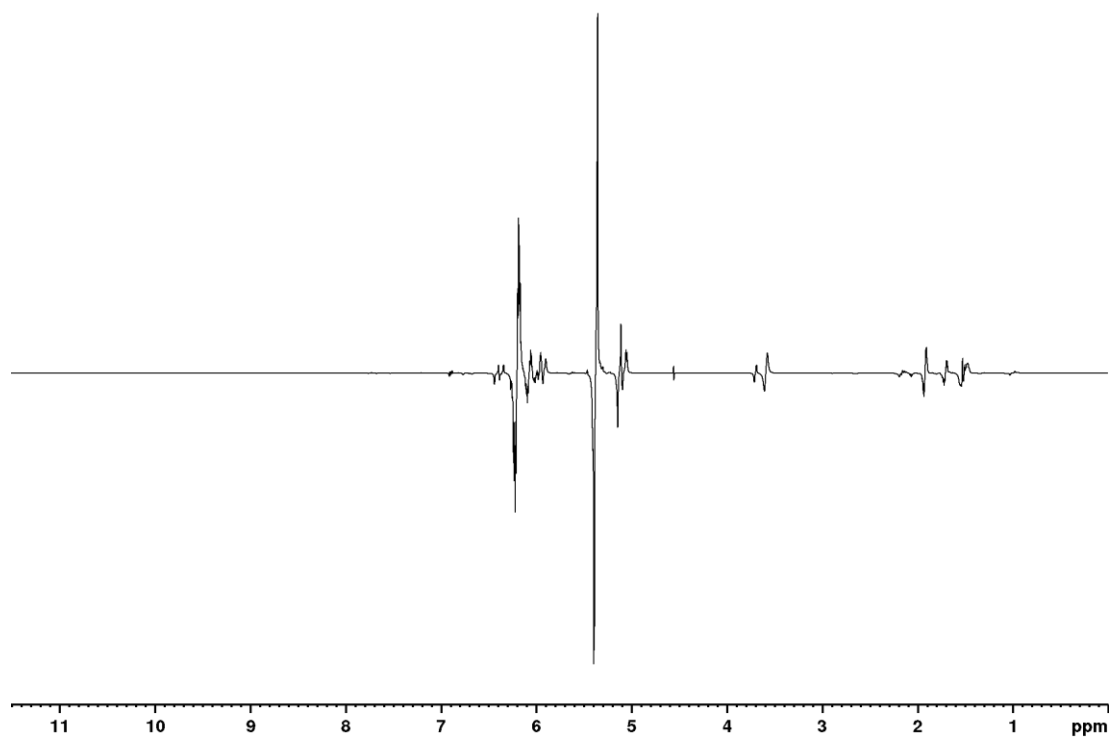
Spectrum 66 ^{1}H spectrum of hyperpolarized 18 in acetone-d$_6$ after a 45° pulse.
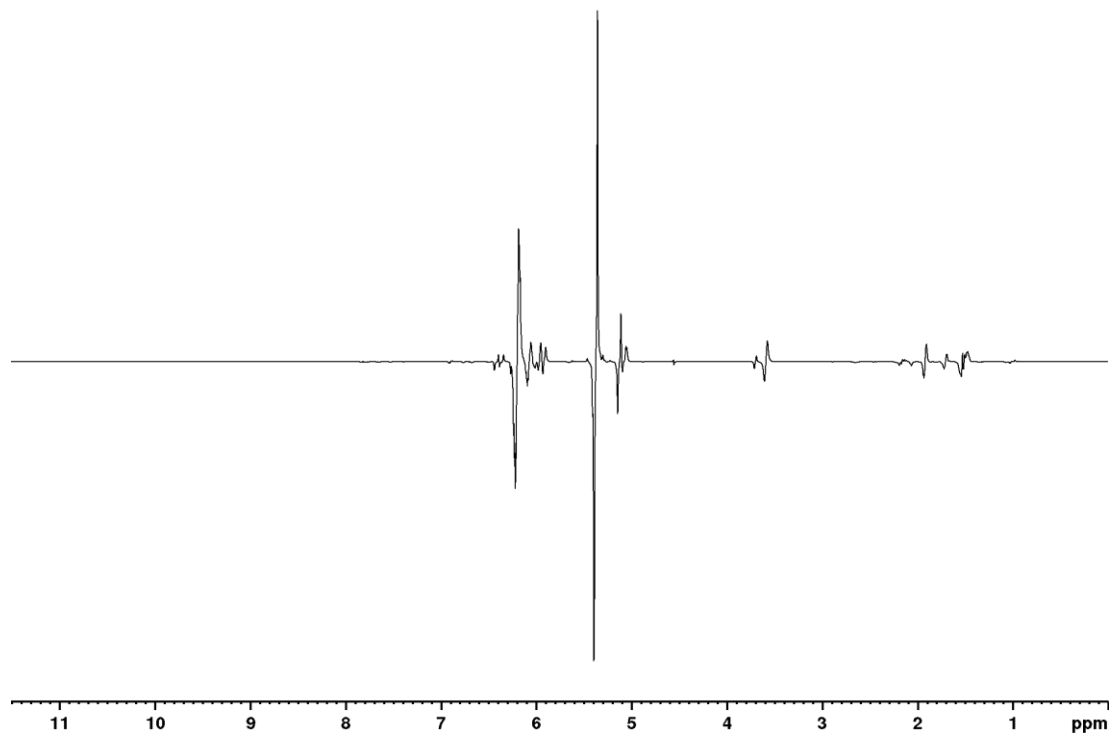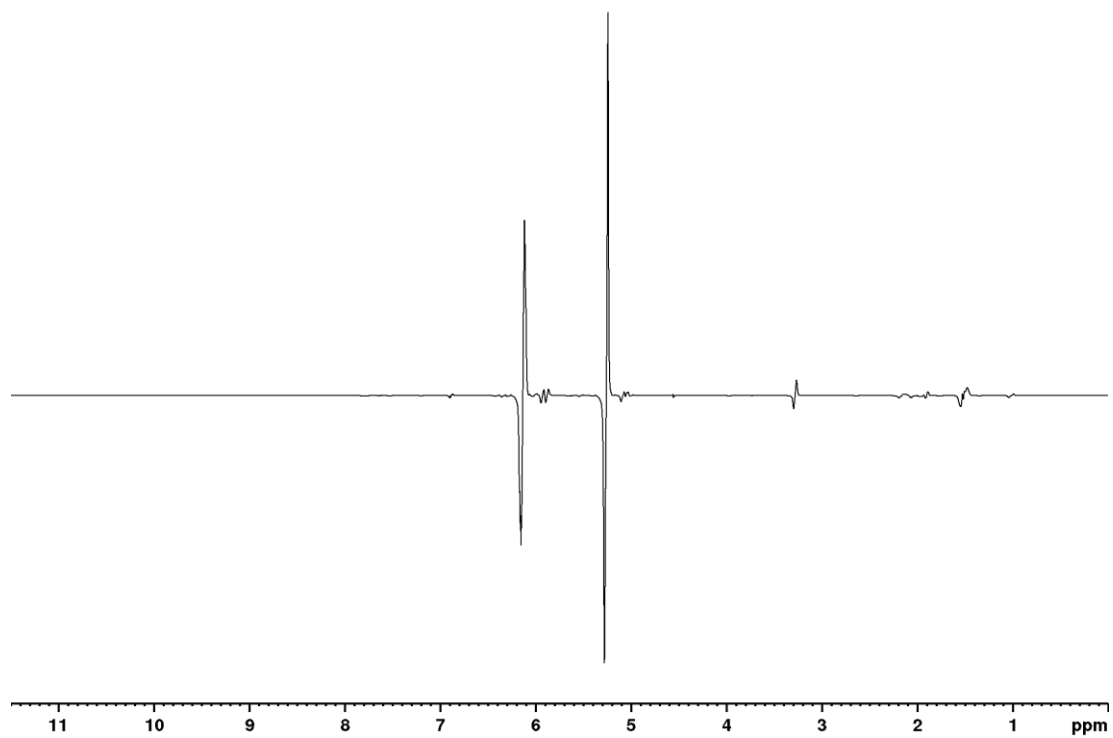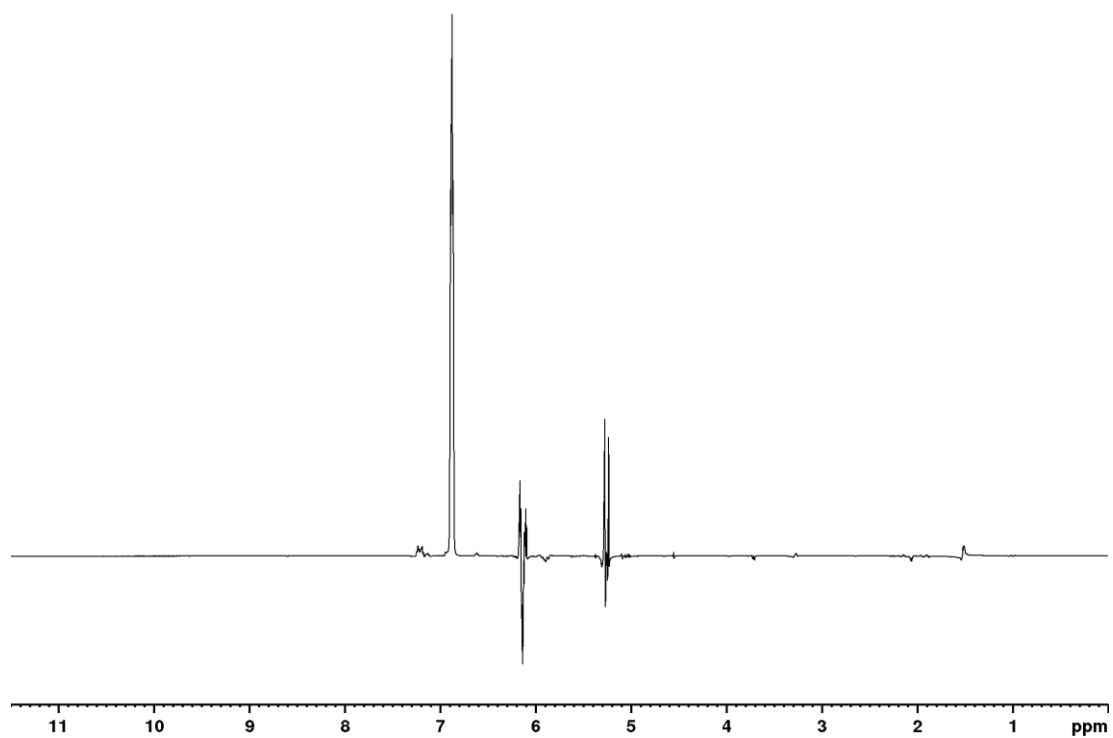
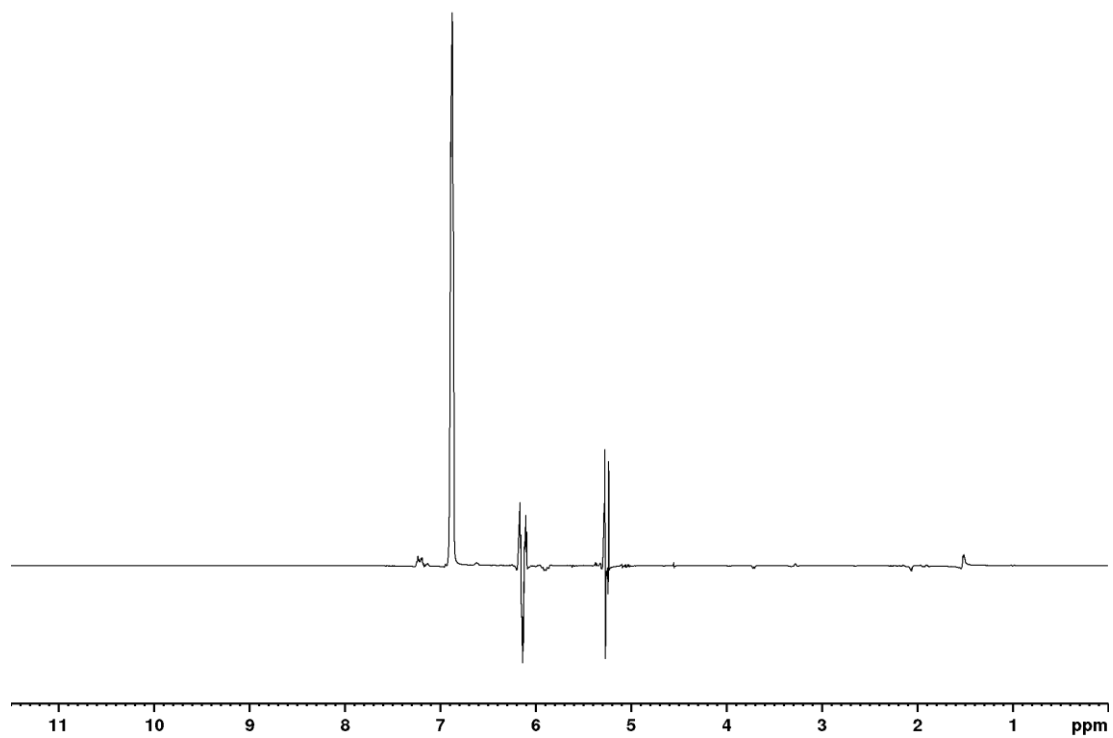Spectrum 67 ^{1}H spectrum of hyperpolarized 18 in acetone-d$_6$ after a 45° pulse.
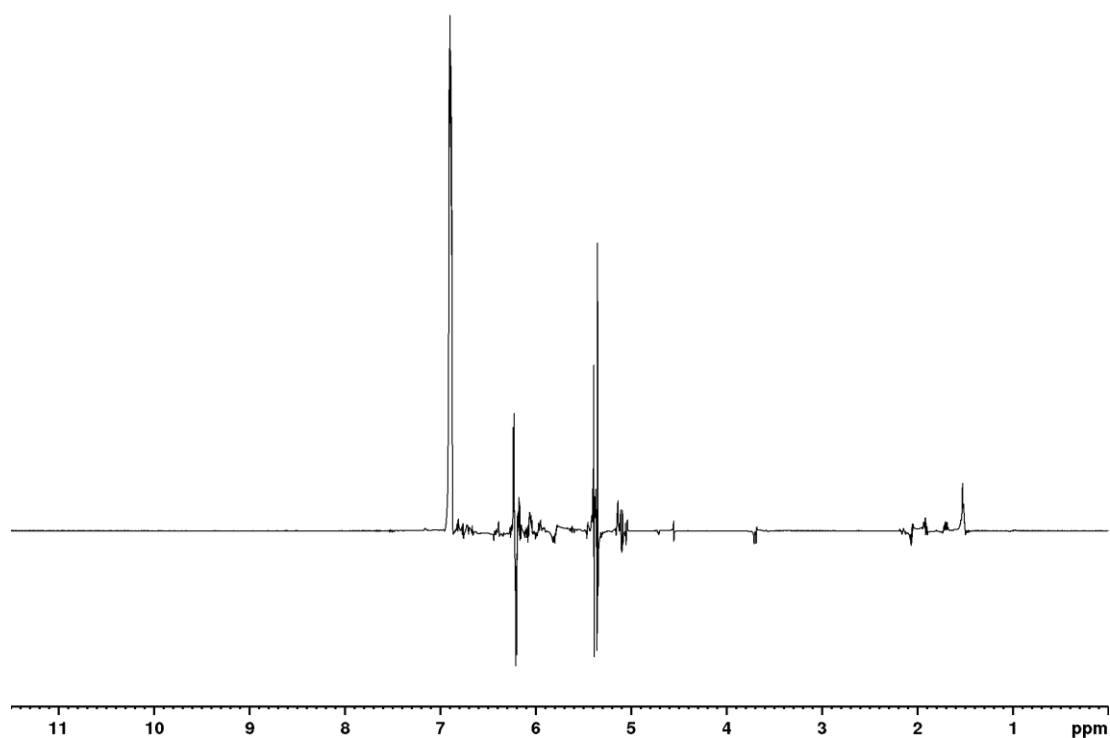
Spectrum 68 ^{1}H spectrum of hyperpolarized 18 in acetone-d$_6$ after the polarization transfer to H^3.
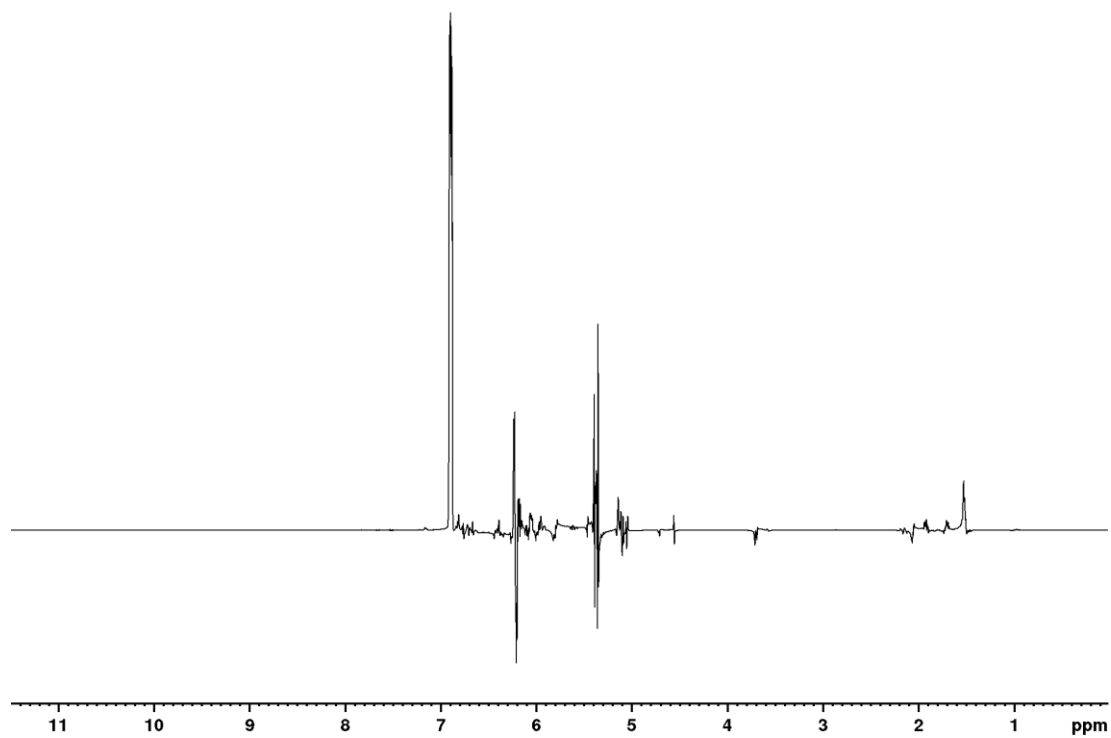
Spectrum 69 ^{1}H spectrum of hyperpolarized 18 in acetone-d_6 after the polarization transfer to H^3.
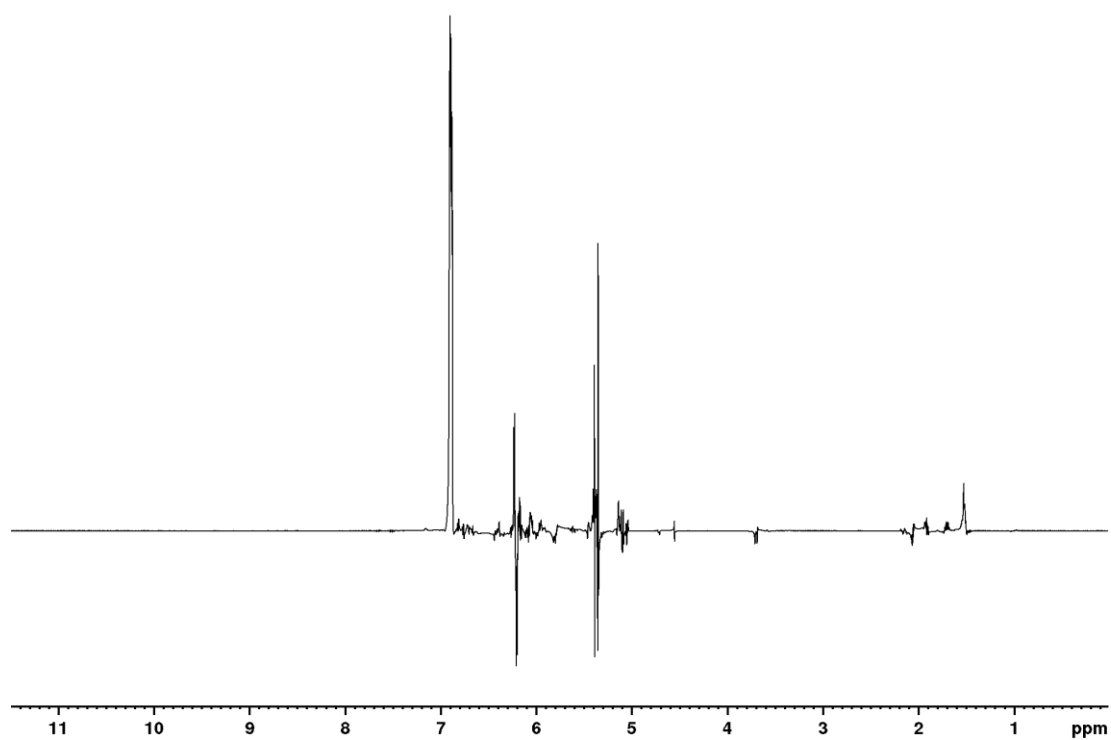
Spectrum 70 ^{1}H spectrum of hyperpolarized 18 in acetone-d_6 after the polarization transfer to H^3.
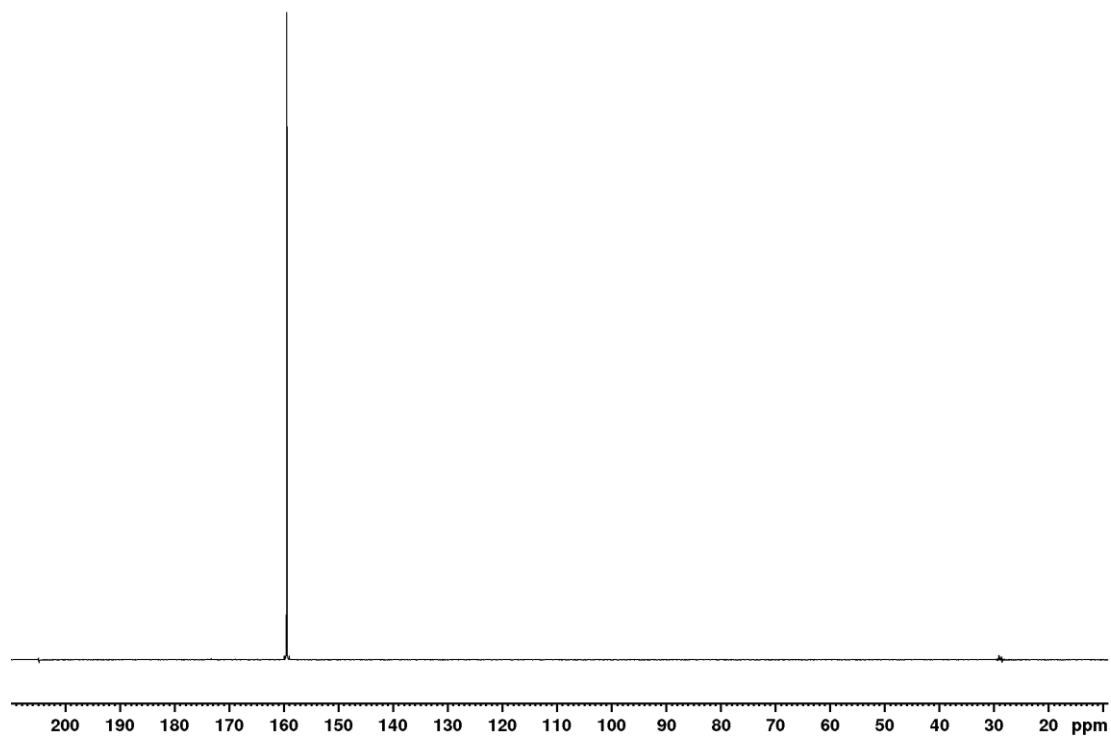
Spectrum 71 ^{13}C spectrum of hyperpolarized 18 in acetone-d$_6$ after the polarization transfer.
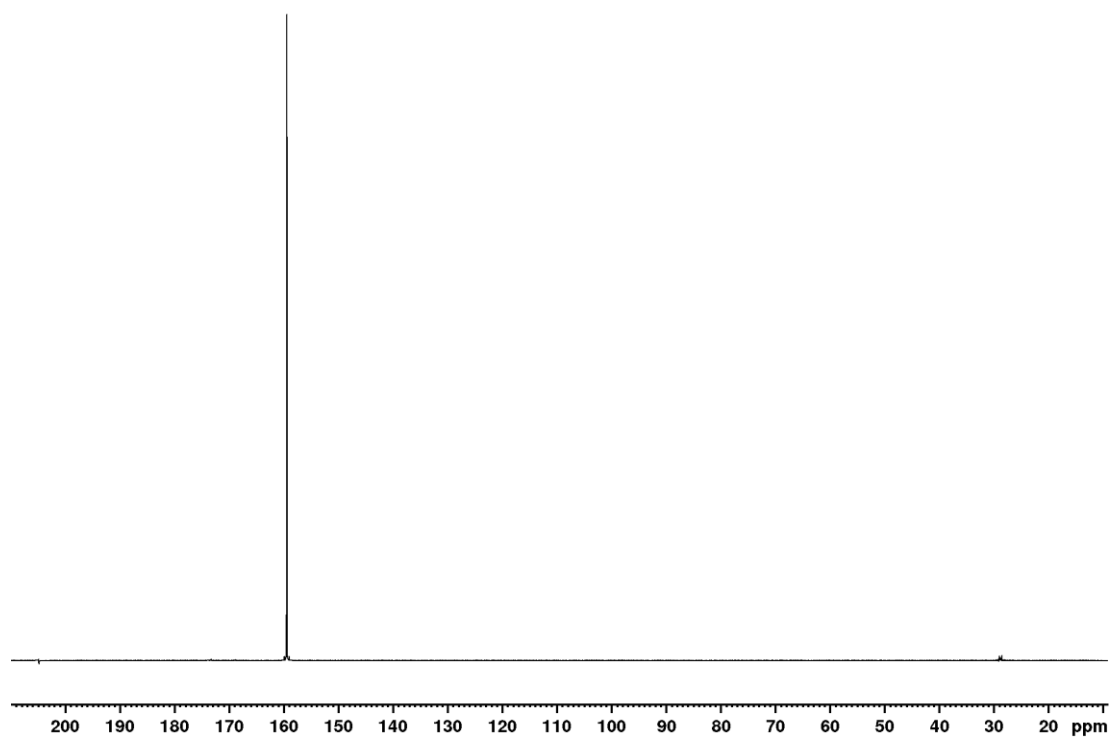
Spectrum 72 ^{13}C spectrum of hyperpolarized 18 in acetone-d$_6$ after the polarization transfer.
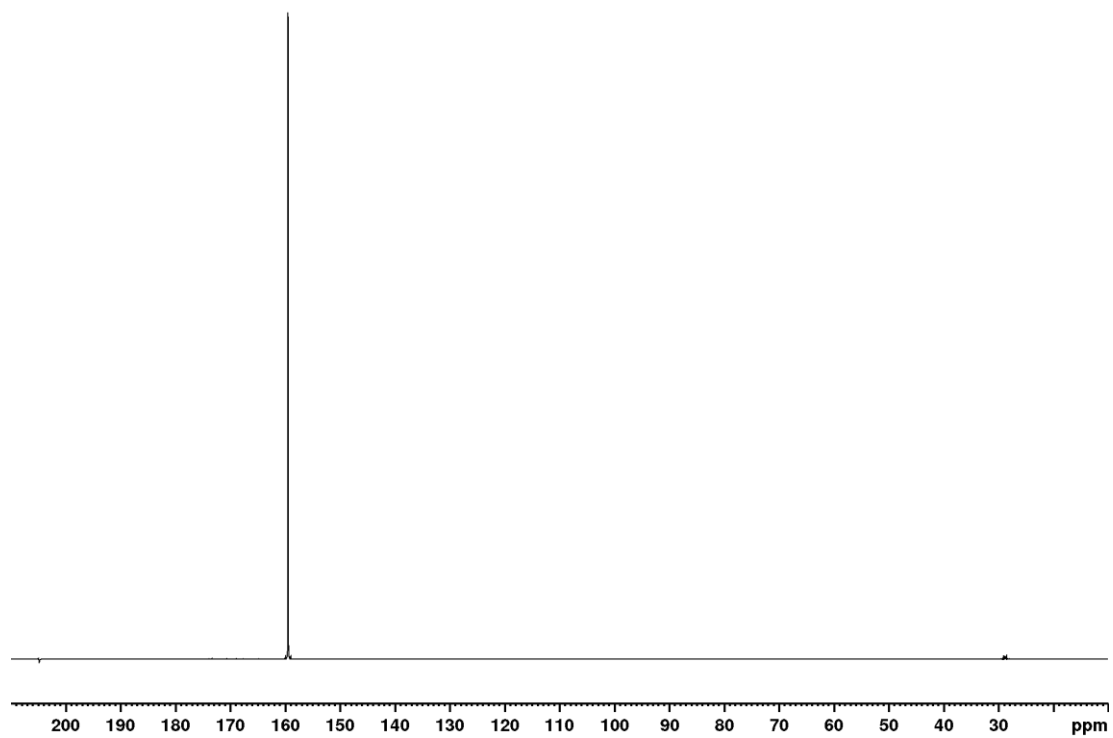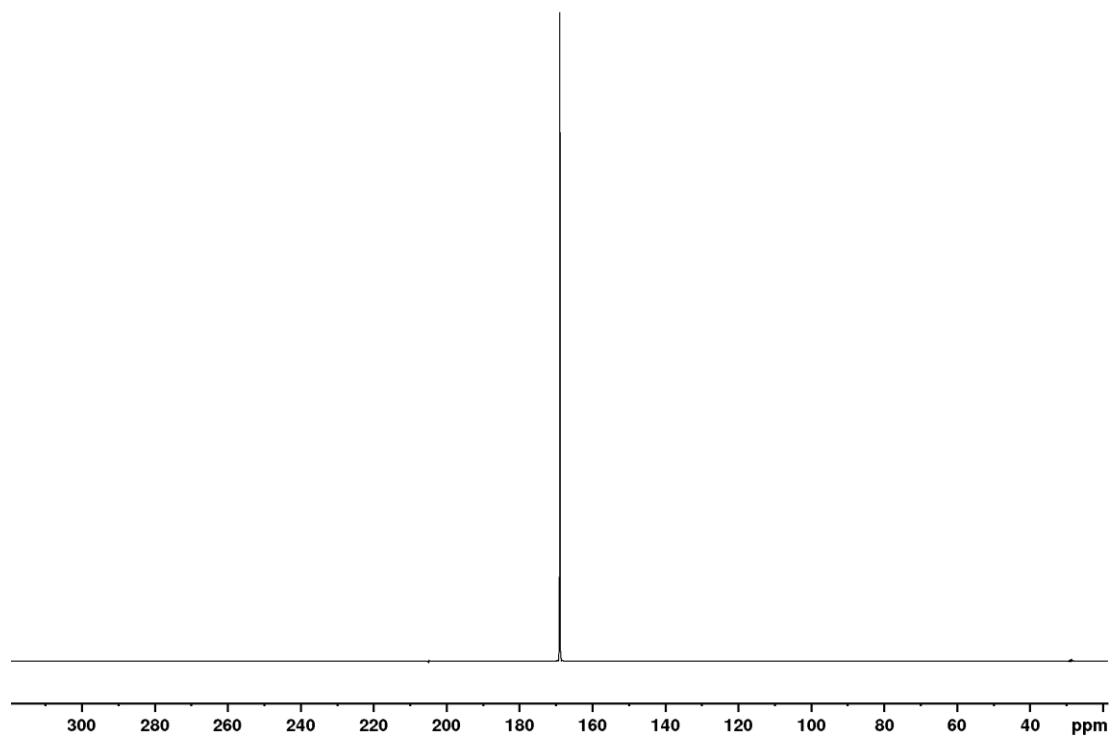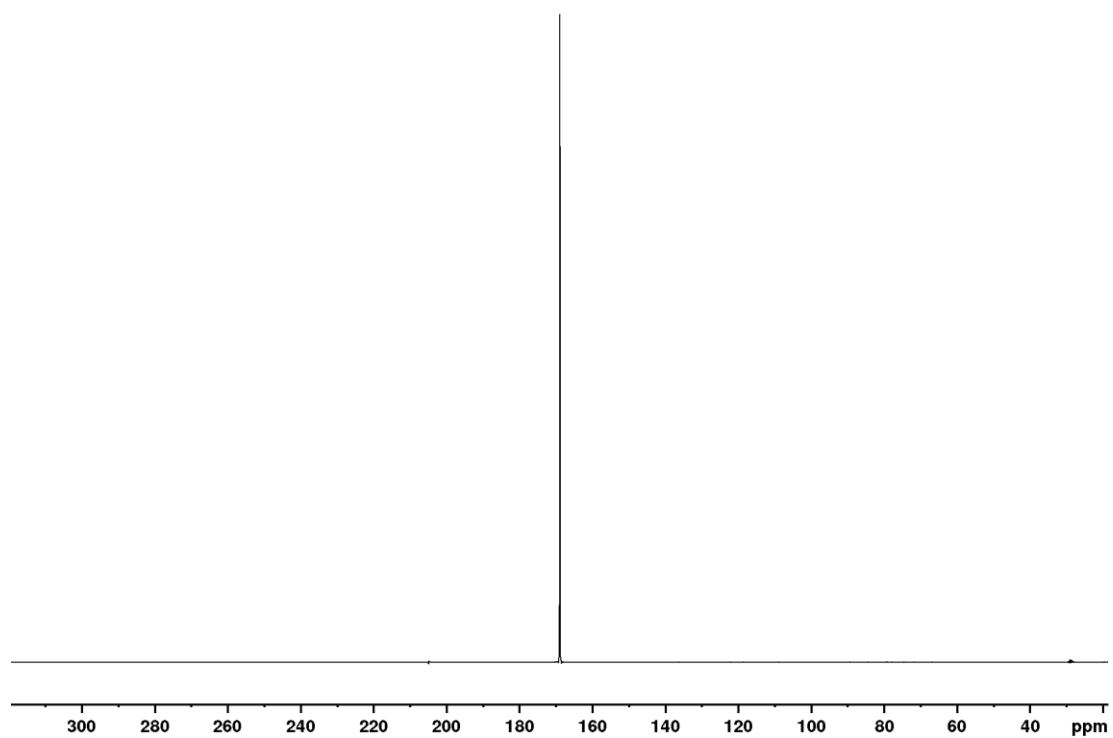
Spectrum 73 ^{13}C spectrum of hyperpolarized 18 in acetone-d$_6$ after the polarization transfer.
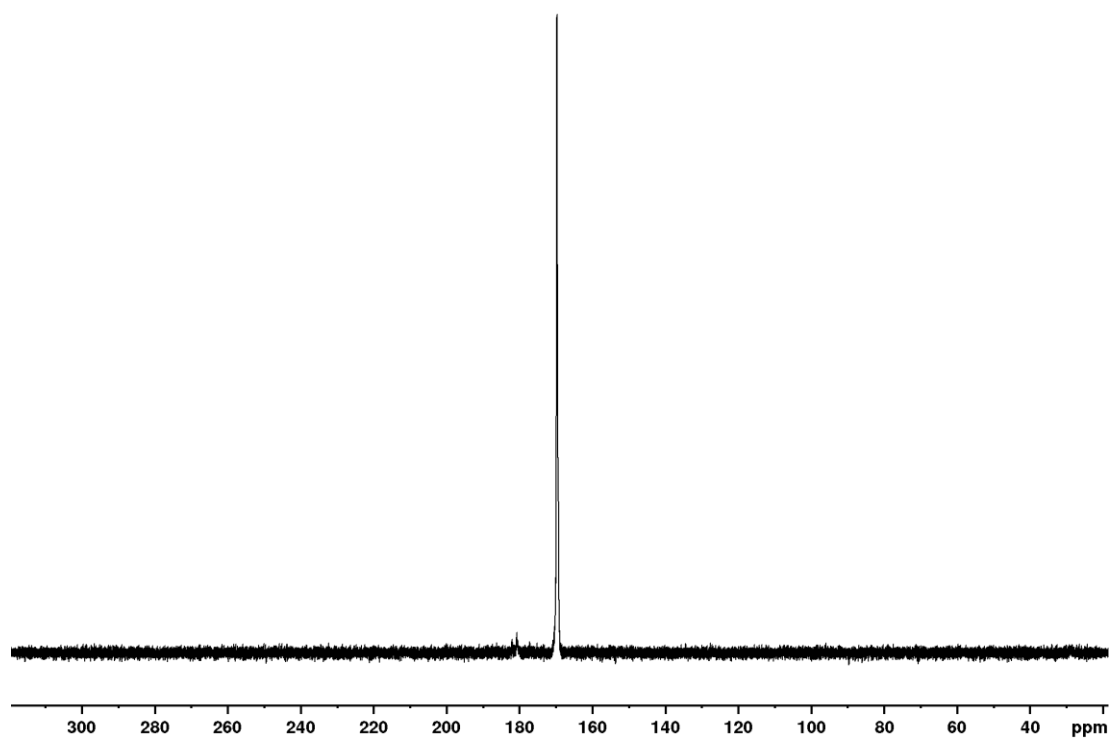
Spectrum 74 ^{13}C spectrum of hyperpolarized 18 in acetone-d$_6$ after the aqueous cleavage.

Spectrum 75 ^{13}C spectrum of hyperpolarized 18 in acetone-d$_6$ after the aqueous cleavage.

Spectrum 76 ^{13}C spectrum of hyperpolarized 18 in acetone-d$_6$ after the aqueous cleavage.

7.3.3   1-(4,5-dimethoxy-2-nitrophenyl)prop-2-yn-1yl-3-d-acetate-1-^{13}C-d$_3$

Spectrum 77 ^{1}H spectrum of hyperpolarized 19 in acetone-d$_6$ after a 45° pulse.

Spectrum 78 ^{1}H spectrum of hyperpolarized 19 in acetone-d$_6$ after a 45° pulse

Spectrum 79 ¹H spectrum of hyperpolarized 19 in acetone-d_6 after a 45° pulse.

Spectrum 80 ¹H spectrum of hyperpolarized 19 in acetone-d_6 after the polarization transfer to H³

Spectrum 81 ^{1}H spectrum of hyperpolarized 19 in acetone-d$_6$ after the polarization transfer to H^3.
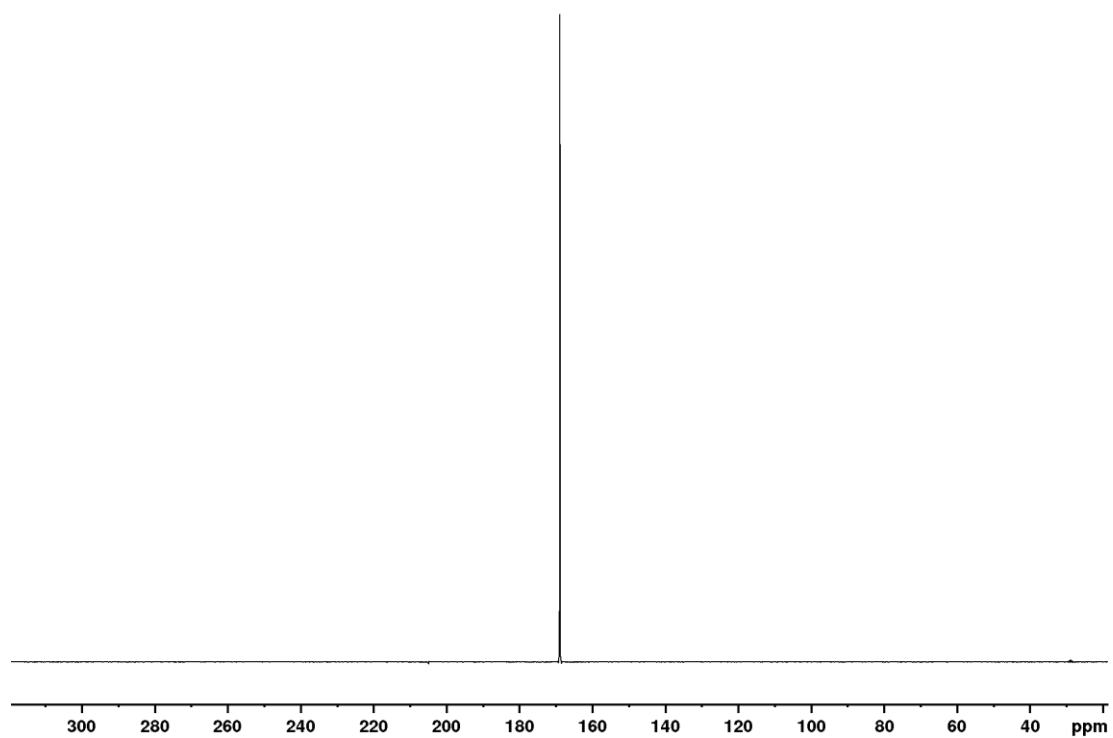
Spectrum 82 ^{13}C spectrum of hyperpolarized 19 in acetone-d$_6$ after the polarization transfer.
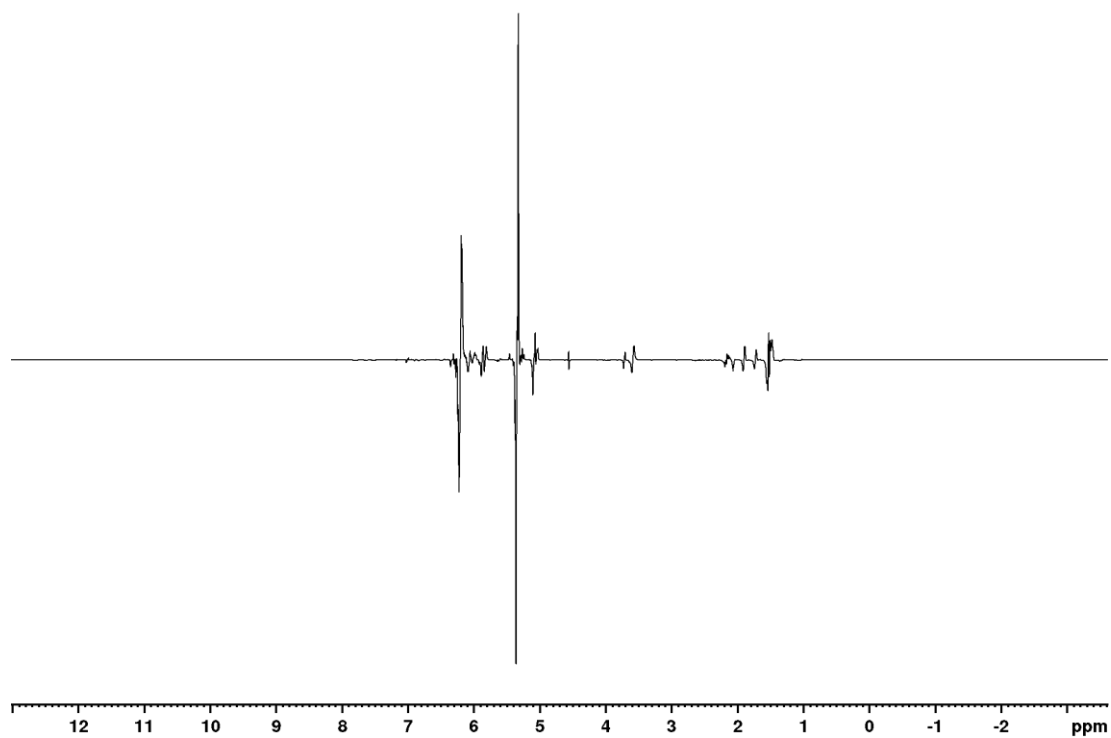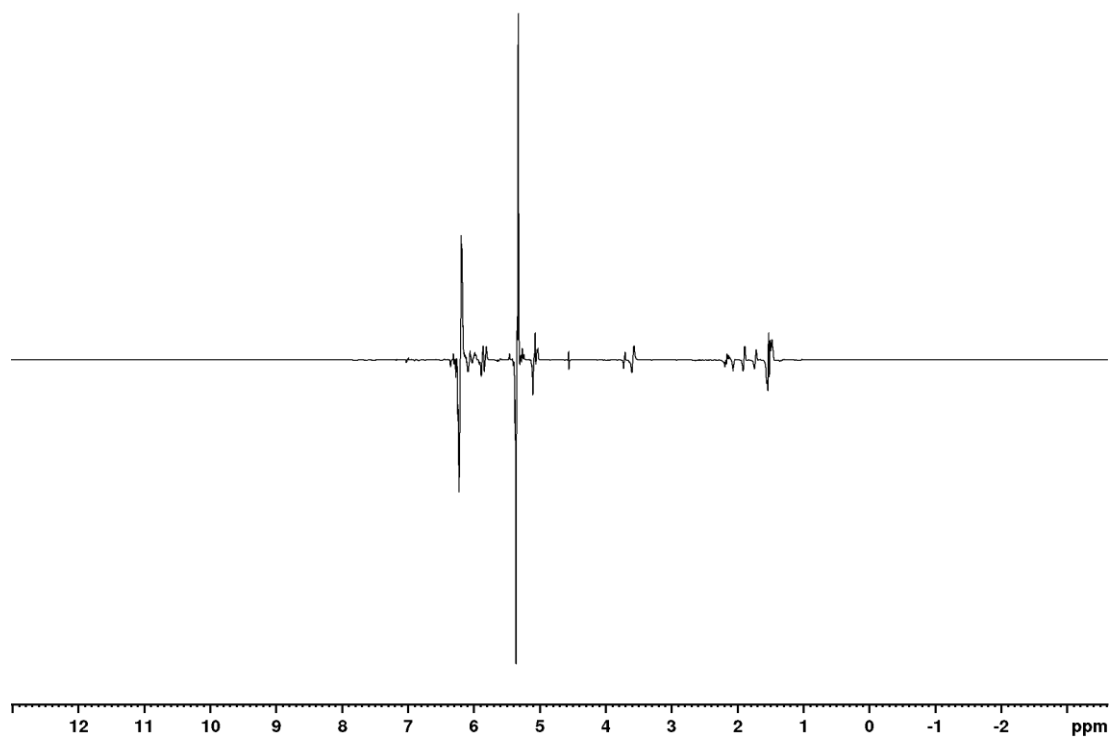
Spectrum 83 ^{13}C spectrum of hyperpolarized 19 in acetone-d$_6$ after the polarization transfer.

Spectrum 84 ^{13}C spectrum of hyperpolarized 19 in acetone-d$_6$ after the polarization transfer.

Appendix

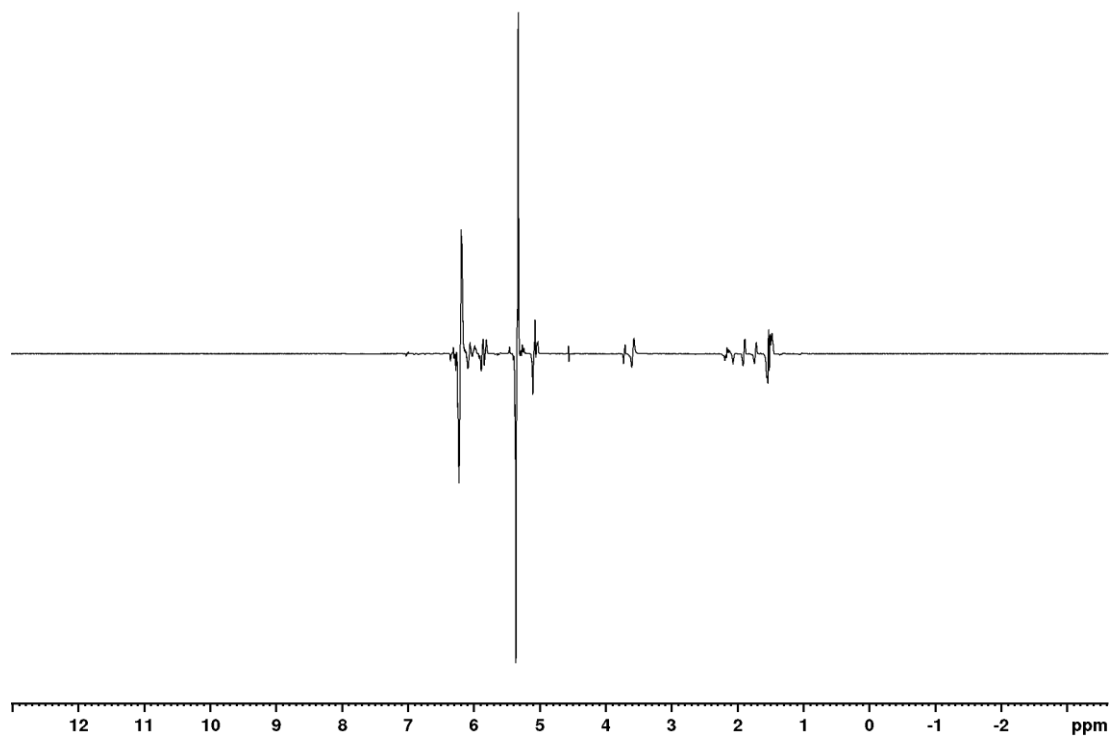## 7.3.4   1-(4,5-dimethoxy-2-nitrophenyl)prop-2-yn-1-yl-3-d-2-oxopropanoate-1-^{13}C-d$_3$

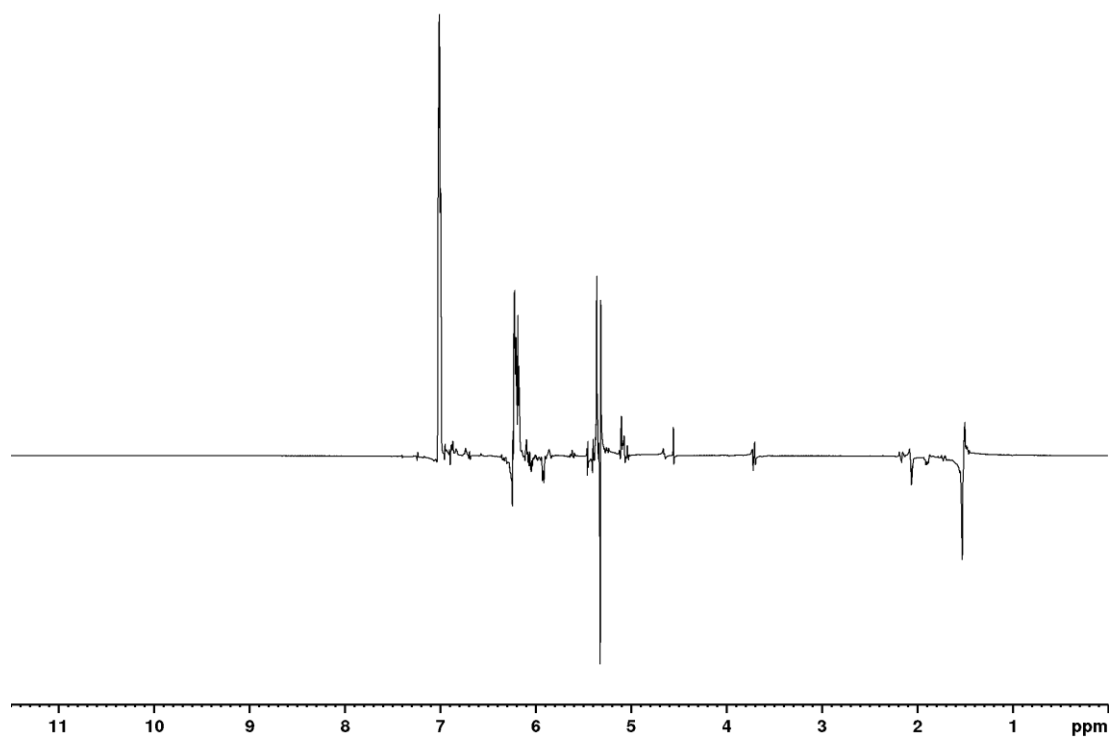Spectrum 85 ^{1}H spectrum of hyperpolarized 20 in acetone-d$_6$ after a 45° pulse.

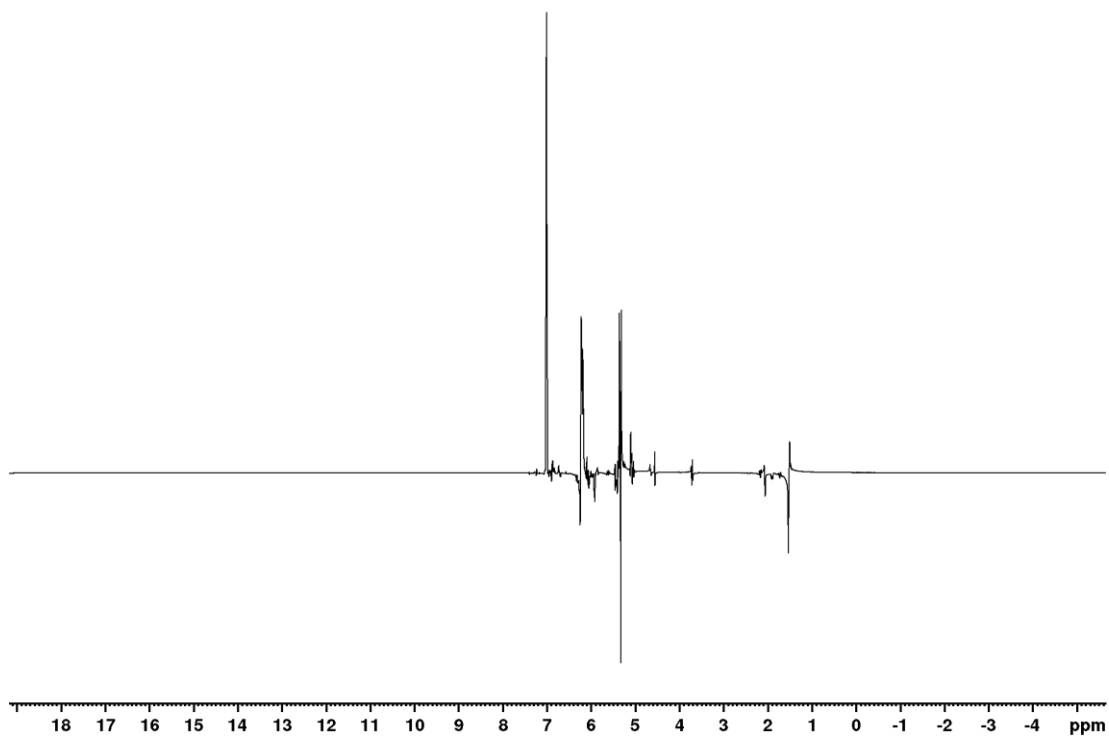Spectrum 86 ^{1}H spectrum of hyperpolarized 20 in acetone-d$_6$ after a 45° pulse.

Spectrum 87 ^{1}H spectrum of hyperpolarized 20 in acetone-d$_6$ after a 45° pulse.

Spectrum 88 ^{1}H spectrum of hyperpolarized 20 in acetone-d$_6$ after the polarization transfer to H^3.
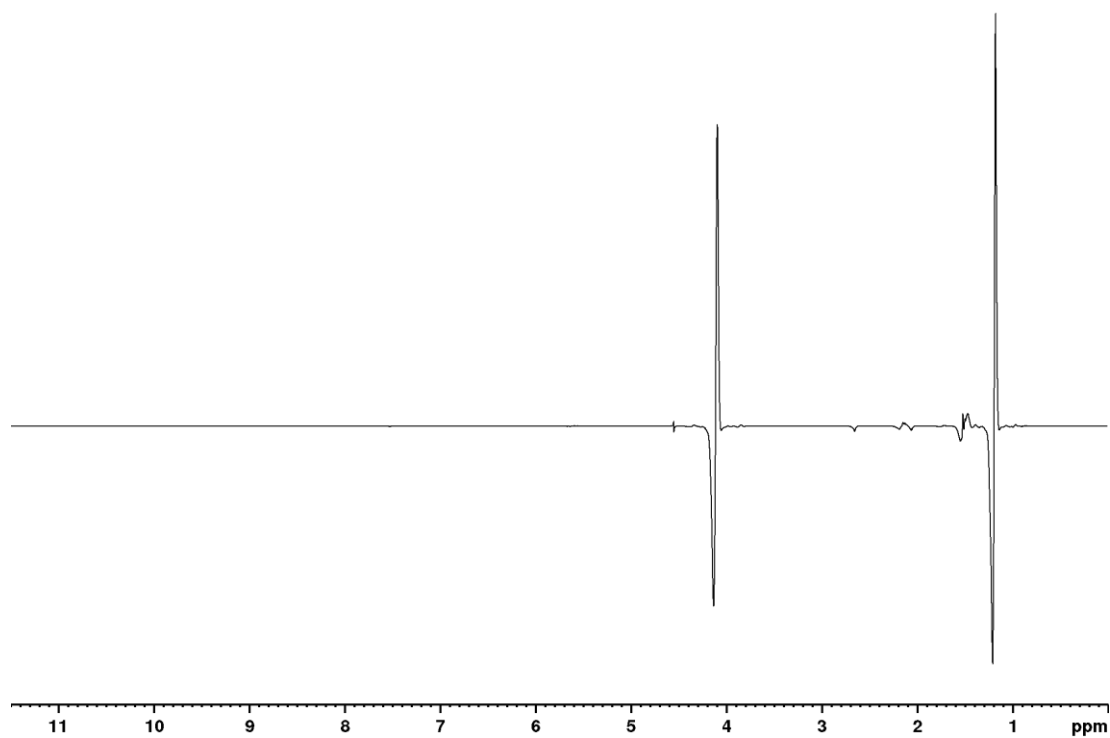
Spectrum 89 ^{1}H spectrum of hyperpolarized 20 in acetone-d$_6$ after the polarization transfer to H^3.
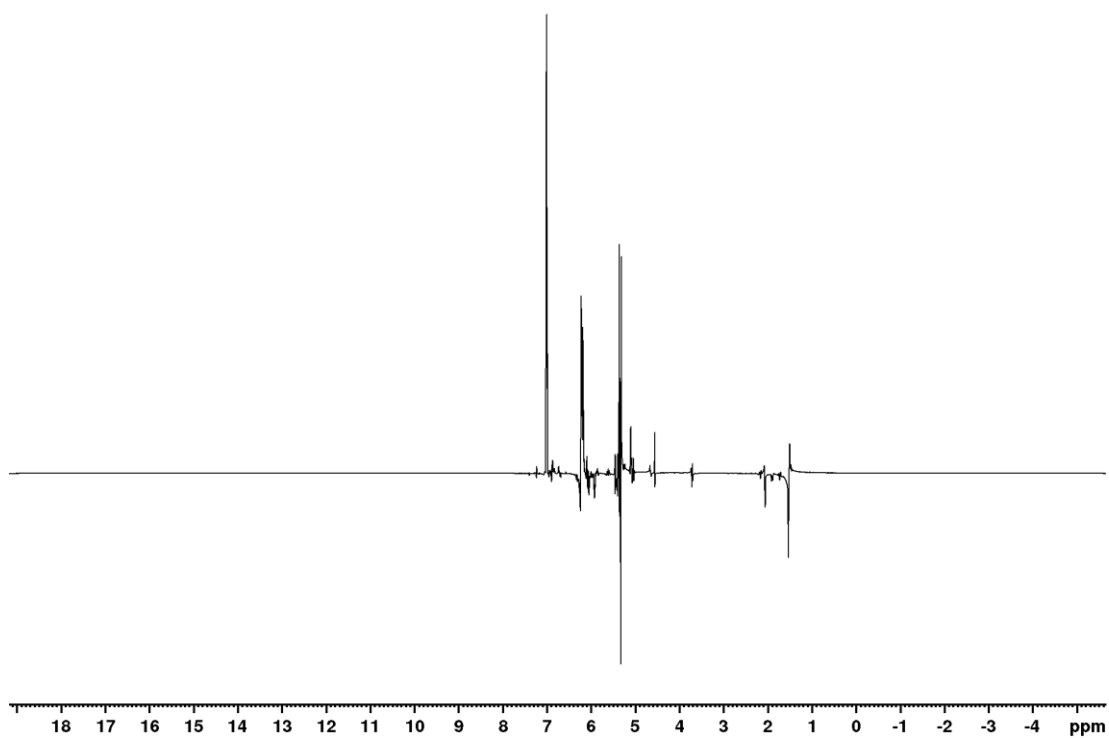
Spectrum 90 ^{1}H spectrum of hyperpolarized 20 in acetone-d$_6$ after the polarization transfer to H^3.

7.3.5 Vinyl-d$_3$ (acetyl-d$_3$)-L-alaninate-1-^{13}C-2-d

Spectrum 91 ^{1}H spectrum of hyperpolarized 28 in acetone-d$_6$ after a 45° pulse.
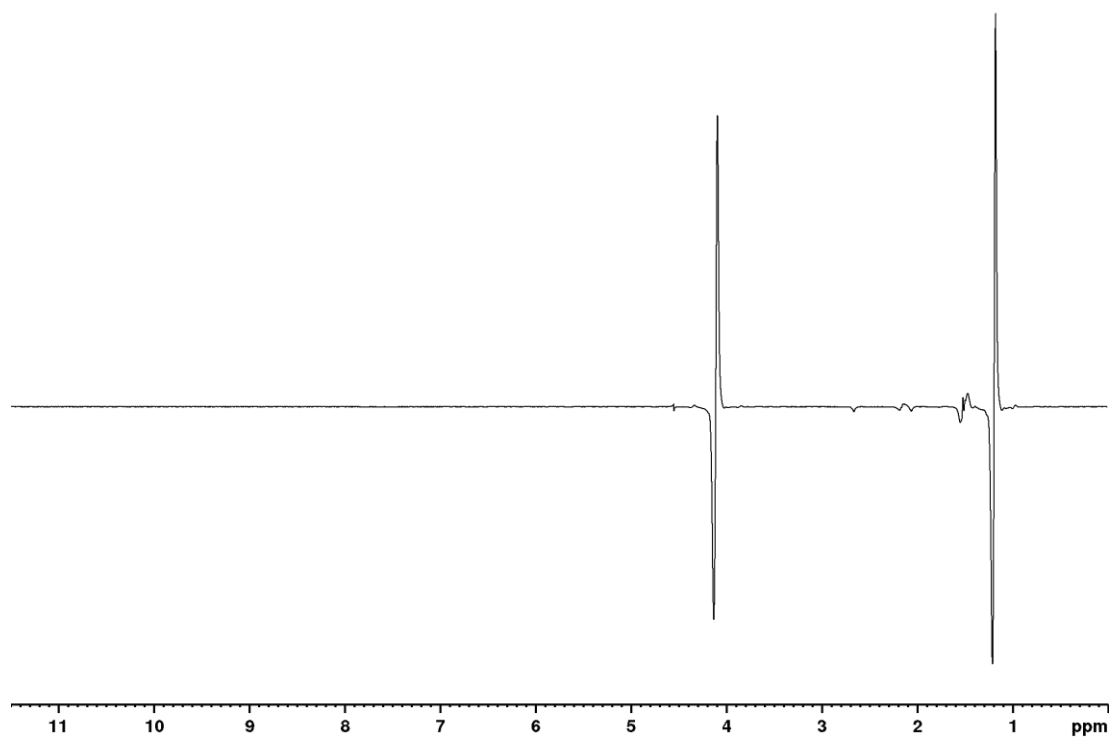
Spectrum 92 ^{1}H spectrum of hyperpolarized 28 in acetone-d$_6$ after a 45° pulse.

Spectrum 93 ^{1}H spectrum of hyperpolarized 28 in acetone-d$_6$ after a 45° pulse.

Spectrum 94 ^{13}C spectrum of hyperpolarized 28 in acetone-d$_6$ after the polarization transfer.

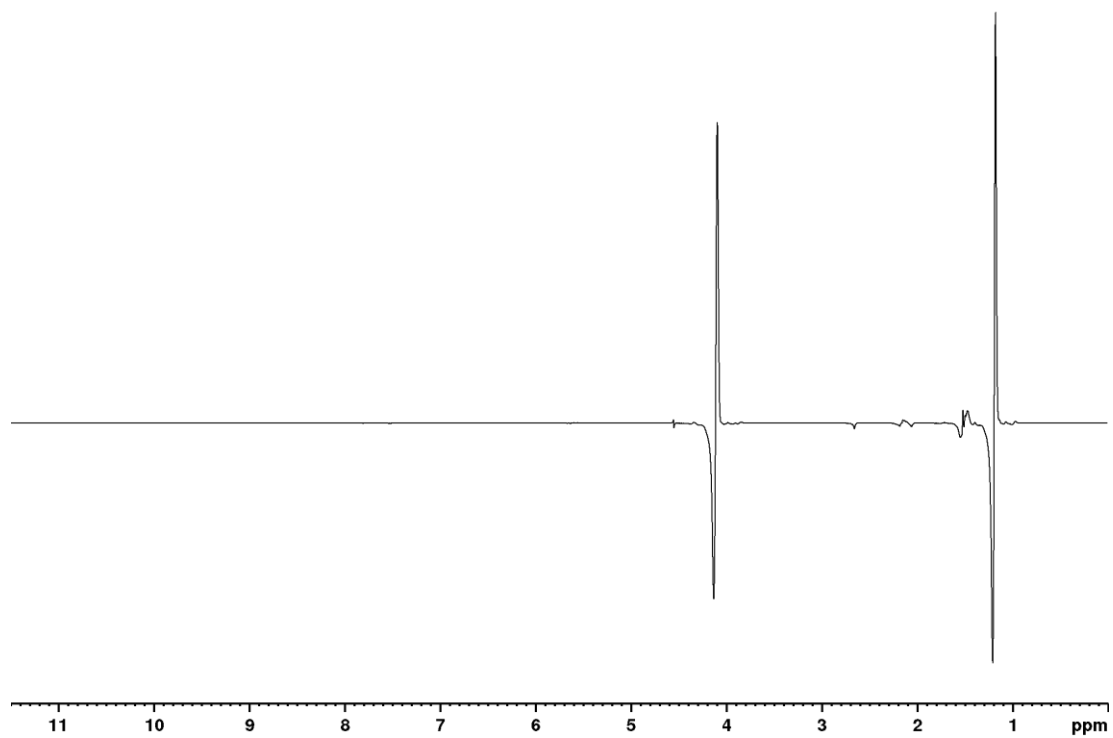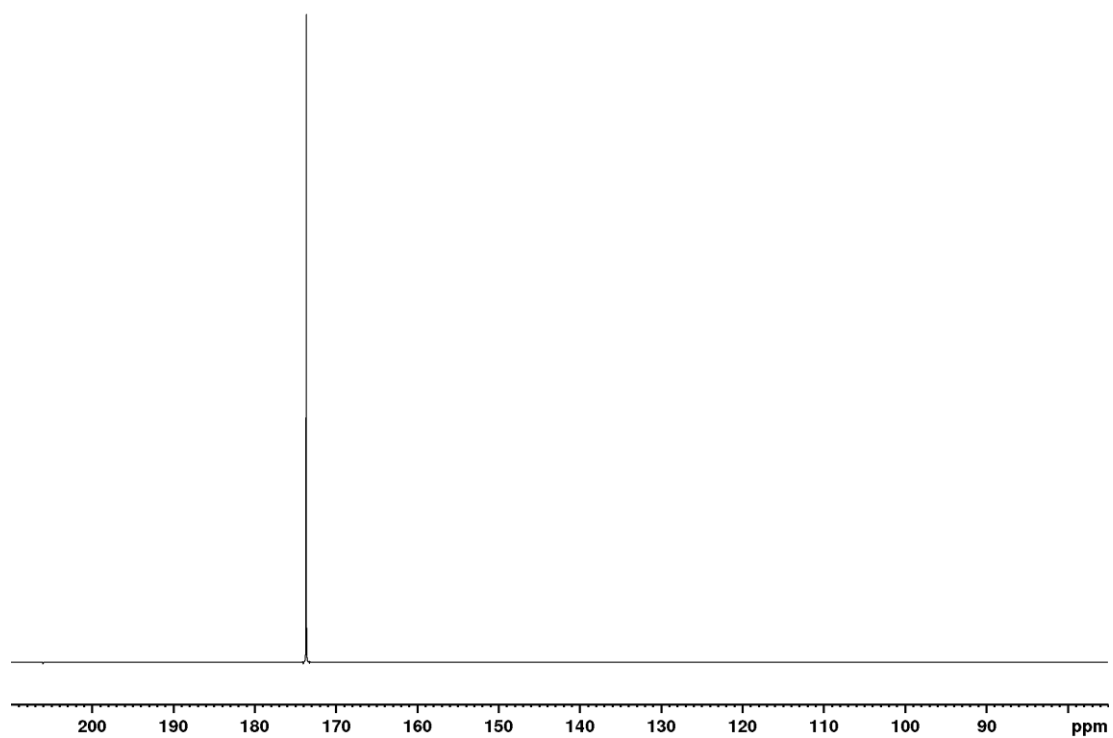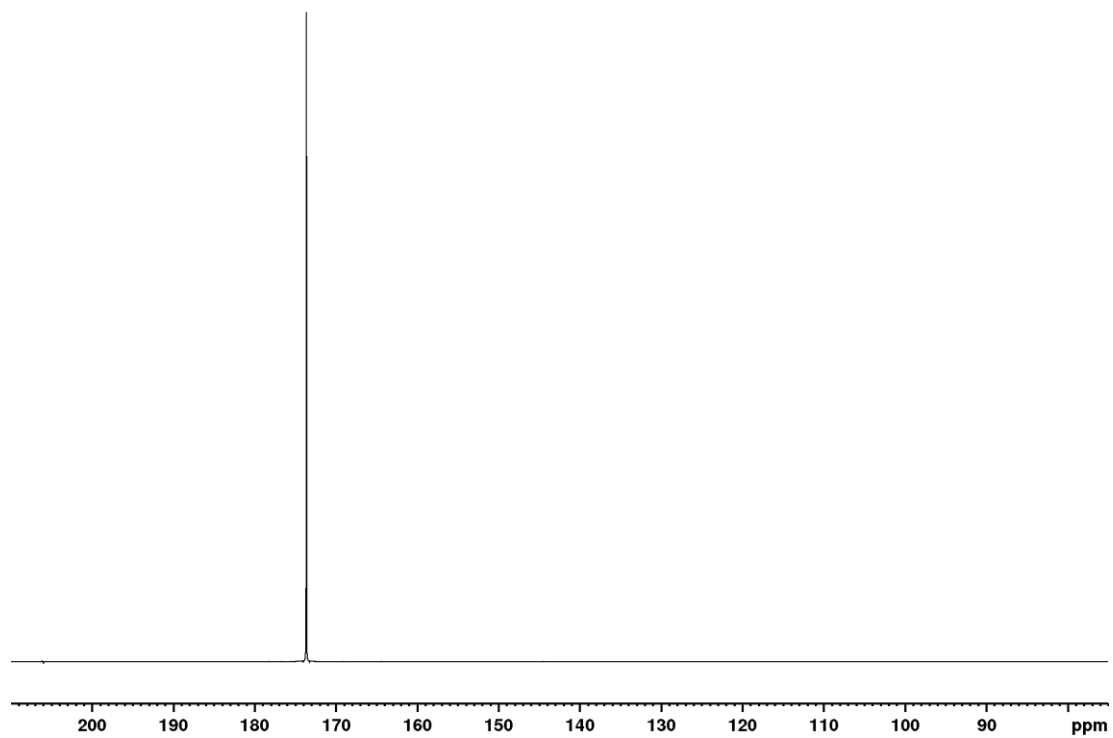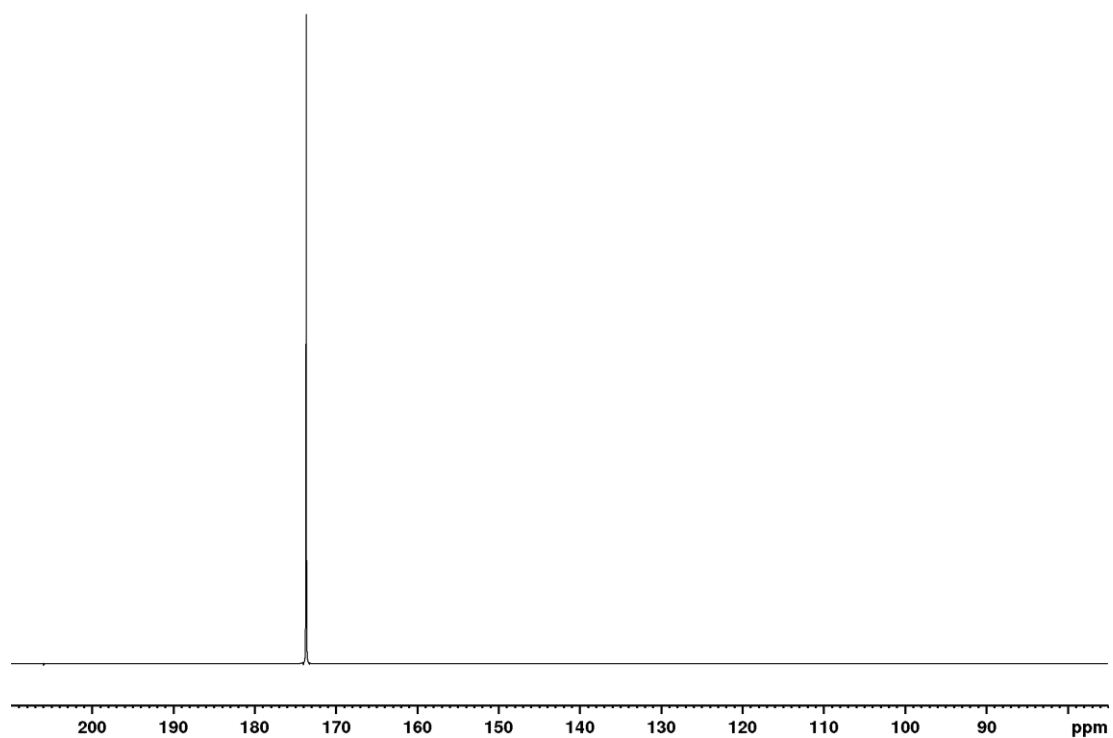Spectrum 95 ^{13}C spectrum of hyperpolarized 28 in acetone-d$_6$ after the polarization transfer.

Spectrum 96 ^{13}C spectrum of hyperpolarized 28 in acetone-d$_6$ after the polarization transfer.

Appendix

7.4 Numerical simulations

Calculation of the delay for the transfer of polarization from the proton H^3 to ^{13}C for the esters 17 to 20.

The relayed-ESOTHERIC pulse sequence described in chapter 1.3.3.3 is based on several INEPT blocks addressing several J couplings. The transfer delay τ_4 is usually set to $\frac{1}{4J_{23}}$ if the coupling between H_1 and H_3 is negligible. In the used molecules the coupling is around 1 Hz leading to the unwanted mixing of the spin states when transferring the polarization onto the heteronucleus (J coupling from 2.7-3.2 Hz). To avoid the unwanted mixing, the delay τ_4 was adjusted in such a way, that any evolution under the coupling of H_1 and H_3 makes a complete cycle. The delay was determined by numerical simulation using SpinDynamica implemented in Mathematica in order to optimize the sequence towards maximum efficiency. The delays used were 0.49 s for both side arms with an efficiency of 60% (2-NBn) and 90% (6-NV). For the pyruvate ester 18 0.617 s and 0.444 s for the ester 20 with 75% and 50% efficiencies were determined, respectively.

Calculation of the refocusing element for the ester 28 for an efficient polarization transfer.

The refocused ESOTHERIC pulse sequence described in chapter 3.3.2 adjusts the delays of the last transfer pulse. Due to the coupling of the methyl protons only 24% transfer efficiency can be expected for the N-acetyl-ethyl-d$_3$-alanine-d-2 using the standard $\frac{1}{4J_{23}}$ delay. To enhance the transfer efficiency numerical simulations were executed showing that close to the optimal transfer $\Delta_4 = \frac{1}{8J_{23}} - \delta$ 99.5% efficiency can be restored when selectively inverting the methyl protons. The used delay was 35.2 ms.

172

7.5 Optical rotation data

The measurements were performed as stated in chapter 2.6.

Table 10 Optical rotation measurements of L-alanine-d_4.

Sample	Temp	optical rotation monitor	specific optical rotation	Path length	concentration [g/mL]	solvent
L-Ala-d_4	20,65	0,3275	3,0218	100	0,1	H_2O
	20,66	0,3028	2,7748			
	20,67	0,3152	2,8988			
	20,69	0,3082	2,8288			
	20,7	0,2792	2,5388			
average	20,674	0,30658	2,8126			
L-Ala-d_4	20,74	0,2471	2,2178	100	0,1	H_2O
	20,75	0,2592	2,3388			
	20,77	0,2817	2,5638			
	20,78	0,2631	2,3778			
	20,8	0,28	2,5468			
average	20,768	0,26622	2,409			
L-Ala-d_4	20,82	0,284	2,5868	100	0,1	H_2O
	20,83	0,274	2,4868			
	20,85	0,2277	2,0238			
	20,86	0,2724	2,4708			
	20,88	0,2468	2,2148			
average	20,848	0,26098	2,3566			

Table 11 Optical rotation measurements of L-1-^{13}C-alanine-d_4.

Sample	Temp	optical rotation monitor	specific optical rotation	Path length	concentration [g/mL]	solvent
L-1-^{13}C-Ala-2-d	22,13	0,1982	2,0306	100	0,1	H_2O
	22,14	0,2335	2,3836			
	22,15	0,2261	2,3096			
	22,16	0,2333	2,3816			
	22,17	0,216	2,2886			
average	22,15	0,22142	2,2788			
L-1-^{13}C-Ala-2-d	22,21	0,2177	2,2256	100	0,1	H_2O
	22,22	0,2244	2,2926			
	22,23	0,2252	2,3005			
	22,24	0,2204	2,2526			
	22,24	0,2262	2,3106			
average	22,228	0,22278	2,27638			
L-1-^{13}C-Ala-2-d	22,26	0,2164	2,2126	100	0,1	H_2O
	22,27	0,2136	2,1846			
	22,28	0,2083	2,1316			
	22,28	0,2143	2,1916			
	22,29	0,2152	2,2006			
average	22,276	0,21356	2,1842			